1993

Precious-metal Mineralization And Sulfide-silicate Relationships In Some Canadian Nickel-copper Sulfide Deposits: Thompson Mine, Manitoba; Sudbury, Ontario; Dundonald Beach, Ontario

Yuan Chen

PRECIOUS-METAL MINERALIZATION AND SULFIDE-SILICATE RELATIONSHIPS IN SOME CANADIAN Ni-Cu SULFIDE DEPOSITS: THOMPSON MINE, MANITOBA; SUDBURY, ONTARIO; DUNDONALD BEACH, ONTARIO

by

Yuan Chen

Department of Geology

Submitted in partial fulfilment
of the requirements for the degree of
Doctor of Philosophy

Faculty of Graduate Studies
The University of Western Ontario
London, Ontario
November 1992

ISBN 0-315-81321-0

Canada

ABSTRACT

Platinum-group minerals (PGMs) and native gold are reported in association with gersdorffite and nickeline from the Thompson mine, Thompson Nickel Belt, Manitoba. Four PGM-gold-bearing ore types are distinguished on the basis of mineral assemblages and host rocks: I) irarsite in massive Ni sulfide ore hosted by metapelite; II) gold, sudburyite, testibiopalladite-antimonian michenerite, unnamed PGM, and merenskyite in As-rich Ni sulfide ore hosted by metapelite from the T-1 mine; III) gold with tellurides in As-rich Ni sulfide ore hosted by metapelite from the open pit; and IV) gold, majakite, kotulskite, merenskyite, and michenerite in As-rich Ni sulfide ore hosted by pegmatite from the T-1 mine. Native gold is argentian (Ag_{22}-Ag_{32}), and most Ag-rich in pegmatite-hosted samples. Testibiopalladite compositions straddle the previously inferred miscibility gap with michenerite. The unnamed PGM has a composition of $(Pd,Ni)_{0.44}(Te,Sb)_{0.56}$, and is distinctly anisotropic. Sporadic, minor amounts of PGEs are present in gersdorffite and nickeline.

All ore types are associated with a pervasive hydrothermal alteration event that post-dates the regional amphibolite facies metamorphism (presently constrained around 600-700°C and 6-7 kbar). The alteration assemblages include: (1) biotite, muscovite, chlorite, albite, calcite, siderite, allanite, quartz and sulfide (mainly pyrite, violarite and chalcopyrite) in metapelite;

(2) secondary grunerite and ferropyrosmalite in silicate-facies banded iron formation; (3) serpentine, tremolite, chlorite, epidote-zoisite and prehnite in skarn; (4) Fe-rich talc, serpentine, chlorite, actinolite, and hisingerite in ultramafic rocks. Spinel in metapelite and ultramafic rocks has been modified by Cr-Zn-rich fluids, and the oscillatory zonation in its composition reflects fluctuation in fluid composition. The latest hydrothermal alteration is characterized by high Cl concentrations, indicated by Cl-bearing allanite and ferropyrosmalite (up to 5.0 wt% Cl). The chlorite geothermometer and muscovite geobarometer suggest that the PGE-Au mineralization occurred at 250-300°C, 3-4 kbar.

PGMs and gold presently reported from the Sudbury mining camp include michenerite and merenskyite at the Lindsley mine, and sperrylite, michenerite, merenskyite, Pd-melonite, and electrum at the Lockerby mine. At the Dundonald Beach exploration property, Ontario, electrum, Os-Ni-Fe alloy, froodite, and an unnamed PGM phase (Pd-Sb-Bi) occur in komatiite. The alteration assemblages in these deposits also favour the possible involvement of hydrothermal fluids in the PGE-Au mineralization.

Investigation of the partitioning of Ni between olivine and Fe-Ni monosulfide reveals that the Fe/Ni distribution coefficient (K_{D3}) is in the range 4-15 at the Whistle, Levack, Trillabelle, and Ministic Lake mines of the Sudbury mining camp. However, K_{D3} values are somewhat higher (17-20) for

the Thompson mine peridotite. These results are consistent with literature observations that K_{D3} is generally significantly lower than the value (of 30-35) for equilibration of sulfide and olivine under magmatic conditions, but increases toward the high-temperature experimental value with increasing metamorphic grade. The komatiite from the Dundonald Beach property gave a K_{D3} value of 26, which could be attributed to either hydrothermal alteration of Fe-Ni sulfide, giving Ni-enriched sulfides, or equilibrium of primary (magmatic) sulfides with olivine.

Acknowledgements

I am indebted to my supervisor, Dr. M.E. Fleet for his patience, valuable ideas, and constructive criticism and editing during the preparation of this thesis; his time and effort contributed greatly to this research.

I owe particular thanks to Drs. R.W. Hodder and N.A. Duke for their help with provision of samples, their encouragement and enlightening discussions.

I wish to thank Y. Pan for providing helpful information concerning the thermobarometry and some hydrothermal minerals. I am grateful to M.L. Thompson, F. Puskas, M.M. Toderian, G.G. Morrison and other INCO staff for the provision of the samples. I would like to thank R.L. Barnett and D.M. Kingston for assistance with electron microprobe analyses, J.A. Forth for preparation of polished thin sections, Dr. T.-W. Wu for whole-rock contents of Pt, Pd and Au, Dr. S.L. Chryssoulis for SIMS analysis, Y. Cheng for XRD analysis, and D. Dillon, P. Davis, and K. Barron for provision of samples.

Funding for this study was provided by an NSERC research grant to Dr. M.E. Fleet. Additional financial support was a teaching assistantship from the University of Western Ontario awarded to the writer.

Lastly, I would like to thank my husband, W. Zang for helpful discussions, and assistance in preparation of the thesis.

TABLE OF CONTENTS

LIST OF PHOTOGRAPHIC PLATES

LIST OF TABLES

LIST OF FIGURES

LIST OF APPENDICES

PART I: PREFACE

CHAPTER 1 GENERAL STATEMENT

The first part of this thesis (Part I, Chapter 2) is an extensive review of the paragenesis of platinum-group minerals (PGMs) from different occurrences worldwide. Earlier reviews (e.g., Cabri, 1981) largely emphasized early-magmatic hypotheses for the origin of PGM deposits. The common evidence cited is the spatial association of platinum-group minerals (PGMs) with Cu-Ni sulfide, which is considered to indicate the primary concentration of precious metals by early-magmatic processes (i.e., sulfide liquation; e.g., Naldrett, 1989). However, numerous PGM-sulfide occurrences show evidence of the involvement of late-magmatic and hydrothermal fluids in either the concentration or remobilization of platinum-group elements (PGEs, McCallum et al., 1976; Ballhaus and Stumpfl, 1986; Mogessie et al., 1991; Farrow and Watkinson, 1992). Additionally, recent experimentation points to the feasibility of the quantitative transport of PGEs in high-temperature, Cl- and S-bearing fluids (Fleet, 1992).

In addition to the paragenesis of PGMs in mafic-ultramafic layered complexes, ophiolite complexes, Alaskan-type complexes, and other Cu-Ni sulfide deposits, the current review includes progress in the study of hydrothermal aspects of PGE deposits, and late-magmatic hydrothermal models

for the genesis of these deposits. Special attention is also given to progress in experimentation on the partitioning of PGEs between alloys, sulfides and silicates, which provides laboratory evidence for late-magmatic, hydrothermal processes.

The main part of the thesis (Part II, Chapters 3-8) is devoted to investigation of precious-metal mineralization in the Thompson mine, Thompson Nickel Belt, Manitoba, where PGE and gold mineralization, together with Ni-sulfide ores occur mainly in metasedimentary rocks. The association of PGMs and native gold with Fe-Ni-Cu sulfide has been reported from a wide variety of Cu-Ni sulfide deposits, including Noril'sk, Russia (Genkin and Evstigneeva, 1986), O'Toole, Brazil (Marchetto, 1990), Waterfall Gorge, Pondoland (Tischler et al., 1981), Ivrea-Verbano Basic Complex, Western Italian Alps (Garuti and Rinaldi, 1986), Sudbury, Ontario (Cabri, 1981), and Kambalda, Australia (Hudson, 1986). These deposits, however, are either hosted in or closely related to mafic-ultramafic magmatic bodies.

In contrast to other deposits, the host rocks at the Thompson mine are metapelite and related pegmatite, and the PGMs are proximally related to a pervasive, late hydrothermal alteration. Lack of large-volume mafic-ultramafic magmatic bodies and distinct relationships between the precious-metal mineralization and metasedimentary rocks make this area perhaps a unique example for the investigation of hydrothermal processes in PGM mineralization. In this study, the general geology and mineral chemistry (including silicates,

oxides, carbonates, sulfides and arsenides) are documented. The metamorphic history of the country rocks in the context of the mineral chemistry is discussed. Metamorphic temperatures and pressures are estimated. Emphasis is also given to investigation of the late hydrothermal minerals, which provide information not only on temperature and pressure, but also on mineralizing fluids.

In addition to the Thompson mine, PGMs from two Cu-Ni sulfide deposits of the Sudbury mining camp (Lindsley and Lockerby) and from the Dundonald Beach prospect in the Archean Abitibi greenstone belt are also documented in Parts III and IV of the study, respectively. The PGMs are the first reported from these deposits.

The last part of the thesis (Part V) is concerned with the partitioning of Ni between olivine and Fe-Ni monosulfide. The general association of Cu-Ni sulfide deposits with ultramafic and mafic igneous rocks and their stratigraphic position in komatiite flow units has encouraged many investigators to favour ore formation by magmatic processes, most commonly magmatic segregation of immiscible sulfide liquid. However, the low Ni contents of sulfides in unmetamorphosed or low-grade metamorphosed Cu-Ni deposits compared with the content expected for equilibration with magmatic olivine are inconsistent with ore formation by magmatic segregation (Fleet et al., 1977; Fleet and MacRae, 1983; 1987; 1988). In the present study, the partitioning of Ni between olivine and Fe-Ni-Cu sulfide is investigated in the presently studied

mining camps, and includes data for the Thompson ultramafic rocks, exotic inclusions and olivine norite from the Sudbury area and komatiite from Dundonald Beach, Ontario.

CHAPTER 2 REVIEW OF PARAGENESIS OF PLATINUM-GROUP MINERALS

2.1 Introduction

Platinum-group minerals (PGMs) are well known to be mainly associated with mafic-ultramafic igneous rocks. The PGMs occur either as PGM-dominant deposits or as by-products of Cu-Ni- dominant deposits. The PGM-dominant deposits are associated with mafic-ultramafic layered complexes, ophiolite complexes, and Alaskan-type complexes. The Cu-Ni-dominant deposits containing PGMs are associated with noritic rocks (such as Sudbury), intrusive equivalent of flood basalts (such as Noril'sk), and komatiitic lavas and intrusions (such as Kambalda). PGMs are also found associated with hydrothermal Cu(Au) deposits.

In Cabri (1981a), the geochemistry, mineralogy and geology of PGMs were reviewed by a group of authors who emphasized early-magmatic hypotheses for their origin. Over the past decade, there have been significant advances in the study of PGM mineralization. New PGM deposits and occurrences have been found worldwide. Progress is particularly noticeable in the studies of fluid inclusions and Cl-bearing hydrous silicates from PGM deposits. Hydrothermal PGM deposits have been recognized in a variety of environments, even in the mafic-ultramafic complexes, such as in the Bushveld Complex (Stumpfl, 1986) and the Stillwater Complex (Boudreau et al., 1986).

Current models for the genesis of these deposits involve transport of PGEs and associated metals by chloride complexes during late-stage magmatic-hydrothermal processes (Nyman et al., 1990; Mogessie et al., 1991; Ferrow and Watkinson, 1992). PGMs of hydrothermal origin occurring within shear zones cutting mafic-ultramafic rocks and PGMs associated with other hydrothermal deposits have also been reported in the literature.

Another noticeable area of progress is in the study of the partitioning of PGEs between alloys, sulfides and silicates. Numerous investigations on the products of laboratory experiments (Stone et al., 1990; Fleet and Stone, 1991; Fleet et al., 1991) show that early-magmatic processes are not consistent with both the concentration and fraction patterns of PGEs in ore deposits. These discrepancies question an exclusive role for immiscible sulfide liquid in fractionating and concentrating PGEs in nature.

The aim of this chapter is to review the paragenesis of PGMs in different types of deposits, including the mafic-ultramafic layered complexes, ophiolite complexes, Alaskan-type complexes, PGMs associated with Cu-Ni sulfide deposits, and Cu mineralization. The relationship between PGMs and chromite, and PGE concentrations and their distribution patterns in different deposits will also be discussed.

2.2 Mafic-Ultramafic Layered Complexes

The mafic-ultramafic layered complexes occur in cratonic areas, and

consist of a sequence(s) of differentiated, layered mafic and ultramafic rocks. The overall compositions of these complexes tend to be mafic rather than ultramafic, although ultramafic zones are present in each of them. The best examples are the Bushveld Complex in South Africa and the Stillwater Complex in Montana.

Four distinct lithostratigraphic zones are recognized in the Bushveld Complex . The lower zone is composed mainly of bronzitites, harzburgites and dunites (Cameron, 1978). It is overlain by the Critical zone, which hosts the PGE-bearing Merensky Reef and UG-2 chromitite (Cameron, 1980; 1982). The Critical zone is overlain, in turn, by the norites, gabbros and anorthosites of the Main zone, which are themselves capped by the ferrogabbros and ferrodiorites of the Upper zone (von Gruenewaldt, 1973). The principal PGE mineralization in the Bushveld Complex occurs within or very close to the Upper Critical zone. Six to eight chromitite layers with high concentrations of PGE occur in this zone. The more important PGE concentrations occur in the upper part of the Upper Critical zone. Five or six well-defined cyclic units occur in this part of the stratigraphy; these are UG-1, UG-2, UG-3 (in some areas only), Pseudoreef (in some areas only), Merensky Reef, and Bastard Reef units. According to Kinloch (1982), most PGMs from the Merensky Reef and UG-2 are associated with base-metal sulfides and silicates. The PGMs are also associated with chromite in UG-2.

The Stillwater Complex is divided into the Basal, Ultramafic and Banded

series (Zientek et al., 1985). The Basal series is in turn subdivided into the Basal Norite zone and the Basal Bronzite Cumulate zone, the Ultramafic series into the Peridotite zone and the Bronzitite zone, and the Banded series into Lower, Middle and Upper Banded series. The Basal series is a laterally continuous but petrologically variable unit consisting of bronzite cumulates or bronzite plus plagioclase cumulates. The Peridotite zone of the Ultramafic series consists of an alternating sequence of olivine-, chromite-, and bronzite-bearing cumulate layers. Talkington and Lipin (1986) noted that in the chromite seams of the Stillwater Complex, laurite (RuS_2) is the most common PGM inclusion in unfractured chromite, and Pt-, Pd-, and Rh-bearing minerals occur as interstitial phases, adjacent to chromite grains, in an altered interstitial sulfide and silicate host.

The J-M Reef of the Stillwater Complex (Cabri, 1981) which contains very high concentration of PGMs occurs within the lowest olivine-bearing zone within the Lower Banded series. The lower portion of the mineralized reef consists of about 1 m of olivine cumulate, enclosed in large bronzite oikocrysts, together with interstitial plagioclase. Minor amounts of Cl-rich phlogopite, apatite and chromite are also present. The common sulfides are chalcopyrite, pyrrhotite, pentlandite and pyrite, which generally occur as blebs or as an interstitial network in the lower part of the reef, and as a fine dissemination towards the top.

The PGMs associated with the mafic-ultramafic layered complexes are

dominated by Pt-Pd sulfides, Pt-Fe alloys, Ru sulfides (mainly laurite, occurring as inclusions in chromite), Rh sulfides, Pt-Pd tellurides, Pt arsenides (mainly sperrylite, $PtAs_2$) and Pd alloys (Table 2.1). In general, laurite is commonly a solitary mineral within grains of chromite, but may also be in direct contact with a silicate, sulfide, oxide or alloy phase.

In the Sompujarvi PGE Reef of the Penikat Layered Intrusion, two types of PGM mineralization were recognized by Halkoaho et al. (1990a), namely, the sulfide-disseminated type and the chromite-disseminated type. The former is associated with base-metal sulfides (mainly pyrite, chalcopyrite and pentlandite) whereas the latter is with chromite disseminations.

From the above discussions, three principal categories of mode of occurrence of PGMs are evident:

(1) association with base-metal sulfides

(2) association with silicates

(3) association with chromite or other oxides.

The PGMs can be either enclosed in or attached to the associated minerals. The sulfides are dominated by an assemblage of chalcopyrite, pyrrhotite and pentlandite. Among the PGMs, laurite is only developed in significant amounts in the chromite layers, occurring as inclusions in the chromite. In the Bushveld Complex, for instance, the chromitites contain about twice the amount of Ru as the silicate ore (Kinloch, 1982).

The association of PGMs with base-metal sulfides and chromite are well

known in the layered mafic-ultramafic complexes. Magma mixing and sulfide immiscibility have been suggested to explain the formation of massive chromitite layers, and the association of PGEs with particular chromitite layers in the layered intrusions. Cyclic layering is generally attributed to the entry of a new pulse of magma into the chamber, suggesting that the formation of these zones is genetically related to the multiple injection process (Campbell et al., 1983; Campbell and Turner, 1986). Irvine (1977) showed that the mixing of two magmas, one that has reached a higher degree of fractionation than the other, can inhibit the fractional crystallization of silicate minerals such as olivine and orthopyroxene and permit the crystallization of chromite alone. Thus massive chromitite layers can develop. Several authors have proposed that PGMs in these associations could result from the crystallization of an immiscible sulfide liquid enriched in PGEs (e.g., Cabri and Laflamme, 1976). This suggestion seems consistent with observations on the J-M Reef in which sulfide-silicate textures were interpreted as equilibrium crystallization (Bow et al., 1982; Barnes and Naldrett, 1985). However, this interpretation was challenged by experimental studies (e.g., Fleet and MacRae, 1983). Fleet (1986) interpreted the same textures as indicating progressive metasomatic replacement of preexisting silicates by sulfides rather than equilibrium crystallization. Therefore, the role of fluids in the formation of PGMs in the layered complexes may be more important than has previously been recognized.

Suggestions have been made in recent years which highlight the role of

volatiles in the formation of PGM-enriched zones in the mafic-ultramafic layered complexes. This model maintains that PGM enriched zones were formed either from fluids migrating upwards (Boudreau et al., 1986) or from a fluid-enriched intercumulus melt introduced from the footwall units (Ballhaus and Stumpfl, 1986).

2.3 Ophiolite Complexes

Ophiolite complexes are interpreted as a portion of the oceanic crust and upper mantle. In ophiolitic complexes the host rocks for the PGMs are dunite, harzburgite and lherzolite. PGMs are found associated with chromitites in all types of dunite (including barren dunite bodies, dunite dykes, dunite interlayered with harzburgite, and dunite associated with the chromite ore). In most cases, the PGMs are included in chromite (including chrome-bearing spinel) grains (e.g., Stockman and Hlava, 1984; Talkington et al., 1984; Auge, 1985; 1988; Thalhammer et al., 1990). An exception is the Shetland ophiolite where PGMs occur also interstitially to chromite (Prichard et al., 1986). Auge (1986) described silicates attached to most of the PGMs from chromitite in Oman and gave the example of laurite enclosed in a two-phase silicate inclusion. Auge concluded that the Oman case seems to indicate that, when the silicate inclusions are abundant in chromitite, PGM inclusions are often attached to silicates.

The PGMs associated with ophiolite complexes are summarized in Table

2.2. They consist predominantly of just three of the PGE: Ru, Ir and Os. Pt, Pd and Rh enter only in minor amounts or very rarely from discrete minerals. The PGMs are mainly restricted to the four groups:

(1) alloys (Os-Ru-Ir, Os-Ir, Ir-Os, Pt-Pd-Fe, Pd-Sb-Pt, Pt);

(2) sulfides (RuS_2, OsS_2, Ir-Cu-sulfides);

(3) sulfarsenides (OsAsS, IrAsS, PtAsS, RhAsS);

(4) arsenides ($PtAs_2$).

The first three groups are much common whereas the fourth group (arsenides) is not so common in ophiolite complexes. However, in the Shetland ophiolite complex, sperrylite and stibiopalladinite ($Pd_{3+x}Sb_{2-x}$) are the most common PGMs (Prichard and Tarkian, 1988), which may suggest that Pt- and Pd-bearing minerals may be more common in ophiolite complexes than previously concluded. Also, PGE-Sb-sulfides (Ir-Sb-S, Rh-Sb-S, Rh-Ni-Sb) were recognized in the Shetland ophiolite complex (Tarkian and Prichard, 1987).

In some cases the alloys are absent and laurite (RuS_2) is dominant, which has been attributed to a high sulfur fugacity during hydrothermal PGM mineralization (Ferrario and Garuti, 1990). In the Tiebaghi (New Caledonia) and Finero (Italy) ophiolites, for example, even the chromite concentration is considered to be formed by metasomatic processes (Ferrario and Graruti, 1990), and the PGM assemblage is characterized by the absence of Ru-Os-Ir alloys, and the presence of laurite along with a variety of Ir PGM-sulfides (Legendre and Auge, 1986; Ferrario and Garuti, 1990).

In most ophiolite complexes two paragenetic groups of PGMs can be recognized based on mineral assemblages and textures. At Kraubath, Austria (Thalhammer et al., 1990), for example, two different groups of inclusions in chrome-spinel are present: the first group occurs within the chromite core, and comprises olivine, orthopyroxene, amphibole, sulfides and PGMs, that are dominated by Ru-Os-Ir sulfides. The second group is formed by chlorite, serpentine, galena, pyrite, arsenopyrite, Pt-Pd-Rh-dominated sulfarsenides and sperrylite. The first group is intimately related to the crystallization of the chromite host, the second group of inclusions clearly displays a secondary formation during serpentinization and metamorphism, closely related to the alteration of chrome-spinel and the development of "ferritchromite".

A similar paragenesis for PGMs was documented from the Osthammeren ultramafic tectonite body, Norway (Nilsson, 1990), where the PGM-inclusions occur in two distinctly different textural groups. Group 1 is totally enclosed in fresh magmatic chromite, and consists of Os-free laurite, Os-laurite, osmiridium (Ir,Os) and $Pt_2(Ir,Os)Fe_{0.65}$. Group 2 occurs within or in contact with late-formed cataclastic cracks or fine fissures in the primary magmatic chromite grains, and consists of Os-free laurite, Os-laurite, erlichmanite (OsS_2), Ir-rich erlichmanite, native Os, iridosmine (Os,Ir), osarsite (OsAsS), irarsite (IrAsS), hollingworthite (RhAsS), Rh-rich platarsite (PtAsS), Ru-rich platarsite, sperrylite, (Ir,Rh)SbS, IrSbS, and $(Ir,Pt,Pb)S_2$. The second group is associated with pentlandite, heazlewoodite, and nickeline. Nilsson suggested that the first

group may have an association with hydrous silicates (phlogopite and Na-bearing hornblende), i.e., that the PGMs may have nucleated in the presence of, or in contact with, volatile bearing silicates. This group is likely to have a magmatic or "magmatic-hydrothermal" origin. The second group is formed during metamorphism and hydrothermal alteration which involve brittle fracturing of the chromite grains and percolation of As and Sb-bearing fluids through the cracks. At the stage of PGM-formation Os-availability decreases whereas Rh and lastly Pd are introduced.

The presence of inclusions of base-metal sulfides in chromitite has been reported by Talkington et al (1984), Whittaker and Watkinson (1984), Auge (1988) and Thalhammer et al. (1990). Chalcopyrite and pentlandite are the most common sulfide minerals. The presence of PGE in solid solution in the sulfides has been proposed by Vermaak and Hendricks (1976), and Mostert et al. (1982) described laurite exsolusion in pyrrhotite. Some PGE have been detected in the sulfides. Ross and Keays (1979) described the presence of Pd in pentlandite. Cabri (1981) noted up to 0.66 wt% Pd in pentlandite from Lac des Iles, Ontario; Bow et al. (1982) reported 2 wt% Pd and Todd et al. (1982) 3.3 wt% in pentlandite from the Stillwater complex. The highest contents of PGE in pentlandite were reported from the Vourinos ophiolitic complex, Greece (Auge, 1988). The content of Ru is up to 24.3, Rh 20.3, Pt 0.9, and Pd 17.5 wt% in pentlandite included in chromite grains. The Ir content is generally low, around 0.2 wt%, except in one grain, where it is 21.4 wt%. An interesting feature is

the lack of Os in the sulfides.

Positive Pt and Au anomalies have been identified by Ohnenstetter (1992) in ophiolite mantle peridotite from the Monte Maggiore Massif, Corsica, France, where PGMs are associated with native gold. PGMs are mainly alloys (native Os, Ir, Pt, Pd), the Cu-bearing equivalent of rustenburgite, potarite, moncheite and Ni-rich merenskyite. The PGMs and native gold are generally located close to base metal sulfides. Ohnenstetter (1992) suggested that the PGMs were directly precipitated from a fluid phase that remobilized PGE originally dissolved in base-metal sulfides.

In summary, PGMs associated with ophiolite complexes concentrate mainly the three most refractory of the PGE: Ru, Ir and Os. Pt, Pd and Rh enter only in minor amounts. The PGMs are present as alloys, sulfides, sulfarsenides and arsenides. A high sulfur fugacity contributes to the absence of alloys and dominance of laurite (RuS_2). Two paragenetic groups of PGMs can be recognized based on mineral assemblages and textures. The first group is intimately related to the crystallization of the chromite host grains. The second group is associated with base-metal sulfides, related to the development of "ferritchromite", and displays a secondary formation during serpentinization and metamorphism. The first group may be associated with hydrous silicates, suggesting that the PGMs have nucleated in the presence of volatile bearing silicates.

2.4 Alaskan-Type Complexes

Alaskan-type ultramafic complexes draw their name from a series of distinctive bodies exposed along the mainland of southeast Alaska. Similar bodies are known in the Urals, south-central British Columbia, Colombia, Venezuela and New South Wales, Australia. The most extensively studied of all is the Duke Island Complex, described by Irvine (1974). The complexes characteristically lack orthopyroxene, have no plagioclase in the ultramafic units, and contain highly magnesian olivine (Fo_{75} to Fo_{93}; Wyllie, 1967), abundant hornblende, iron-rich chromite, and magnetite. The complexes usually show a rough concentric zoning which, when best developed, consists of a dunitic core surrounded by successive shells of minor peridotite, olivine clinopyroxenite, magnetite-rich clinopyroxenite, and hornblendite, with felsic rocks on the margin.

The core of most complexes consists of massive chromite that has indistinct crystal outlines and is locally cross-cut by irregular fractures. Subhedral to euhedral chromite crystals are interspersed with olivine in the enveloping dunite. The chromitites are highly enriched in Pt and, to a much lesser extent, Ir, relative to other PGEs. The (Pt+Pd)/(Ru+Os+Ir) and Pt/Pd ratios are extremely high.

The PGMs in the complexes (Table 2.3) occur primarily as Pt-Fe(-Ni-Cu) alloys, geversite ($PtSb_2$), cooperite (PtS), sperrylite, erlichmanite, and malanite [$(Pt,Ir)_2CuS_4$]. Paragenetically, the PGMs can be subdivided into two

groups. Group 1 consists predominantly of platinum-bearing alloys associated with chromite and silicates that are considered to have segregated from high-temperature silicate melts and coprecipitated with chromite (Amosse et al., 1990), and Group 2 includes other PGMs associated with base-metal sulfides and arsenides that are considered to have formed during later metamorphism and serpentinization (Nixon et al., 1990). However, St. Louis et al. (1986) assumed the PGMs associated with serpentine and Fe-Ni sulfides to have been originally deposited as complex sulfide droplets, alloys, or possibly monosulfide solid solution.

In Alaskan-type complexes, in general, the chromitite-PGE association appears to be the most widespread type of lode mineralization, though not the sole economic target. PGE-enriched chromitites are even more important in stratiform mafic intrusions, and also have potential in the ophiolitic settings (see above discussions). Alaskan-type complexes tend to have PGE contents greater than ophiolite complexes, but the Pt/(Pt+Pd) ratio of the former (0.68) tends to be somewhat lower than that of the latter (0.73). However, the Pt/(Pt+Pd) ratios of both are substantially higher than is observed in large layered complexes (0.51; Naldrett and Cabri, 1976; Raicevic and Cabri, 1976).

In the Alaskan-type intrusions, PGEs are primarily contained in Pt-Fe and Pt-Ir alloys, and are not associated with primary magmatic base-metal sulfides (Cabri, 1981; Nixon et al., 1990). The high (Pt+Pd)/(Ru+Os+Ir) ratios of PGE-enriched chromitites are typically accompanied by high Pt/Pd

(e.g., Nixon and Hammack, 1990), and the latter feature is inconsistent with collection by base-metal sulfides, which are known to concentrate both Pt and Pd (e.g., Talkington and Watkinson, 1986; Naldrett, 1989). Therefore, the concentration of PGEs in chromitites of Alaskan-type intrusions is best explained by the accumulation of platinum-rich alloys that segregated directly from the melt at an early stage in the evolution of the complex (Nixon et al., 1990).

2.5 Nickel-Copper Sulfide Deposits

PGM mineralization is frequently reported from Cu-Ni sulfide deposits. These PGMs are dominated by Pd and Pt minerals (Table 2.4). Cu-Ni sulfide deposits are associated with noritic rocks, flood basalt magma and intracontinental rifting, and komatiitic rocks in Precambrian greenstone belts. These deposits are well represented by the major deposits at Sudbury, Ontario, Noril'sk, Siberia, and Kambalda, Western Australia.

2.5.1 Sudbury Cu-Ni sulfide deposits

The Cu-Ni sulfide deposits of the Sudbury area are peripherally located around the structure of an elliptical basin-shaped stratiform complex referred to as the "Nickel Irruptive", which consists of an outer part of noritic rocks and an inner part of granophyre. The orebodies are associated with the sublayer unit and offset dykes. The geological evolution of the rocks and ores of the Sudbury

area has been actively discussed in the literature. The Ni-Cu ore deposits can be divided into three categories (cf., Naldrett, 1981a): South Range deposits, North Range deposits, and Offset deposits. The South Range deposits are generally zoned from massive ore at the footwall to disseminated sulfide ore toward the hanging wall. The North Range deposits occur not only within sublayer norite, but also within brecciated country rocks and in fractures in the country rock underlying the breccias. The Offset deposits occur in dyke-like offsets of quartz diorite and gabbros, in which the sulfides form lens-like pods of massive and interstitial disseminated ore. At the Frood deposit, a siliceous mineralized zone which is anomalously rich in PGE occurs at the bottom of the orebody. This zone probably represents a hydrothermal aspect of the mineralization (Naldrett, 1981a).

The PGMs found in the Sudbury deposits are dominated by Pd and Pt phases (Table 2.4). According to Cabri and Laflamme (1976), the South Range and Offset deposits are characterized by the presence of arsenides and antimonides and the scarcity of Sn-bearing PGMs. In the North Range deposits, arsenides and antimonides are sparse and Sn is present in the PGMs. Sperrylite is the principal Pt mineral in the South Range deposits, whereas moncheite ($PtTe_2$), insizwaite ($PtBi_2$), and niggliite (PtSn) are the principal Pt minerals in the North Range deposits.

The principal sulfides are pyrrhotite, chalcopyrite and pentlandite. Michenerite (PdBiTe) is the principal Pd mineral and sperrylite ($PtAs_2$) is the

most common Pt mineral for many deposits in the Sudbury area. Sperrylite characteristically occurs as monocrystalline inclusions and the other PGMs are present more frequently as complex multimineralic intergrowths, often with Bi and Ag tellurides within other minerals, especially sulfides (mainly chalcopyrite and pyrrhotite), arsenides and sulfarsenides (Cabri and Laflamme, 1976).

Farrow and Watkinson (1992) investigated the hydrothermal alterations and role of fluids in Ni, Cu and PGE deposition at Onaping-Levack area of the North Range of the Sudbury Structure. Two significant alteration assemblages were recognized: (1) amphibole (actinolite) + epidote + chlorite + quartz ± albite ± K-feldspar ± calcite adjacent to Cu-rich veins in the Deep Copper Zone of Strathcona mine, and (2) amphibole (actinolite to ferro-actinolite) + epidote + titanite + pentlandite + pyrite ± quartz ± magnetite in the Fraser mine Epidote Zone. Investigation of fluid inclusions showed that salinities are high, between 20.8 to 34.4 NaCl wt% equivalent. The high salinity fluid inclusions suggests that they were the result of late-stage hydrothermal activity within contact units of the Sudbury Igneous complex. They suggested that the Cl-rich fluids deposited Cu and PGE in the Deep Copper Zone. They also found that alteration temperatures decreases from the Epidote Zone (230-340°C) to the most distal Deep Copper Zone (175-280°C).

2.5.2 Noril'sk Cu-Ni sulfide deposits

The Noril'sk Cu-Ni sulfide deposits in Siberia (Genkin and Evstigneeva,

1986) are associated with continental rifting. Basaltic magma derived from the underlying mantle has ascended along fractures to form flood basalt. The Cu-Ni sulfide deposits are closely associated with the intrusive feeders to the flood basalt. The PGMs are characterized by Pd and Pt minerals associated with sulfides occurring in both disseminated ore and massive ores (Table 2.4). In disseminated sulfide ores, the main PGMs are represented by isoferroplatinum (Pt_3Fe) and cooperite (PtS) whereas in massive ores a great diversity of Pd intermetallic compounds and tetraferroplatinum (PtFe) commonly occur. Pd and Pt sulfides, tellurides, and bismuthotellurides are characteristic of veinlet-disseminated and breccia ores. The textural features in the massive ores indicate that the PGMs formed at a late stage in the crystallization history of the ores. These textural features include metacrystals and veinlets of PGMs in the main ore-forming sulfides (pyrrhotite, chalcopyrite and pentlandite), and the close association of PGMs with galena, sphalerite, and Cl-bearing djerfisherite. According to Genkin and Evstigneeva (1986), cooperite and isoferroplatinum in disseminated ores were crystallized directly from a sulfide melt whereas the PGMs of various intermetallic compounds of Pd in massive ores composed of chalcopyrite-group minerals were formed from the residual liquid enriched in Pt, Pd, Sn, Pb, As, Sb, Bi, Cu, Ag, Au, and volatile components.

2.5.3 Komatiitic Ni-Cu sulfide deposits

Kambalda Ni-Cu sulfide deposits of Western Australia (Hudson, 1986)

are the best example of sulfide deposits associated with komatiitic rocks in Precambrian greenstone belts. The deposits at Kambalda are comprised of a number of elongate, high-grade sulfide orebodies that occur at or near the base of a thick sequence of metamorphosed, highly magnesian ultramafic flows (komatiites) of Archean age. Ore zones at Kambalda include both massive and matrix ores, with massive sulfides generally underlying the more continous matrix (disseminated) ores. The massive ores consist predominantly of banded pyrrhotite-pentlandite ore with irregular bands and lenses of pyrite. Chalcopyrite occurs dispersed throughout the massive ore but also occurs in zones of local enrichment, particularly associated with pyrite, as cross-cutting veins and as a major component of sulfide stringers that occur within the footwall mafic flow rocks at the base of the massive sulfide ore.

Studies of PGE concentrations in samples from Kambalda ore shoots (Cowden et al., 1986) suggest the following values (expressed as ppb in 100% sulfides): Pt, 1,650; Pd 2,050; Os, 480; Ir, 230; Rh, 320; Ru, 980. The major Pt minerals are sperrylite and moncheite, and the major Pd minerals are sudburyite (PdSb), merenskyite ($PdTe_2$), stibiopalladinite, palladoarsenide (Pd_2As), michenerite (PdBiTe), and testibiopalladite (PdSbTe); Pd also occurs in solid solution in Pd-melonite (Table 2.4). Irarsite is the only Ir mineral recognized. Sperrylite is the most abundant PGM and occurs within massive sulfide ores. It is particularly abundant in chalcopyrite-rich massive ores. Sudburyite, moncheite, merenskyite, michenerite, testibiopalladite, and

Pd-melonite occur predominantly within crosscutting sulfide veins in the massive and matrix ores, within stringers of sulfide in the footwall rocks, or in association with postore hydrothermal veins and porphyries.

According to Hudson (1986), the occurrence within the ore zones of Pt as sperrylite and Pd dispersed in pentlandite is believed to reflect a primary magmatic distribution. The presence of sudburyite, moncheite, merenskyite, michenerite, testibiopalladite, and Pd-melonite in stringers and reaction zones indicates that their formation may be related to postmagmatic processes, in particular metamorphic segregation of sulfides and the interaction of Pd-bearing ore sulfides (pentlandite) with younger hydrothermal veins.

Other examples of komatiitic Ni-Cu sulfide deposits include the O'Toole Ni-Cu-Co deposits, Brazil; the Pipe Mine, Thompson, Manitoba, etc. are summarized in Table 2.4

2.5.4 Other Cu-Ni sulfide deposits

The Ivrea-Verbano occurrences in the western Italian Alps, have been considered as belonging to the Sudbury-type paragenesis (Garuti and Rinaldi, 1986). Melonite, merenskyite, and moncheite occur as minute grains dispersed within the main sulfide minerals (pyrrhotite, pentlandite and chlcopyrite) in sulfide concentrations of the basic complex. Garuti et al. (1986) suggest that these sulfides may be regarded as either primary or remobilized, based on their textures. Primary sulfides occur as low- to high-grade disseminations interstitial

to the mafic silicates in the cyclic units, and also intergrown with the hydrous silicates in the main gabbro and with cross-cutting pipes. The mobilized sulfides are represented by high-grade to fairly massive ore redistributed during late- to postmagmatic stages, mainly in reponse to deformation. They may occur either as sulfide cementing silicate breccias redeposited along shear zones in the cyclic units and the main gabrro, or as sulfide intergrown with secondary silicates (chlorite, tremolite, and serpentine) remobilized and redeposited in veinlike bodies, within the late pipes.

At Waterfall Gorge, Insizwa, Pondoland, Transkei (Tischler et al., 1981), the sulfide mineralization is spatially confined to the lower contact of an intrusive gabbroic sill. The composition of the parental magma is a high-MgO tholeiite. The underlying sediments, which are host to some of the fracture-filled veins of sulfide, are siliceous shales. There are twc principle sulfide ore types. Type 1 consists of disseminations of chalcopyrite, pentlandite, and pyrrhotite, mainly in basal hypersthene gabbro and, to a lesser extent, in proximal chill-zones and picrite dykes. Type 2 is massive ore in sheets and veins, both in the basal hypersthene gabbro and adjacent hornfelsic sedimentary rocks. In this deposit, sperrylite ($PtAs_2$), niggliite (PtSn) and insizwaite ($PtBi_2$) are common PGMs in the massive ore, where they occur as small idiomorphic crystals in contact with pyrrhotite, cubanite, parkerite, and pentlandite. Froodite ($PdBi_2$) is a common PGM in the pyrrhotite-chalcopyrite disseminated sulfide ore. Also sperrylite and irarsite were identified from the disseminated ore.

2.6 Copper (Gold) Deposits

As noted above, PGMs are also associated with hydrothermal Cu-Au deposits. These PGMs are dominated by Pd and Pt tellurides, arsenides, and bismuthotellurides (Table 2.5). Pd-Pt mineralization associated with copper deposits was reported from several localities in South Africa (Mihalik et al., 1974), where the PGMs are closely associated with bornite, chalcocite, digenite, clausthalite, epidote and chlorite, within a propylitized alteration zone. The PGE contents of the sulfide ore are as follows (in ppm): Pd, 116; Pt, 24; Ir, 2.5; Rh, 1.3; Ru, 0.6. A $(Pd,Pt)_3(Te,Bi)_5$ phase was identified.

The Geordie Lake Intrusion of the Coldwell alkaline complex in northen Ontario hosts a variety of PGMs (Mulja and Mitchell, 1990). The intrusion consists of alternating zones of unlayered troctolite and ophitic olivine gabbro. The PGMs are dominated by palladium minerals, including kotulskite (PdTe), Bi-rich kotulskite, merenskyite, michenerite, sopcheite ($Pd_3Ag_4Te_4$), paolovite (Pd_2Sn), guanglinite, Pd bismuthotelluride, arsenides and antimonides, and unnamed $Pd_{1.6}NiAs_{1.5}$. Sperrylite is the only platinum mineral present, and Ir-, Os-, and Rh-based PGMs were not observed. Most PGMs are contained within disseminated chalcopyrite grains, although some occur in bornite, silicate minerals, massive chalcopyrite and magnetite. The abundance of the disseminated chalcopyrite is positively correlated with the proportion of hydrous silicates (actinolite, amphibole, and biotite).

The best example within this category of PGE association is the New

Rambler Pt-Cu-Au deposit, Wyoming (McCallum et al., 1976). This deposit formed as a result of the leaching of PGE from the mafic wallrocks by hydrothermal fluids, and deposition of PGMs and associated sulfides within shear zones cutting the mafic to ultramafic rocks. The deposit is characterized by higher concentrations of soluble (Pd and Pt) relative to less soluble (Ru, Rh, Os, and Ir) PGEs. The PGMs in the New Rambler deposit include sperrylite ($PtAs_2$), merenskyite ($PdTe_2$), kotulskite (PdTe), michenerite (PdBiTe), moncheite ($PtTe_2$), $Pd_5(Te,Bi,Sb)_2$, and $Pd_5(BiSb)_2Te_4$. They occur as anhedral grains enclosed within chalcopyrite and pyrrhotite. Fluid inclusions in quartz segregations, associated with propylitic (chlorite + epidote + clinozoisite + albite + magnetite ± pyrite) and phyllic (quartz + sericite + pyrite) alteration assemblages record a minimum formation temperature of 335°C for the associated PGM mineralization (Nyman et al., 1990). Nyman et al. also investigated the composition of the fluid inclusions and noted that the close temporal and spatial association of high-salinity H_2O-NaCl-$CaCl_2$ fluid inclusions with propylitic and phyllic alteration assemblages supports the transport of PGEs as chloride complexes.

2.7 Relationships between PGMs and Chromite

PGMs are found associated with chromitites in the layered mafic-ultramafic complexes, ophiolites and Alaskan-type complexes. Laurite is the dominant PGM inclusion in chromites; Pt-, Pd-, and Rh-bearing minerals

occur, in general, as interstitial phases.

According to Naldrett and von Gruenewaldt (1989), ophiolitic chromitites are characterized by Os, Ir and Ru abundances in the range of 0.1 to 1.0 times chondritic values and Pt and Pd abundances about 0.01 times chondritic values. The Middle and Upper Group chromitites of the Bushveld Complex are very different, with Ir and Ru 0.5 to 1.0 times and Pt and Pd 0.5 to 4 times chondritic values. The Stillwater chromitites are intermediate between those from ophiolites and those of the Bushveld Middle and Upper Group. In general, chromitites from the layered complexes contain much higher proportions of Pt and Pd relative to Ru, Ir and Os than do those from ophiolite complexes.

The mechanism by which chromite concentrates PGE has been debated in the literature. Naldrett and Cabri (1976) proposed that these elements substitute in the crystal structure of chromite, but microscopic studies tend to support the view that chromite nucleates around small particles of laurite or metallic alloy (Stockman and Hlava, 1984). Naldrett and van Gruenewaldt (1989) proposed that the original process of PGE concentration was that of collection of a base metal sulfide liquid, with subsequent crystallization of the PGMs which may be present as nonsulfide minerals. Small amounts of sulfides that are trapped within chromitite at high temperature may suffer appreciable modification during cooling. Naldrett and Lehmann (1988) investigated the nonstoichiometry in chromite thermodynamically; they concluded that the data

are consistent with the model that, as chromite cools, vacancies within its structure take up Fe from any associated base metal sulfide, causing a loss of sulfur to surrounding rocks, and a resultant increase in the Cu, Ni, and PGE contents of the remaining base-metal sulfide.

Many investigations (e.g., Talkington et al., 1983; Stockman and Hlava, 1984) agree that laurite inclusions in unfractured chromites are magmatic in origin as opposed to an earlier view (e.g., Gijbels et al., 1974) that ascribed the formation of laurite to exsolution of PGE from the host chromite during cooling. The latter hypothesis has largely been refuted by textural and detailed petrographic evidence and mineral and whole-rock geochemistry.

However, experimental data are still needed to explain the ubiquitous association of Ru sulfide as inclusions in chromites, and Pt-, Pd-, and Rh-bearing minerals as interstitial phases.

2.8 PGE Contents in Different Classes of Deposits

As discussed before, the PGM species vary from one class of deposits to another. In the mafic-ultramafic layered complexes, PGMs are dominated by Pt-, Pd-bearing minerals, and Ru sulfide occurs as inclusions in chromite within the chromitite layers. In ophiolite complexes, PGMs are dominated by Ru-, Ir-, and Os-bearing minerals. In Alaskan-type complexes, PGMs are dominated by Pt-bearing minerals with some Os-, Ir-, Rh-sulfides occurring in chromite. In both Cu-Ni sulfide deposits and Cu sulfide deposits, PGMs are dominated by

Pd-, Pt-bearing minerals.

Chondrite-normalized PGE data from different classes of deposits, conventionally plotted in left-to-right sequence (Os, Ir, Ru, Rh, Pt, Pd) of decreasing melting point (Fig. 2.1), reflect the principal features of the PGM distributions. The chondrite-normalized PGE patterns from different lithologies vary from strongly negative for chromitites from ophiolitic complexes, to flat for mantle material, to weakly positive for komatiites, to strongly positive for various tholeiites and mineralized layers in layered intrusions (Page and Talkington, 1984; Barnes et al., 1985; von Gruenewaldt et al., 1989).

It is suggested that such fractionation of PGEs (whether by fractional crystallization or partial melting) results from partitioning between alloy and liquid-sulfide phases. Thus, Os, Ir, and Ru are concentrated in refractory alloy particles entrapped in chromite and olivine, and Pt and Pd are partitioned strongly into an immiscible sulfide liquid dispersed within the partial melt. However, recent estimates of partition coefficients for PGEs make this and similar hypothesis less plausible. Sulfide-liquid/silicate melt partition coefficients derived from MORB (Peach et al., 1989) and obtained from experimentation (Stone et al., 1990) indicate strong but approximately equal partitioning for both Pd and Ir, in the absence of coexisting alloy phases. Further experimental investigations (Fleet and Stone, 1991) indicate that Pt would partition strongly into the alloy phases. The experimental results suggest that partitioning of PGEs between refractory alloys and an immiscible sulfide

Fig. 2.1 Chondrite-normalized PGE distribution pattern

(M.E. Fleet, pers. comm.)

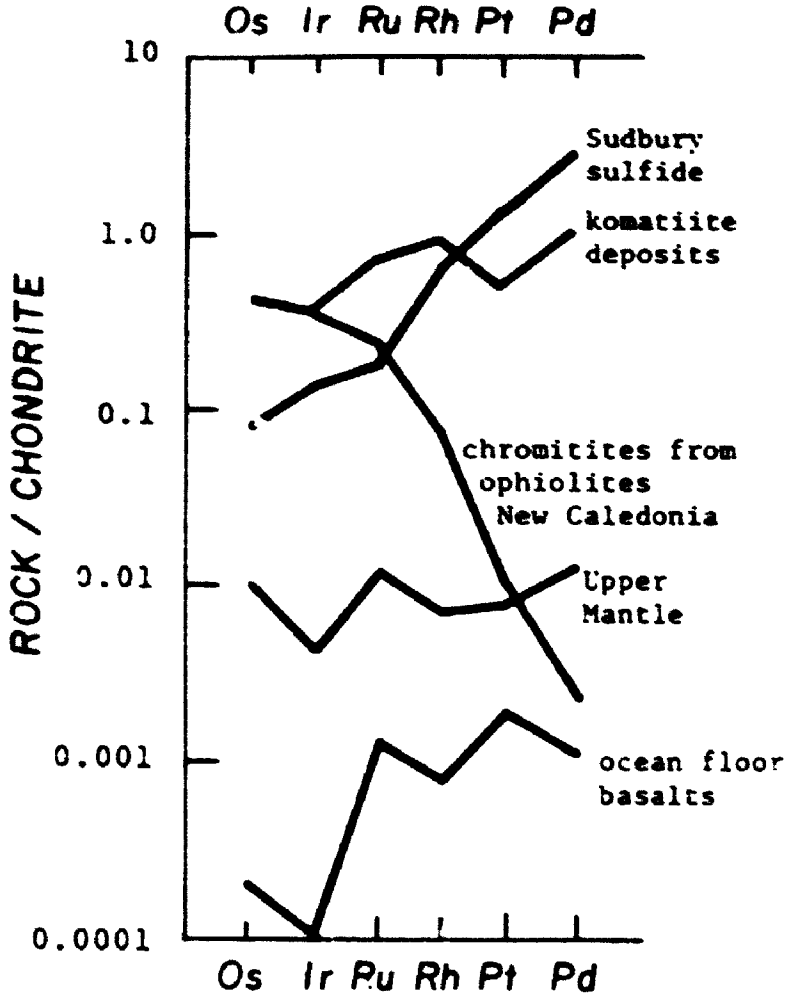
Os Ir Ru Rh Pt Pd
10
1.0
0.1
0.01
0.001
0.0001
ROCK / CHONDRITE
Sudbury sulfide
komatiite deposits
chromitites from ophiolites New Caledonia
Upper Mantle
ocean floor basalts
Os Ir Ru Rh Pt Pd

liquid would result in fractionation of light from heavy platinoids, which is quite different from that observed in nature.

Table 2.1 PGMs in Mafic-Ultramafic Layered Complexes

location (reference)	host rocks gangue minerals	metamorphic grade	PGM assemblage
	1. Bushveld Complex, South Africa		
UG-2 Chromitite layer (Kinloch, 1982; von Gruenewaldt et al., 1990)	chromitite layers Orthopyroxene plagioclase pentlandite bornite millerite galena acanthite chalcocite covellite godlevskite arsenopyrite clausthalite		major: laurite(RuS_2) vysotskite(PdS) cooperite(PtS) braggite((Pt,Pd,Ni)S) Pt-Fe alloy sperrylite($PtAs_2$) minor: Ir-Os, Os-Ir hollingworthite moncheite($PtTe_2$) michenerite(PdBiTe) kotulskite(PdTe) irarsite(IrAsS) stumpflite(PtBiSb) Pt-Cu-Ni-S Pt-Pb-Cu-Ni-S Pt-Ir-Cu-Fe-Ni -Os-Pd-S Pt-Pd-Ir-Pb-Ni-S Ir-Pt-Cu-Ni-Co-S Ir-Os-Rh-Pd-Cu-Fe -Ni-S Pt-Cu-Rh-S, Rh-Ir-S Pd-Cu-S Pt-Cu-Ni-Fe-As-S Pt-Pd-As, Pt-Pd-Fe-As Pd-Pt-As, Ir-As merenskyite($PdTe_2$) (Pt,Ru,Pd)AsS ruarsite(RuAsS) paolovite(Pd_2Sn) Pt-Sn-Pd-S, Pd-Bi-Sn Pt-Rh-Co-S Pt-Rh-Cu-Co-S Pt-Co-Cu-S, electrum
Merensky Reef (Kinloch, 1982	pegmatoidal feldspathic pyroxenite chromitite -layers pyrrhotite pentlandite chalcopyrite pyrite voilarite		major: braggite(Pt,Pd)S cooperite(PtS) laurite(RuS_2) Pt-Fe alloys sperrylite($PtAs_2$) moncheite($PtTe_2$) kotulskite(PdTe) michenerite(PdBiTe) merenskyite($PdTe_2$) minor: potarite(PdHg) froodite($PdBi_2$) Pt-Cu-Ir-Rh-S. Pd-Pb Pd-Sn, Pt-Sn, Au-Te Pt-Cu-Fe, Pd-Hg-Te AuAg

Table 2.1 Continued.

location (reference)	host rocks gangue minerals	metamorphic grade	PGM assemblage
Platreef (KinLoch, 1982)	pyroxenite & harzburgite with dolomite & ironstone as country rock sulfides		major: Pt-Fe alloys sperrylite($PtAs_2$) cooperite(Pt(Pd,Ni)S) insizwaite($PtBi_2$) moncheite($PtTe_2$) michenerite(PdBiTe) merenskyite($PdTe_2$) braggite(PtPdNiS) Pd-Sb-As laurite(RuS_2) minor: Pt-Au, Pt-Pd-Sn Pd-Pb Pd-Hg, Pd-Sn, Pd-Sb Pd-Tl, AuAg vysotskite(Pd(Pt,Ni)S PtPdAsS RhAsS(Pt,Pd,Co) Pd-Ni-As, Pd-As Ru-Os-As, Au-Te Pd-Te-Sn-Fe-Sb-Pt Pt-Pd-Sn-Te, Pd-Pt-Hg kotulskite(PdTe)
Eastern Bushveld (Harney and Merkle, 1990)	anorthosite with minor Ti-magnetite clinopyroxene pyrrhotite chalcopyrite pentlandite pyrite, galena sphalerite Ag-pentlandite cobaltite mackinawite marcasite covellite	greenschist facies (chlorite, sericite, quartz, calcite, hornblende)	michenerite(PdBiSb) moncheite($PtTe_2$) merenskyite($PdTe_2$) froodite($PdBi_2$) sperrylite($PtAs_2$)
2. Stillwater Complex, Montana, USA			
J-M Reef (Cabri, 1981; Volborth, et al., 1986)	anorthosite -troctolite -peridotite pyrrhotite chalcopyrite pentlandite pyrite millerite cubanite	greenschist facies (localized)	major: braggite((Pt,Pd)S) vysotskite(PdS) moncheite($PtTe_2$) Pt-Fe alloys minor: cooperite(PtS) kotulskite(PdTe) rare: telluropalladinite (Pd_9Te_4) keithconnite($Pd_{3-x}Te$) zvyagintsevite(Pd_3Pb)

Table 2.1 Continued.

location (reference)	host rocks gangue minerals	metamorphic grade	PGM assemblage
	violarite graphite chlorapatite calcite quartz Cl-Cr-phlogopite		merenskyite($PdTe_2$) sperrylite($PtAs_2$) temagamite(Pd_3HgTe_3) rustenburgite(Pt_3Sn) laurite(RuS_2) hollingworthite(RhAsS) stillwaterite(Pd_8As_3) arsenopalladinite ($Pd_8(As,Sb)_3$ palladobismutharsenide ($Pd_2As_{0.8}Bi_{0.2}$) mertieite ($Pd_8(Sb,As)_3$) palladoarsenide(Pd_2As) plumbopalladinite (Pd_3Pb_2) michenerite(PdBiTe) (Pt,Rh), (Rh,Pt) (Au,Pd), (Au,Ag)
The Lower Chromitites (Cabri, 1981; Talkington and Lipin, 1986)	chromite olivine pentlandite pyrrhotite nickeline		Pt-Fe alloy cooperite(PtS) laurite(RuS2) sperrylite($PtAs_2$) Pt-Pd-Ni-As
	3. Penikat Layered Intrution, Northern Finland		
Passivaara PGE Reef (Huhtelin et al., 1990)	anorthosite chalcopyrite pyrrhotite pentlandite	lower amphibolite facies (uralite, talc, sericite, rutile chlorite epidote serpentine	sperrylite(PtAs2) kotulskite(PdTe) merenskyite($PdTe_2$) isomertieite($Pd_{11}Sb_2As_2$) stibiopalladinite (Pd_3Sb_2) cooperite(PtS) braggite(Pt,Pd)S AuAg, native gold
Ala-Penikka PGE Reef (Halkoaho et al., 1990b)	plagioclase -augite -bronzite, plagioclase cumulates pyrrhotite chalcopyrite pentlandite pyrite galena	greenschist facies	kotulskite(PdTe) merenskyite($PdTe_2$) sperrylite($PtAs_2$) palladoarsenide ($Pd_2(AsSb)$) braggite(Pd,Pt,Ni)S cooperite(PtS) vysotskite(PdS) hollingworthite(RhAsS) moncheite($PtTe_2$)

Table 2.1 Continued.

location (reference)	host rocks gangue minerals	metamorphic grade	PGM assemblage
	sphalerite cobaltite gersdorfite Ag-pentlandite		$Pd_{1.68}As$ AuAg
Sompujaevi PGE Reef (Halkoaho et al., 1990a)	bronzitite peridotite pyrite chalcopyrite pentlandite chromite uralite apatite phlogopite	greenschist facies	(1) PGMs with sulfides: major: laurite(RuS_2) kotulskite(PdTe) sperrylite($PtAs_2$) hollingworthite(RhAsS) isomertietie($Pd_{11}Sb_2As_2$) minor: irarsite(IrAsS), AuAg stibiopalladinite ($Pd_3Sb_{1.5}As_{0.5}$) isoferroplatinum(Pt_3Fe) rare: merenskyite($PdTe_2$) (2) PGMs with chromite: major: sperrylite($PtAs_2$) isomertietie($Pd_{11}As_2Sb_2$) (Pt,Pd,Cu,Rh,Au,Fe,Cr, Mn,Pb)-hydroxides minor: $(Pt_3CuPd)_3S_3$ hollingworthite(RhAsS) stibiopalladinite ($Pd_3Sb_{1.6}As_{0.4}$) rare: laurite(RuS_2) braggite(PdS) $(Pt_{0.3}Cu_{0.2}Pb_{0.2}Fe_{0.2}Ni_{0.1})S$ cuprorhodsite $(Cu_{0.9}Rh_{0.9}Pt_{0.9}Ir_{0.3})_3S_4$ keithconnite $(Pd_3(Te_{0.7}Bi_{0.3}))$ guanglinite(Pd_3As) Pd3($As_{0.8}Sn_{0.2}$) $Pd_3Sb_{1.3}As_{0.7}$ palarstanide ($Pd_8(Sn,As,Te)_3$) zvyagintsevite(Pd_3Sb) Pd_8Pb_2 hongshiite(PtCu) isoferroplatinum(Pt_3Fe)
	4. Complexes in Canada		
Lac Des Iles Complex, Ontario (Cabri, 1981)	gabbro pentlandite pyrrhotite chalcopyrite pyrite galena		major: braggite(Pt,Pd)S vysotskite(PdS) kotulskite(PdTe) isomertieite ($Pd_{11}(As,Sb)_4$) merenskyite($PdTe_2$)

Table 2.1 Continued.

location (reference)	host rocks gangue minerals	metamorphic grade	PGM assemblage
	magnetite		sperrylite($PtAs_2$)
	sphalerite		moncheite($PtTe_2$)
	minor: millerite		minor: stillwaterite(Pd_8As_3)
	siegenite		palladoarsenide(Pd_2As)
	arsenopyrite		$Ag_4Pd_3Te_4$
	cobaltite		
	gersdorffite		
	loellingite		
	skutterudite		
	nickeline		
	cubanite		
	bornite		
	covelline		
	molybdenite		
	marcasite		
	ilmenite		
	cassiterite		
Bird River Sill, Manitoba (Talkington et al, 1983)	chromite in peridotite		laurite(RuS_2) Os-Ir-Ru alloy

Table 2.2 PGMs from Ophiolite Complexes

location (reference)	host rocks, gangue minerals	metamorphic grade	PGM assemblage
Cliff, Shetland, Scotland (Prichard and Tarkian, 1988)	dunite within harzburgite chrome spinel(50-90%) serpentine chlorite magnetite Ni-carbonate Ru-pentlandite	greenschist facies	sperrylite($PtAs_2$) stibiopalladite hollingworthite(RhAsS) minor: Pt-Pd-Au-Cu, Au-Pd potarite(PdHg) laurite(RuS_2) native Os
Harold's Shetland, Scotland (Prichard and Tarkian, 1988)	dunite within harzburgite chrome spinel(50-90%) serpentine chlorite magnetite Ni-carbonate Ru-pentlandite	greenschist facies	native Os, laurite(RuS_2) irarsite(IrAsS) hollingworthite(RuAsS) minor: genkinite$(Pt,Pd)_4Sb_3$ hongshiite(PtCu) Pt-Pd-Cu stibiopalladinite $Pd_{3-x}Sb_{2+x}$
Shetland (Tarkian and Prichard, 1987)	podiform chromite serpentine chlorite Ni-carbonate	greenschist facies	irarsite(Os rich) -hollingworthite Os-Ir-Ru Ir-Sb-S Rh-Sb-S
Troodos, Cyprus (McElduff and Stumpfl, 1990)	chromitites within harzburgite Fe-serpentine calcite Cr-chlorite magnetite pentlandite chalcopyrite awaruite trevoite	greenschist facies	laurite(90%) (RuS_2) cooperite (PtS) Ru-Ir-rich Ni-Fe-Cu-S Pt-Ir-S Pt-Pd-S Os,Ir Ru,Os Ru-Fe Ru-Ir-Fe
Finero Complex, Italy (Ferrario and Garuti, 1990)	Chromitites in phlogopite-rich peridotite Rh-pentlandite Rh-millerite Ir-digenite		laurite(RuS_2) native Ir Ir-Cu-Rh-sulfide Ir-Ni-Fe-Cu sulfide Cu-Rh-Fe, Cu-Pt-Ag Cu-Pb-Rh, Pb-Rh

Table 2.2 Continued

location (reference)	host rocks, gangue minerals	metamorphic grade	PGM assemblage
Hochgrossen and Kraubath, Austria (Thalhammer et al., 1990)	ultramafic chrome spinel olivine,opx amphibole pentlandite chalcopyrite heazlewoodite pyrite,galena arsenopyrite chlorite serpentine	greenschist to amphibolite facies	laurite(RuS_2) irarsite(IrAsS) sperryite($PtAs_2$) laurite(RuS_2) minor:hollingworthite(RhAsS) platarsite(PtAsS) cooperite(PtS) Pd-Pt-Sb, Pt-alloy
Tiebaghi New Caledonite (Auge, 1988)	chromitite dunite		laurite(RuS_2)(50-77%) erlichmanite(OsS_2)(13%) $(Ir,Cu)_2S_3$, Ir-Os Ir-Os-Ru xingzhongite(Ir,Cu)S prassoite($Rh_{17}S_{15}$) $(Ir,Cu)_2S_3$ Pt-Pd-Fe
Josephine, Onion Mt. Oregon (Stockman and Hlava, 1984)	podiform chromitite in dunite millerite Ni-Fe alloy Cr-chlorite	greenschist facies	laurite[$(Ru,Os,Ir)S_2$] Ru-rich alloy Pt-rich alloy Os-Ir-rich alloy Ir-rich sulfide Pt-arsenide
Osthammaren Ultramafic Tectonic Body, South Central Norway (Nilsson, 1990)	chromitite in serpentinite Na-hornblende phlogopite pentlandite niccolite heazlewoodite		primary:laurite, Os-laurite Ir, Os, $Pt_2(Ir,Os)Fe_{0.6}$ secondary:laurite, Os-laurite erlichmanite$(Os,Ir)S_2$ irarsite(IrAsS) hollingworthite(RhAsS) platarsite(PtAsS) sperrylite($PtAs_2$) (Os,Ir), native Os IrSbS, (Ir,Rh)SbS $(Ir,Pt,Pb)S_2$ osarsite(OsAsS)? stibiopalladinite (Pd,Sb)?
Vourinos Greece (Auge, 1985; 1988)	chromitite olivine Opx,Cpx	greenschist facies	Os-laurite(50%) osarsite(OsAsS) irarsite(IrAsS) Ru-Ir-Os, Os-Ir, Ir-Os Ir, Os-Ir, Os-Ir-Ru hollingworthite(RhAsS)

Table 2.3 PGMs in Alaskan-type complexes

location (reference)	host rocks gangue minerals	metamorphic grade	PGM assemblage
Tulameen, British Columbia (St. Louis et al., 1986; Nixon et al., 1990)	chromitite in dunite, serpentine carbonate pentlandite violarite bravoite	greenschist facies	Pt(Fe,Ni,Cu) $Pt_{2-3}(Fe,Ni,Cu)_{1-3}$ $Pt_2(Fe,Cu,Ni,Sb)_2$ tulameenite(Pt_2FeCu) geversite($PtSb_2$) hollingworthite -irarsite(Rh-Ir(AsS)) sperrylite($PtAs_2$) tulameenite(Pt_2FeCu) minor: erlichmanite(OsS_2) genkinite$(Pt,Pd)_4Sb_3$ laurite(RuS_2) Pt-Fe, Pt-O stumpflite(PtSb)
Finfield, New South, Wales, Australia (Johan et al., 1989)	pegmatoidal clinopyroxenite		erlichmanite$(Os,Ir,Rh)S_2$ Pt-Fe cooperite(PtS) cuprorhodsite malanite$(Pt,Ir)_2CuS_4$? geversite($PtSb_2$) sperrylite($PtAs_2$) stumpflite(PtSb) Pd_2Sb, Pd_4Sb
Nizhnii Tagil, Ural (Razin, 1976)	apodunitic clinopyroxene & forsterite dunite		Pt-Fe(mainly Pt_3Fe) Ir-Pt Ir-Os Os-Ir cooperite(PtS) tulameenite(Pt_2FeCu)
Inagli Aldan shield (Razin, 1976)	forsterite dunite		laurite(RuS_2) PtFe irarsite(IrAsS)

Table 2.4 PGMs in Cu-Ni sulfide deposits

location (reference)	host rocks gangue minerals	metamorphic grade	PGM assemblage
Sudbury, Ontario (Cabri, 1981)	mafic norite & footwall rocks pyrrhotite chalcopyrite pentlandite minor: cobaltite gersdorffite pyrite, galena marcasite millerite, cubanite violarite, sphalerite magnetite, ilmenite mackinawite argentopentlandite rare: hessite, altaite arsenopyrite maucherite, nickeline molybdenite, parkerite Bi-tellurite		major: michenerite(PdBiTe) sperrylite($PtAs_2$) moncheite($PtTe_2$) minor: froodite($PdBi_2$) insizwaite($PtBi_2$) sudburyite(PdS) rare: hollingworthite(RhAsS) irarsite(IrAsS) kotulskite(PdTe) merenskyite($PdTe_2$) niggliite(PtSn) mertieiteII(Pd_8Sb_3) electrum
Noril'sk Siberia (Genkin and Evstigneeva, 1986)	gabbrodolerites galena sphalerite djerfisherite shadlunite talnakhite cubanite mooihoekite putoranite chalcopyrite pyrrhotite Cu-pentlandite(7.5%Cu) millerite		atokite(Pd_3Sn) braggite[Pd,Pt,Ni)S] cabriite(Pd_2SnCu) cooperite(PtS) froodite($PdBi_2$) geversite(PtSb2) hollingworthite(RhAsS) insizwaite($PtBi_2$) isoferroplatinum(Pt_3Fe) isomertieite($Pd_{11}Sb_2As_2$) kharaelakhite [$(Cu,Pt,Pb,Fe,Ni)_9S_8$] kotulskite(PdTe) majakite(PdNiAs) maslovite(PtBiTe) merenskyite[(Pd(TeBi)$_2$)] mertieite [$(Pd,Pt)_8(Sb,As)_3$] michenerite(PdBiTe) niggliite(PtSn) palarstanide [$(Pd_5(As,Sn)_2)$] palladoarsenide(Pd_2As) paolovite[(Pd_2Sn)] plumbopalladinite(Pd_3Pb_2) polarite[Pd(Bi,Pb)] rustenburgite(Pt_3Sn)

Table 2.4 Continued.

location (reference)	host rocks gangue minerals	metamorphic grade	PGM assemblage
			sobolevskite(PdBi) sperrylite($PtAs_2$) stannopalladinite [$(Pd,Pt)_3Sn_2Cu$] stibiopalladinite taimyrite[$(Pd,Pt)_3Sn_2Cu_3$] telargpalite[$(Pd,Ag)_{4-x}Te$] tetraferroplatinum(PtFe) urvantsevite[$Pd(Bi,Pb)_2$] vysotskite(Pd,Ni)S zvyagintsevite(Pd_3Pb) $Pd_3(As_{0.6}Te_{0.4})$, Pd_2As_2 $(Pd,Ni)_3As_2$, $Pd_2Ni_6As_4$ $Pd_5(Sb,As)_2$, $Pd_2(Sn,Sb)$ Pd_8Sn_2As, $Pd_4Bi_3Cl_3$, AuAg
Kambalda, Australia (Hudson, 1986)	komatiite (1) within chalco-pyrite rich ore (2) in chalcopyrite-rich stringers (3)within nickeline in quartz-carbonate vein (4) in nickeline (5) with tellurrides in quartz-carbonate-andradite vein (6) in gersdorffite, pyrite-chalcopyrite-pyrrhotite-pentlandite massive ore	low amphibolite facies	sperrylite($PtAs_2$)(1) moncheite($PtTe_2$)(2) sudburyite(PdSb)(3)(4) merenskyite($PdTe_2$)(1)(2) stibiopalladinite(4) palladoarsenide(Pd_2As) michenerite(5)(1)(2) testibiopalladite(5)(1) Pd-melonite Irarsite(IrAsS)(6) calverite($AuTe_2$) native Au
C'Toole Brazil (Marchetto, 1990)	serpentinite talc schist metachert pyrrhotite pentlandite chalcopyrite sphalerite cobaltite gersdorffite pyrite, marcasite violarite, bravoite native Bi, cobaltite-gersdorffite, ReS_2	upper greenschist-lower amphibolite facies	kotulskite(PdTe) irarsite(IrAsS) sperrylite($PtAs_2$) omeiite($OsAs_2$) osarsite(OsAsS) $OsAs_3$ OsRhAsS RuTeAs OsRuAs Os-Re-As-Te-Fe-Y-Rh native Au native Ag

Table 2.4 Continued.

location (reference)	host rocks gangue minerals	metamorphic grade	PGM assemblage
Pipe Mine, Thompson, Manitoba (Cabri, 1981)	sulfide veins in serpentinite maucherite cubanite, galena Bi-telluride marcasite arsenopyrite mellonite, nickeline hessite, cobaltite		sperrylite($PtAs_2$) michenerite(PdBiTe) froodite($PdBi_2$) irarsite(IrAsS)
Ivrea-Verbano Basic Complex, Western Italian Alps (Garuti and Rinaldi, 1986)	gabbro: chalcopyrite pentlandite pyrrhotite molybdenite crosscuting pipe: melonite altaite hessite wehrlite	greenschist facies	merenskyite($PdTe_2$) moncheite($PtTe_2$) AuAg
Waterfall Gorge, Insizwa, Pondoland, Transkei. (Tischler et al., 1981)	gabbroic sill & siliceous shales pentlandite chalcopyrite pyrrhotite cubanite parkerite bismuthinite native Bi		sperrylite($PtAs_2$) froodite($PdBi_2$) irarsite(IrAsS) niggliite(PtSn) insizwaite($PtBi_2$) Au-Ag-Cu alloy

Table 2.5 PGMs associated with Cu sulfide mineralization

location (reference)	host rocks gangue minerals	metamorphic grade	PGM assemblage
Geordie Lake Intrusion, Coldwell complex, Ontario (Mulja and Mitchell, 1990)	troctolite olivine gabbro chalcopyrite hessite melonite altaite bornite magnetite	greenschist facies	kotulskite(PdTe) merenskyite($PdTe_2$) michenerite(PdBiTe) sopcheite($Pd_3Ag_4Te_4$) paolovite(Pd_2Sn) guanglinite(Pd_3As) sperrylite($PtAs_2$) $Pd_{1.6}NiAs_{1.5}$ Pd-Bismuthotelluride $Pd_8Bi_4Te_3$, Pd-As Pd-Sb, Ag_3Te_2
New Rambler Pt-Cu-Au Deposit Wyoming (McCallum et al., 1976)	amphibolitized metagabbro chalcopyrite pyrrhotite pyrite sphalerite mackinawite thiospinel pentlandite	greenschist facies	Rh-sperrylite($PtAs_2$) merenskyite($PdTe_2$) kotulskite(PdTe) michenerite(PdBiTe) $Pd_3(Te,Bi,Sb)_2$ $Pd_3(Bi,Sb)_2Te_4$ moncheite($PtTe_2$) electrum

PART II: THOMPSON NICKEL BELT, MANITOBA

CHAPTER 3 INTRODUCTION

3.1 General Remarks

The Thompson nickel deposit in the Thompson Nickel Belt, Manitoba, was discovered in 1956, and has been known as a producer of Ni for over 30 years. The Thompson nickel mine is distinct from other PGM-bearing Ni-deposits in that it is hosted by metasedimentary rocks, and the PGMs are proximally related to a pervasive, late hydrothermal alteration associated with remobilisation of rare-earth elements. In this study nine varieties of PGMs have been identified, with paragenesis directly or indirectly related to the metasedimentary rocks. Gold, Ni-telluride and bisimuthtelluride have also been found associated with PGMs. The aims of this investigation were to study the unusual As-rich nickel ore at the Thompson mine and evaluate the nature of the PGM-Au and Ni-sulfide mineralization in the area. Special emphasis is placed on: (1) documentation of PGM-Au compositions, PGM optical properties, mode of occurrence, and mineral association; (2) documentation of mineral chemistry of gangue minerals, such as silicates, carbonates and other related minerals; (3) metamorphic petrology, including early prograde metamorphism and the late hydrothermal alteration spatially associated with the PGE-Au mineralization.

PGMs have been previously reported from only one of the numerous Ni

sulfide deposits of the Thompson Nickel Belt, at the Pipe mine, where an assemblage of sperrylite + michenerite + froodite + irarsite has been documented from a sulfide vein in serpentinite, associated with maucherite, nickeline, Bi-telluride, mellonite, hessite, arsenopyrite-cobaltite, cubanite and galena (Cabri, 1981b). The thesis study area is within the Thompson nickel mine, which is located about 30 km northeast of the Pipe mine.

It was anticipated that this study might contribute to a better understanding of the PGM mineralization in the Thompson Nickel Belt, particularly in respect to the relative roles of hydrothermal and metamorphic processes in either forming or modifying the PGM mineralization.

3.2 Location and Sample Description

The Thompson mine is situated in the Thompson Nickel Belt, which defines the boundary between the Churchill and Superior Provinces in north-central Manitoba, 644 km north of Winnipeg (Fig. 3.1). The Thompson mine is operated by INCO Limited. The property is presently developed as an open pit, the T-1 mine and the T-3 mine. Most of the material studied was collected by INCO personnel. M.L. Thompson provided hand samples and drill core material from the T-1 mine, including four As-rich nickel ore samples (pegmatite and metapelite), three sulfide iron formation (barren massive sulfide) samples from drillhole 74317, 4000 level drilling, and eight Ni-Fe sulfide bearing peridotite samples. She also provided an unlocated drillcore sequence

Fig. 3.1 Geological setting of the Thompson Nickel Belt

(after Cumming et al. 1982, Paktunc 1984)

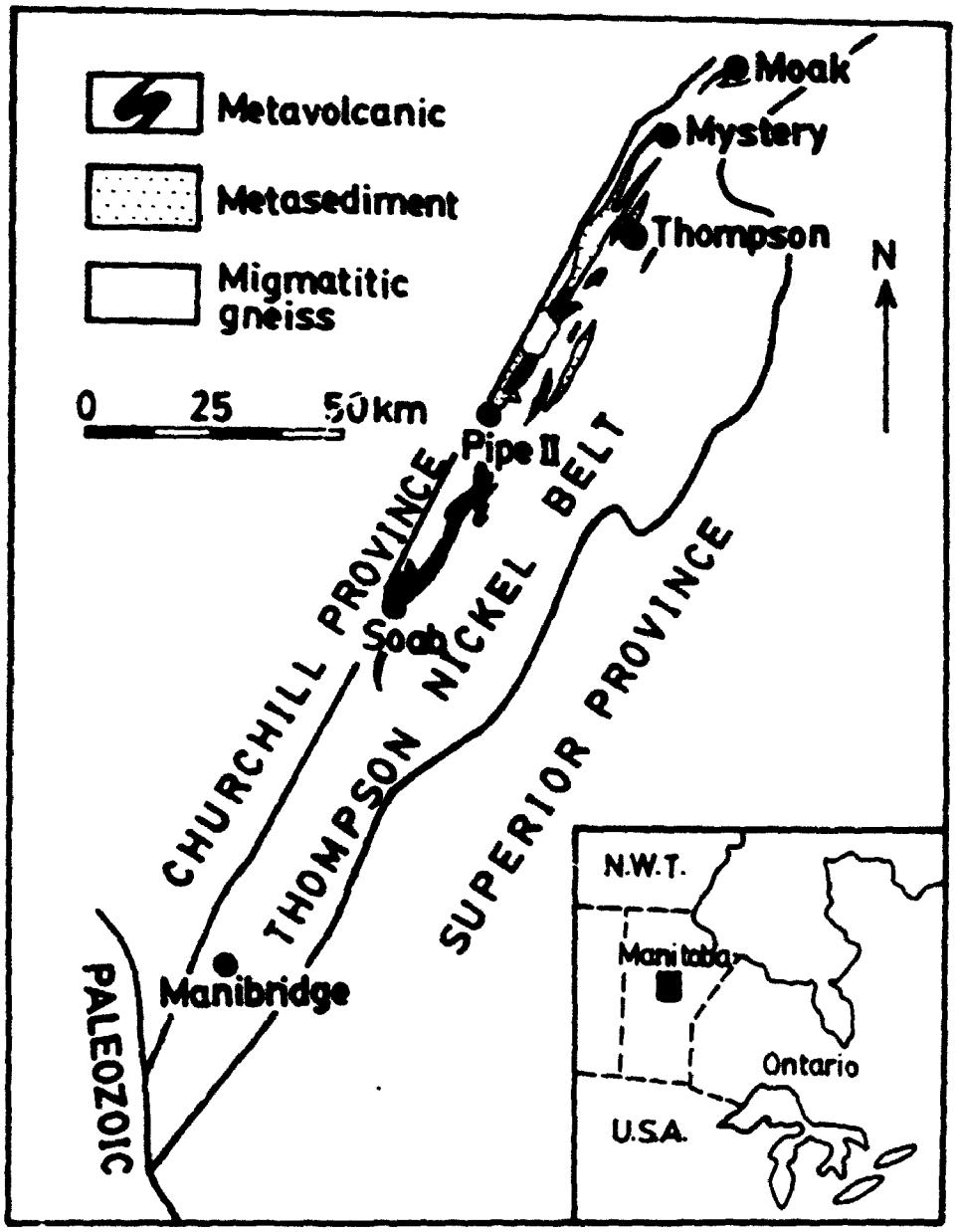
Metavolcanic
Metasediment
Migmatitic gneiss
0 25 50km
Moak
Mystery
Thompson
N
Pipe II
Soab
CHURCHILL PROVINCE
THOMPSON NICKEL BELT
SUPERIOR PROVINCE
PALEOZOIC
Manibridge
N.W.T.
Manitoba
Ontario
U.S.A.

through the ore zone and F. Ruskas provided a slab (15x10x3 cm^3, sample T1FP) of As-rich nickel ore from the 200 level underground in the T-1 mine. Several hand specimens from the open pit (Fig. 4.1), including representative material of the troublesome As-rich Ni ore, were obtained from M.L. Thompson and M. Toderian. Additionally, 48 samples from the Thompson T-3 mine were obtained from the Gordon Suffel Collection in the Department of Geology, University of Western Ontario.

3.3 Previous Study

INCO Limited was attracted to the Thompson Nickel Belt in 1946 because of known nickel occurrences at Lynn Lake, Ospwagan Lake, and elsewhere. By 1948, with the help of an aeromagnetic survey carried out by the Company, the Thompson Belt came into focus. In 1951, the Company carried out its first airborne electromagnetic survey. This added impetus to exploration and culminated in nickel sulfide discoveries in the Nickel Belt.

INCO Limited has two operating mines in the Thompson Nickel Belt, Thompson mine and Pipe 2 mine. Operations at four other INCO mines, Birchtree, Soab North, Soab south and Pipe 1, have been temporarily suspended. Falconbridge's Manibridge Mine, operational since 1971, was closed in April of 1977. In addition to these mines, there are a number of subeconomic sulfide deposits and numerous sulfide occurrences within the belt.

The Thompson mine ore deposit was discovered in 1956. Five years

later, full production, at an annual rate of more than 75,000,000 lbs. of refined nickel, was attained. At the close of 1960, with production about to begin, the ore reserves at the Thompson mine amounted to 25,000,000 tons, containing 2.97 percent nickel-copper. A figure for the total tonnage has not been published but is estimated at 50 to 100 million tons at a similar or slightly higher grade (Bleeker, 1990).

The geology of the Thompson mine has been studied by Zurbrigg (1963), Peredery (1979), Peredery and Geological Staff (1982), and Paktunc (1984). Fueten et al. (1986) and Bleeker (1990) studied the structural features of the mine and proposed different structural models for the Thompson Nickel Belt. Geochronologic study on the Thompson Nickel Belt was carried out by Brooks and Thayer (1981) and Cumming et al. (1982).

3.4 Methodology

Numerous polished thin sections were made from representative samples for this study at the Department of Geology, the University of Western Ontario. Microscopic investigation was carried out on the polished thin sections to identify mineral assemblages and to select minerals for electron microprobe study. In order to identify PGMs, the polished thin sections were scanned by optical microscopy at 100x magnification. Mineral grains of interest were then examined at 500x magnification, both in air and oil. X-ray powder diffraction was used to identify hisingerite.

Chemical compositions of minerals were determined with the JEOL JXA-8600 Superprobe at the Department of Geology, University of Western Ontario. Analyses for platinum group minerals, gold, base-metal sulfides, gersdorffite, and nickeline were performed using an accelerating voltage of 20 kV and cup current of 20 nA. Beam diameter was 2-3 μm and counting time for each element was 20 seconds.

Spinel, garnet, sheet-silicate minerals, amphibole and feldspar were analyzed at 15 kV with a beam current of 10 nA and a beam diameter of 1 to 5 μm. The counting time for each element was 20 seconds except for the Ni in garnet for which counting time was 50 seconds. Olivine was analyzed at 15 kV with a beam current of 50 nA. Allanite grains were analyzed at 25 kV, 20 nA, with a beam diameter 2 to 3 μm.

The following standards were used for PGMs and gold analyses: pure metals of Pt, Pd, Ru, Rh, Os, Ir, Au and Ag; pure Bi, Te and Sb; synthetic FeS and NiS for Fe and Ni; FeS for S, and natural arsenopyrite for As. To avoid fluorescence interference from surrounding minerals, the size of most PGM grains for electron microprobe analysis was larger than 10 μm.

For gersdorffite and nickeline analyses the following standards were used: pure Au, Ag, Co, Pt, Pd, Ru, Rh, Os and Ir; millerite for Ni; arsenopyrite for As and S; and pyrrhotite for Fe.

The standards for analyses of sphalerite were sphalerite (Zn and S), chalcopyrite (Cu), pyrrhotite (Fe), greenockite (Cd), cinnabar (Hg), pure Mn,

synthetic GaAs, and InAs (Ga and In). The standards for analyses of pyrite were pyrite (Fe and S), millerite (Ni), chalcopyrite (Cu), arsenopyrite (As), sphalerite (Zn), and pure Co. The standards for analyses of pyrrhotite were pyrrhotite (Fe and S), millerite (Ni), and pure Co, Pd, and Mn. The standards for analyses of pentlandite were pyrrhotite (Fe and S), millerite (Ni), and pure Co, Pd, Rh, and Ag. The standards for analyses on chalcopyrite were chalcopyrite (Cu and S), pyrrhotite (Fe), millerite (Ni), sphalerite (Zn), and pure Co.

Spinel analysis was made using the following standards: chromite for Al, Cr, and Mg; orthopyroxene for Si; kaersutite for Ti; rhodonite for Mn; magnetite for Fe; pure V for V; sphalerite for Zn; millerite for Ni; and barite for S.

Sheet-silicate minerals and amphiboles were analyzed with the following standards: orthopyroxene for Si, Fe, and Mg; kaersutite for Ti and Al; chromite for Cr; rhodonite for Mn; millerite for Ni; wakefield diopside for Ca; orthoclase for K; albite for Na; barite for Ba; tugtupite for Cl, and synthetic LiF for F.

Albite (An0), anorthite (An90) and orthoclase were used as standards for feldspar analyses.

Almandine, spessartine and grossular were used as standards for (Si, Al, Fe), Mn and Ca in garnet analyses. Other standards for garnet analyses include kaersutite for Ti, chromite for Cr, olivine for Ni, orthopyroxene for Mg,

synthetic LiF for F, and pure V.

A natural olivine with 0.305 wt% NiO was used as standard for olivine analysis. NiO data were obtained with 50 second peak counts. Multiple analyses were made on individual grains and data were averaged on each grain.

Allanite analyses used standards of silicate minerals and synthetic REE-bearing calc-silicate glasses, as in Pan and Fleet (1990).

Whole-rock contents of Pt, Pd and Au were determined by lead fire assay and ICP at ACME Analytical Laboratories Ltd., Vancouver. The detection limits for Pt, Pd and Au are 5, 2, and 1 ppb, respectively.

CHAPTER 4 REGIONAL GEOLOGY AND GEOLOGY OF THE THOMPSON MINE

4.1 Regional Geology

The Thompson Nickel Belt is a highly deformed structural belt, 10-35 km wide and over 200 km long. Zurbrigg (1963) noted that the Thompson Nickel Belt is characterized by rocks having a northeasterly strike, in contrast to the east-west trends of the Superior Province and irregular northeasterly trends of the Churchill Province. It is located at the border between the Proterozoic Hudson Orogeny (1.9-1.7 Ga) and the Pikwitonei Domain of the Archean Superior Province (>2.5 Ga) (Lewry et al., 1985; Hoffman, 1988). Wilson and Brisbin (1961) interpreted the Thompson belt as a root of a Precambrian mountain range of the island-arc or alpine type. Bell (1971) considered it might be an autochthonous slice from the Flin Flon subprovince, a "horst" of Archean basement underlying the Churchill Province, or an Archean allochthon related to the Superior continental block.

Fueten et al. (1989) proposed a tectonic model in which the Superior Province has been thrust over the Churchill Province. Bleeker (1990) suggested that the Thompson Nickel Belt represents an early oblique collision zone, due to Churchill terranes thrusting over the Superior plate, which subsequently evolved into a sinistral transform boundary.

The Thompson Nickel Belt is composed of variably reworked Archean

basement gneisses and Early Proterozoic cover rocks. The gneisses constitute 80% or more of the Thompson Nickel Belt and they mainly contain amphibolite-facies mineral assemblages. However, granulite-facies assemblages are also common in the belt and are interpreted as relict Archean granulites that survived the Hudsonian orogeny (Weber and Scoates, 1978; Peredery, 1979; Russell, 1981). This reconstruction is based on Rb/Sr age determinations on the basement gneisses (Cranstone and Turek 1976) that reflect a late Hudsonian overprint (1.7 Ga) and an older metamorphic event (2.8 Ga). Near the western margin of the belt the basement gneisses are overlain by thin (150-1500 m) Early Proterozoic supracrustal rocks that include both metavolcanic assemblages, which chemically are basalts with komatiitic affinities, and metasedimentary assemblages (Peredery, 1979; Peredery et al., 1982).

The supracrustal rocks and basement gneisses are intruded by abundant ultramafic and mafic sills and dykes. Most of the ultramafic rocks in the Thompson Nickel Belt are located in a zone about 6 km wide along the western side of the belt. They occur in the metasedimentary and metavolcanic rocks and gneisses, but the largest bodies are found within the metasedimentary rocks. The ultramafic bodies are generally lensoid or tabular in shape and vary in thickness from several meters to several hundreds of meters. The contacts between the ultramafic bodies and enclosing rocks are so deformed and altered that their true character is uncertain (Peredery et al., 1982). Peredery et al. (1982) divided the ultramafic rocks in the belt into two groups, serpentinites

and ultramafic amphibolites, of which the latter was used as a field name by Peredery to describe a variety of ultramafic rocks ranging from picrite to pyroxenite in composition, whereas serpentinites range in composition from dunite through peridotite to pyroxenite. Some nickel sulfide deposits in the Thompson Belt are spatially related to serpentinites e.g., Pipe mine, Mystery and Moak Lake localities. The sulfides occur as interstitial grains in the serpentinites, as massive and inclusion-bearing sulfides at the contact between the serpentinites and country rocks, and as stringers or veins in the serpentinites and country rocks. However, the Ni sulfides at the Thompson mine are hosted mainly by metasediments, and therefore distinct from almost all other PGM-bearing Ni sulfide deposits.

4.2 Structural Geology and Ore Zones

The major structure controlling the distribution of ore at the Thompson mine was interpreted by Zurbrigg (1963) to be an anticlinical fold striking northeast and plunging steeply to the south. Mine workings include the T-1 and T-3 underground mines, and an open pit. The T-1 mine is at the nose of the anticline whereas the T-3 mine and the open pit are on the eastern limb (Fig. 4.1). Peredery et al. (1982) suggested that the fold could be synclinal. Bleeker (1990) proposed that the dominant structure of the mine is the combination of F1 and F2 isoclinal folds and a nearly upright, high-amplitude, doubly plunging F3 antiform. F3 axial planes dip at 65-90° to the southeast and strike northeast,

Fig. 4.1 Geological map of the Thompson Mine

(after INCO staff 1989, pers. comm.)

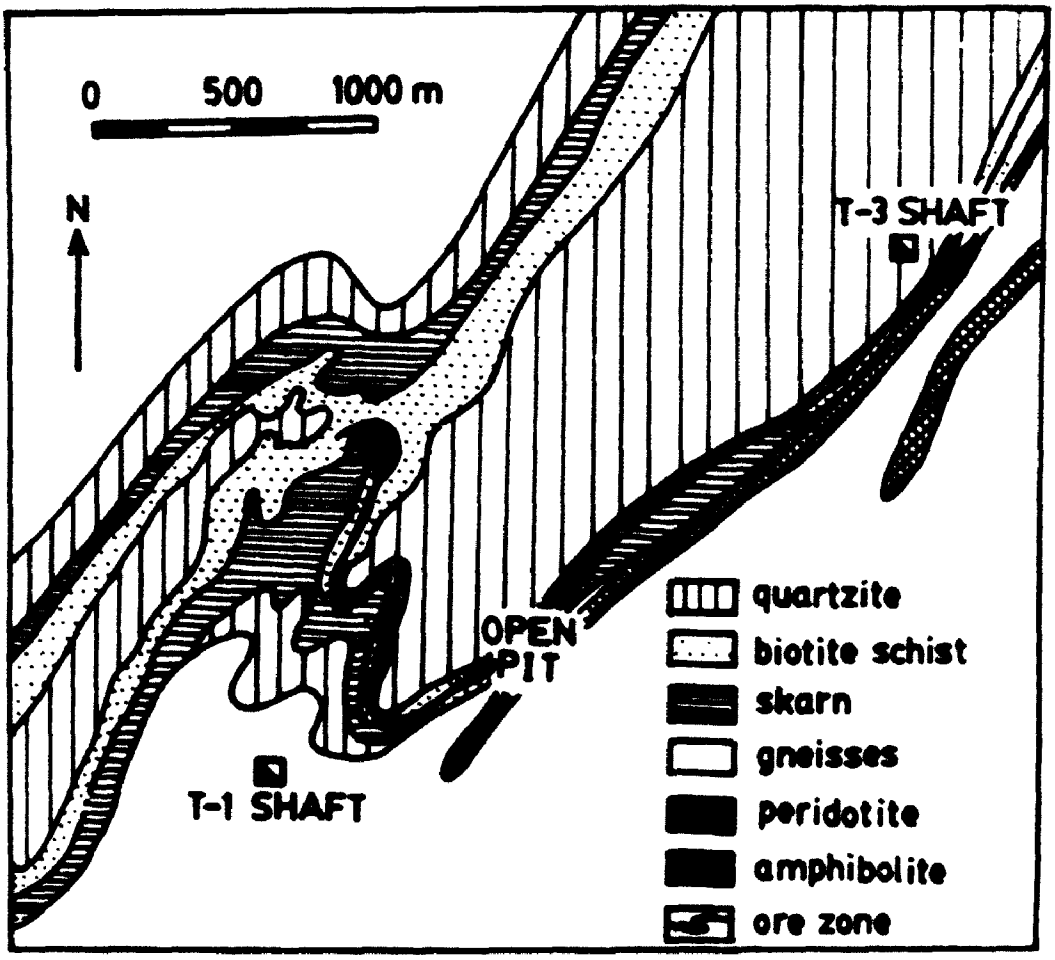
0
500
1000 m
N
T-3 SHAFT
OPEN PIT
T-1 SHAFT
quartzite
biotite schist
skarn
gneisses
peridotite
amphibolite
ore zone

making a 10-20° angle with the trend of the belt. The locus of the nickel sulfide ore is a zone of metapelite (garnet-sillimanite-biotite schist) which is continuous over the length of the antiform structure and conformable with overlying quartzite and skarn and underlying quartzite and iron formation. The nickel sulfide ore itself has an overall length of about 6 km long projected to the surface, has been proven beyond a depth of 1500 m, and has local concentrations along the east limb of the fold, around the nose of the fold, and within associated minor crenulations and drag folds. Ore is only locally associated with serpentinized peridotite, as in the 3-shear orebody of the T-1 mine. Nickel sulfide ore is dominated by pentlandite and pyrrhotite with minor chalcopyrite and pyrite. Violarite occurs after pentlandite. Gersdorffite occurs sporadically, but extremely As-rich ore (gersdorffite ± nickeline) is present locally in both the T-1 mine and open pit. In the latter, the As-rich zone is associated with late white quartz veins and K-feldspar-quartz pegmatite dykes. Both the veins and dykes appear to be boundinaged, and therefore possibly do not postdate the Hudsonian tectonics.

4.3 Local Lithologies

Lithologies defining the fold structures at the Thompson mine include metapelite (garnet-sillimantie-biotite schist), quartzite, skarn, iron formation, gneiss, pegmatite and various ultramafic rocks. The following review includes present observations. Mineral assemblages are consistent with the regional

amphibolite facies metamorphism.

4.3.1 Metapelite

Metapelite is of particular interest because it is the locus of nickel sulfide mineralization. In this study, Au-PGM mineralization is also associated with metapelite and pegmatite which is spatially associated with metapelite.

According to Peredery et al. (1982), essential minerals of metapelite at the Thompson mine are commonly garnet, biotite, sillimanite, graphite and minor cordierite. Metapelite examined in this study consists mainly of almandine, biotite, oligoclase, and quartz with accessory K-feldspar, sillimanite, fluorapatite, titanite, monazite, allanite, graphite and spinel (Plate 1A and 1B). Metapeltie associated with Ni or Au-PGM mineralization is strongly altered. The alterations will be described later.

4.3.2 Quartzite

Quartzite in the core of the anticlinal fold is massive, coarse grained, and contains variable amounts of microcline, plagioclase, biotite, muscovite, zircon, apatite and titanite. Peredery et al. (1982) referred to this rock as a meta-arkose and noted that minor amounts of sillimanite and garnet are associated with micaceous slivers, and microcline appears to be a secondary mineral.

4.3.3 Skarn

Skarn is massive to thinly banded, light green, and medium to coarse grained, and can be classified as diopside-microcline skarn and olivine-diopside-carbonate skarn (Peredery et al., 1982; Bleeker, 1990). The former has essential diopside, microcline, carbonate, plagioclase, scapolite, quartz and minor titanite, apatite and rarely zircon. The alteration products are tremolite, chlorite after diopside, phlogopite after diopside and feldspar. Epidote-zoisite, large retrograde grains of titanite, and prehnite also occur (Bleeker, 1990). The latter skarn type is comprised of mainly olivine, diopside and carbonate minerals (Plate 1C); colorless mica may be present, and locally minor chondrodite. It has been hydrothermally altered; olivine is partially serpentinized, and diopside is altered to tremolite.

4.3.4 Iron formation

In the present study, silicate-facies banded iron formation (BIF, Plate 1D), with only minor magnetite and pyrrhotite, was recognized in material collected from the T-3 mine, within the footwall, 3-15 m below the Ni-sulfide orebodies hosted by metapelite. It is associated with quartzite underlying the metapelite, and is banded on a mm-cm scale. The dark bands are mainly almandine-rich garnet and Fe-rich biotite, with minor ferrosilite, grunerite, cummingtonite and ferropyrosmalite [$(Fe,Mn)_8Si_6O_{15}(OH,Cl)_{10}$]. The light bands consist of coarse-grained quartz and minor amounts of garnet. Two types of sulfide facies iron formations were also encountered. Type I (Plate 1E) was

collected from the 4000 level drilling in the T-1 mine. It is comprised of pyrrhotite, graphite, and silicate minerals (biotite, plagioclase, quartz), and is enclosed by biotite schist. It is interpreted by INCO staff to have been a sulfide-rich sediment contained within the original pelitic sequence. This barren sulfide zone is very closely associated with the ore deposits of the Thompson mine. Type II sulfide facies iron formation (Plate 1F) is from the T-3 mine, and was recognized in material from the Suffel Collection. It is hosted by garnet-amphibole schist, which is composed of garnet, amphibole, biotite, quartz and pyrrhotite with minor pentlandite. Bleeker (1990) also reported trace amounts of sphalerite and molybdenite in sulfide iron formation from the Thompson open pit.

4.3.5 Pegmatite

Pegmatite occurs as large cross-cutting masses spatially associated with ore-bearing metapelite (Zurbrigg, 1963). The pegmatite sample examined in this study is composed of microcline, oligoclase and quartz with minor amounts of biotite and sillimanite (Plate 1G).

4.3.6 Ultramafic rocks

The ultramafic rocks occur as small lenses in metapelite, ranging in size from 1 to 250 meters in maximum dimension. They have been folded and faulted together with their enclosing host rocks, and occur as clusters of angular

blocks either in sulfide matrix or in pelitic schist. The volume of ultramafic rocks in the mine is small relative to the amounts of sulfides. Zurbrigg (1963) distinguished serpentinized peridotite from metaperidotite. The former is composed mainly of pseudomorphs of serpentine after olivine and pyroxene, whereas the latter peridotite is composed of orthopyroxene, magnesian amphibole, olivine, clinochlore and green spinel. He suggested that the latter may have developed from serpentinized peridotite by progressive metamorphism. Peredery et al. (1982) reported that the MgO/(MgO+FeO) ratios of sepentinites (ranging in composition from peridotite to pyroxenite or even picrite) vary from the centre of a lens to its margin, similar to the variation exhibited by differentiated sills.

Paktunc (1984) studied a relatively fresh ultramafic body without Ni-sulfide mineralization occurring at the 400 level of the Thompson T-3 mine, and composed of tremolite peridotite and tremolite pyroxenite units. The tremolite peridotite consists of olivine, orthopyroxene, cummingtonite, tremolite, chlorite and spinel. The tremolite pyroxenite is composed of orthopyroxene, phlogopite, chlorite and tremolite. Paktunc postulated that olivine megacrysts may have recrystallized from partly altered olivine during progressive metamorphism. Orthopyroxene may have formed at the expense of olivine and probably anthophyllite at temperatures above 700°C. Locally developed secondary serpentinization is the latest event observed and probably corresponds to the extensive serpentinization of the ultramafic rocks elsewhere

in the belt.

In the present study, ultramafic rocks (metapyroxenite and metaperidotite) both from the footwall of the nickel orebody and as bulk inclusions in massive sulfide matrix are observed to have been strongly altered and deformed (Plate 1H). These rocks are composed of talc, serpentine, chlorite, actinolite, tremolitic hornblende, magnesio-hornblende, magnesio-cummingtonite, phlogopite and spinel. Hisingerite is closely associated with late carbonate veins and stringers of pentlandite and pyrrhotite also occur.

Mineralized peridotite (named serpentinized peridotite by Zurbrigg, 1963) collected from the T-1 mine is composed of serpentine, talc, carbonate minerals, phlogopite, chlorite and relict olivine, and pyroxene.

4.3.7 PGE-Au mineralization and ore types

The PGE-Au-bearing ores examined in this study are presently divided into four types, on the basis of host rocks and mineral assemblages. Ore types I, II and III are hosted by metapelite whereas ore type IV is hosted by pegmatite.

Ore type I (Plate 2A and 2B) is Ni sulfide ore from the ore zone and was sampled by the unlocated drill core. It consists of pentlandite, pyrrhotite, minor chalcopyrite, pyrite and graphite, with occasional isolated gersdorffite grains. Out of 21 polished thin sections from 7 meters of core, 4 grains of PGMs (all irarsite, IrAsS) were recognized microscopically and analyzed by the electron

microprobe. The host metapelite has been altered, and muscovite and chlorite replace biotite.

Ore type II (Plate 2C) is a PGM-Au-bearing As-rich nickel ore, containing both gersdorffite and nickeline. The slab sample from the T-1 mine (T1FP) contains a vein or segregation, about 8 cm wide and in irregular contact with host metapelite. The vein is asymmetrically zoned from massive Ni-Fe sulfide in metapelite, to a gersdorffite-rich band, a nickeline-rich band, and finally to a massive calcite band against disseminated Ni-Fe sulfide in metapelite. The vein transects the penetrative deformation fabric of the host rock and is not itself penetratively deformed. One hundred and fifty grains of PGMs were recognized microscopically, and analyzed by electron microprobe. The PGMs include sudburyite (PdSb, 60 grains), testibiopalladite-antimonian michenerite [Pd(Sb,Bi)Te, 35 grains] and an unknown PGM [$(Pd,Ni)_{0.44}(Te,Sb)_{0.56}$, 55 grains]. More than 32 gold grains, bismuth telluride, and Cd-rich sphalerite (Appendix I) were identified from this sample T1FP. All precious-metals are closely associated with late gersdorffite and nickeline. Gold is concentrated in both the massive gersdorffite and nickeline bands, whereas PGMs are more concentrated in the massive nickeline band. Also the distribution of PGMs along the gersdorffite-nickeline vein (or zone) is variable with decrease in testibiopalladite-Sb-michenerite associated with increase in sudburyite. The whole-rock assay of the slab (T1FP) yielded Pt 7, Pd 17,261, and Au 4,855 ppb, with about 33 vol% ore minerals.

The host metapelite has been extensively altered by late hydrothermal processes. Biotite has been altered to chlorite and muscovite. Plagioclase has been altered to albite ($Ab_{97}An_3$-Ab_{100}), which in turn has been altered to muscovite and calcite as well. It seems that albitization is closely associated with the PGM-Au mineralization because oligoclase is found outside the vein where only early Ni-Fe sulfide is present.

Ore type II was also recognized in two other samples from the T-1 mine, with massive gersdorffite associated with merenskyite (2 grains) and minor nickeline. Silicate alteration is not as intensive as in the previous sample. Plagioclase and biotite are replaced by minor amounts of muscovite.

Ore type III is As-rich (but nickeline absent) Ni ore from the open pit (N27450, E8500, elevation 10390) that contains native gold, melonite ($NiTe_2$), and Bi-telluride. The host metapelite (biotite schist) has been strongly altered to siliceous chlorite-muscovite schist.

Ore type IV (Plate 2D) is the PGM-Au bearing As-rich Ni ore hosted by the pegmatite from the T-1 mine, that contains gold (24 grains) and four varieties of PGMs: majakite (PdNiAs, 24 grains); kotulskite (PdTe, 7 grains); merenskyite (PdTe2, 4 grains) and michenerite (PdBiTe, 2 grains). PGMs and gold occur as inclusions in late disseminated gersdorffite and nickeline which apparently replace early Ni-Fe sulfides (pentlandite and pyrrhotite). A whole-rock assay yielded Pt 760, Pd 5, Au 12,900 ppb, for a sample with about 20 vol% ore minerals, the low Pd value presumable reflecting a heterogeneous

distribution of PGMs and PGE-enriched arsenides. Microcline and oligoclase are partially altered to muscovite, whereas biotite is altered to chlorite and muscovite.

Plate 1

Lithologies from the Thompson mine

A: Photomicrograph of metapelite host rock for Ni-ore from the Thompson mine, illustrating garnet, biotite, plagioclase and quartz. Scale bar is 0.2 mm. Sample TS-39.

B: Photomicrograph of sillimanite-rich metapelite. Scale bar is 0.2 mm. Sample TOM10.

C: Photomicrograph of olivine-diopside skarn: Di=diopside, Ol=olivine, Phl=phlogopite and Carb=carbonate minerals. Scale bar is 0.2 mm. Sample TC7.

D: Photomicrograph of BIF. Light band is composed of quartz; dark band is composed of biotite and garnet. Scale bar is 0.2 mm. Sample TS-18.

E: Photomicrograph of sulfide iron formation type I, illustrating biotite (grey), quartz and plagioclase (white) and pyrrhotite (black). Scale bar is 0.2 mm. Sample T1B97.

F: Photomicrograph of sulfide iron formation type II: Hbl=hornblende, Cum=cummingtonite, Bt=biotite, Grt=garnet, Qtz=quartz. Scale bar is 0.2 mm. Sample TS-19.

G: Photomicrograph of pegmatite illustrating microcline, biotite, quartz, sulfide and arsenide and sulpharsenide (black). Scale bar is 0.2 mm. Sample T1A4.

H: Photomicrograph of mineralized peridotite illustrating serpentine after olivine. Olivine grain was deformed and penetrated by sulfide veins. Scale bar is 0.2 mm. Sample PT8.

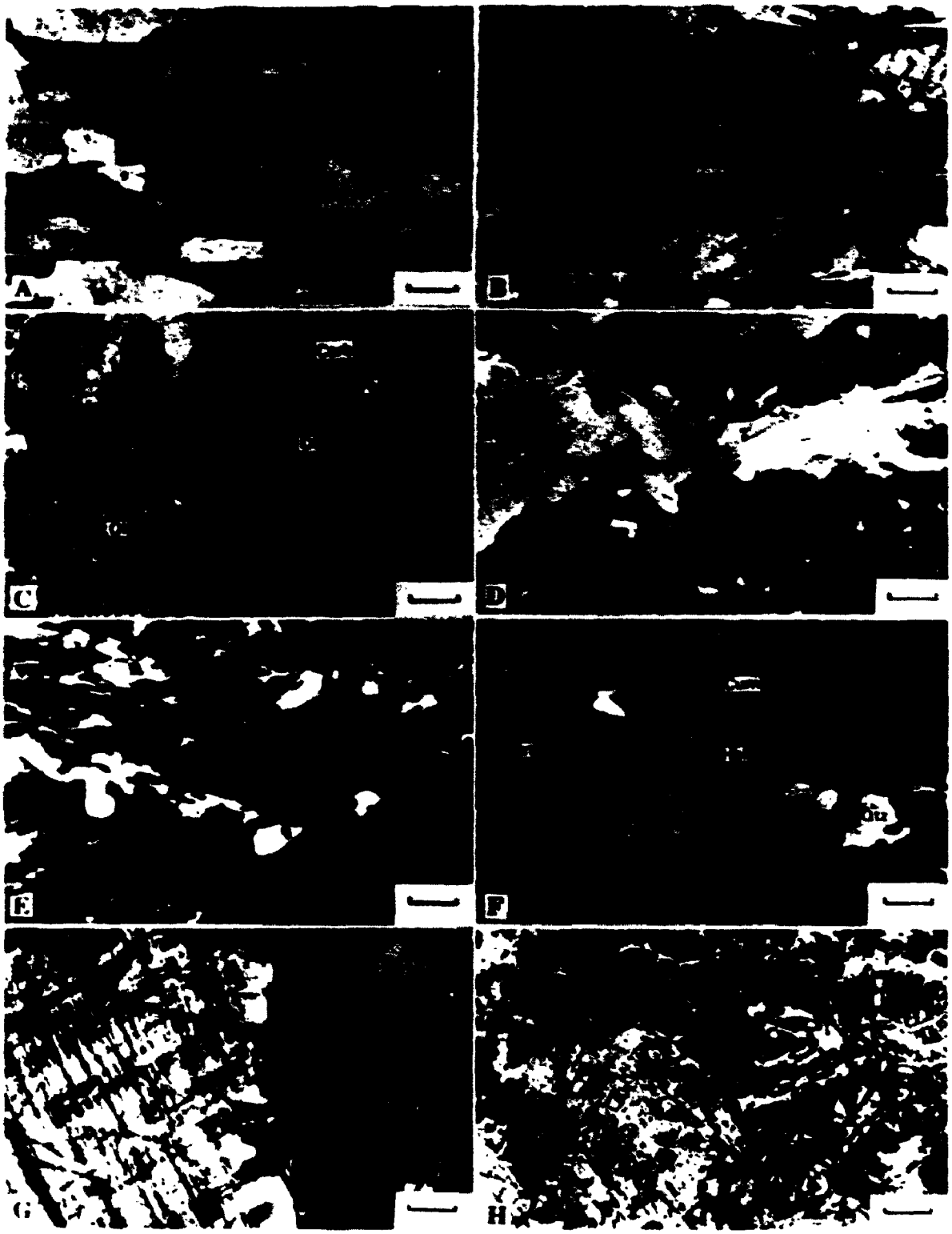
A
B
C
D
E
F
G
H

Plate 2

Some ores from the Thompson mine

A: Photograph of typical nickel ore (ore type I) from the Thompson open pit. Inclusions are biotite rich. Sample TOM-3.

B: Photograph of nickel ore (ore type I) from the Thompson mine. Inclusions are quartz and plagioclase rich. Sample TOM-13.

C: Photograph of PGM-Au bearing As-rich nickel ore (ore type II) from the Thompson T-1 mine. Nc: nickeline-rich band. Gf: gersdorffite-rich band. Slf: massive sulfide. Sample T1FP.

D: photograph of PGM-Au bearing As-rich nickel ore hosted by pegmatite (ore type IV) from the Thompson T-1 mine. Sample T1A4.

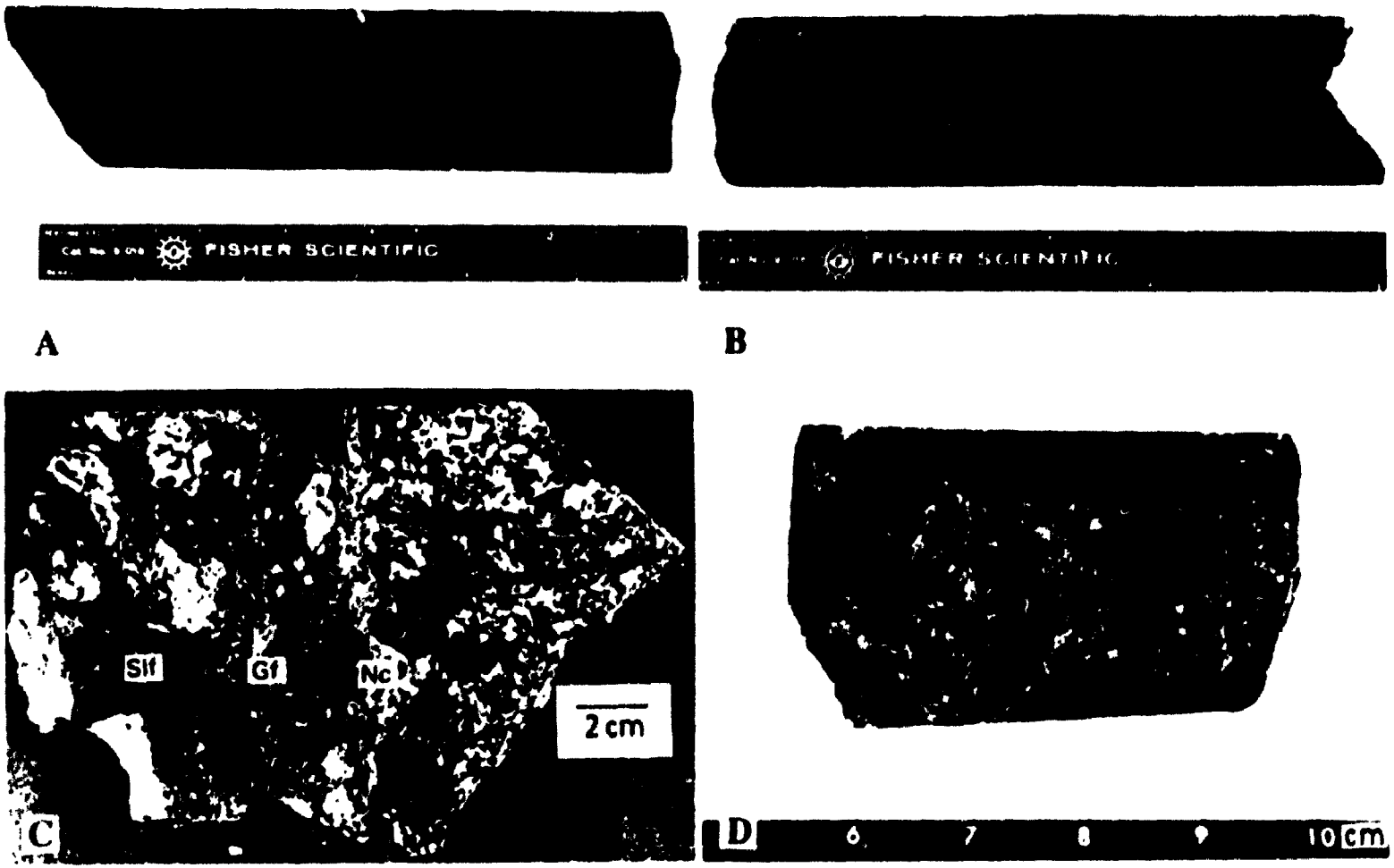
FISHER SCIENTIFIC
FISHER SCIENTIFIC
A
B
Slf
Gl
Nc
2 cm
C
D
6
7
8
9
10 cm

CHAPTER 5 MINERAL CHEMISTRY OF SILICATES, CARBONATES, OXIDES, ARSENIDES AND TELLURIDES

5.1 Introduction

The metasedimentary sequence and ultramafic rocks of the Thompson mine have experienced multi-stage metamorphism. The chemistry of the minerals from these rocks is the best record of this complicated metamorphic history. In this chapter the following minerals are documented: chlorite, biotite, muscovite, talc, hisingerite, ferropyrosmalite, garnet, amphibole, feldspar, carbonate minerals, spinels, nickeline, gersdorffite, bismuth telluride and melonite. Special attention is given to late hydrothermal minerals because they are closely related spatially to the PGE-Au mineralization.

Hydrothermal alteration post-dating the regional amphibolite-facies metamorphism is ubiquitous but variably developed and yet diverse in mineral assemblages in different rock types of the Thompson mine. Alteration assemblages in metapelites contain biotite, muscovite, chlorite, albite, calcite, siderite, allanite (Plate 3A), quartz and sulfides (mainly pyrite and chalcopyrite). Here, biotite, chlorite, and muscovite commonly occur as replacements after early biotite (Plate 3B, 3C and 3D), and albite, chlorite, calcite, and muscovite after more calcic plagioclase (Plate 3E). Ferrosilite and garnet porphyroblasts in silicate-facies banded iron formation (BIF) are extensively replaced by biotite, grunerite (Plate 3F), chlorite, ferropyrosmalite

(Plate 3G), and pyrrhotite. Ferropyrosmalite also is present locally in cross-cutting veins (Plate 3H). Pegmatite has also been affected by a late hydrothermal alteration characterized by similar mineral assemblages to those in metapelites (Plate 3I). Metaperidotites and metapyroxenites examined in this study, both from the footwall of the Ni sulphide orebody and as inclusions in massive sulphide matrix, are strongly altered to talc, dolomite, serpentine, chlorite, actinolite, and phlogopite, with relict tremolitic hornblende, magnesio-hornblende, magnesio-cummingtonite, and spinel. Carbonate micro-veins are very common (Plate 3J). Fingerite is also closely associated with late carbonate veins (Plate 3K). Mineralized peridotite (serpentinized peridotite of Zurbrigg, 1963) collected from the T-1 mine is composed of serpentine, talc, carbonate minerals, phlogopite, and chlorite, as well as relict olivine and pyroxene (Plate 3L).

5.2 Chlorite

Because of the variety of chemical substitutions that are permitted by the chlorite structure, many species names and classification schemes have been proposed. These classification schemes have varied over the years in accordance with our understanding of the composition, properties, and crystal structure of chlorite (summarized by Bailey, 1975).

According to the simplified classification scheme recommended by the Nomenclature Committee of AIPEA (Bailey, 1988), the chlorite group is

subdivided into four sub-groups:

(1) trioctahedral lorite

(2) dioctahedral chlorite

(3) di,trioctohedral cl lorite

(4) tri,dioctahedral chlorite.

Chlorite from the Thompson mine belongs to the trioctahedral chlorite sub-group.

Nomenclature for the trioctahedral chlorite species is based on the suggestions of Bailey (1975), who proposed only four names:

(1) clinochlore $(Mg_5Al)(Si_3Al)O_{10}(OH)_8$

(2) chamosite $(Fe^{2+}{}_5Al)(Si_3Al)O_{10}(OH)_8$

(3) nimite $(Ni_5Al)(Si_3Al)O_{10}(OH)_8$

(4) pennantite $(Mn_5Al)(Si_3Al)O_{10}(OH)_8$.

Electron microprobe analyses of chlorite from the Thompson mine are given in Appendix II. Structural formulae have been calculated on the basis of 28 oxygens, assuming total iron as FeO. The electron microprobe analyses show that the chlorites from the Thompson mine are clinochlore in ultramafic rocks and chamosite in pegmatites and metapelites. Contents of MnO and NiO in the chlorites are relatively low, with maximum values of 0.8 wt% and 0.4, respectively. The tetrahedral-site compositions of trioctahedral chlorite given by Bailey (1975) range from $(Si_{4.8}Al_{3.2})$ to $(Si_{6.4}Al_{1.6})$. Trioctahedral chlorites in the present study have tetrahedrai-site compositions ranging from $(Si_{5.02}Al_{2.98})$ to

($Si_{6.48}Al_{1.52}$), with the exception of three analyses from the ultramafic rocks with compositions from ($Si_{6.62}Al_{1.38}$) to ($Si_{6.88}Al_{1.12}$), which can be named as silician clinochlore according to Bailey (1975).

FeO contents of chlorite from metapelite hosted ore types I, II and III vary from 28.8 to 33.2 wt%, whereas MgO varies from 12.2 to 7.7 wt%. The majority of chlorite in pegmatite-hosted ore type IV is relatively iron-rich, containing 34.1 to 35.8 wt% FeO and 6.6 to 6.0 wt% MgO, with an exception that contains FeO 10.60 wt% and MgO 22.93 wt%. Chlorite from ultramafic rocks is Mg-rich, containing 4.5 to 23.3 wt% FeO and 30.8 to 19.4 wt% MgO, compared with chlorite from metapelite and pegmatite. The highest contents of TiO_2 and MnO are 0.2 and 0.8 wt%, respectively, detected from pegmatite which is the host rock for PGM-Au bearing As-rich nickel ore (ore type IV). The Cr_2O_3 content of chlorite is up to 1.6 wt% in metapelite hosted ore type I from the T-3 mine and ore type III from the open pit. Chlorite in pegmatite hosted ore type IV and metapelite hosted ore type II from the T-1 mine contains none to 0.1 wt% Cr_2O_3. In contrast, chlorite from the ultramafic rocks has Cr_2O_3 contents varying from undetected to 4.7 wt%. Fluorine contents of the chlorite are relatively low, only up to 0.6 wt%, and this is most likely attributable to interference from Fe.

5.2.1 Si and Fe/(Fe+Mg)

The Fe/(Fe+Mg) ratios and Si have been used in the classification and

nomenclature for chlorite (e.g., Hey, 1954). Chlorites in this study have Si contents ranging from 5.06 to 6.88 cations p.f.u., and Fe/(Fe+Mg) ratios ranging from 0.07 to 0.77 (Fig. 5.1). According to Hey (1954), chlorites in ultramafic rocks are chlinochlore, penninite, diabantite and pycnochlorite. Chlorite in ore type III from the open pit is brunsvigite. Chlorite in ore types I and II is ripidolite. And chlorite in ore type IV is ripidolite.

5.2.2 Mg/(Mg+Fe) and Al/(Al+Mg+Fe)

Chlorite is a common mineral in metamorphosed pelitic, felsic, intermediate, mafic, aluminous calc-silicate, and ultramafic rocks. It also occurs in metamorphosed Mn-rich rocks and is rare in metamorphosed iron formation. Laird (1988) introduced an Al/(Al+Mg+Fe)-Mg/(Mg+Fe) binary diagram to show the variation of chlorite composition with different parental rocks. Laird (1988) pointed out that in her diagram pelitic rocks span a wide range of Mg/(Mg+Fe) ratio but within individual rocks chlorite does not usually show a wide variation.

In this study, chlorites from PGM-Au enriched ore types II and IV show a broad variation of Mg/(Mg+Fe) ratios (0.30 to 0.50 and 0.24 to 0.75, respectively) in the same rock sample (Fig. 5.2). Chlorite in ore type I which is associated with nickel ore shows only a relatively narrow range of Mg/(Mg+Fe) ratio (0.30 to 0.40). This may indicate that hydrothermal alteration is more intensive in PGM-Au bearing metapelite. The

Fig. 5.1 Compositions of Thompson mine chlorite in Fe/(Fe+Mg)-Si system. Classification and nomenclature are after Hey (1954). RI=ripidolite, SH=sheridanite, BR=brunsvigite, PY=pycnochlorite, CH=chlinochlore, DI=diabantite, PE=penninite.

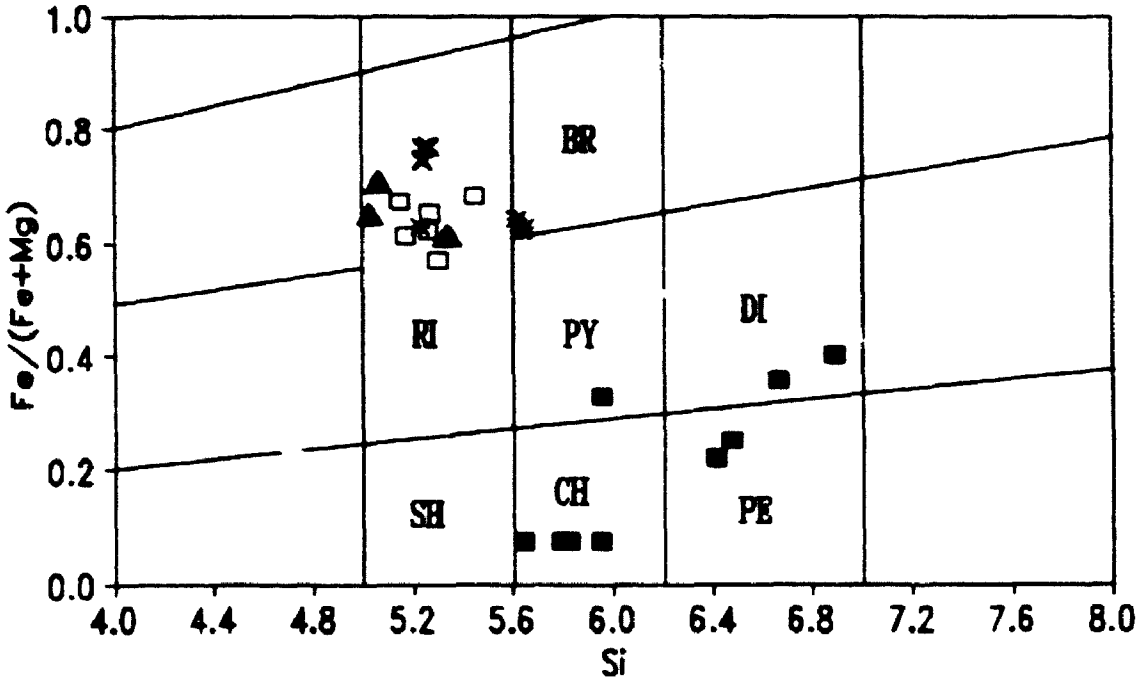
1.0
0.8
0.6
0.4
0.2
0.0
Fe/(Fe+Mg)
4.0
4.4
4.8
5.2
5.6
6.0
6.4
6.8
7.2
7.6
8.0
Si
BR
RI
PY
DI
SH
CH
PE
ore type I
ore type II
ore type III
ore type IV
ultramafic rocks

Fig. 5.2 Compositions of Thompson mine chlorite in Al/(Al+Mg+Fe)-Mg (Mg+Fe) system

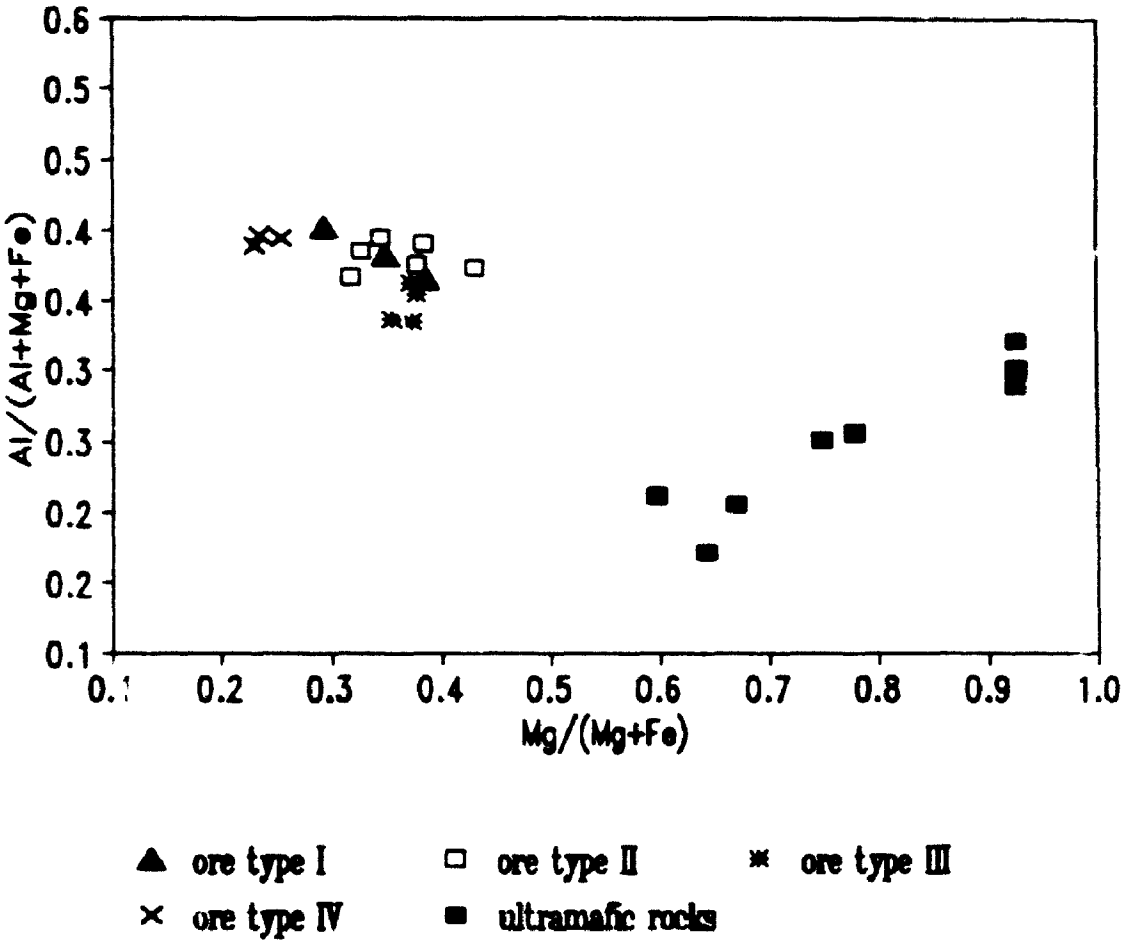
0.6
0.5
0.5
0.4
0.4
0.3
0.3
0.2
0.2
0.1
Al/(Al+Mg+Fe)
0.1
0.2
0.3
0.4
0.5
0.6
0.7
0.8
0.9
1.0
Mg/(Mg+Fe)
ore type I
ore type II
ore type III
ore type IV
ultramafic rocks

Al content of chlorite from the metapelite is higher than the chlorite from ultramafic rocks. In the present study chlorite in some ultramafic rocks has lower Mg/(Mg+Fe) ratios than chlorite in the ultramafic rocks collected by Laird (1988). However, they are still distinct from chlorite in mafic rocks in the literature because of their low Al contents. Chlorites from the present ultramafic rocks show a narrow variation in MgO/(MgO+FeO) ratio, except for one rock sample with values ranging from 0.75 to 0.93.

5.2.3 ^{IV}Al, ^{VI}Al and Fe/(Fe+Mg)

Figure 5.3 is a plot of ^{IV}Al vs. ^{VI}Al of chlorite from different rocks from the Thompson mine. It shows that ^{IV}Al and ^{VI}Al are positively correlated. ^{IV}Al varies from 1.12 to 2.98 (based on 28 oxygens) whereas ^{VI}Al varies from 0.78 to 3.00. ^{IV}Al/^{VI}Al ratios are close to unity in most of the chlorites, which suggests that charge balance of ^{IV}Al ⇌ Si replacement is accomplished by ^{VI}Al replacing either Fe or Mg in octahedral layers. This also suggests that Fe^{3+} is generally low in the chlorites. In ultramafic rocks, however, the octahedral Al of chlorite may be replaced by Cr^{3+} and Fe^{3+}. Two chlorite analyses from the ultramafic rocks show lower ^{VI}Al contents, and the ^{IV}Al/^{VI}Al ratios for these two analyses are 1.72 and 2.27, respectively. One of them contains 4.74 wt% Cr_2O_3, so that charge balance can be accomplished by Cr^{3+}. However, the other one may contain Fe^{3+} since the Cr_2O_3 content is low. Three analyses of chlorite from the ultramafic rocks show an excess of octahedral Al relative to

Fig. 5.3 Compositions of Thompson mine chlorite in ^{IV}Al-^{VI}Al system

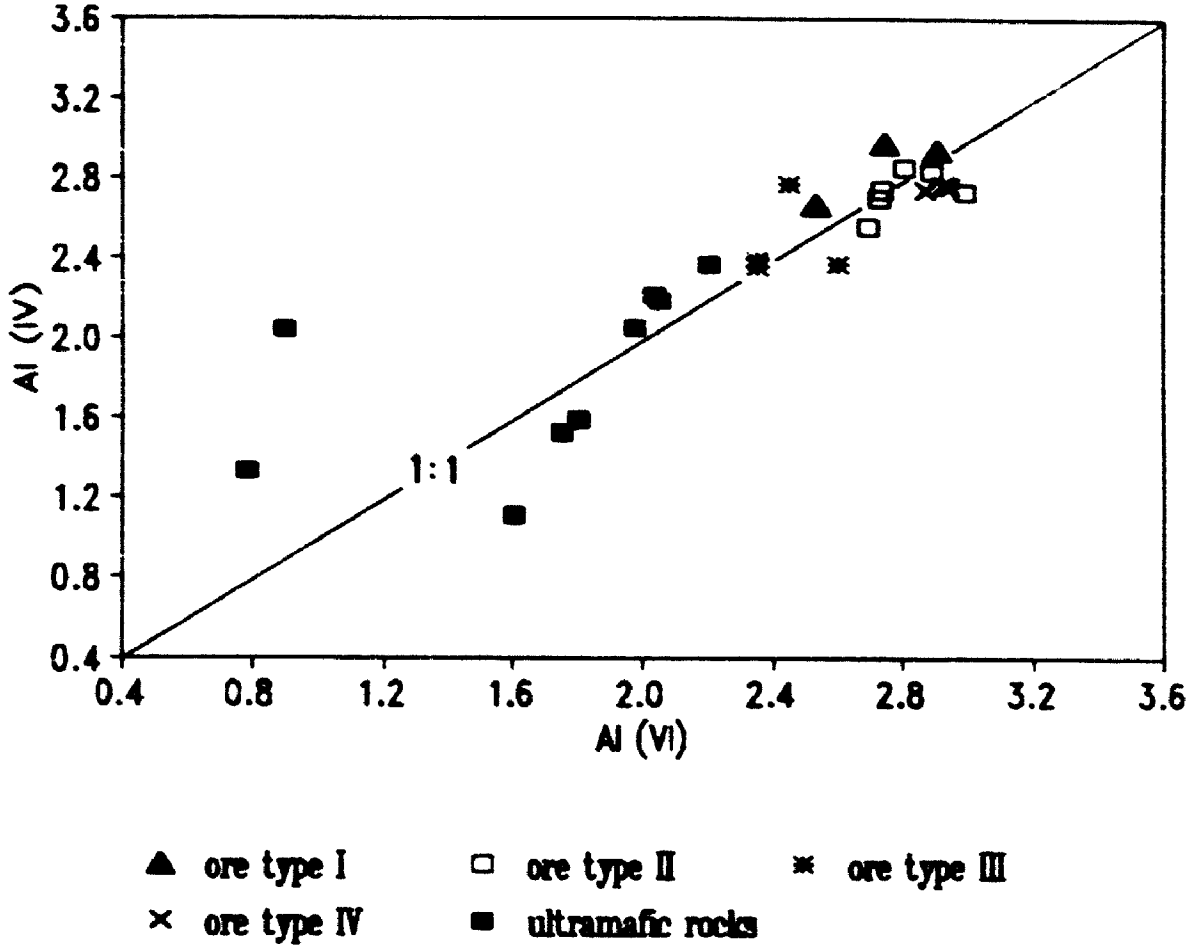
3.6
3.2
2.8
2.4
2.0
1.6
1.2
0.8
0.4
Al (IV)
1:1
0.4
0.8
1.2
1.6
2.0
2.4
2.8
3.2
3.6
Al (VI)
ore type I
ore type II
ore type III
ore type IV
ultramafic rocks

tetrahedral Al, with $^{IV}Al/^{VI}Al$ ratios ranging from 0.70 to 0.87. The excess ^{VI}Al indicates that there are cation vacancies in the octahedral layers.

^{IV}Al is plotted against Fe/(Fe+Mg) ratios for chlorites from different rocks from the Thompson mine in Figure 5.4. It appears that ^{IV}Al increases with increasing Fe/(Fe+Mg) ratios in metapelite. It has been suggested that the increase ^{IV}Al with increase in Fe/(Fe+Mg) ratio can be attributed to structural adjustments in chlorite associated with change in cation size (Kranidiotis and Maclean, 1987). However, ^{IV}Al and Fe/(Fe+Mg) ratios of chlorites in ultramafic rocks are negatively correlated. This may be due to variation of whole-rock compositions.

5.2.4 Replacement of biotite by chlorite

Chlorite replaces biotite in the host metapelite rocks. In some cases, chlorite replaces biotite completely, giving rise to the assemblage of muscovite + quartz + chlorite + ilmenite. The ilmenite is elongated, occurring parallel to chlorite cleavage. Coexistence of ilmenite with chlorite and muscovite suggests reaction of biotite to both chlorite and muscovite, from which excess titanium combines with iron to form ilmenite under relatively reducing conditions. Rutile will appear under oxidizing conditions in the same alteration, in which biotite is replaced by an assemblage of chlorite + rutile + carbonate + epidote + megnetite (Sales and Meger, 1948). Ferry (1979) reported that biotite in granitic rocks from Maine was converted to chlorite and titanite. With

Fig. 5.4 Compositions of Thompson mine chlorite in ^{IV}Al-Fe/(Fe+Mg) system

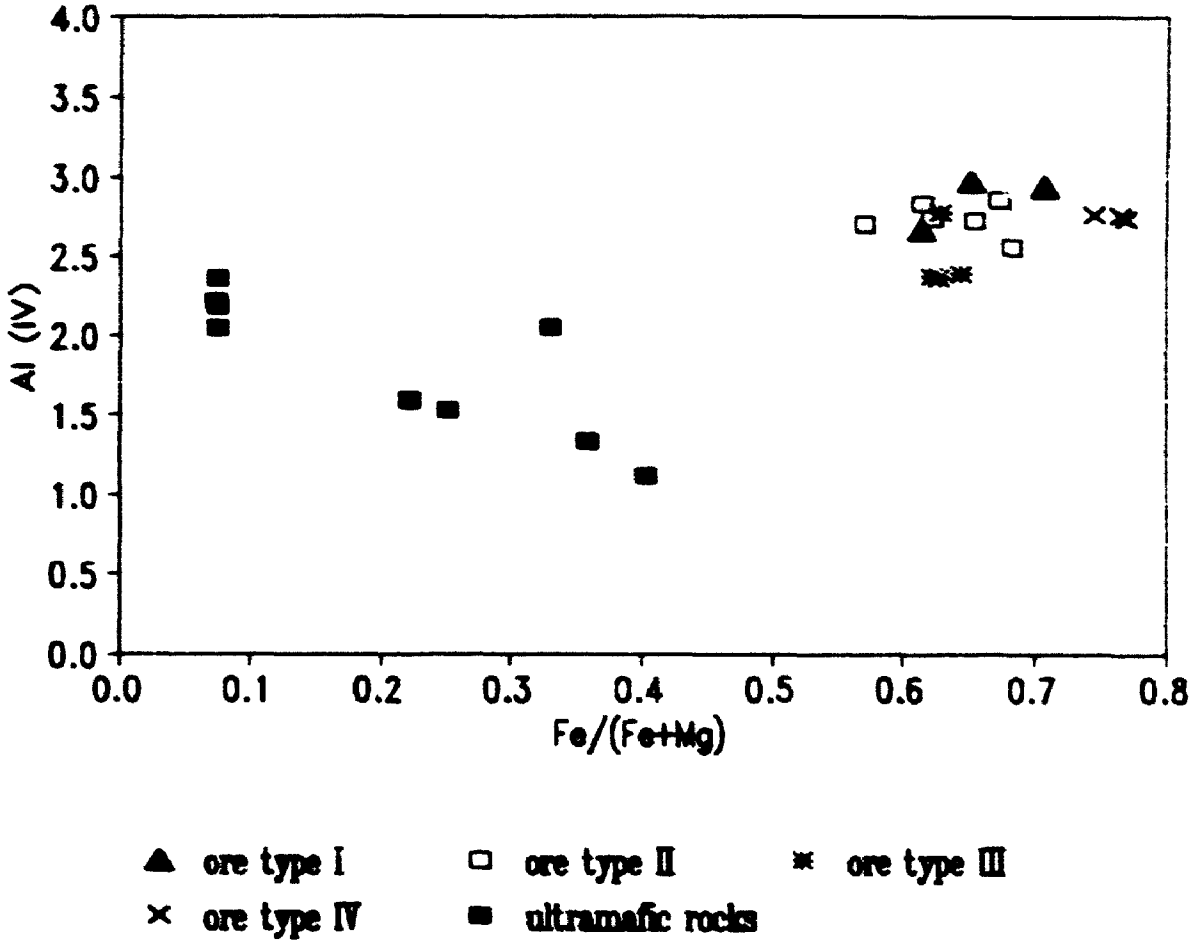
4.0
3.5
3.0
2.5
2.0
1.5
1.0
0.5
0.0
Al (IV)
0.0
0.1
0.2
0.3
0.4
0.5
0.6
0.7
0.8
Fe/(Fe+Mg)
ore type I
ore type II
ore type III
ore type IV
ultramafic rocks

the assumption of conservation of aluminum and titanium in the alteration, he estimated a volume decrease of 13% of parent rocks in mass transfer accompanying the hydrothermal processes. Parry and Downey (1982) examined the chemistry of the replacement of biotite by chlorite in quartz monzonite and proposed two possible chemical reactions. In the first reaction aluminum and silicon are conserved among the solid phases:

$$2KMg_3AlSi_3O_{10}(OH)_2 + 4H^+ = Mg_5Al_2Si_3O_{10}(OH)_8 + 2K^+ + Mg^{2+} + 3SiO_2,$$

where the magnesium end-members phlogopite and clinochlore represent biotite and chlorite, respectively. In the reaction H^+ is consumed whereas K^+ and Mg^{2+} are produced. The second reaction assumes that biotite is replaced by an equivalent volume of chlorite. Since the molar volumes of phlogopite and clinochlore are 149.66 cm^3/mole and 207.11 cm^3/mole, respectively (Helgeson et al., 1978), the reaction is written as

$$1.4KMg_3AlSi_3O_{10}(OH)_2 + 0.8Mg^{2+} + 0.6Al^{3+} + 3.6H_2 = Mg_5Al_2Si_3O_{10}(OH)_8 + 1.4K^+ + 2H^+ + 1.2SiO_2,$$

where Mg^{2+} and Al^{3+} are consumed, and H^+ and K^+ are produced.

These two reactions will give rise to two different mineral assemblages since one reaction consumes H^+ and the other produces H^+. In a phase diagram of $\log(aK^+/aH^+)$ vs. $\log(aMg^{2+}/aH^+)$, these two reactions are represented by two different paths. For the first (Al conserved) reaction the products are phlogopite + clinochlore, whereas for the second (volume conserved) reaction

the products are clinochlore + muscovite ± phlogopite.

Microscopic study revealed that, at the Thompson mine, chlorite replaces biotite along cleavage lamellae without distortion of the lamellae or increased porosity. Also muscovite is a common alteration product of biotite. Therefore, it is concluded that the alteration of biotite to chlorite at the Thompson mine is volume conservative. H^+ and K^+ are produced when hydrothermal chlorite formed.

5.3 Muscovite

Muscovite at the Thompson mine occurs in association with ore types I, II, III and IV as an alteration product of biotite and feldspar, and in most cases it occurs cross cutting the earlier foliation, and even as late veins. Muscovite is most abundant in ore types II and III in the T-1 mine and the open pit. Electron microprobe analyses are given in Appendix III.

5.3.1 Si

The silicon content of muscovite altered from both feldspars and biotite in ore types I, II and III hosted by metapelite ranges from 6.2 to 6.6 cations p.f.u. (Fig. 5.5) with an average value of 6.4 (calculated on 22 oxygens), i.e., equal to 20 mole percent celadonite component ($KMgAlSi_4O_{10}(OH)_2$). The silicon content of muscovite in ore type IV hosted by pegmatite is about 6.2 cations p.f.u. (10 mole percent celadonite) (Fig. 5.5). Numerous studies point

Fig. 5.5 Compositions of Thompson mine muscovite in Si-Fe+Mn+Mg system

1.0
0.8
0.6
0.4
0.2
0.0
Fe+Mn+Mg
6.0
6.2
6.4
6.6
6.8
7.0
Si
ore type I
ore type II
ore type III
ore type IV

out that increase in the temperature of formation of muscovite generally results in a progressive decrease in the celadonite component (cf. review of Guidotti and Sassi, 1976). This suggests that although muscovite could be stable up to upper-amphibolite grade metamorphism, the muscovite in the study area may have formed under a relatively low metamorphic temperature.

5.3.2 Mg^{2+} and Fe^{2+}

It is well known that Fe^{2+} and Mg^{2+} can replace Al^{3+} in octahedral sites with concomitant replacement of Al^{3+} by Si^{4+} in the tetrahedral sites of muscovite to balance the charge. Electron microprobe analyses show that the FeO and MgO contents of muscovite in ore type IV, which is hosted in pegmatite, are up to 1.5 and 0.8 wt%, respectively. Also FeO and MgO contents of muscovite in ore types I, II and III hosted by metapelite are up to 2.7 and 1.8 wt%, respectively.

5.3.3 Cr^{3+} and V^{3+}

Cr^{3+} sometimes replaces Al^{3+} in muscovite. The Cr_2O_3 contents of muscovite in ore-types II and IV from the T1 mine are very low, only up to 0.1 wt%, whereas those of muscovite in ore types I and III are relatively high, up to 2.1 and 1.5 wt%, respectively. One grain of Cr-bearing muscovite in ore type I shows green to greenish yellow pleochroism. Other grains are slightly greenish. Such grains usually occur in the assemblage muscovite + quartz ±

chlorite ± spinel. The V_2O_3 content of all muscovites is only up to 0.2 wt%.

5.3.4 Ti

Titanium can enter the octahedral site of muscovite as Ti^{4+}, and substitutes for Al^{3+}, Fe^{3+}, Mg^{2+} or Fe^{2+}. The increase in Ti content of muscovite with metamorphic grade has been summarized by Guidotti (1984). This author suggests that over the range from greenschist facies to upper amphibolite facies (chlorite zone to K-feldspar + sillimanite zone, where muscovite finally breaks down) the Ti content increases fairly steadily from about 0.02 to about 0.12 cations p.f.u..

Electron microprobe analyses show that the Ti content of muscovite in metapelite (garnet-sillimanite-biotite schist) associated with nickel and PGM-Au mineralization (ore types I, II and III) from the Thompson mine is 0.02 cations p.f.u.. Because a Ti-saturating phase (ilmenite) usually coexists with muscovite, the Ti content in the muscovite should be at saturation levels for the P-T conditions prevailing during its formation. Hence, the amount of Ti present is probably controlled by crystal-chemical factors. Therefore, we suggest that muscovite in this study was formed under greenschist facies metamorphism. This confirms that muscovite is the hydrothermal alteration product of biotite.

5.4 Biotite

Among the samples examined in this study, biotite occurs in metapelite,

both sulfide and silicate-facies banded iron formations, and Ni and PGM-Au ores (ore types I, II, III and IV) hosted by both metapelite and pegmatite. Two generations of biotite were observed from metapelite, silicate-facies banded iron formation and pegmatite. The secondary biotite occurs as fine-grained aggregates and cross-cutting foliations. There is no distinct compositional variation between the two generations of biotite with the same bulk rock compositions, except that some secondary biotite associated with PGMs and native gold has slightly higher contents of both ^{IV}Al and Mn. Phlogopite is present in strongly altered ultramafic rocks (probably originally pyroxenite) both from the footwall of the nickel orebody and as bulk inclusions in massive sulfide matrix.

In comparison with muscovite, biotite from different rocks shows much more variation in proportions of major elements, including Fe, Mg, Tschermak exchange, etc. This compositional variation occurs in r·sponse to variation in bulk composition and/or mineral assemblage variation, and metamorphic conditions.

Biotite compositions can be approximated by end-members representing the simple substitution $Mg \leftrightarrow Fe^{2+}$ and the coupled substitution $^{VI}Al + {}^{IV}Al = (Fe^{2+},Mg) + Si$. Electron microprobe analyses of biotite and phlogopite in different types of rocks from the Thompson mine are given in Appendix VI. Structural formulae have been calculated on the basis of 22 oxygens, assuming total iron as FeO. The microprobe data show a slight positive correlation

between ^{IV}Al and Fe/(Fe+Mg) (Fig. 5.6), indicating that another substitution may be involved as well as the Tschermak substitution. Also, ^{VI}Al is very often in excess of that required to balance ^{IV}Al.

5.4.1 Compositional variation within the biotite compositional plane

The electron microprobe analyses are plotted in the ideal biotite plane in Figure 5.7. This diagram shows that all the metamorphic biotite and phlogopite from the Thompson mine deviate from having the ideal tetrahedral Si:Al ratio of 3:1 as in annite or phlogopite end-members. This is because substitution of Al for Si in tetrahedral sites is the primary way of maintaining charge balance for Al replacing Mg or Fe^{2+} in octahedral sites. The Mg/(Mg+Fe) ratios of phlogopite in ultramafic rocks vary from 0.67 to 0.83 with tetrahedral Al/Si occupancies of 1.12/2.88 and 1.21/2.79, respectively.

The Mg/(Mg+Fe) ratio of biotite in silicate-facies banded iron formation is in the range of 0.19 to 0.24. The FeO content of the biotite in the iron formation is the highest among all biotite in different host rocks from the Thompson mine. Since natural metamorphic biotites rarely have Mg/(Mg+Fe)$<$0.3, the composition of this biotite from the iron formation is unusual relative to biotite data in the literature (Bailey, 1984). The ^{VI}Al content of the biotite ranges from 0.34 to 0.52 p.f.u. Biotite in sulfide iron formation type I is relatively Mg-rich as expected, with Mg/(Mg+Fe) ranging from 0.57 to 0.59, compared with biotite in the silicate-facies banded iron formation, but

Fig. 5.6 Compositions of Thompson mine biotite in ^{IV}Al-Fe/(Fe+Mg) system

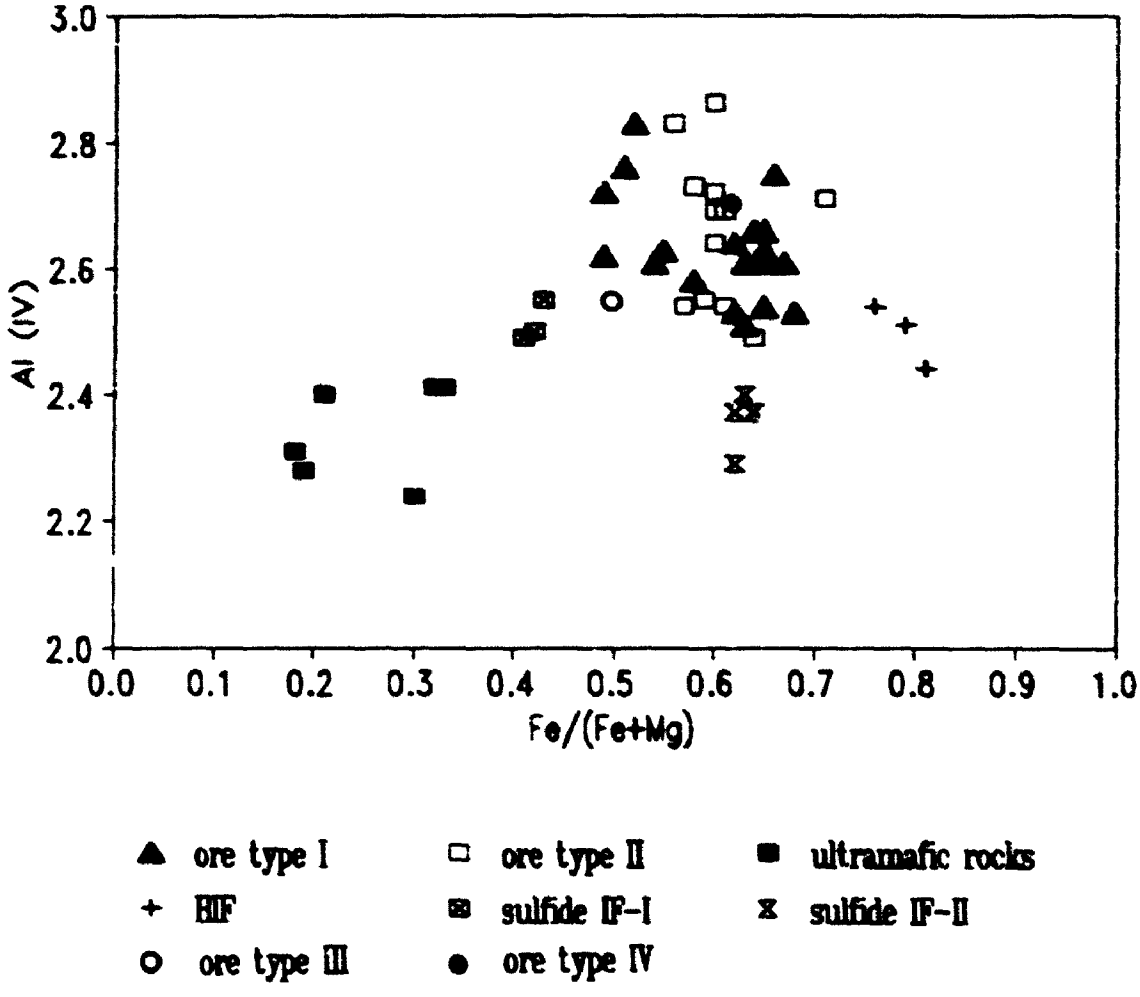
3.0
2.8
2.6
2.4
2.2
2.0
Al (IV)
0.0
0.1
0.2
0.3
0.4
0.5
0.6
0.7
0.8
0.9
1.0
Fe/(Fe+Mg)
ore type I
ore type II
ultramafic rocks
BIF
sulfide IF-I
sulfide IF-II
ore type III
ore type IV

Fig. 5.7 Compositions of Thompson mine biotite in biotite compositional plane ^{VI}Al-Mg/(Mg+Fe) system

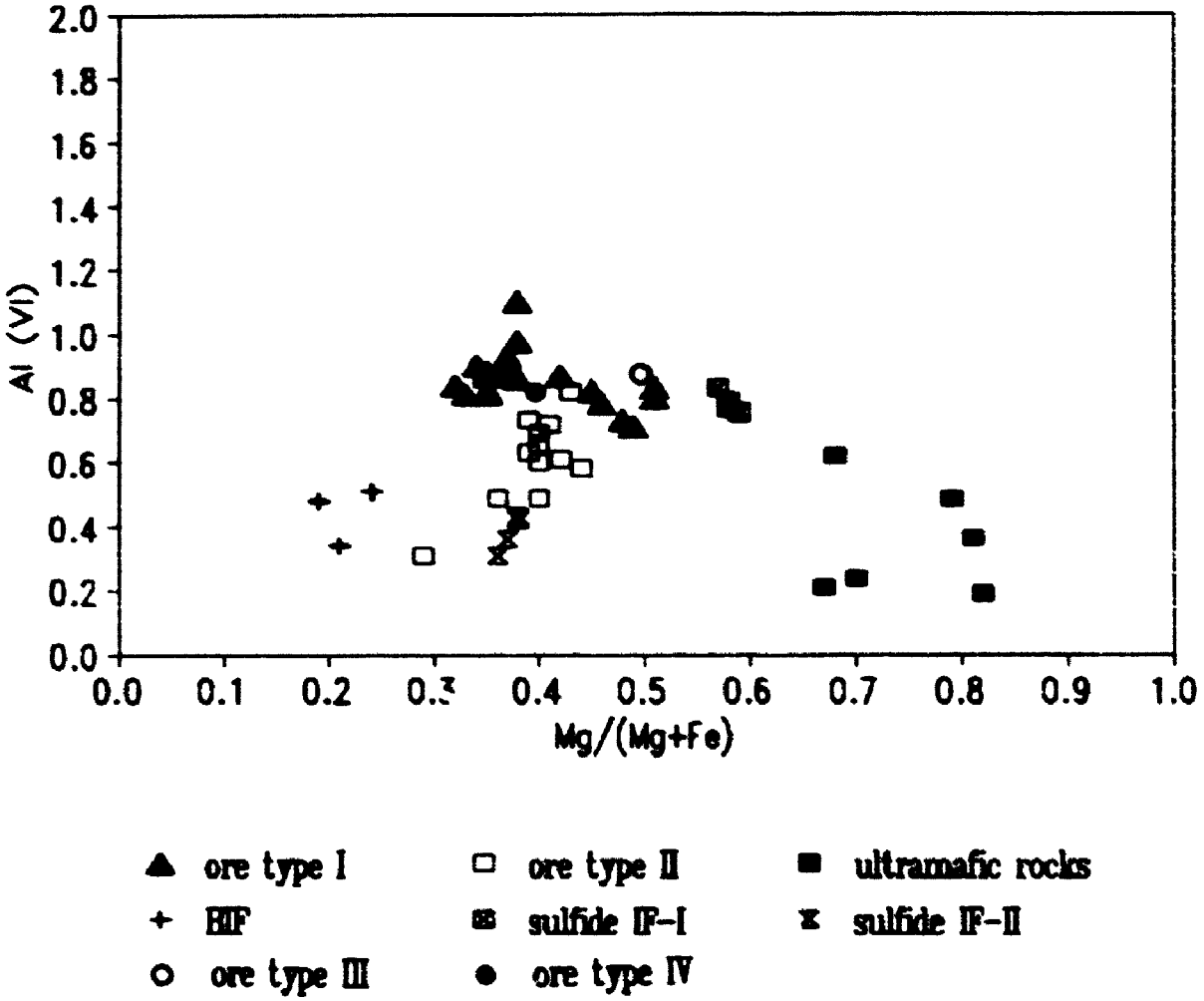
2.0
1.8
1.6
1.4
1.2
1.0
0.8
0.6
0.4
0.2
0.0
Al (VI)
0.0
0.1
0.2
0.3
0.4
0.5
0.6
0.7
0.8
0.9
1.0
Mg/(Mg+Fe)
ore type I
ore type II
ultramafic rocks
BIF
sulfide IF-I
sulfide IF-II
ore type III
ore type IV

has a higher ^{VI}Al content (0.74 to 0.84 p.f.u.).

Biotite in ore type IV (pegmatite hosted Au-PGM-Ni ore) has a Mg/(Mg+Fe) ratio of 0.5 and ^{VI}Al content of 0.82 p.f.u., which are within the range for biotite in metapelite both from the Thompson mine and from other localities worldwide (Guidotti, 1984). This may indicate that the pegmatite is related to metapelite and probably formed by segregation from the metapelite during metamorphic processes.

Biotites in metapelite hosting ore types I (Ni ore) and II (PGM-Au-Ni ore) have similar Mg/(Mg+Fe) ratios, with average values of 0.40 and 0.39, respectively, and the same mineral assemblages. Also biotites from ore types I and II have identical Ti contents (0.22 p.f.u.). However, their ^{VI}Al contents are distinctly different. The ^{VI}Al content of biotite in ore type I ranges from 0.72 to 1.10 p.f.u., with an average value of 0.86, whereas the ^{VI}Al content of biotite in ore type II ranges from 0.32 to 0.82, with an average value of 0.62. It has been noted that besides bulk composition of host rocks and mineral assemblages, the ^{VI}Al content of the biotite also depends on the formation temperature, decreasing with decrease in formation temperature (Guidotti, 1984). Therefore, the difference in ^{VI}Al content of biotites from ore types I and II may suggest that the alteration to secondary biotite in ore type II was more pervasive due to late hydrothermal processes related to the PGM-Au mineralization. Biotite in ore type III hosted in metapelite has an ^{VI}Al content of 0.86 p.f.u. and a Mg/(Mg+Fe) ratio of 0.5, which is higher than in biotites

from ore types I and II.

5.4.2 Mn substitution

Manganese is commonly present in small amounts in the octahedral sites of biotite. Figure 5.8 shows the Mn content vs. Fe/(Fe+Mg) ratio for biotite in different host rocks from the Thompson mine. There is a positive correlation between Fe/(Fe+Mg) ratio and Mn content, except for biotite from iron formations. The Fe content of biotite in sulfide iron formation type I is relatively low, but the Mn content is distinctly high, ranging from 0.08 to 0.10 cations p.f.u. (0.65 to 0.84 wt% MnO). Biotite in oxide iron formation has a very high Fe content, but the Mn content is only up to 0.04 cations p.f.u. (0.3 wt% MnO). The Mn content in biotite may be controlled by not only the bulk compostion of parent rocks, but also the mineral assemblages. It is well known that Mn is a lithophile element, being present in oxide minerals or silicates. In sulfide iron formation type I, Mn prefers to enter biotite rather than sulfides. In silicate-facies banded iron formation from the study area Mn concentrates in other silicate minerals, such as ferropyrosmalite (MnO, 5.6-5.8 wt%), garnet (MnO, 4.0-4.7 wt%), ferrosilite (MnO, 1.7-1.9 wt%).

In general, biotite in ore type II which is enriched in PGM and Au has a slightly higher Mn content than that in ore type I which is a nickel ore. The difference in Mn content between these two ores can be attributed to different intensities of hydrothermal alterations of the same host rocks, since some Mn

Fig. 5.8 Manganese contents of Thompson mine biotite

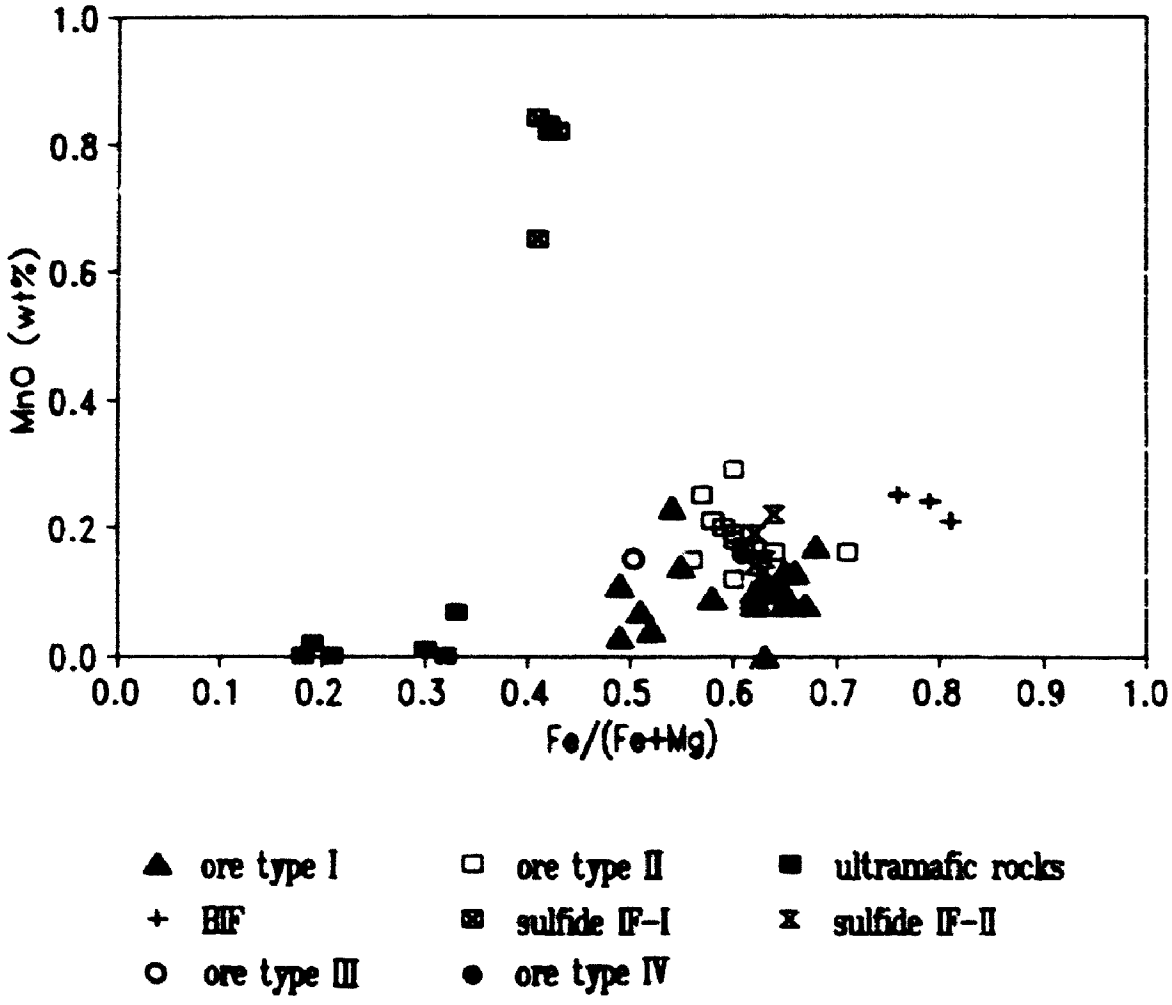
1.0
0.8
0.6
0.4
0.2
0.0
MnO (wt%)
0.0 0.1 0.2 0.3 0.4 0.5 0.6 0.7 0.8 0.9 1.0
Fe/(Fe+Mg)
ore type I
ore type II
ultramafic rocks
BIF
sulfide IF-I
sulfide IF-II
ore type III
ore type IV

may have been introduced metasomatically. The high Mn content in biotite from ore type II may suggest strong alteration of its host rock. The Mn content of phlogopite from ultramafic rocks in the study area is very low, ranging from 0.00 to 0.02 cations p.f.u., mainly due to low Mn content in the parent rocks.

5.3.3 Cr substitution

The content of Cr in biotite is generally low. The maximum Cr content of biotite in the review of Guidotti (1984) is 0.026 cations p.f.u. (per 22 oxygens). In this study, biotite in ore types I (Ni ore) and III (Au-bearing Ni ore) and Ni-sulfide-bearing ultramafic rocks (probably originally metapyroxenite or metaperidotite) contains relatively higher Cr than that in other rock (ore) types, with contents up to 1.0 wt% Cr_2O_3, i.e. 0.12 cations p.f.u. Biotite in sulfide iron formation type I contains relatively more Cr (0.02 cations p.f.u. on average) than that in oxide iron formation (0.006 cations p.f.u. on average). The contents of Cr in biotite from PGM-Au-rich Ni ores (types II and IV hosted by metapelite and pegmatite, respectively) and non-mineralized metapelite are very low to not detected. It may be concluded that biotite in Ni ore is more enriched in Cr than biotite in late PGM-Au-rich Ni ores.

5.4.4 Ti substitution

Although there is discussion in the literature on the possibility of Ti

being in the trivalent state or substituting for Si in tetrahedral sites, there is a general consensus that Ti in biotite is quadrivalent and substitutes into octahedral sites. Many studies show that the Ti content of the biotite depends on both Fe/(Fe+Mg) ratio and metamorphic grade. Figure 5.9 shows that Ti is obviously correlated with Fe/(Fe+Mg) ratio in biotite-phlogopite from the Thompson mine.

The Ti content of phlogopite, ranging from 0.04 to 0.10 cations p.f.u. (0.41 to 0.94 wt% TiO_2), is lower than that in all the biotites. The Ti content of biotite from sulfide iron formation type I ranges from 0.28 to 0.34 cations p.f.u. (2.5 to 2.9 wt% TiO_2), with an average value of 0.32, which is the highest among biotites in this study. Biotite in silicate-facies banded iron formation contains 0.14 to 0.24 cations p.f.u. (1.2 to 2.0 wt% TiO_2) with an average value of 0.20. The Ti content of biotite in ore type I (Ni ore) ranges from 0.20 to 0.32 cations p.f.u. (1.75 to 2.69 wt% TiO_2) with 0.22 cations on average. The Ti content of biotite in ore type II (PGM-Au-rich Ni ore) ranges from 0.14 to 0.28 cations p.f.u. (1.2 to 2.3 wt% TiO_2) with 0.22 cations on average. Biotite in ore type IV (pegmatite hosted PGM-rich Ni ore) contains Ti of 0.26 cations p.f.u. (2.3 wt% TiO_2).

5.5 Talc

In this study talc has been identified in strongly altered ultramafic rocks (probably metapyroxenite or metaperidotite). The ultramafic rocks occur as the

Fig. 5.9 Titanium contents of Thompson mine biotite

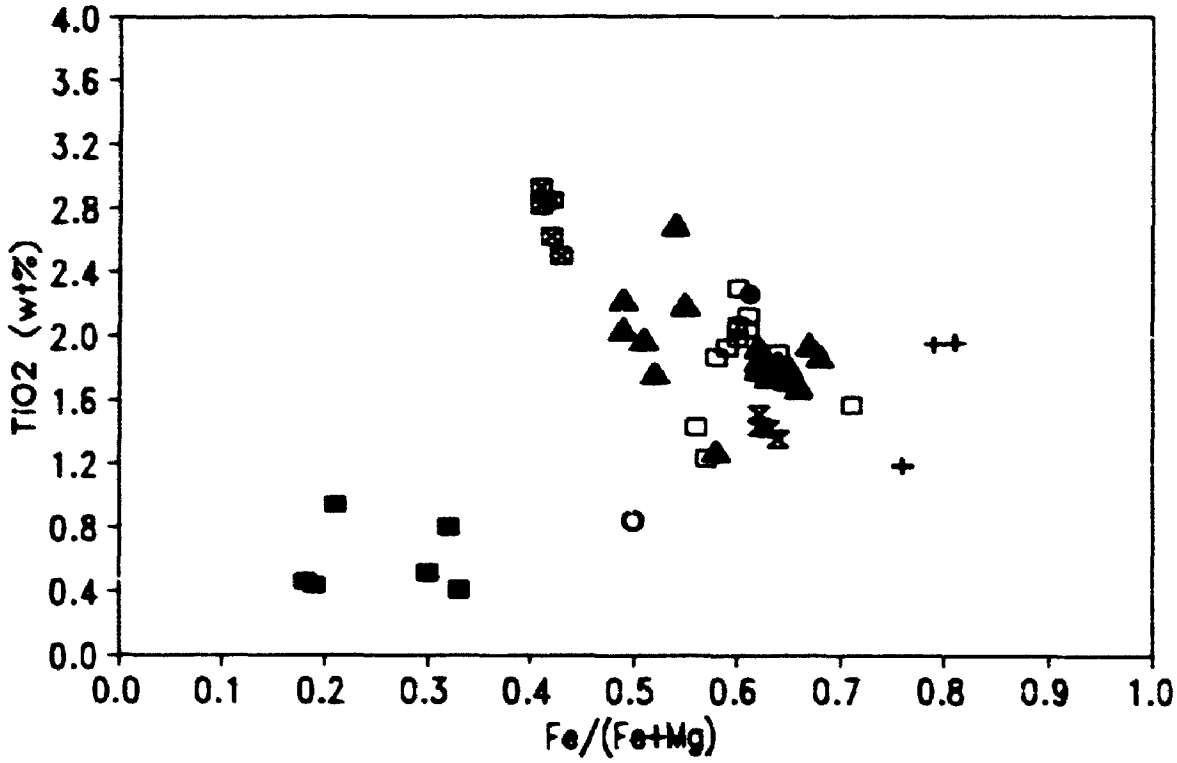
4.0
3.6
3.2
2.8
2.4
2.0
1.6
1.2
0.8
0.4
0.0
TiO2 (wt%)
0.0
0.1
0.2
0.3
0.4
0.5
0.6
0.7
0.8
0.9
1.0
Fe/(Fe+Mg)
ore type I
ore type II
ultramafic rocks
HIF
sulfide IF-I
sulfide IF-II
ore type III
ore type IV

footwall of the nickel orebody and as inclusions in the Ni-Fe sulfide matrix. Massive talc has been found associated with chlorite, spinel, phlogopite and amphiboles. Ferrous talc has a similar composition to minnesotaite. Evans and Guggenheim (1988) suggested that only X-ray diffraction analysis could distinguish ferrous talc from minnesotaite. However, these two minerals have distinctly different parageneses. Minnesotaite is usually limited to very low-grade Fe-rich metasediments. A few occurrences of Mn-rich minnesotaites have also been reported in hydrothermal deposits developed in limestone and marbles (Oen et al., 1975; Kager and Oen, 1983). Minnesotaite has not been reported from ultramafic rocks. The formation of talc in ultramafic rocks is attributed to the introduction of SiO_2-saturated, frequently CO_2-bearing fluid (Evans and Guggenheim, 1988). The close association of talc with carbonate minerals in the study area also supports this interpretation.

Electron microprobe analyses of talc are given in Appendix V. The formulae were calculated on the basis of 22 oxygens. The data show that the talc is dominated by MgO, with small amounts of FeO. Minor amounts of Al_2O_3 (up to 1.1 wt% and 0.18 p.f.u.), Cr_2O_3 (up to 0.1 wt% and 0.02 p.f.u.), MnO (up to 0.2 wt% and 0.02 p.f.u.), Na_2O (0.3 wt% and 0.08 p.f.u.) and Cl (up to 0.1 wt%) have been detected.

Talc usually has the end-member composition ($Mg_3Si_4O_{10}(OH)_2$). Wet chemical and electron microprobe analyses of talc from metamorphosed ultramafic rocks in the literature reveal that most talc compositions fall in the

range 1-4 mol% Fe-talc end-member (cf., summary by Evans and Guggenheim, 1988). However, the composition of talc in ultramafic rocks from the Thompson mine shows more extensive Fe^{2+} substitution (up to 0.52 Fe^{2+} cation per 3 octahedral sites). The composition of talc ranges from 4 to 16 mol% Fe-talc end-member (2.20-8.85 wt% FeO), with an average value of 10 mol% Fe-talc. Most of the talc compositional data fall in the range of 8-12 mol% of Fe-talc component.

It has been reported that talc formed in a hydrothermal environment is distinctly Fe-rich. For instance, Fe-rich talc has been recognized along with Fe-sulfide as a chemical precipitate in a modern submarine hydrothermal environment (Guaymas Basin, the Gulf of California), where Lonsdale et al. (1980) reported 19-25 mol% of Fe-talc component, and Koski et al. (1985) reported 7.5 mol% of Fe-talc component. Also in massive sulfide deposits, such as the Mattagami Lake deposit within the Archean Abitibi greenstone belt in Quebec, talc contains 5 to 34 mol% of Fe-talc end-member (Costa et al., 1983). From the above discussion, it is suggested that the formation of the ferrous talc in the present study may indicate the introduction of a SiO_2-Fe-rich fluid during the proposed hydrothermal alteration related to Ni-mineralization.

5.6 Hisingerite

Hisingerite is a hydrous oxidised sheet silicate mineral of uncertain structure and classification. In the present study, hisingerite has been found in

extensively altered ultramafic rocks (probably originally metaperidotite or metapyroxenite). In the literature, hisingerite is frequently reported associated with hydrothermal Cu, Ni, Zn, Pb and U deposits (Sudo and Nakamura, 1952; Osborn and Archambault, 1950; Aplonov and Sereda, 1983; Ludwig et al., 1981). In these occurrences, hisingerite is an alteration product derived variously from hypersthene (Schwartz, 1924), stilpnomelane (Ioan et al., 1974), pyrrhotite and other iron minerals (Sudo and Nakamura, 1952), diopside, and siderite (Osborn and Archambault, 1950), and is also found in late hydrothermal veins (Ludwig et al., 1981; Aplonov and Sereda, 1983). In Fe-rich gabbroic rocks hisingerite has been reported as an alteration product of either olivine (Lebedev, 1936) or Fe-Mn wollastonite (Nel'nitskaya, 1967). Hisingerite also occurs in altered rhyolitic tuffs, in which it is derived from Fe-rich saponite (Kohyama and Sudo, 1975). Thus, the Thompson mine occurrence is the first record of hisingerite associated with ultramafic rocks.

In the ultramafic rocks at the Thompson mine, hisingerite occurs together with carbonate minerals as micro-veinlets cross-cutting chlorite, talc, etc. (Plate 3K). This probably indicates formation in the latest alteration event, similar to that reported from the Talnakh Cu-Ni deposits, Russia (Aplonov and Sereda, 1983), where hisingerite occurs in post-ore cross-cutting veins, together with quartz, carbonates, pyrite, pyrrhotite and galena.

In transmitted light, hisingerite is brownish red and isotropic. The X-ray power diffraction (XRD) pattern of the hisingerite obtained with a Gandoffi

camera (CrKα radiation) reveals broad and diffuse lines corresponding to d_{hkl}-spacings of 7.46, 5.45, 4.36, 3.50, 2.59 and 1.54 Å, in good agreement with hisingerite reported in the literature (Table 5.1).

Representative electron microprobe analyses of hisingerite are given in Table 5.2. FeO was recalculated to Fe_2O_3 since most hisingerite in the literature is oxidized and contains less than 1.0 wt% FeO.

Since hisingerite is a very poorly crystalline (semi-amorphous) hydrous iron silicate of variable composition, its structural formula is rather controversial. It has been considered variously to have a nontronite structure (Gruner, 1934; Sudo and Nakamura, 1952; Bowie, 1955), an Fe-rich saponite structure (Whelan and Goldich, 1961; Kohyama and Sudo, 1975) and even a mica structure (Lindgvist and Jansson, 1962). Kohyama and Sudo (1975) suggested that hisingerite has a chemical composition variable between a trioctahedral Fe-rich saponite and a dioctahedral nontronite.

Clark et al. (1978) considered hisingerite to be the Fe-rich end-member of the solid solution series between $MnSiO_3 \bullet H_2O$ and $FeSiO_3 \bullet H_2O$. Hisingerite from Balan, Romania gives a formula of $Fe_2Si_2O_5(OH)_4 \bullet 2H_2O$ (Marza et al., 1974). Brigatti (1982) concluded that there is a structure-composition continuity between Fe-rich saponite and hisingerite corresponding to a hypothetical series of (Mg, Fe^{2+}) saponites in which the Fe^{2+} is subsequently oxidized to Fe^{3+}. Eggleton et al. (1983) and Val'ter et al. (1988) gave two more, different empirical formulae for hisingerite from Broken Hill, Australia ((Fe,

Table 5.1 X-ray diffraction patterns of hisingerite

1		2		3		4		5	
d(Å)	I	d(Å)	I	d(Å)	I	d(Å)	I	d(Å)	I
7.46	s	7.53	w						
5.45	w								
4.36	w	4.33	w	4.39	s	4.40	s	4.40	s
3.50	w	3.50	w	3.58	s	3.55	s	3.55	s
2.59	s	2.55	w	2.57	s	2.58	s	2.56	s
				1.71	w	1.70	w	1.70	w
1.54	w	1.54	w	1.54	s	1.53	s	1.53	s
		1.21	w						

1. This study.
2. East Mesabi (Whelan and Goldich, 1961).
3. Langanshyttan, Sweden (Bowie, 1955).
4. Nicholson Mine, Saskatchewan (Bowie, 1955).
5. Blaine County, Idaho (Bowie, 1955).

s=strong intensity, w=weak intensity.

$Mn)_{0.85}SiO_{3.25}\bullet 2H_2O$) and the Terrovage astrobleme, former USSR [$(Ca_{0.04}Na_{0.02}K_{0.01})(Fe^{3+}_{1.33}Mg_{0.50}Al_{0.08}Fe^{2+}_{0.06})SiO_2O_{5.88}(OH)_{2.02}\bullet 2.16H_2O$], respectively.

In this study, the smectite structure was adopted for hisingerite because it is relatively popular in the literature. Therefore, the electron microprobe data were calculated based on 11 oxygens (Table 5.2).

Aplonov and Sereda (1983) studied a hisingerite-quartz vein in the Talnakh Cu-Ni deposits, Russia, and estimated the formation temperature of hisingerite to be 120-140°C, based on decrepitation of fluid inclusions in the associated quartz.

In summary, the occurrence of hisingerite-carbonate veinlets at the Thompson mine indicates a late metamorphic event of oxidizing conditions and low temperature in the ultramafic rocks.

5.7 Ferropyrosmalite

Pyrosmalite was originally established as a mineral species (Zambonini, 1901; Dana, 1920; Frondel and Baner, 1953), but presently refers to the solid solution series $(Mn,Fe)_8Si_6O_{15}(OH,Cl)_{10}$, including the end-members manganpyrosmalite and ferropyrosmalite (Vaughan, 1987).

Although pyrosmalite was originally thought to be exceedingly rare, it has since been observed with increasing frequency in base-metal associated localities worldwide, including Sterling Hill, New Jersey; Broken Hill,

Table 5.2 Electron microprobe analyses of hisingerite

No.	1 TS24	2 TS24	3 TS24	4 TS29
SiO_2	41.88	40.79	41.33	40.89
TiO_2	0.00	0.04	0.06	0.00
Al_2O_3	0.24	1.34	1.49	0.08
Cr_2O_3	0.01	0.06	0.01	0.00
MnO	0.34	0.35	0.35	0.30
Fe_2O_3	41.38	39.43	39.14	40.92
MgO	6.00	5.95	6.27	5.95
V_2O_3	0.00	-	-	0.00
CaO	-	1.55	1.54	-
NiO	0.21	0.00	0.00	0.00
K_2O	0.04	0.19	0.18	0.28
Na_2O	0.00	0.03	0.08	0.12
F	0.20	0.10	0.12	0.23
Cl	0.07	0.01	0.01	0.01
F,Cl=O	0.10	0.04	0.05	0.10
total	90.27	89.79	90.53	88.68
	ions on the basis of 11 oxygen			
Si	3.28	3.22	3.22	3.27
Ti	0.00	0.00	0.00	0.00
Al	0.02	0.12	0.14	0.01
Cr	0.00	0.00	0.00	0.00
Mn	0.02	0.02	0.02	0.02
Fe^{3+}	2.44	2.34	2.30	2.46
Mg	0.70	0.70	0.73	0.71
V	0.00	-	-	0.00
Ca	-	0.13	0.13	-
Ni	0.01	0.00	0.00	0.00
K	0.00	0.02	0.02	0.03
Na	0.00	0.01	0.01	0.02
F	0.05	0.03	0.03	0.06
Cl	0.01	0.00	0.00	0.00

Australia; Geco mine, Ontario, etc. (Frondel and Bauer, 1953; Vaughan, 1986; Pan and Fleet, 1992). Ferropyrosmalite resembles white mica in transmitted light. It was observed and confirmed by electron microprobe analyses at the Thompson mine, in one sample of silicate-facies banded iron formation (BIF) that was collected within the footwall and 3 to 15 meters below the nickel sulfide orebodies. Two distinct textural varieties of ferropyrosmalite are present. Firstly and more commonly, ferropyrosmalite occurs as aggregates with grunerite, quartz and pyrrhotite after ferrosilite. Although replacement along or parallel to the cleavage of ferrosilite is observed locally, most aggregates occur around grain boundaries and show no preferred crystallographic orientation to the host ferrosilite. Secondly, ferropyrosmalite is also present in association with pyrrhotite as cross-cutting veins (Plate 3H).

Electron microprobe analyses of ferropyrosmalite and associated silicates (ferrisilite, grunerite and biotite) are given in Table 5.3. Most pyrosmalite analyses in the literature have a Mn/(Fe+Mn) atomic ratio ranging from 0.41 to 0.85. An Fe-rich end-member with Mn/(Fe+Mn)=0.08 was described only recently from the Pegmont mine, Australia (Vaughan, 1986). The two texturally distinct varieties of ferropyrosmalite in BIF of the Thompson mine show no distinct compositional difference and have an Mn/(Fe+Mn) ratio ranging from 0.10 to 0.15, which is similar to that of the most Fe-rich end-member from the Pegmont mine (Vaughan, 1986). The Cl content of the ferropyrosmalite ranges from 3.14 to 4.87 wt%. Biotite and grunerite coexisting with ferropyrosmalite

Table 5.3 Electron microprobe analyses of pyrosmalite and its associated minerals

	ferrisilite	grunurite	biotite	pyrosmalite	
				1	2
			wt%		
SiO_2	47.10	50.16	33.29	34.12	34.48
TiO_2	0.08	0.00	1.68	0.00	0.11
Al_2O_3	0.39	1.12	16.36	0.24	0.24
Cr_2O_3	0.01	-	-	0.04	0.05
MnO	1.85	1.50	0.22	7.04	5.76
FeO*	46.48	36.29	32.31	46.77	46.73
MgO	4.27	7.42	3.73	0.54	0.58
ZnO	-	-	-	0.00	-
CaO	0.26	0.03	0.08	0.03	0.09
Na_2O	0.01	0.45	0.07	0.02	0.03
K_2O	0.01	0.10	8.91	0.01	0.12
F	0.00	0.00	0.48	-	-
Cl	0.00	0.20	0.19	4.87	3.17
H_2O^{**}	-	-	-	7.35	7.77
O=F,Cl	-	0.05	0.26	1.10	0.71
Total	100.46	97.22	97.06	99.93	98.42
			structural formulae		
Si	1.99	7.93	5.36	5.95	6.02
Ti	-	0.01	0.20	-	-
^{IV}Al	0.01	0.07	2.64	0.05	0.00
^{VI}Al	0.01	0.14	0.46	0.01	0.06
Cr	0.00	-	-	0.00	0.02
Fe	0.00	4.79	3.25	6.81	6.82
Mg	1.65	1.79	0.89	0.14	0.16
Mn	0.27	0.20	0.03	1.04	0.86
Zn	0.07	-	-	0.00	-
Ca	-	0.00	0.01	0.00	0.01
Na	0.01	0.14	0.02	0.00	0.01
K	0.00	0.02	1.83	0.00	0.02
F	-	0.00	0.24	-	-
Cl	0.00	0.05	0.05	1.44	0.94
OH	-	-	-	8.56	9.06

* total iron content as FeO; ** H_2O calculated from OH=(10-Cl).
1. in cross-cutting vein;
2. replacing ferrosilite.

also contain minor Cl content (Table 5.3).

5.8 Garnet

Garnet occurs in sillimanite-garnet schist, silicate-facies banded iron formation and sulfide iron formation type II in the Thompson mine. Electron microprobe analyses of garnet are given in Appendix VI. Structural formulae have been calculated on the basis of cation stiochiometry (8 cations) and Fe^{3+} was calculated assuming charge balance. The electron microprobe analyses show that the garnet in this study is dominated by almandine component, which ranges from 59 to 84 mol%, with corresponding FeO content from 26.55 to 36.88 wt%. The Fe_2O_3 content calculated from charge balance is generally low, with a maximum value of 1.0 wt% in the garnet from the oxide iron formation, corresponding to 3 mol% of andradite component. Other end-members include spessartine (4-16 mol%, MnO 1.5-7.2 wt%), pyrope (2-20 mol%, MgO 0.6-4.9 wt%), and grossular (2-17 mol%, CaO 1.0-6.7 wt%). The contents of TiO_2 and Cr_2O_3 are relatively low with a maximum value of 0.08 wt% for both components. The electron microprobe investigation shows that the garnet in the present study is homogeneous, and without any zoning.

The composition of garnet varies in different host rocks (ores). The electron microprobe data are plotted on a Fe^{2+}-Mg-Ca ternary diagram (Fig. 5.10), which shows the variation of almandine component. Garnet in silicate-facies banded iron formation is most enriched in Fe^{2+} with 83 mol% of

Fig. 5.10 Compositions of Thompson mine garnet in Fe^{2+}-Mg-Ca system. Solid triangle = ore type I, hour glass = sulfide iron formation type II, cross = BIF.

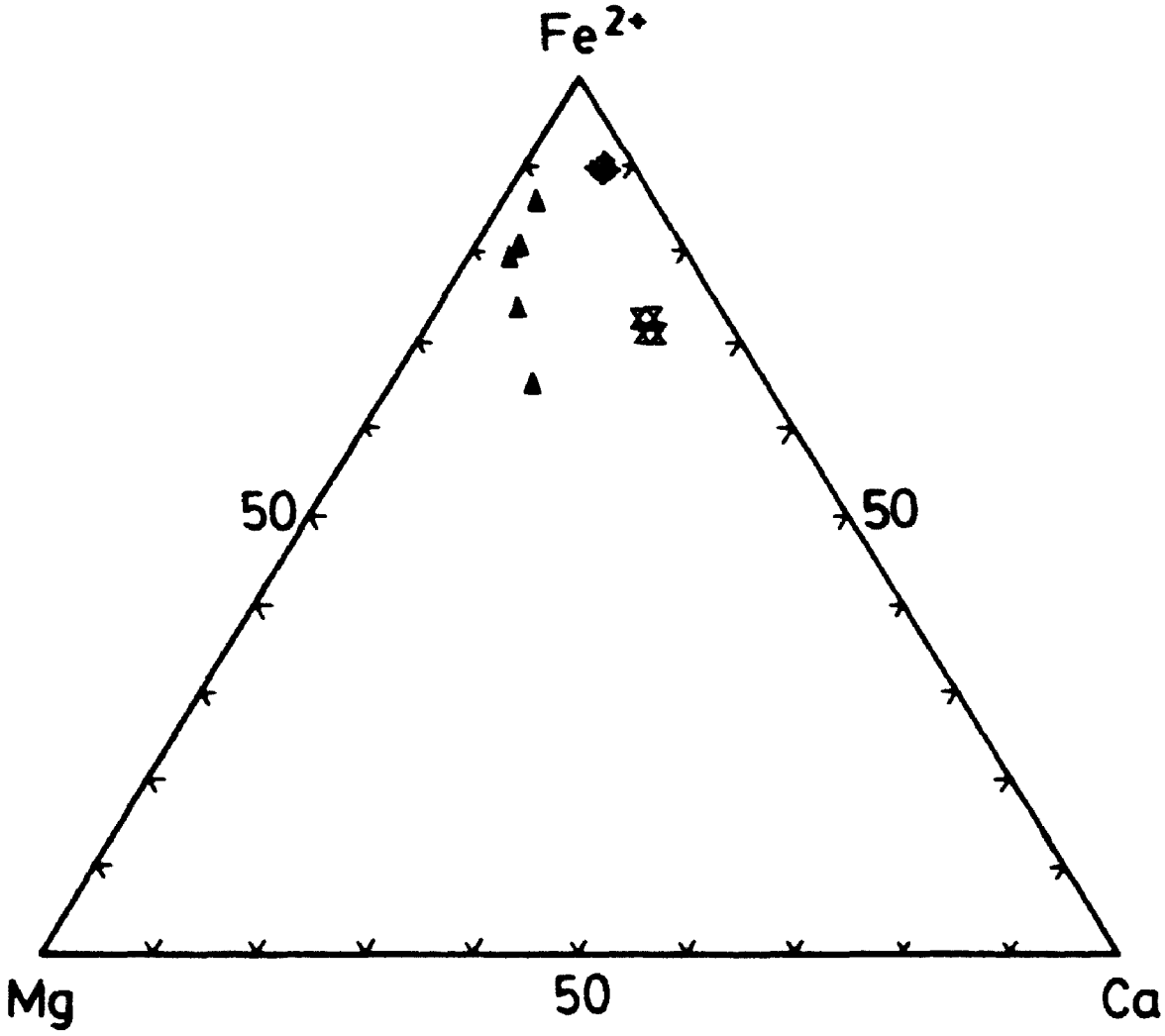
Fe2+
50
50
Mg
50
Ca

almandine (FeO 35.5 wt%) on average. Garnet in sulfide iron formation type II contains only 64 mol% of almandine (FeO 28.7 wt%). The FeO contents of garnet in garnet-sillimanite schist, which occurs as host or inclusions in Ni-ore (ore type I), vary from 26.6 to 36.9 wt% FeO (59-83 mol% of almandine). From this diagram one can also see that garnet from both iron formations contains less Mg than the Ni-ore.

The compositional variation in garnet from different rocks and ore types is also represented by a Mn-Mg-Ca ternary diagram (Fig. 5.11) It is apparent that garnet in sulfide iron formation type II is relatively Ca-rich, garnet in oxide iron formation is Mn-rich and garnet in ore type I (garnet-sillimanite schist) is relatively Mg-rich.

5.9 Amphibole

Among the samples examined in this study, amphibole occurs in silicate-facies banded iron formation, sulfide iron formation type II and strongly altered ultramafic rocks. Electron microprobe analyses of the amphibole in different types of rocks from the Thompson mine are given in Appendices VII and VIII. Structural formulae were calculated on the basis of 23 oxygen, assuming total iron as FeO. According to Leake's (1978) classification, the amphiboles in the present study belong to calcic amphibole and Fe-Mg amphibole groups.

The silicate-facies banded iron formation in the study area contains only Fe-Mg amphibole, i.e., grunerite-cummingtonite, replacing ferrosilite in

Fig. 5.11 Compositions of Thompson mine garnet in Mn-Mg-Ca system. Solid triangle=ore type I, hour glass=sulfide iron formation type II, cross=BIF.

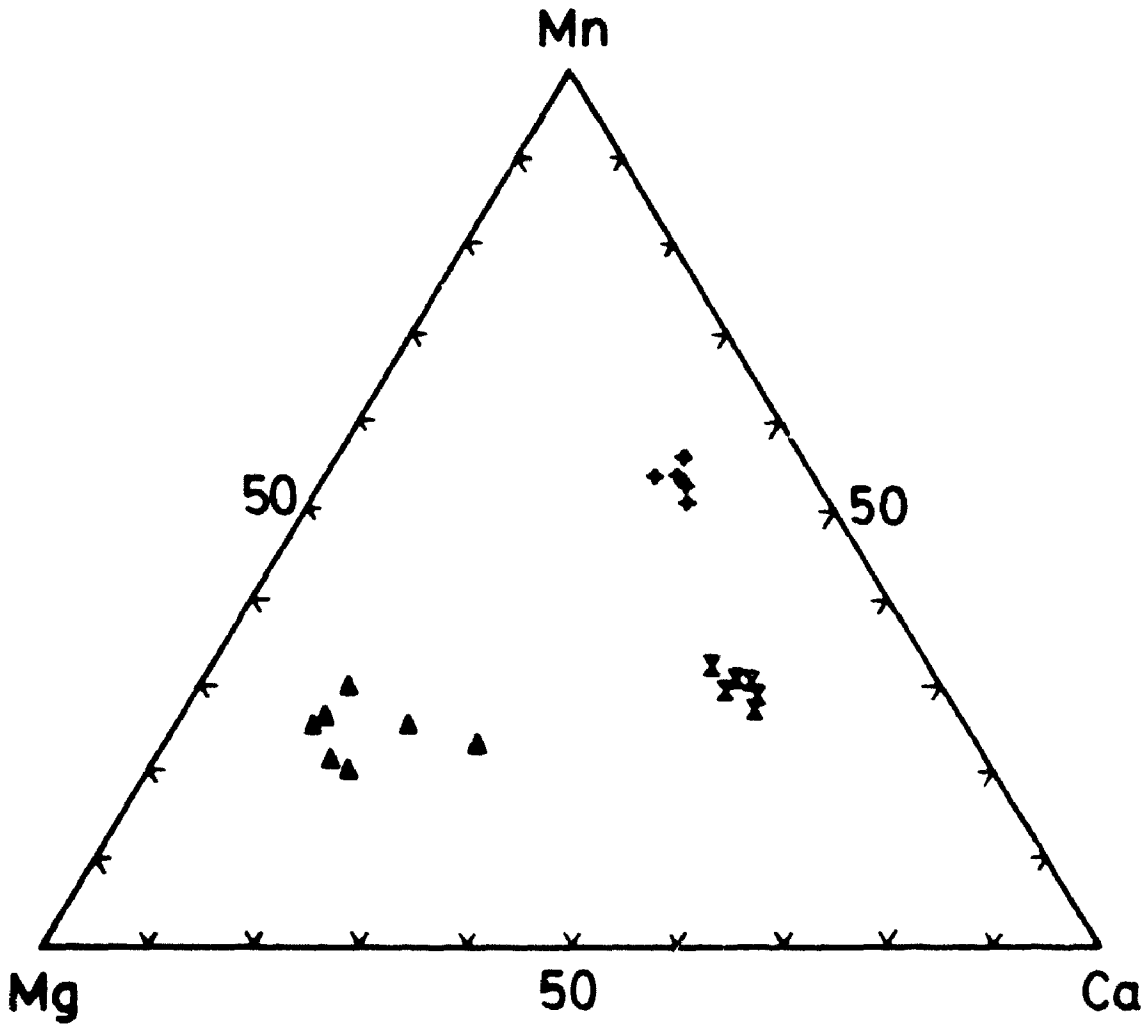
Mn
50
50
Mg
50
Ca

association with garnet, biotite, quartz, ferropyrosmalite and magnetite. The sulfide iron formation type II contains both primary calcic amphibole (ferro-hornblende) and Fe-Mg amphibole (cummingtonite), associated with garnet, biotite, quartz and pyrrhotite. Also both secondary calcic amphibole (tremolite (actinolite)-tschermakite) and Fe-Mg amphibole (magnesio-cummingtonite) occur in the strongly altered ultramafic rocks (probably metapyroxenite or peridotite), in association with talc, serpentine, clinochlore, phlogopite, hisingerite, spinel, and carbonate minerals.

5.9.1 Fe-Mg amphibole

Grunerite has been identified only in silicate-facies banded iron formation with Mg/(Mg+Fe) ratio ranging from 0.08 to 0.17. Cummingtonites from sulfide iron formation type II and silicate-facies banded iron formation have similar Mg/(Mg+Fe) ratios (0.38 and 0.37, respectively). Magnesio-cummingtonite in ultramafic rocks has the highest Mg/(Mg+Fe) ratio, ranging from 0.78 to 0.81, reflecting the Mg-rich nature of the host rocks. The magnesio-cummingtonite in the ultramafic rocks also contains more Cr_2O_3 (up to 0.2 wt%) than the Fe-Mg amphibole from other rocks in the Thompson mine.

In the Fe-Mg amphibole group, grunerite contains more MnO than cummingtonite, reflecting the general correlation of Mn with Fe. In silicate-facies banded iron formation grunerite contains MnO up to 1.7 wt% whereas

cummingtonite contains only up to 0.3 wt%. However, in sulfide iron formation type II, cummingtonite contains MnO up to 1.3 wt%. In the ultramafic rocks cummingtonite contains MnO up to only 0.5 wt%, which can be attributed to the lower content of Mn in the host rocks.

The TiO_2 content of the Fe-Mg amphibole is low, only up to 0.1 wt%. The contents of Al_2O_3, K_2O and Na_2O are up to 5.5, 0.2, 0.2 wt%, respectively. The Cl content is very low with a maximum value of 0.1 wt%.

Grunerite-cummingtonite is very common in iron formation, whereas in igneous rocks, the only member of the Fe-Mg amphibole group known to occur is cummingtonite, and it is rare. All such occurrences are in silicic volcanic rocks except the one in amphibole-rich diorite (Seitsaari, 1956; Klein, 1968) and several reported by Hall (1975) in Eocene hypabyssal intrusions. Therefore, the colorless magnesio-cummingtonite found in altered ultramafic rocks is probably secondary in origin.

5.9.2 Calcic amphibole

5.9.2.1 Mg/(Mg+Fe) and Si

The Mg/(Mg+Fe) ratio of calcic amphibole in the present study permits us to distinguish two major groups of amphibole, Mg-amphibole from strongly altered ultramafic rocks and Fe-amphibole in sulfide iron formation type II. According the classification of Leake (1978), the Fe amphibole is ferro-

hornblende, and the Mg-enriched amphibole falls in the interval of composition between tremolite (actinolite) and tschermakite end-members (Fig. 5.12).

The calcic amphibole in the strongly altered ultramafic rocks has a higher Mg/(Mg+Fe) ratio than the amphibole in the sulfide iron formation type II, for which Mg/(Mg+Fe)=0.40. In ultramafic rocks, actinolite is colorless, and has a relatively lower Mg/(Mg+Fe) ratio of 0.76, tremolite, tremolitic hornblende and magnesio-hornblende are also colorless, and have similar Mg/(Mg+Fe) ratios, ranging from 0.87 to 0.94.

The Si content of the calcic amphibole in the ultramafic rocks ranges from 7.96 to 6.91 p.f.u., corresponding to variation of mineral species from actinolite, tremolite, tremolitic hornblende, to magnesio-hornblende.

5.9.2.2 Na and K

In contrast with magmatic calcic amphibole, metamorphic calcic amphibole is usually characterized by low contents of Na and K. The contents of Na and K in the calcic amphibole of this study are very low, ranging only from 0.01 to 0.49 p.f.u. On a Al(IV)-(Na+K) diagram (Fig. 5.13), the data fall in the field of metamorphic amphiboles defined by Jamieson (1981).

5.9.2.3 ^{IV}Al and ^{VI}Al

The Al content of calcic amphiboles has been used as an indicator of metamorphic grade. Raase (1974) plotted calcic amphibole compositions from

Fig. 5.12 Compositions of Thompson mine calcic amphibole in Mg/(Mg+Fe)-Si system. Classification and nomenclature are after Leake (1978). TH=tremolitic hornblende, AH=actinolitic hornblende, FAH=ferroactinolitic hornblende

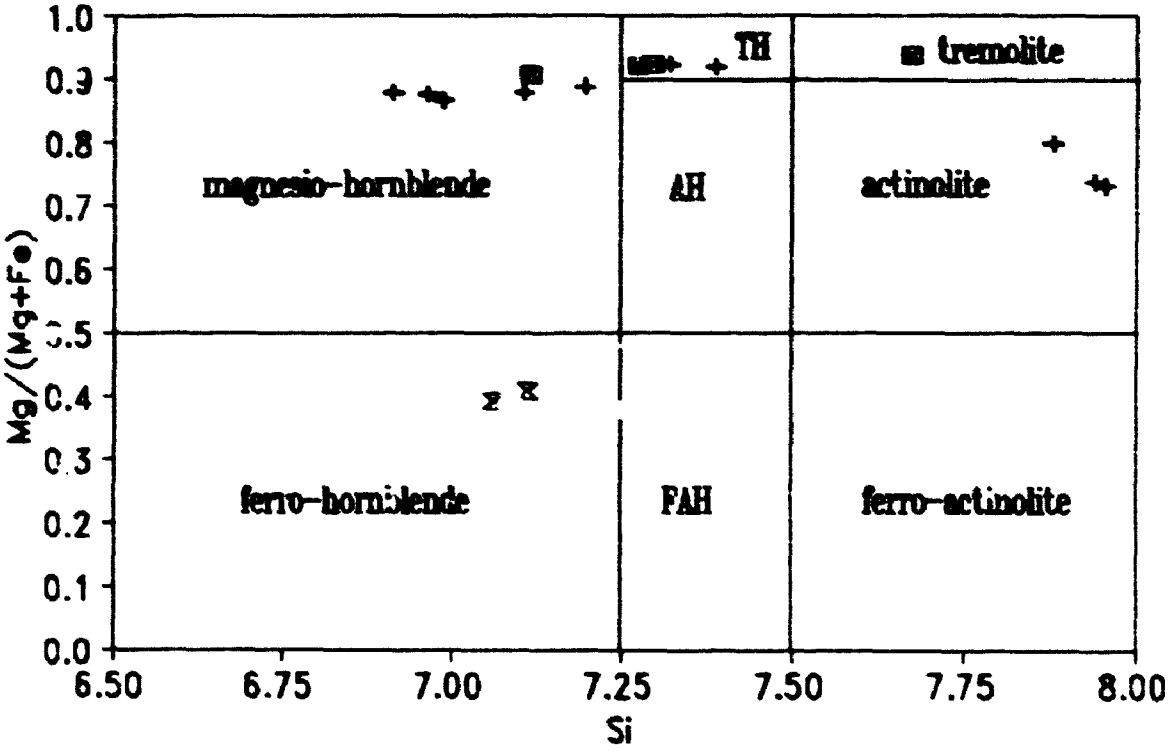

+ metapyroxenite ▣ peridotite ⧗ sulfide IF-II

Fig. 5.13 Compositions of Thompson mine calcic amphibole in ^{IV}Al-Na+K system.

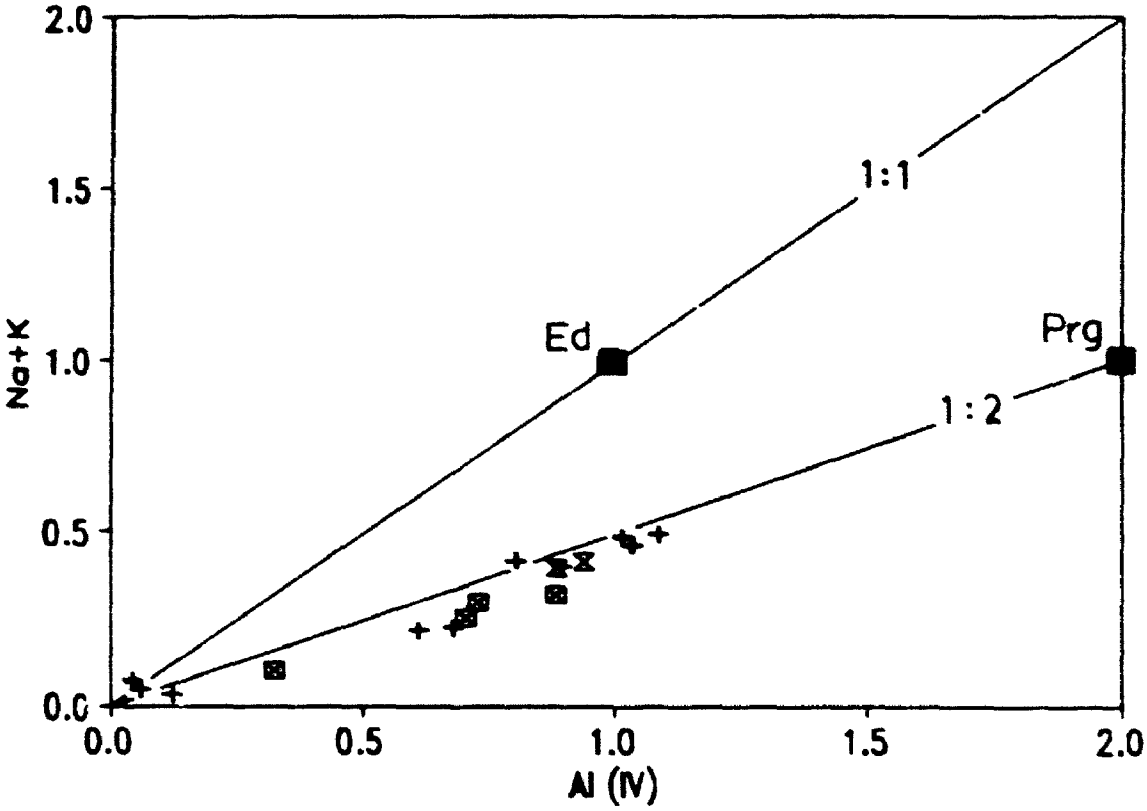

+ metapyroxenite ⊠ peridotite ⧗ sulfide IF-II

some well-characterized regional metamorphic terrains on a Si-Al(VI) diagram. Combined with the maximum possible Al(VI) content of the calcic amphibole given by Leake (1965), the diagram permits a distinction between calcic amphibole of low-pressure type (<5 kbar), which has low Si and Al(VI) contents, and high pressure type (>5 kbar). In the Al(VI)-Si diagram (Fig. 5.14), the amphibole in ultramafic rocks from the Thompson mine plot below the 5 kbar line, whereas the calcic amphibole in sulfide iron formation type II plot above the 5 kbar line.

Fleet and Barnett (1978) suggested that Al(VI) increases with pressure and that Al(IV) is temperature dependent. However, they pointed out that the introduction of Fe^{3+} in the lattice may limit the quantitative application of this relationship and caution has to be exercised when interpreting the compositional variations of the Fe-enriched amphiboles in Fe-Ti gabbros. Since calcic amphibole in the ultramafic rocks in this study is Mg-rich, and calcic amphibole in sulfide iron formation type II is only moderately Fe-enriched. The Al(IV)-Al(VI) diagram still can be used. In the diagram, Fleet and Barnett (1978) defined the field of metamorphic amphibole from unaltered igneous amphibole by Al(IV)/Al(VI)<3. All the data in this study fall in the field of metamorphic amphibole (Fig. 5.15).

5.9.2.4 Mn, Cr and Ti

The MnO content of the calcic amphibole in this study ranges from 0.01

Fig. 5.14 Compositions of Thompson mine calcic amphibole in Si-^{VI}Al system, illustrating their formation pressure (after Raase, 1974).

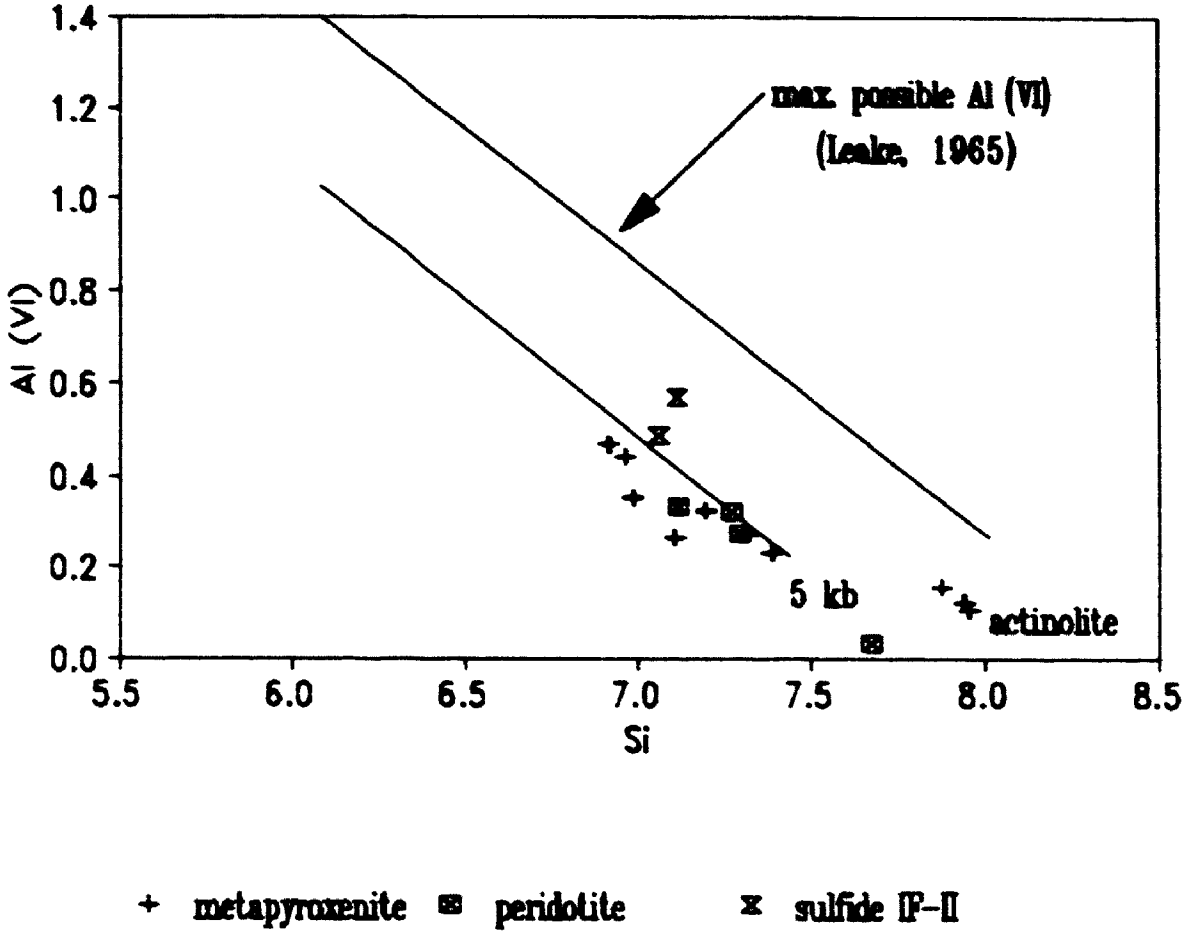
1.4
1.2
1.0
0.8
0.6
0.4
0.2
0.0
Al (VI)
5.5
6.0
6.5
7.0
7.5
8.0
8.5
Si
max. possible Al (VI)
(Leake, 1965)
5 kb
actinolite
metapyroxenite
peridotite
sulfide IF-II

Fig. 5.15 ^{IV}Al and ^{VI}Al contents of calcic amphibole from the Thompson mine. According to Fleet and Barnett (1978) field of unaltered igneous calciferous amphibole defined by $^{IV}Al/^{VI}Al \geq 3.3$; solid line with $^{IV}Al/^{VI}Al = 2.0$ approximates the 5 kbar boundary of Raase (1974); field of low-pressure metamorphic hornblende defined by $^{IV}Al/^{VI}Al > 2.0$; field of high-pressure metamorphic hornblende defined by $^{IV}Al/^{VI}Al < 2.0$.

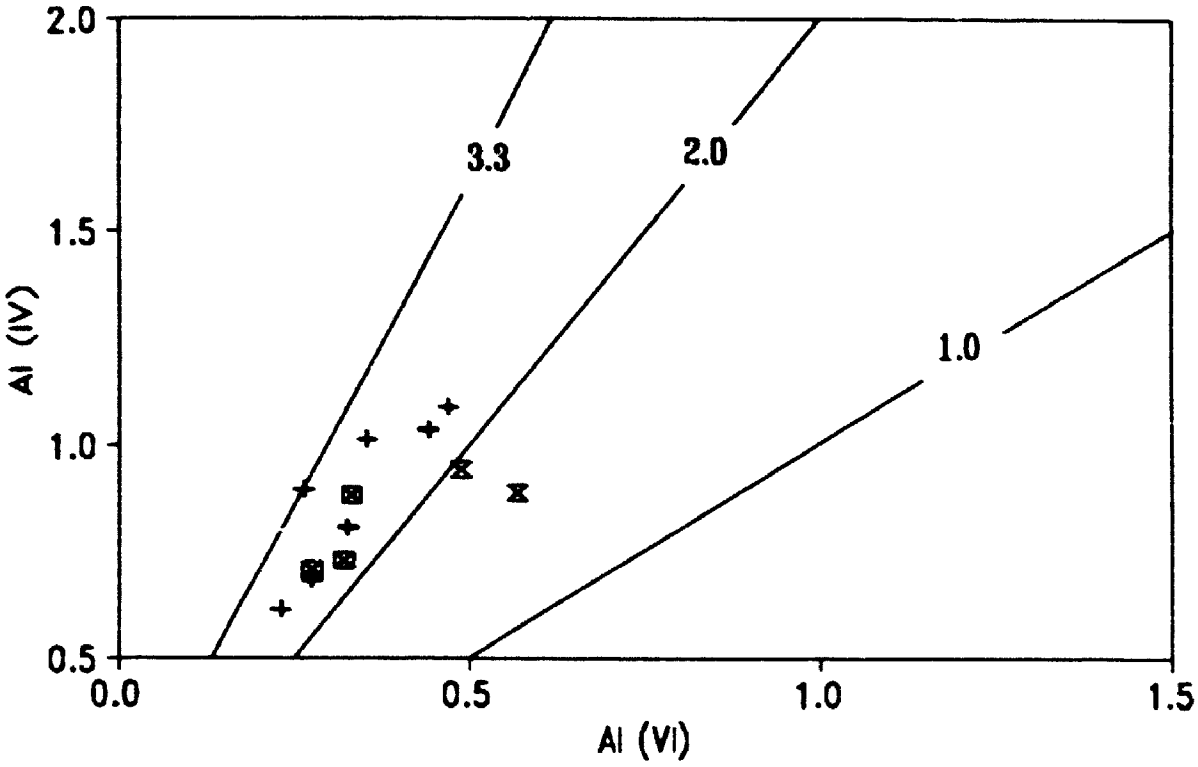

+ metapyroxenite ⊠ peridotite ⧗ sulfide IF-II

wt% in tremolitic hornblende to 0.8 wt% in actinolite. Magnesio-hornblende contains the highest Cr_2O_3 (up to 0.9 wt%) whereas ferro-hornblende contains the lowest Cr_2O_3 (0.01 wt%).

The Ti content of calcic amphibole has been used also as an indicator of metamorphic grade because it increases with temperature. Raase (1974) summarized the Ti content of calcic amphiboles from rocks of different metamorphic facies. In his histogram, the Ti content of calcic amphibole in epidote- amphibolite facies ranges from 0.02 to 0.08 p.f.u., with an average value of 0.05. The Ti content in calcic amphibole from the Thompson mine is very low, ranging from 0.01 to 0.05, with an average value of 0.03. The low Ti content indicates a greenschist to lower epidote-amphibolite facies metamorphic event for the ultramafic rocks.

5.10 Feldspar

5.10.1 K-feldspar

Based on samples investigated in this study, K-feldspar present in pegmatite hosted PGM-Au ore (ore type IV) is microcline on the basis of commonly occurring cross-hatched twinning. Orthoclase is present in metapelite hosted ores (ore types I, II and III). Electron microprobe analyses of the two K-feldspars are given in Appendix IX. The Na_2O content of microcline is up to

1.0 wt% whereas Na_2O content of the K-feldspar in ore types I, II and III is up to 0.2 wt%.

5.10.2 Plagioclase

Electron microprobe analyses of plagioclase are given in Appendix X. Plagioclase in sulfide iron formation type I ranges from oligoclase (An25) to andesine (An36), with K_2O up to 0.2 wt%. Oligoclase also occurs in pegmatite hosted PGM-Au-Ni ore (ore type IV) and metapelite rocks with average compositions of An25 and An29, respectively, and K_2O contents up to 0.5 wt% and 0.2 wt%, respectively.

In metapelite hosted Ni-ore (ore type I), albite (An2 with K_2O not detectable) replaces oligoclase (An26 with K_2O 0.2 wt%) along fractures. In metapelite-hosted PGM-Au-Ni ore (ore type II), oligoclase is completely replaced by albite (An0.27 with K_2O up to 0.3 wt%). Zoning of plagioclase is not pronounced in all four ore types. The maximum variation observed from core to margin is An30 to An27.

Oligoclase and/or andesine in metapelite rocks and sulfide iron formation type I are relatively fresh, whereas both oligoclase and albite in Ni-ore and PGM-Au-Ni ore are extensively altered to sericite and carbonates.

5.11 Carbonate Minerals

Based on samples examined in this study, carbonate minerals occur in

metapelite-hosted ore type II (PGM-Au-Ni ore) and ore type III (Au-Ni ore), and extensively altered ultramafic rocks. In ore type II, calcite occurs as micro-bands in-between the wall rock of metapelite containing disseminated sulfides and the late massive gersdorffite-nickeline veins in which PGMs and gold are enriched. Therefore, the precipitation of these calcite bands is probably associated with the hydrothermal processes related to PGM-Au mineralization. In ore type III siderite, containing 0.1 wt% Cr_2O_3, 0.2 wt% MnO and 0.1 wt% MgO, occurs in association with other secondary alteration minerals, such as muscovite and chlorite.

Dolomite ($Ca_{1.1}Mg_{0.9}Fe_{0.04}(CO_3)_2$) in association with talc and serpentine occurs in ultramafic rocks and also attributable to the hydrothermal alteration.

5.12 Spinel

Spinel occurs as an accessory mineral in ultramafic rocks, metapelite hosted Ni-ore (ore type I) and Au-Ni ore (ore type III). Electron microprobe analyses show that spinels from the Thompson mine are solid solutions of spinel ($MgAl_2O_4$)-chromite ($FeCr_2O_4$)-hercynite ($FeAl_2O_4$). In the ultramafic rocks, spinel is mainly composed of spinel-chromite solid solutions, whereas in metapelite-hosted Ni-ore and Au-Ni ore, the spinel compositions are close to the hercynite-chromite join. All the spinels are ZnO bearing, except those in unaltered peridotite (Figs. 5.16, 5.17). Unlike those spinels in metamorphosed peridotite reported in the literature (Beeson and Jackson, 1969; Frisch, 1971;

Fig. 5.6 Compositions of spinel from Thompson mine ultramafic rocks in $ZnAl_2O_4$-$(Mg,Fe)Al_2O_4$-$FeCr_2O_4$ system. Circles, solid triangles and dots represent spinels from mineralized peridotite, serpentinite and unaltered metaperidotite, respectively.

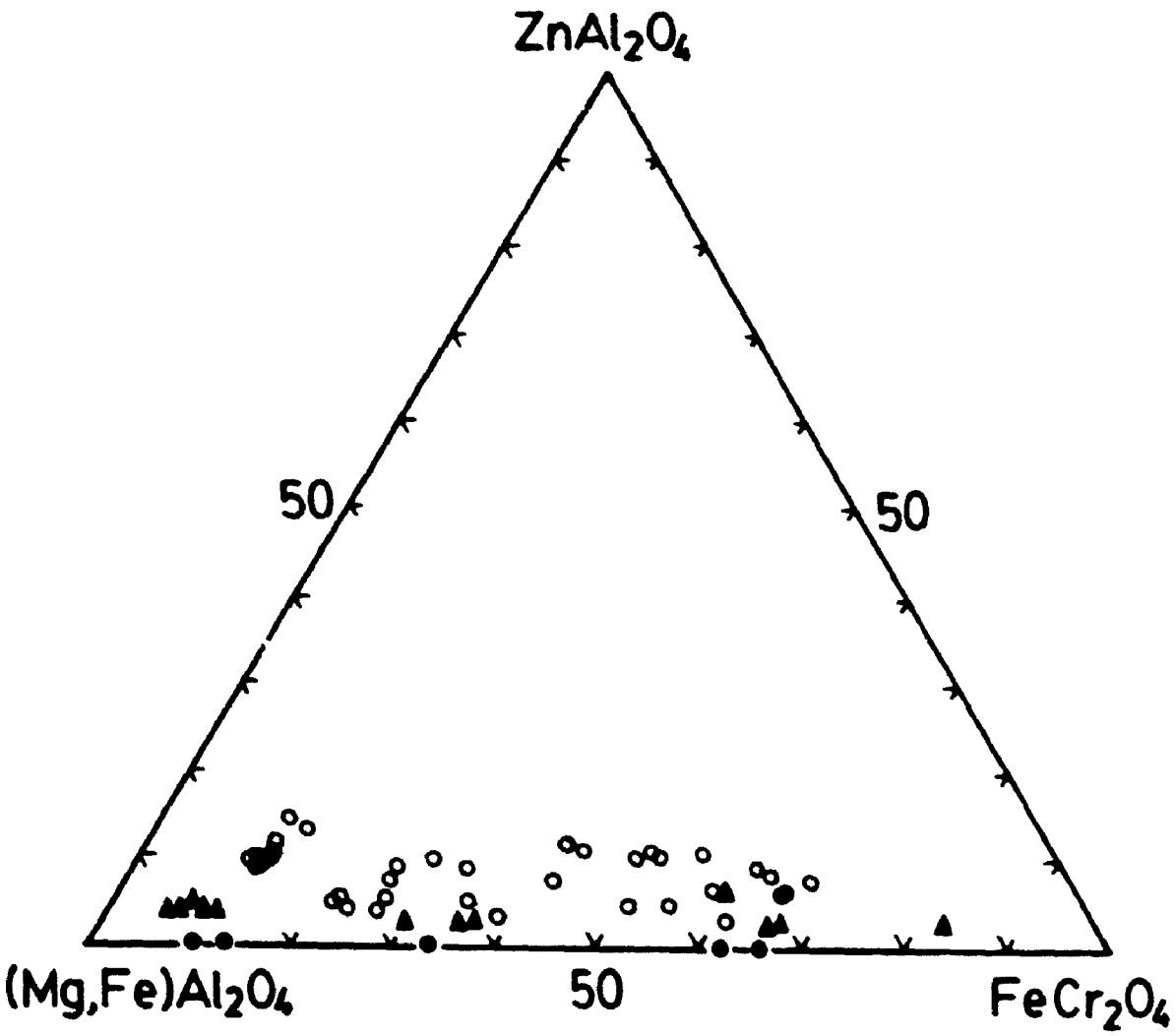
ZnAl2O4
50
50
(Mg,Fe)Al2O4
50
FeCr2O4

Fig. 5.17 Compositions of spinel from Thompson mine metapelite in $ZnAl_2O_4$-$(Mg,Fe)Al_2O_4$-$FeCr_2O_4$ system. Dots and solid triangles represent spinels from ore types I and III, respectively.

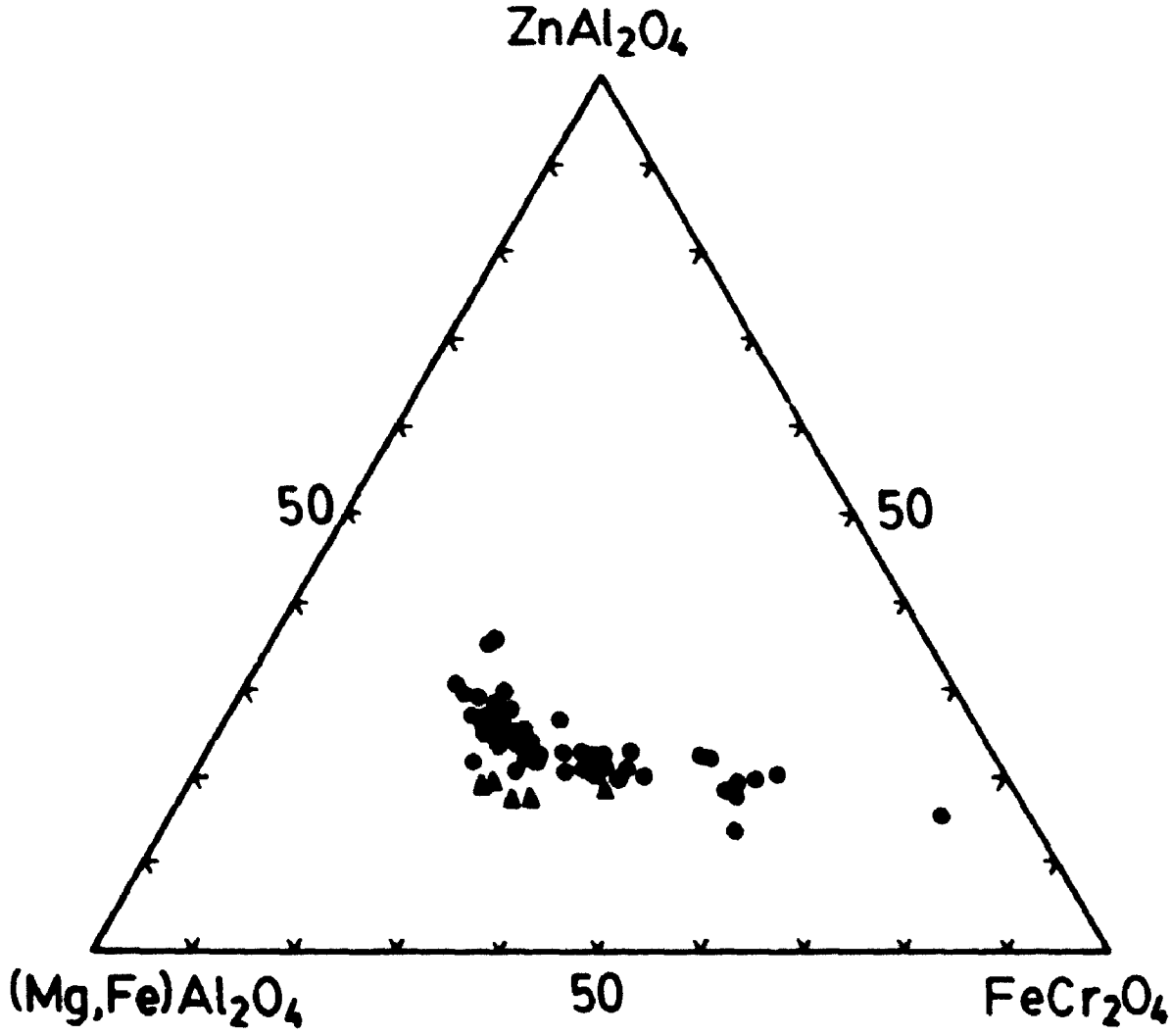
$ZnAl_2O_4$
50
50
$(Mg,Fe)Al_2O_4$
50
$FeCr_2O_4$

Onyeagocha, 1974; Bliss and Maclean, 1975; Evans and Frost, 1975; Shen et al., 1988; Michailidis, 1990; Thalhammer et al., 1990; Fleet et al., 1992), spinel in Thompson mine ultramafic rocks is not rimmed by "ferritchromite". The Fe^{3+} contents of spinel are generally very low (Fig. 5.18), an outer rim of wustite is present (see detailed describtion below) indicating very reducing metamorphic conditions. Spinel compositions are given in Appendices XI and XII; the structural formulae were calculated on 4 oxygens. The ferric iron content was calculated by the following procedure: $FeO_{excess}=\Sigma M^{2+}O-2(TiO_2+SiO_2)-\Sigma M^{3+}{}_2O_3$, where $\Sigma M^{2+}O$ is the sum of molecular proportions of FeO^t, MgO, MnO, ZnO, and NiO, and $\Sigma M^{3+}{}_2O_3$ is the sum of Al_2O_3, V_2O_3, and Cr_2O_3. The FeO_{excess} was then calculated to magnetite (Fe_3O_4) component.

5.12.1 Spinel in ultramafic rocks of the Thompson mine

5.12.1.1 Spinel in unaltered metaperidotite

Zoned spinel in fresh peridotite has a Mg-Al-chromite core [$Mg/(Mg+Fe^{2+})=0.26$, $Cr/(Cr+Al)=0.65$] and Cr-spinel margin [$Mg/(Mg+Fe^{2+})=0.61$, $Cr/(Cr+Al)=0.14$]. From core to rim, $MgAl_2O_4$ and $FeAl_2O_4$ increase from 25.3 to 61.0 mol% and 6.6 to 24.3 mol%, respectively. Whereas $FeCr_2O_4$ and Fe_3O_4 decrease from 62.6 to 13.7 mol% and 3.3 to 0.8 mol%, respectively. Minor amounts of V_2O_3 (up to 0.7 wt%), MnO (up to 0.4), NiO (up to 0.1) and ZnO (up to 0.1) have also been detected. According

Fig. 5.18 Compositions of spinel from Thompson mine ultramafic rocks in Fe^{3+}-Al-Cr system. Circles, solid triangles and dots represent spinels from mineralized peridotite, serpentinite and unaltered metaperidotite, respectively.

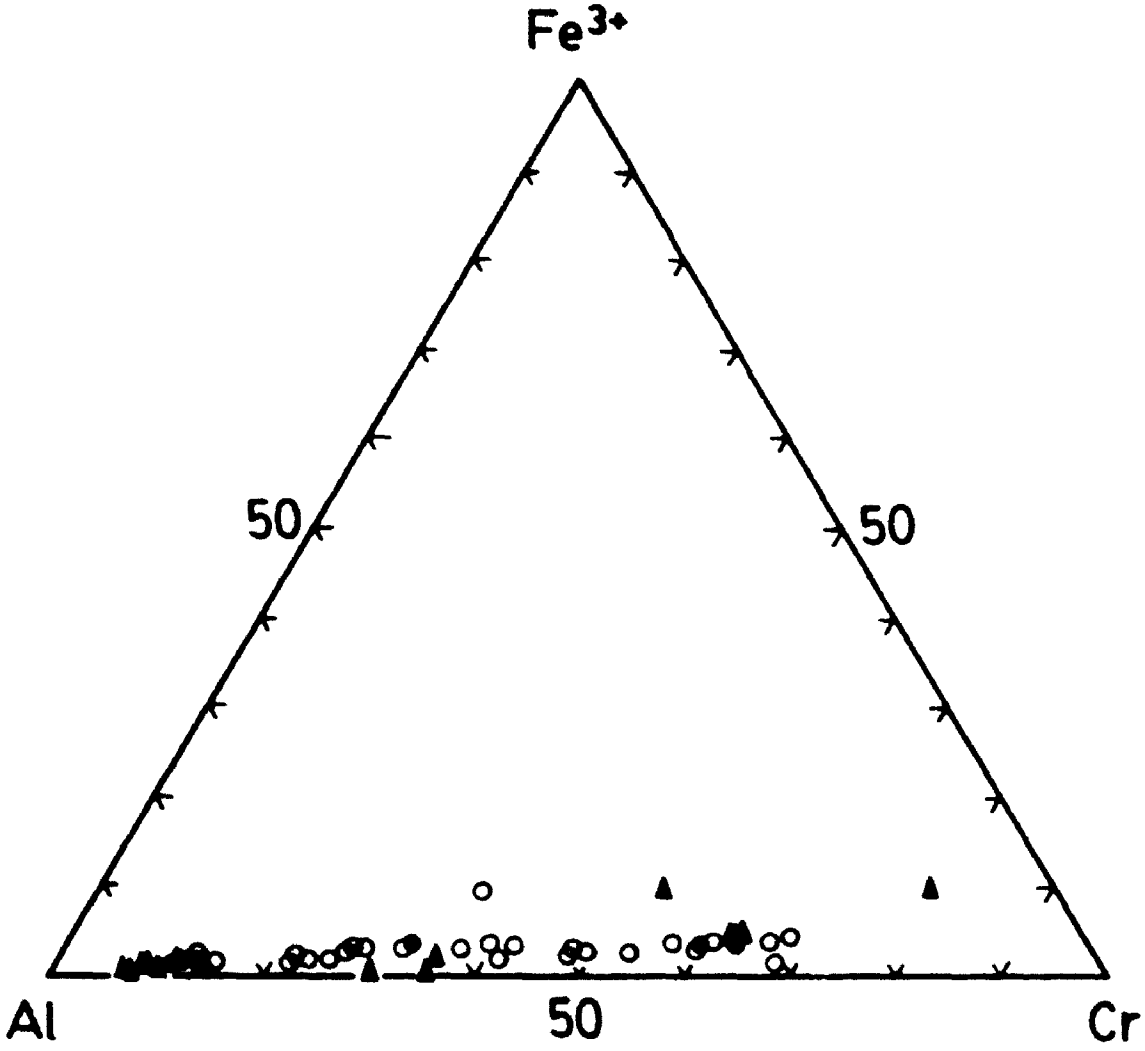
Fe3+
50
50
Al
50
Cr

to Evans and Frost (1975), spinel becomes more Al- and Mg-rich during prograde metamorphism. Paktunc (1984) observed a spinel from a fresh ultramafic body at 4000 level underground of the Thompson T-3 mine, which has the same zoning pattern as that described above, and suggested that the zoning is the result of prograde amphibolite grade metamorphism.

5.12.1.2 Spinel in serpentinite

Two peridotite samples collected from the Thompson T-3 mine are composed of serpentine with minor amounts of spinel, magnetite, pentlandite and pyrrhotite. Two different varieties of spinel have been documented from the samples: Mg-Al-chromite with dark red color under transmitted light has $Mg/(Mg+Fe^{2+})$ from 0.13 to 0.28 and $Cr/(Cr+Al)$ from 0.59 to 0.87, and Cr-spinel with greenish yellow color has $Mg/(Mg+Fe^{2+})$ from 0.43 to 0.65 and $Cr/(Cr+Al)$ from 0.07 to 0.36. The TiO_2, V_2O_3, MnO, NiO contents of both spinels are less than 1.0 wt% (Appendix XI). ZnO contents of both spinels are similar (up to 2.5 wt%) and higher than in spinels from unaltered peridotite. One chromite grain shows compositional zoning with increase $FeCr_2O_4$ (52.7 to 77.1 mol%) and decrease in both $MgAl_2O_4$ and $FeAl_2O_4$ (25.8 to 12.8 and 3.9 to 0.0 mol%, respectively from core to margin. The ZnO content of this spinel also decreases slightly from 2.5 to 1.3 wt% ($ZnAl_2O_4$ from 6.3 to 3.6 mol%). Another chromite grain exhibits the opposite zoning, with Mg and Al enriched and Cr and Fe depleted at the margin. ZnO content increases from 1.1

to 1.7 wt% ($ZnAl_2O_4$ from 3.7 to 2.7 mol%).

5.12.1.3 Spinel in mineralized peridotite

The mineralized peridotite has experienced extensive hydrothermal alteration accompanied by Ni-mineralization. Spinel is present in association with serpentine, chlorite, carbonate minerals and Ni-Fe sulfide. The most striking feature of spinel in this peridotite is that it contains distinctly higher ZnO content (up to 7.2 wt% or 14.3 mol% of $ZnAl_2O_4$) compared to both unmineralized serpentinite (up to 2.5 wt% or 6.6 mol% of $ZnAl_2O_4$) and unaltered peridotite (only up to 0.1 wt%).

Although a few grains of dark red chromite have been observed (Appendix XI), the majority of the spinels are Cr-spinel with yellow to orange color in transmitted light and in close association with Ni sulfide. The spinel is composed mainly of Cr-spinel with varied amounts of FeO and ZnO and minor V_2O_3, MnO and NiO (less than 1.0 wt%); the Fe_2O_3 content is low, ranging from 0.7 to 3.0 wt%.

In spinel grains which are optically unzoned, the $ZnAi_2O_4$ content is enriched from core to margin and coupled with depletion in $FeAl_2O_4$ content. For example, in one grain, $ZnAl_2O_4$ increases from 11.6 to 14.3 mol% (4.9 to 7.2 wt% of ZnO) and $FeAl_2O_4$ correspondingly decreases from 10.2 to 6.1 mol%. The compositional variation is dominated by substitution of $ZnAl_2O_4$ by $FeAl_2O_4$.

The dominant zoning pattern of the spinel enclosed by Ni-Fe-sulfide has both Zn and Cr enriched and Mg, Fe and Al depleted outwards. The following substitution scheme is suggested:

$$FeCr_2O_4 + ZnAl_2O_4 \leftrightarrows MgAl_2O_4 + FeAl_2O_4.$$

This zoning pattern is the reverse of that for spinel in unaltered peridotite. In the transmitted light one can see that the brown Cr-spinel core has been rimmed by reddish-brown Mg-Al chromite. For instance, in one spinel grain which is surrounded by Ni-Fe-sulfide, $MgAl_2O_4$ and $FeAl_2O_4$ decrease toward the margin from 61.5 to 37.1 and 7.7 to 0.0 mol%, respectively, whereas $FeCr_2O_4$ increases from 25.5 to 49.5 mol%. Additionally, this chromite is rimmed by opaque wustite with $[(Fe_{0.98}Cr_{0.01})_{0.99}O]$ (Plate 3N). The $ZnAl_2O_4$ component of the spinel is 7.7 mol% (3.8 wt% of ZnO) in the spinel core, 10.2 mol% (4.4 wt% of ZnO) in the chromite inner margin and only 0.5 mol% (0.2 wt% of ZnO) in the wustite outer rim.

In the literature, ZnO in chromian spinel and chromite from metamorphosed peridotite is usually present in abundances of less than 1 wt% (Frost, 1991). The only recorded exception is Zn-rich chromite reported from the Sykesville district of Maryland where chromite in serpentine contains up to 11.1 wt% of ZnO (Wylie et al., 1987). As described above, the ZnO content of chromian spinel and chromite in ultramafic rocks at the Thompson mine is closely related to hydrothermal activity associated with Ni-mineralization. The spinel containing the highest ZnO content has been found in strongly

mineralized peridotite which occurs as lenses enclosed in Ni-ore hosted in metapelite.

The zoning pattern of spinel is also very interesting. According to Evans and Frost (1975), spinel becomes more Al- and Mg-rich relative to Cr and Fe^{2+} as the grade of metamorphism increases. Therefore, the zoning of spinel in mineralized peridotite may indicate a lower crystallization temperature for the grain margin. Also the $ZnAl_2O_4$-$FeCr_2O_4$ enriched margin of spinel probably indicates late hydrothermal activity.

As described above, many authors have noted the "ferritchromite" margin of chromite in serpentinite. However, the Fe_2O_3 content of the margin of spinel grains in the Thompson ultramafic rocks is very low (up to 3.76 wt%). The occurrence of an outer rim of wustite on spinel is a further indication of very-low oxygen fugacity. It suggests that the hydrothermal fluid related to the precipitation of wustite was very reducing. In the Fe-O system, wustite is unstable below 570°C at 1 atm. (Lindsley, 1991). However, Shen et al. (1983) found that this temperature will decrease when pressure increases. Therefore, the formation temperature of wustite in this study area is likely to be lower than 570°C.

In addition to those enclosed by Ni-Fe sulfide, other spinel grains are associated with talc and chlorite. Chlorite associated with spinel contains up to 4.7 wt% of Cr_2O_3 and talc contains up to 0.2 wt% of Cr_2O_3. The high Cr_2O_3 content of these minerals also indicates that the hydrothermal fluid is locally

Cr-bearing (Pan and Fleet, 1988) and correlated to the formation of the chromite-rich margin of the spinels. The ZnO content of the spinel in mineralized pyroxenite is also higher than in non-mineralized peridotite.

In summary, it seems unlikely that the high ZnO content of the spinel in the ultramafic rocks at the Thompson mine is a primary magmatic feature. Therefore, it is suggested that metamorphism by Cr-Zn-rich hydrothermal solutions modified the original chromian spinel and Mg-Al chromite compositions. The evidence suggests that the Zn metasomatism started in the earliest stage of serpentinization of the the ultramafic rocks and became intensified with the Ni-mineralization.

5.13.2 Spinel in metapelite-hosted Ni-ore

Compared with spinel in ultramafic rocks, the composition of spinel in metapelite-hosted Ni-ore (ore type I) and Au-Ni-ore (ore type III) is distinctly Fe^{2+}-rich and Mg-poor, but both are Cr-rich. The Cr_2O_3 content of these spinels ranges from 16.6 to 42.6 wt%, and FeO from 22.8 to 29.9 wt%. MgO is only up to 1.3 wt%. The spinel compositions are close to the hercynite-chromite join. According to the classification scheme of Haggerty (1991), these spinels belong to either picotite or Al-chromite. In transmitted light they are red-brown or dark red in color.

Spinels in ore type I and III are associated with not only primary metamorphic minerals but also late alteration minerals. The former include

garnet, biotite, and quartz, whereas the latter includes calcite, chlorite, quartz, and muscovite. Spinel is also associated as inclusions with Ni-Fe sulfide.

It is noteworthy that both picotite and Al-chromite contain the highest ZnO concentration of analyzed samples from the Thompson mine. A maximum ZnO content of 14.6 wt% was obtained from a picotite grain included in Ni-Fe sulfide. The maximum Cr_2O_3 content of this grain was 17 wt%.

Zinc-rich spinel has been reported frequently from metapelite (c.f., summary of Frost, 1991). However, Zn-rich spinel is commonly green $(Mg,Fe)Al_2O_4$ spinel, and Cr_2O_3 is usually present in only minor amounts (Frost, 1991). One exception is the chromite with ZnO up to 19.1 wt% in metapelite from Sykesville district of Maryland (Wylie et al., 1987). Therefore, the present occurrence of zincian chromian spinel and chromite in metapelite from the Thompson mine is not unique.

Spinel compositions are plotted on a $ZnAl_2O_4$-$(Fe,Mg)Al_2O_4$-$FeCr_2O_4$ ternary diagram (Fig. 5.17). This diagram also shows that the ZnO content correlates with host rocks but Cr_2O_3 content does not. For example, the ZnO content of spinel in Ni-ore (ore type I) is generally higher than that in As-rich Ni-ore (ore type III), but the Cr_2O_3 contents are similar. This can be largely attributed to their conditions of formation. The As-rich Ni-ore was formed later than the Ni-ore during the late hydrothermal alteration. Also the PGMs in the Thompson mine are associated in the As-rich Ni-ore with Cd-rich sphalerite and chalcopyrite, whereas in Ni-ore only a few tiny inclusions of sphalerite have

been observed in spinel grains.

Another important factor which influences spinel chemistry is mineral assemblage (Frost, 1991). However, spinels with different Zn contents occur in metapelite with the same silicate mineral assemblage, having chlorite, calcite, and muscovite as late alteration minerals. In the present study, spinel composition is more closely correlated with the ore-forming mineral assemblage which in turn is associated with different stages of hydrothermal mineralization.

Under reflected light, both picotite and Al-chromite appear either homogeneous or zoned. However, even "optically homogeneous grains" exhibited chemical zonation by electron microprobe investigation. In general, zoning occurs in the contents of ZnO and FeO; ZnO increases from the grain core and reaches a maximum content at the margin, whereas FeO decreases correspondingly. For example, from core to margin in one grain, ZnO increases from 12.7 to 14.6 wt% and FeO decreases from 25.2 to 23.1 wt%.

The majority of the picotite and Al-chromite grains are optically zoned, generally with a more Cr-rich and slightly Zn-poor Al-chromite margin. This suggests a coupled substitution between $FeCr_2O_4$ and $ZnAl_2O_4$ (see also Treloar, 1987).

In metapelite-hosted Ni ore, homogeneous spinel with high ZnO content occurs included in unaltered biotite and interlocking with garnet, a texture suggesting formation by amphibolite grade metamorphism. In the literature the

origin of Zn in gahnite-hercynite spinel has been a matter of debate. Stoddard (1979) and Spry (1982) suggested that gahnitic spinels can be breakdown products of staurolite. Spry and Scott (1986) argued that gahnitic spinel can form by desulfurization of sphalerite and noted the Zn-bearing spinels are found in many rock types in association with metamorphosed ore deposits. Staurolite is not present in rocks of the Thompson mine, but several sphalerite grains do occur as inclusions in picotite-Al-chromite within Ni-ore. Therefore, the Zn in the spinel may have been present originally as sphalerite.

In contrast to the optically unzoned spinel, the spinel with distinct chromite-rich margin occurs as corroded inclusions in sulfide, replaced by sulfide, and generally associated with quartz, calcite and chlorite. These observations suggest that the chromite-rich margin of the spinel may have resulted from hydrothermal fluids enriched in Cr. The hydrothermal alteration processes are also responsible for Ni-mineralization. Both Cr and Ni in the hydrothermal fluids were probably taken from the ultramafic rocks.

Oscillatory zonation has also been observed on one spinel grain in which a $FeAl_2O_4$-rich core is surrounded by a $FeCr_2O_4$-rich inner zone with an $FeAl_2O_4$-rich band at the grain boundary. The ZnO content decreases from 11.3 at the core to 7.8 in the inner zone and increases to 12.3 wt% at the grain edge. The $FeAl_2O_4$ of this spinel varies from 40 to 33, and finally back to 39 mol%. $MgAl_2O_4$ also shows a similar variation trend as $FeAl_2O_4$ although it is present as a minor component of the spinel. $FeCr_2O_4$ varies inversely from 25

to 40, and then back to 25 mol% at the grain boundary.

The oscillatory zonation in this spinel is analogous to that of the growth-banded pyrite studied by Fleet et al. (1989). It is unlikely to have formed by diffusion after crystal growth due to its uniform composition. Compositional growth banding in crystals can arise from either rapid crystallization or changes in the physico-chemical conditions of the mineralizing fluids. It seems unlikely that rate of crystallization would be a significant factor in the present case. Therefore, it is probably that the composition of the fluids in the immediate vicinity of growing spinel grains fluctuated in some episodic manner.

5.14 Allanite

Allanite is an epidote-group mineral with the general formula $A_2M_3Si_3O_{12}(OH)$. The ten-fold-coordinated A(1) site is always fully occupied by Ca; the large cations, such as the REE and possible Mn^{2+}, which may substitute for Ca, partly occupying the nine-fold-coordinated A(2) site. Ferrous iron, along with Fe^{3+}, Mn^{3+}, Mn^{2+}, Mg and Ti, is present in the relatively large M(3) site (Dollase, 1971). The ideal end-member composition for allanite, then, may be represented as $Ca(REE)Fe^{2+}Al_2Si_3O_{12}(OH)$.

In the literature varieties of allanite with volatile anion species other than OH^- are considered to be rare (Deer et al., 1986). Fluorine-bearing allanite has been reported at the contact between calc-granulite and microcline pegmatite from India (Rao et al., 1979) and in quartz veins in granites of the Itulin Sn-W

Table 5.4 Electron microprobe analyses of allanite

No.	1	2	3
		wt%	
SiO_2	33.76	34.12	33.37
TiO_2	0.22	0.10	0.01
Al_2O_3	21.99	20.71	21.23
FeO*	7.73	8.75	8.79
MgO	0.21	0.32	0.29
MnO	0.35	0.30	0.38
CaO	16.31	15.67	14.46
Y_2O_3	0.41	0.42	0.23
La_2O_3	3.96	4.28	4.50
Ce_2O_3	7.18	7.98	8.29
Pr_2O_3	0.66	0.79	0.96
Nd_2O_3	2.67	2.97	3.14
Sm_2O_3	0.44	0.45	0.43
Gd_2O_3	0.30	0.22	0.20
Dy_2O_3	0.12	0.16	0.14
Yb_2O_3	0.22	0.05	0.05
Na_2O	0.02	0.08	0.00
K_2O	0.03	0.02	0.00
F	0.55	0.46	0.32
Cl	0.81	0.72	0.46
O=F,Cl	0.41	0.35	0.24
Total	97.53	98.62	97.01
	ions on the basis of 12 oxygen		
Si	3.01	3.04	3.01
Ti	0.01	0.01	0.00
Al	2.31	2.18	2.26
Fe^{3+}	0.12	0.14	0.14
Fe^{2+}	0.46	0.51	0.52
Mg	0.03	0.04	0.04
Mn	0.03	0.02	0.03
Ca	1.57	1.50	1.40
REE	0.52	0.57	0.59
Na	0.02	0.01	0.00
K	0.00	0.00	0.00
F	0.15	0.13	0.09
Cl	0.12	0.10	0.07

* total iron content as FeO, Fe^{3+} and Fe^{2+} calculated by charge balance.
1. ore type II, metapelite host;
2. ore type III, metapelite host;
3. ore type IV, pegmatite host.

deposit from the former USSR (Ivnov et al. 1981). Pan and Fleet (1990) reported a halogen-bearing (F, Cl) variety of allanite in an assemblage associated with a gold occurrence from the Hemlo area, Ontario.

In the present study, allanite is a minor or trace constituent (< 1 vol%) in most samples of all four of the present ore types of the Thompson mine, but it is most abundant (up to 5 vol%) in ore type II, in which it occurs as large isolated crystals (up to 0.2 x 0.6 mm) and aggregates associated with biotite and/or sulfide. Allanite in ore types I, II and III (all hosted in metapelite) contains significant amounts of both F and Cl (up to 0.6 and 0.8 wt% F and Cl, respectively) (Table 5.4), and therefore is an unusual halogen-bearing variety (cf., Pan and Fleet, 1990). Similarly, minor contents of halogens have been detected also in allanite grains of the pegmatite-hosted ore type IV (Table 5.4).

5.14 Gersdorffite and Nickeline

Arsenides (nickeline and maucherite) and sulpharsenides (cobaltite and gersdorffite) have been reported from various Cu-Ni sulfide and Ni sulfide deposits, such as Sudbury, Ontario; Pechenga, former USSR; Kanichee, Ontario; and Pipe Mine, Thompson Nickel Belt, Manitoba. Only in the Sudbury area, has a PGM (sudburyite) been reported directly related to either cobaltite-gersdorffite or maucherite. In contrast, at the Thompson mine, gersdorffite and nickeline are the only host minerals for PGMs and for most of

gold.

In nickel ore hosted by metapelite (ore type I), gersdorffite occurs occasionally as isolated grains, and some of them have inclusions of irarsite (IrAsS). In As-rich nickel ore, late gersdorffite and/or nickeline occur either in massive (metapelite, ore types II and III) or as disseminated (pegmatite, ore type IV) assemblages, replacing early sulfides. They are both enriched in PGMs and gold.

Compositions of gersdorffite and nickeline are given in Appendices XIII and XIV, respectively. The composition of gersdorffite in this study has been plotted in a FeAsS-CoAsS-NiAsS ternary diagram (Fig. 5.19). Gersdorffite from Ni-ore (ore type I) is mostly Fe- and Co-rich, which probably indicates a relatively high crystallization temperature. However, gersdorffite from pegmatite is relatively depleted in Co, and gersdorffite from As-rich nickel ore (ore type II and III) has the lowest Fe content, which probably indicates a lower formation temperature (Klemm, 1965).

All of the present precious-metal assemblages are associated with As-rich ores. The assemblage (gersdorffite $\pm$ nickeline) characterises all of the present PGE-Au ore types. Significantly, both minerals contain local elevated contents of PGEs; Ru being the only PGE not detected by electron microprobe analyses. Maximum substitutions (wt%) in gersdorffite from PGM-Au-Ni ore (type II) are Pt 0.1, Ir 0.1, Os 0.2, Pd <0.1 and Rh <0.1. Maximum substitutions (wt%) in nickeline from the same ore type are Pt 0.3, Ir 0.3, Os 0.2, Pd 0.1

Fig. 5.19 Compositions of gersdorffite from the Thompson mine in FeAsS-CoAsS-NiAsS system. Solid triangle, dots, solid square and circles represent gersdorffite from ore types I, II, III and IV, respectively.

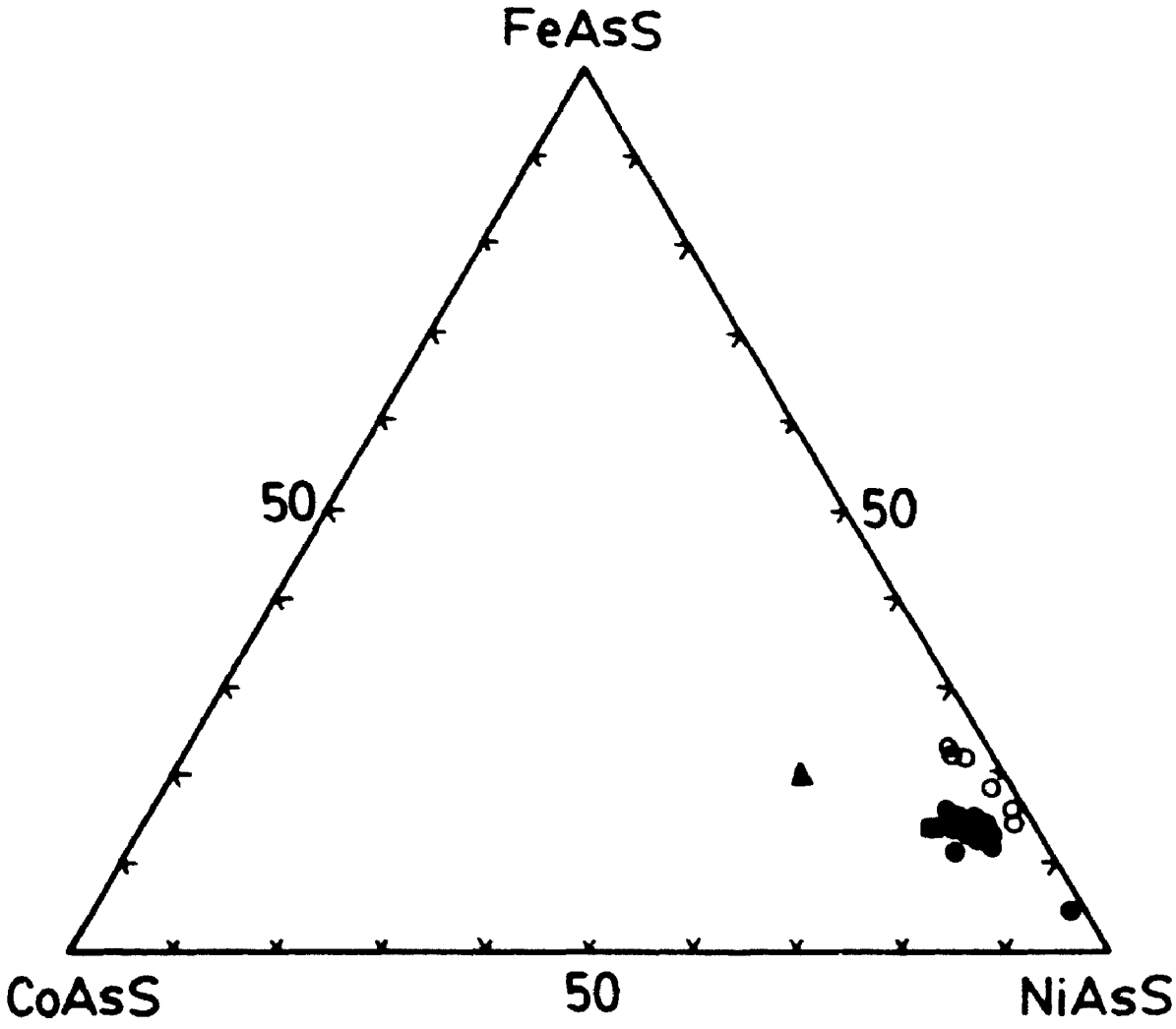
FeAsS
50
50
CoAsS
50
NiAsS

and Rh <0.1. The Pt, Os and Ir contents of nickeline are higher than those reported in the literature (Cabri and Laflamme, 1981). The higher contents of Pt, Ir, and Os compared to Pd in both gersdorffite and nickeline may indicate fractionation of PGEs between gersdorffite/nickeline and PGMs (mainly Pd-Ni-Sb-telluride).

In ore type IV (Au-PGM) hosted in pegmatite, PGMs are less abundant than in ore type II and, correspondingly, so are the PGE contents of gersdorffite (0.1 wt% of Pd) and nickeline (0.1 wt% of Pd, less than 0.1 wt% of Ir and Rh). The positive correlation between abundance of PGMs and PGE contents of gersdorffite and nickeline suggests that the formation of these sulpharsenide and arsenides is closely related to the PGM-Au mineralization.

5.15 Bismuth Telluride

Wehrlite was identified in ore type II associated with gersdorffite, pentlandite and calcite. Electron microprobe analysis (in wt%) gave Te 40.3, Bi 55.0, Ni 1.5, Pt 1.0, Ir 0.1, Fe 0.1 and Os 0.02, total 98.0, with a corresponding formula of $Pt_{0.02}Ni_{0.08}Bi_{0.83}Te_{1.00}$. Tellurobismuthite also occurs in ore type III associated with chalcopyrite, gold, and gersdorffite. Electron microprobe analysis (in wt%) gave Bi 53.1, Te 45.9, Pt 1.0, Ir 0.1, Ag 0.6, Fe 0.3, Ni 0.1, and S 0.03, total 101.0 and a corresponding formula of $(Te_{2.84}Pt_{0.04}Ag_{0.04}Fe_{0.04}Ni_{0.02})_{2.98}Bi_{2.00}$.

5.16 Melonite

Melonite ($NiTe_2$) was observed in ore type III as inclusions in pentlandite. Electron microprobe analysis (in wt%) shows that the mineral consists mainly of Ni 19.6, Te 73.7, and Bi 4.6, with minor amounts of Fe 1.6, Ag 0.1, Pt 0.02, and S 0.1, and total 99.8, and a corresponding formula of $(Ni_{1.04}Fe_{0.09})_{1.13}(Te_{1.79}Bi_{0.07}S_{0.01})_{1.87}$.

Plate 3

Minerals from the Thompson mine

A: Photomicrograph of allanite from ore type II, in association with biotite and opaque ore minerals (black). Scale bar is 0.2 mm. Sample TAB-1AB.

B: Photomicrograph of secondary fibrous biotite replacing large primary large biotite grain in matrix of opaque ore minerals (black) from ore type II. Scale bar is 0.2 mm. Sample TD-3.

C: Photomicrograph of massive chlorite (grey) after biotite (black) from ore type III. Plagioclase and quartz are white. Scale bar is 0.2 mm. Sample TO42.

D: Photomicrograph of secondary radial aggregates of muscovite replacing biotite. Scale bar is 0.2 mm. Sample TOM-TOP.

E: Photomicrograph of muscovite and calcite (white) after plagioclase from ore type II. Scale bar is 0.2 mm. Sample TAB-1AA.

F: Photomicrograph of grunerite replacing ferrosilite in BIF. Gru=grunerite, Fs=ferrosilite. Scale bar is 0.2 mm. Sample TS-18.

G: Electron back-scattered image of ferropyrosmalite and grunerite replacing ferrosilite in BIF. Fps=ferropyrosmalite, Gru=grunerite. Fs=ferrosilite. Black matrix is magnetite and pyrrhotite. Sample TS-18.

H: Photomicrograph of ferropyrosmalite vein in pyrrhotite matrix from BIF. Scale bar is 0.2 mm. Sample TS-18.

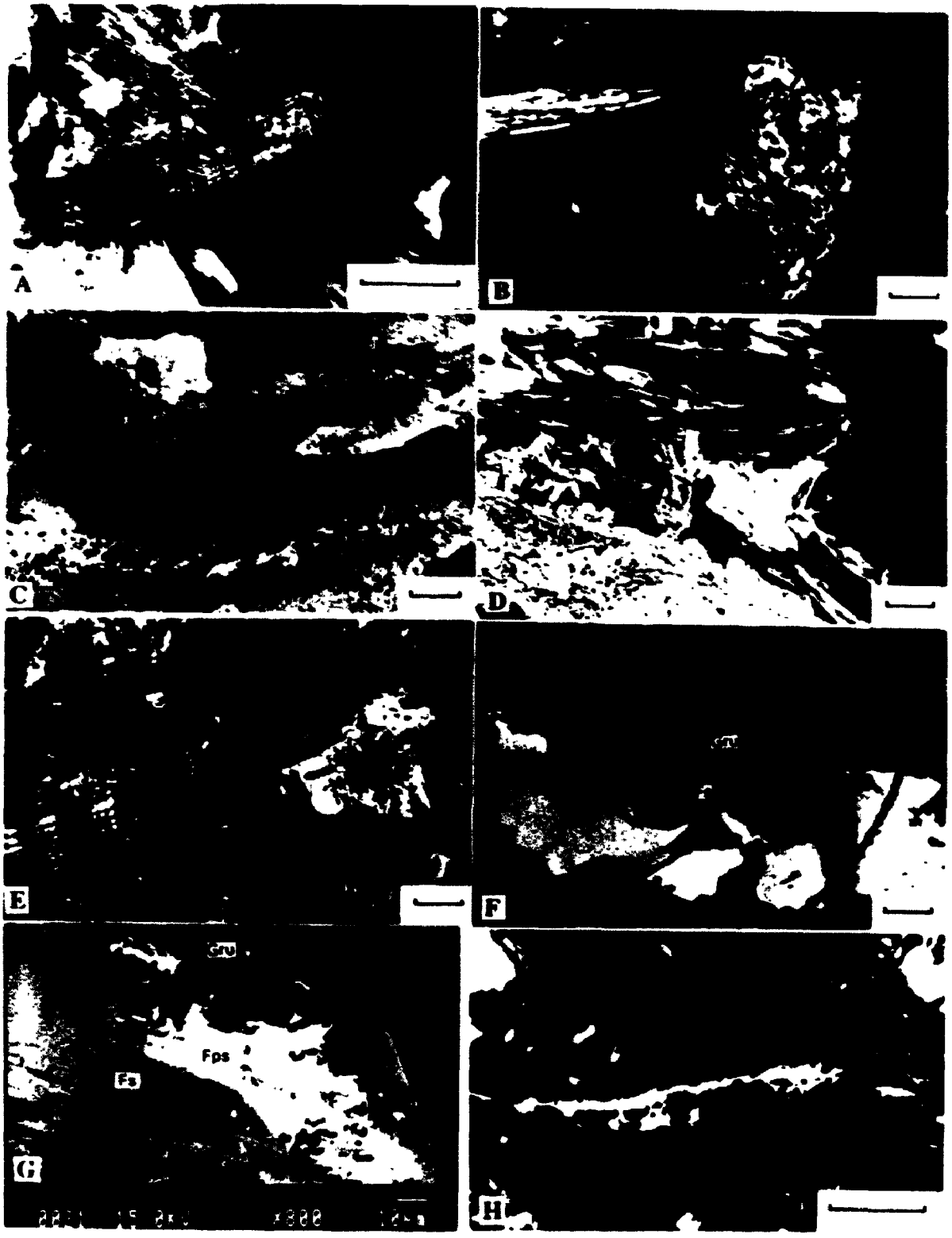
A
B
C
D
E
F
G
Fps
Fs
H

Plate 3 (continued)

I: Photomicrograph of muscovite replacing plagioclase in opaque ore mineral matrix from ore type IV. Scale bar is 0.2 mm. Sample A4.

J: Photomicrograph of a carbonate vein cutting chlorite, talc and Fe-Ni sulfide minerals from metapyroxenite. Scale bar is 0.2 mm. Sample 24A.

K: Photomicrograph of hisingerite-carbonate vein cutting talc and chlorite from metapyroxenite. Hsg=hisingerite. Scale bar is 0.2 mm. Sample 24.

L: Photomicrograph illustrating serpentinite replacing olivine in association with chlorite, talc and carbonate minerals from mineralized peridotite. Scale bar is 0.2 mm. Sample PT3.

M: Electron back-scattered image of Mg-Al-chromite (light grey) core mantled by Cr-spinel margin in unaltered metaperidotite. Sample TS44.

N: Photomicrograph illustrating a zincian Cr-spinel with zincian Mg-Al chromite inner rim (grey) and wustite outer rim (light grey) in pyrrhotite and pentlandite matrix from mineralized peridotite. Gangue minerals (black) are chlorite and serpentine. Wus=wustite. Scale bar is 0.2 mm. Sample PT8II.

O: Electron back-scattered image illustrating the dominant zoning pattern of zincian spinel from ore type I: pictite core and Al-chromite rim. Silicate gangue minerals (black) are chlorite and calcite. Sample TS-21.

P: Electron back-scattered image of zincian spinel with oscillatory zonation from ore type I. Silicate gangue mineral is quartz. Sample TOM-13

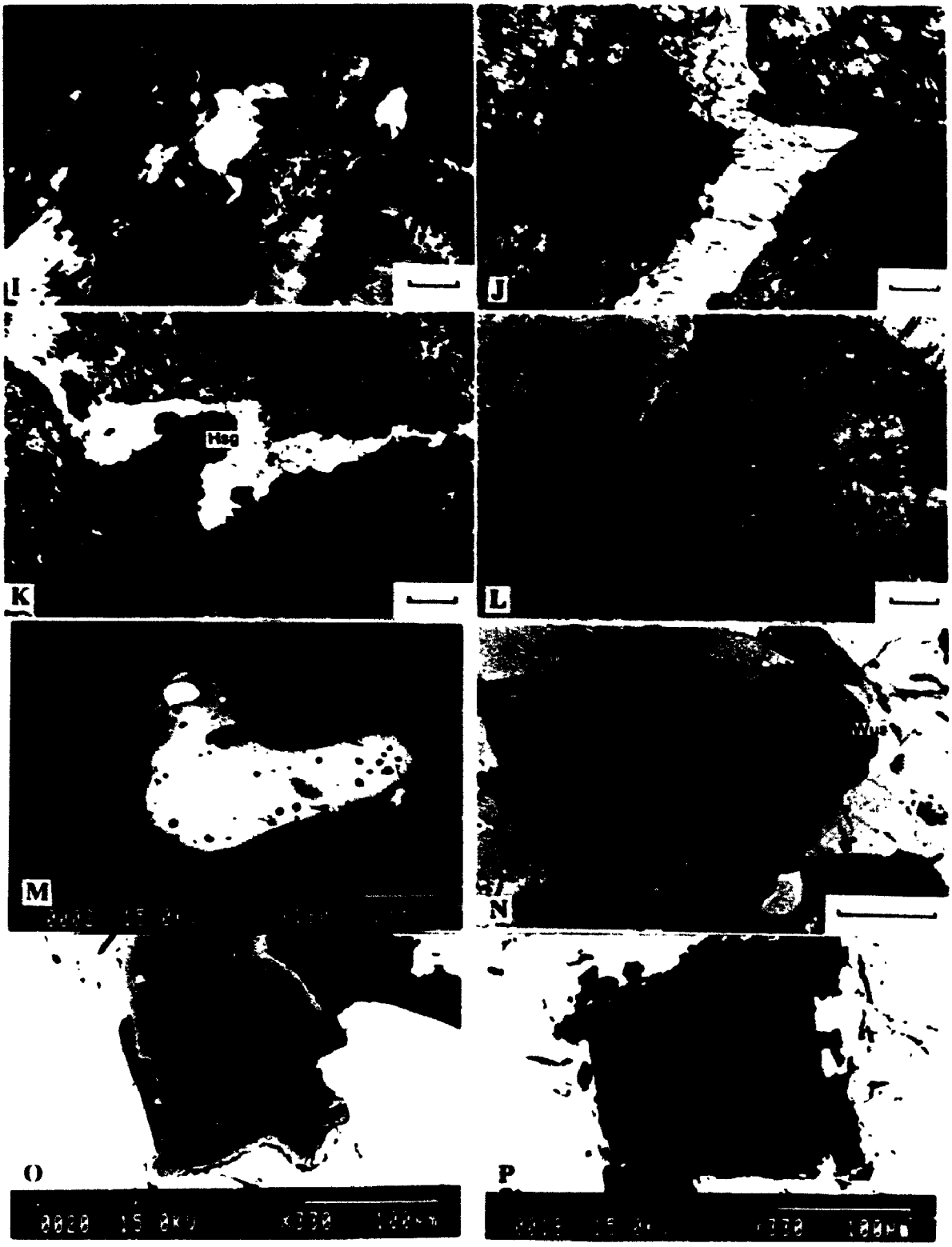
I
J
K
Hsg
L
M
N
O
P

CHAPTER 6 PRECIOUS-METAL MINERALOGY

6.1 Sudburyite

Sudburyite was first reported from the Copper Cliff South Mine and the Frood mine, Sudbury area by Cabri and Laflamme (1974). The Copper Cliff samples consist of disseminated sulfide in quartz diorite. Sudburyite is generally present as inclusions in cobaltite and maucherite. In the Frood mine, sudburyite is closely associated with chalcopyrite, wehrlite and cubanite (Cabri and Laflamme, 1975). Sudburyite from the Kambalda nickel deposits, Western Australia occurs within nickeline in a quartz-carbonate veinlet (Hudson and Donaldson, 1984). Sudburyite has been described from a serpentinite-hosted Cu-Ni sulfide deposit in southwestern China (Platinum Metal Research Group, 1974). Sudburyite from the Blue Lake Cu-Ni-PGE massive sulfide deposit occurs at Cu-rich sheared margins of massive sulfide lenses and their adjacent chloritized peridotite host rock. Most sudburyite grains are associated with amphibole, pyrrhotite and chalcopyrite (Beaudoin et al., 1990).

In our study, sudburyite is observed most frequently within nickeline, but it is associated also with gersdorffite, pyrrhotite and chalcopyrite and quartz (Plate 4A), and coexists with native gold (Plate 4B) and an unnamed PGM phase (Plate 4C). Sudburyite inclusions are 10x10 μm to about 20x50 μm in size. It occurs predominantly as anhedral grains or occasionally as euhedral grains. Under reflected light, in air and in oil, sudburyite is whitish creamy

with weak reflection pleochroism from yellowish white to creamy with a pink tint. Sudburyite coexisting with gold in gersdorffite appears more greyish in air, appearing yellowish grey with pale greenish or bluish-grey tint. Under oil, the mineral is greyish yellow. For the more Bi-rich composition, sudburyite is distinctly greenish in air from yellowish white to greenish yellow. Under oil, the mineral is creamy to yellowish white with a distinct bluish tint. Sudburyite in chalcopyrite is distinctly pinkish, creamy to pinkish creamy in air, and yellowish white to pinkish creamy in oil. The anisotropism is moderate to strong in air and in oil, with pinkish grey to bluish grey colours.

Compositions of sudburyite are given in Appendix XV. Figure 6.1 shows the range in composition of sudburyite from the Thompson mine in the PdSb-PdBi-PdTe system. Representative electron microprobe analyses and structural formulae of sudburyite are given in Table 6.1. Maximum contents of substitutions (in wt%) are Pt 0.3, Ir 0.2, Os 0.2, Ni 2.3, Fe 0.7, Bi 3.4, Te 3.1 and As 1.0, of which Os is not reported in the literature. Platinum, Ir, Os, Fe, and Ni substitute for Pd, whereas As, Bi, and Te substitute for Sb.

6.2 Testibiopalladite-Antimonian Michenerite

Testibiopalladite is a rare mineral. It was first described from two Cu-Ni sulfide deposits in China (Platinum Metal Research Group, 1974). In southwestern China a mineralized serpentinite contains testibiopalladite inclusions in an assemblage comprised of gersdorffite, cobaltite, pyrrhotite,

Fig. 6.1 Compositions of Thompson mine sudburyite in PdSb-PdBi-PdTe system.

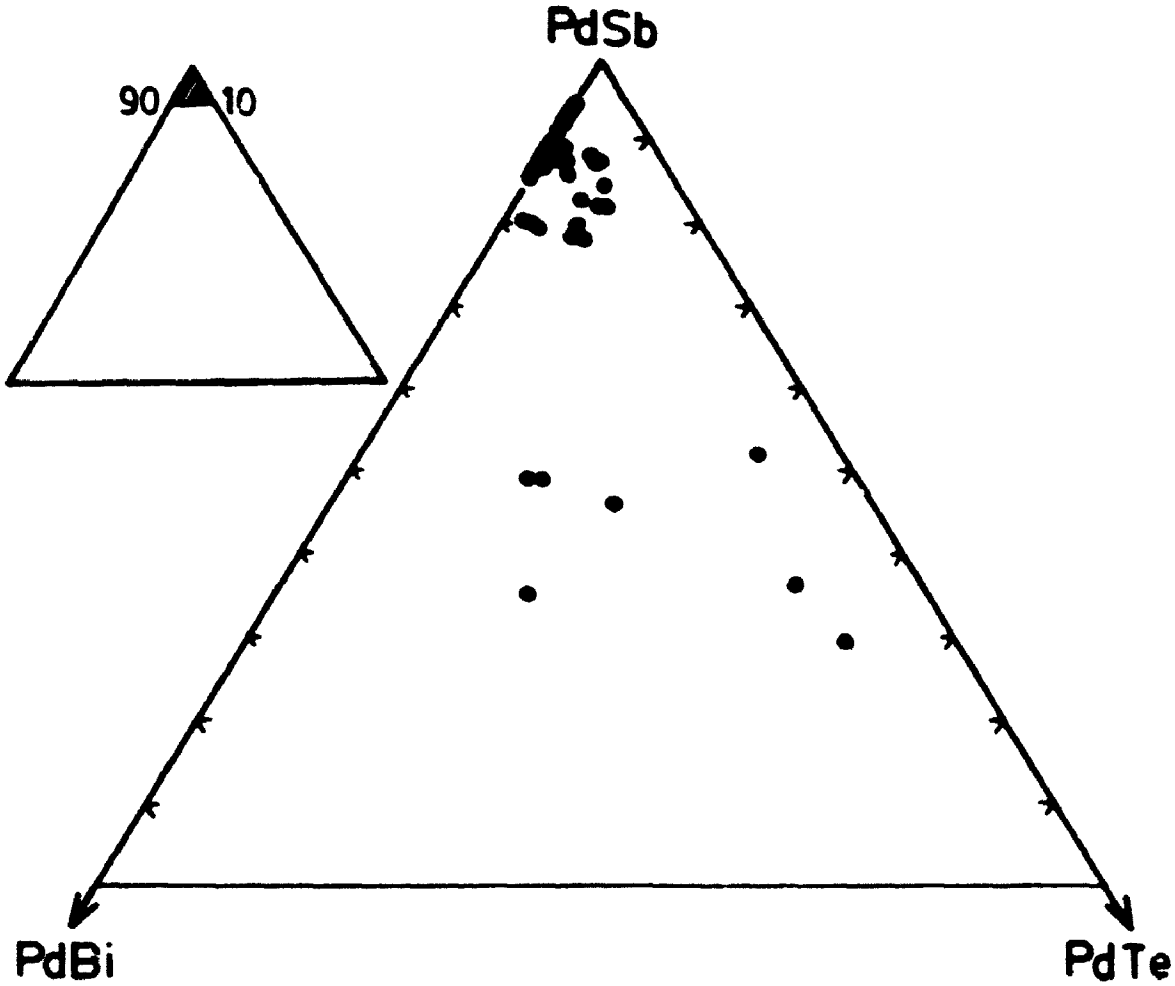
PdSb
90
10
PdBi
PdTe

Table 6.1 Representative electron microprobe analyses of sudburyite from ore type II, metapelite host

sample	1	2	3	4	5	6
			weight percent			
Pt	0.00	0.25	0.00	0.00	0.08	0.00
Pd	44.37	44.61	44.87	45.71	47.87	47.66
Ir	0.00	0.04	0.00	0.00	0.15	0.00
Os	0.19	0.09	0.00	0.00	0.00	0.12
Rh	0.01	-	-	-	-	-
Ru	0.00	-	-	-	-	-
Fe	0.21	0.04	0.07	0.14	0.00	0.73
Ni	2.33	1.37	1.31	0.97	1.99	0.11
As	0.95	0.52	0.39	0.41	0.52	0.06
Bi	1.15	2.72	0.96	3.42	0.74	0.71
Te	2.76	1.01	3.13	1.31	0.00	2.08
Sb	48.52	47.60	46.94	47.17	48.27	48.06
S	-	0.01	0.02	0.00	0.02	0.05
Total	100.49	98.26	97.69	99.13	99.64	99.50
			atomic percent			
Pt	0.0	0.2	0.0	0.0	0.1	0.0
Pd	46.3	48.3	48.7	49.5	50.4	50.9
Ir	0.0	0.0	0.0	0.0	0.1	0.0
Os	0.1	0.1	0.0	0.0	0.0	0.1
Rh	0.0	-	-	-	-	-
Ru	0.0	-	-	-	-	-
Fe	0.4	0.1	0.1	0.3	0.0	1.5
Ni	4.4	2.7	2.6	1.9	3.8	0.2
As	1.4	0.8	0.6	0.6	0.8	0.1
Bi	0.6	1.5	0.5	1.9	0.4	0.4
Te	2.4	0.9	2.8	1.2	0.0	1.9
Sb	44.3	45.2	44.5	44.6	44.4	44.8
S	-	0.0	0.1	0.0	0.1	0.2

1. $(Pd_{0.91}Ni_{0.06}Fe_{0.01})_{0.98}(Sb_{0.95}Te_{0.03}As_{0.02}Bi_{0.01})_{1.01}$
2. $(Pd_{0.94}Ni_{0.05})_{0.99}(Sb_{0.96}Te_{0.02}As_{0.02}Bi_{0.01})_{1.01}$
3. $(Pd_{0.95}Ni_{0.04})_{0.99}(Sb_{0.93}Te_{0.06}As_{0.01}Bi_{0.01})_{1.01}$
4. $(Pd_{0.96}Ni_{0.04}Fe_{0.01})_{1.01}(Sb_{0.94}Te_{0.02}As_{0.01}Bi_{0.04})_{1.01}$
5. $(Pd_{1.01}Ni_{0.02})_{1.03}(Sb_{0.93}As_{0.02}Bi_{0.01})_{0.96}$
6. $(Pd_{1.02}Fe_{0.01})_{1.03}(Sb_{0.93}Te_{0.04}Bi_{0.01})_{0.98}$

chalcopyrite, and pentlandite. The second locality is in northeastern China where the mineral occurs in sulfide-bearing clinopyroxenite. Testibiopalladite has been reported also from Kambalda, Australia. Hudson et al. (1978) described a euhedral grain zoned from a core of testibiopalladite to a margin of michenerite, associated with other tellurides (hessite, rucklidgeite, volynskite, and melonite) in a quartz-carbonate vein that cuts massive nickel sulfide in the Lunnon shoot, Kambalda.

In this study, testibiopalladite is usually present as anhedral to subhedral inclusions in gersdorffite, and occasionally attached to sphalerite, pyrrhotite, and chalcopyrite when included within gersdorffite. Only one grain has been found to be attached to gersdorffite and calcite, surrounded by nickeline. Testibiopalladite also coexists with gold (Plate 4D) and an unnamed PGM (Plate 4E). Testibiopalladite inclusions vary in size from a few μm in diameter to about 140x80 μm. In a few cases, compositional variation from Sb-michenerite to testibiopalladite has been observed in the same grain (Plate 4F). No colour contrast is apparent between testibiopalladite and Sb-michenerite under reflected light. In air, when next to gersdorffite the grains have pale greenish-yellow colour with weak reflection pleochroism from greyish yellow with greenish tint to pale creamy. Reflection pleochroism is moderate to distinct in oil from bluish white to yellowish white. Under crossed nicols, it is weakly anisotropic in air, but more distinct in oil, from bluish grey to dark brownish grey.

Electron microprobe analyses of testibiopalladite and Sb-michenerite are given in Appendix XVI. Compositions of testibiopalladite and Sb-michenerite from the Thompson mine plotted on a Pd_2Te-Bi_2Te-Sb_2Te triangular diagram (Fig. 6.2) straddle the previously inferred immiscible gap between michenerite and testibiopalladite. The complete solid solution between these two end-members in nature is therefore demonstrated. Representative compositions of testibiopalladite and Sb-michenerite are given in Table 6.2. Palladium contents vary from 24.8 to 28.2 wt%. The corresponding formulae vary from $(Pd_{0.90}Pt_{0.01}Fe_{0.01}Ni_{0.13})_{1.05}Te_{0.96}(Sb_{0.52}AS_{0.04}Bi_{0.43})_{0.99}$ to $(Pd_{0.99}Fe_{0.01}Ni_{0.02})_{1.02}Te_{0.95}(Sb_{0.83}As_{0.01}Bi_{0.20})_{1.04}$. Antimony contents range from 26.8 to 13.6 wt%, whereas Bi varies from 10.9 to 28.9 wt%, corresponding to $(Pd_{0.99}Fe_{0.01}Ni_{0.02})_{1.02}Te_{0.95}(Sb_{0.83}As_{0.01}Bi_{0.20})_{1.04}$ and $(Pd_{0.97}Pt_{0.01}Ni_{0.02})_{1.00}Te_{0.95}(Sb_{0.45}As_{0.04}Bi_{0.55})_{1.04}$, respectively. Maximum content of substitutions (in wt%) are Ni 2.0 [illegible] t 1.1, Ir 0.4, Os 0.3, and Fe 0.57; Ir, Os and Fe were detected for the first time. Trace amounts of As (substituting for Sb) have also been detected. The relatively large grain size analysed (90x20 μm) excludes the possibility of contamination of As from the host mineral during electron microprobe analysis. A few grains were inhomogeneous in back-scattered electron mode due to variation of Bi/Sb ratio with a distribution different or even reverse in comparison with grains from Kambalda, Australia. One grain is 50x20 μm in size with two different compositions: $(Pd_{0.97}Pt_{0.01}Ir_{0.01}Fe_{0.01}Ni_{0.04})_{1.04}Te_{0.96}(Sb_{0.70}Bi_{0.29})_{0.99}$ and

Fig. 6.2 Compositions of Thompson mine testibiopalladite-Sb-michenerite in Pd_2Te-Bi_2Te-Sb_2Te system (small filled circles) relative to data from the literature. Pd=(Pd+Pt+Ni).

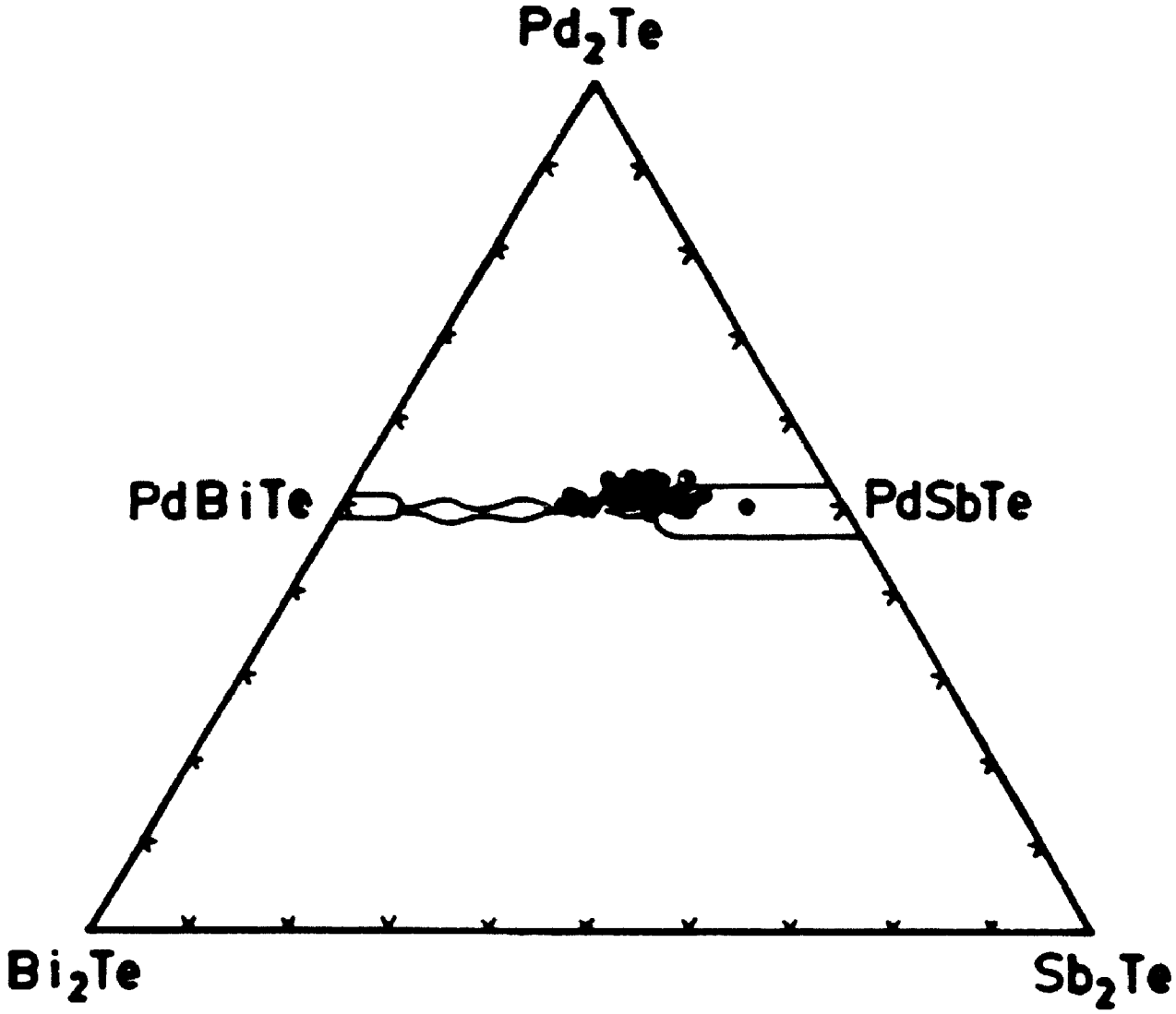
Pd_2Te
PdBiTe
PdSbTe
Bi_2Te
Sb_2Te

Table 6.2 Representative electron microprobe analyses of testibiopalladite-Sb-michenerite from ore type II, metapelite host

sample	1	2	3	4	5	6	7	8	9
					weight percent				
Pt	0.14	0.55	0.24	0.69	0.79	0.54	0.97	1.13	0.42
Pd	28.22	27.28	27.22	26.56	26.58	24.84	25.58	25.90	26.01
Ir	0.00	0.34	0.00	0.25	0.44	0.00	0.36	0.32	0.04
Os	0.00	0.14	0.00	0.12	0.23	0.00	0.34	0.18	0.09
Rh	-	-	-	-	-	0.00	-	-	0.00
Ru	-	-	-	-	-	0.00	-	-	0.00
Fe	0.12	0.08	0.57	0.31	0.10	0.16	0.04	0.06	0.00
Ni	0.32	0.64	0.37	0.87	0.56	2.02	0.15	0.29	0.31
As	0.14	0.05	0.12	0.06	0.00	0.69	0.00	0.45	0.81
Bi	10.89	16.24	18.56	20.98	22.21	23.40	26.10	27.15	28.93
Te	32.23	32.31	31.23	31.63	31.84	31.79	31.09	29.80	30.52
Sb	26.84	22.49	20.98	19.36	18.03	16.49	14.05	13.78	13.62
S	0.01	0.03	0.01	0.03	0.03	-	0.02	0.02	-
Total	98.91	100.15	99.30	100.86	100.81	99.93	98.70	99.08	100.75
					atomic percent				
Pt	0.1	0.4	0.2	0.5	0.5	0.4	0.7	0.8	0.3
Pd	33.1	32.4	32.7	31.8	32.3	30.0	32.6	32.9	32.5
Ir	0.0	0.2	0.0	0.2	0.3	0.0	0.3	0.2	0.0
Os	0.0	0.1	0.0	0.1	0.2	0.0	0.2	0.1	0.1
Rh	-	-	-	-	-	0.0	-	-	0.0
Ru	-	-	-	-	-	0.0	-	-	0.0
Fe	0.3	0.2	1.3	0.7	0.2	0.4	0.1	0.1	0.0
Ni	0.7	1.4	0.8	1.9	1.2	4.4	0.4	0.7	0.7
As	0.2	0.1	0.2	0.1	0.0	1.2	0.0	0.8	1.4
Bi	6.5	9.8	11.4	12.8	13.7	14.4	17.0	17.5	18.4
Te	31.5	32.0	31.3	31.6	32.3	32.0	33.1	31.5	31.8
Sb	27.5	23.4	22.1	20.3	19.2	17.4	15.7	15.3	14.9
S	0.1	0.1	0.1	0.1	0.1	-	0.1	0.1	-

1. $(Pd_{0.99}Ni_{0.02}Fe_{0.01})_{1.02}(Sb_{0.83}Bi_{0.20}As_{0.01})_{1.04}Te_{0.99}$
2. $(Pd_{0.97}Ir_{0.01}Ni_{0.04}Fe_{0.01}Pt_{0.01})_{1.04}(Sb_{0.79}Bi_{0.19})_{0.98}Te_{0.98}$
3. $(Pd_{0.98}Ni_{0.02}Fe_{0.04})_{1.04}(Sb_{0.66}Bi_{0.34}As_{0.01})_{1.01}Te_{0.94}$
4. $(Pd_{0.93}Ni_{0.06}Fe_{0.02}Pt_{0.01})_{1.04}(Sb_{0.61}Bi_{0.38})_{0.99}Te_{0.99}$
5. $(Pd_{0.97}Ir_{0.01}Ni_{0.04}Fe_{0.01}Pt_{0.02})_{1.03}(Sb_{0.57}Bi_{0.41})_{0.98}Te_{0.97}$
6. $(Pd_{0.90}Ni_{0.13}Fe_{0.01}Pt_{0.01})_{1.05}(Sb_{0.52}Bi_{0.43}As_{0.04})_{0.99}Te_{0.96}$
7. $(Pd_{0.98}Ir_{0.01}Os_{0.01}Ni_{0.01}Pt_{0.02})_{1.03}(Sb_{0.47}Bi_{0.51})_{0.98}Te_{0.99}$
8. $(Pd_{0.99}Ir_{0.01}Ni_{0.02}Pt_{0.02})_{1.04}(Sb_{0.46}Bi_{0.53}As_{0.02})_{1.01}Te_{0.95}$
9. $(Pd_{0.97}Ni_{0.02}Pt_{0.01})_{1.00}(Sb_{0.45}Bi_{0.53}As_{0.04})_{1.02}Te_{0.98}$

$(Pd_{0.97}Pt_{0.02}Ir_{0.01}Fe_{0.01}Ni_{0.06})_{1.07}Te_{0.98}(Sb_{0.58}Bi_{0.40})_{0.98}$. Another grain is about 90x30 μm in size. A traverse along the long axis of the latter grain reveals asymmetrical compositional zoning with Sb-michenerite in the core and testibiopalladite towards the margins (Plate 4F, Table 6.3).

6.3 Unnamed PGM

One variety of PGMs observed at the Thompson mine is composed of mainly Pd, Ni, Te and Sb with an average formula of $(Pd,Ni)_{0.44}(Te,Sb)_{0.56}$, based on electron microprobe analyses of over 50 grains (Appendix XVII). Both in air and in oil, the mineral appears slightly anisotropic, from yellowish white with a green tint to a pink tint, when next to pyrrhotite and gersdorffite, respectively. The mineral is pure yellowish white when next to pentlandite, only slightly whiter than pentlandite itself. Next to chalcopyrite, the Pd-rich variety of the mineral (white with a yellowish tint) is distinctly brighter than Ni-rich grains (yellowish white to creamy). The mineral is creamy next to testibiopalladite, but distinctly yellower than the latter. The mineral is greyish green with bluish tint next to sudburyite, whereas sudburyite is yellowish white. But in oil, the mineral becomes yellowish grey The mineral is more greenish next to gold. It is distinctly anisotropic under crossed nicols, from brownish grey to bluish grey. The high Ni-content variety is strongly anisotropic. Over 50 percent of the grains occur as inclusions in gersdorffite. Grains associated with nickeline are less common and are usually attached to pyrrhotite and

Table 6.3 Electron microprobe analyses of zoning from Sb-michenerite to testibiopalladite in a single grain from ore type II, metapelite host

location	1	2	3	4	5	6	7
	margin			core			margin
				weight percent			
Pt	0.26	0.33	0.54	0.42	0.44	0.48	0.43
Pd	27.38	27.33	26.57	26.01	26.27	26.77	26.75
Ir	0.00	0.00	0.00	0.04	0.00	0.00	0.00
Os	0.04	0.00	0.00	0.09	0.00	0.11	0.00
Rh	0.02	0.03	0.04	0.00	0.04	0.01	0.00
Ru	0.00	0.00	0.00	0.00	0.00	0.00	0.00
Fe	0.04	0.00	0.01	0.00	0.02	0.00	0.01
Ni	1.12	0.43	0.22	0.31	0.36	0.47	0.54
As	0.10	0.03	0.00	0.81	0.00	0.00	0.04
Bi	19.98	21.06	26.28	28.93	27.54	27.22	23.61
Te	32.37	32.31	31.54	30.52	31.43	31.85	31.59
Sb	19.95	19.76	15.50	13.62	14.24	15.33	17.50
Total	101.26	101.28	100.70	100.75	100.34	102.24	100.47
				atomic percent			
Pt	0.2	0.2	0.4	0.3	0.3	0.3	0.3
Pd	32.4	32.8	33.0	32.5	32.9	32.7	32.7
Ir	0.0	0.0	0.0	0.0	0.0	0.0	0.0
Os	0.0	0.0	0.0	0.1	0.0	0.1	0.0
Rh	0.0	0.0	0.1	0.0	0.1	0.0	0.0
Ru	0.0	0.0	0.0	0.0	0.0	0.0	0.0
Fe	0.1	0.0	0.0	0.0	0.0	0.0	0.0
Ni	2.4	0.9	0.5	0.7	0.8	1.1	1.2
As	0.2	0.1	0.0	1.4	0.0	0.0	0.1
Bi	12.6	12.9	16.6	18.4	17.6	17.0	14.7
Te	32.0	32.4	32.7	31.8	32.8	32.5	32.2
Sb	20.7	20.7	16.8	14.9	15.6	16.4	18.7

1. $(Pd_{0.97}Ni_{0.01}Pt_{0.01})_{1.03}(Sb_{0.62}Bi_{0.36}As_{0.01})_{0.99}Te_{0.98}$
2. $(Pd_{0.98}Ni_{0.00}Pt_{0.01})_{1.02}(Sb_{0.62}Bi_{0.39})_{1.01}Te_{0.97}$
3. $(Pd_{0.99}Ni_{0.01}Pt_{0.01})_{1.01}(Sb_{0.50}Bi_{0.50})_{1.00}Te_{0.98}$
4. $(Pd_{0.97}Ni_{0.02}Pt_{0.01})_{1.00}(Sb_{0.45}Bi_{0.55}As_{0.04})_{1.04}Te_{0.95}$
5. $(Pd_{0.99}Ni_{0.02}Pt_{0.01})_{1.02}(Sb_{0.47}Bi_{0.53})_{1.00}Te_{0.98}$
6. $(Pd_{0.98}Ni_{0.00}Pt_{0.01})_{1.02}(Sb_{0.49}Bi_{0.51})_{1.00}Te_{0.97}$
7. $(Pd_{0.98}Ni_{0.04}Pt_{0.01})_{1.03}(Sb_{0.56}Bi_{0.44})_{1.00}Te_{0.97}$

gersdorffite (Plate 4G). The mineral has also been found to be associated with chalcopyrite, pentlandite, and silicates such as chlorite, biotite, and quartz. Two grains coexist with gold (Plate 4H), two with testibiopalladite (Plate 4E) and four with sudburyite (Plate 4G). The grain size ranges from 10x10 μm to 80x30 μm and the grain shape is anhedral to euhedral (six-sided). Representative compositions of the unnamed PGM are given in Table 6.4. The Ni content, substituting for Pd, varies from 5.8 to 11.4 wt% (i.e., atomic ratio of Ni/(Ni+Pd) is 0.26 to 0.48) with corresponding formula of $(Pd_{0.32}Ni_{0.11}Fe_{0.01})_{0.44}(Sb_{0.28}Te_{0.27}Bi_{0.01})_{0.54}$ to $(Pd_{0.23}Ni_{0.21})_{0.44}(Te_{0.27}Sb_{0.27}Bi_{0.01}As_{0.01})_{0.56}$. The atomic ratio of Te to Sb remains unchanged from grain to grain, and is approximately one. Compositions of the mineral have been plotted in the system (Pd+Pt+Ir+Os+Rh+Ru)-(Ni+Fe)-(Te+Sb+Bi+As) (Fig. 6.3). Maximum contents of substitutions (in wt%) are Pt 0.2, Ir 0.1, Os 0.4, Rh 0.02), Fe 0.8, Bi 2.6, and As 0.5.

6.4 Majakite

Majakite is a rare mineral. It was first discovered and described from chalcopyrite and talnakhite ores of the Majak mine, Talnakh deposit, in Noril'sk region, Russia, where it often occurs as inclusions in polarite and also as intergrowths with stannopalladinite and ferroplatinum (Genkin, 1978). Majakite has been described also associated with djerfisherite and polarite from that area (Genkin and Evstigneeva, 1986). Recently, majakite has been reported

Table 6.4 Representative electron microprobe analyses of unnamed PGM phase from ore type II, metapelite host

sample	1	2	3	4	5	6	7	8	9
				weight percent					
Pt	0.00	0.14	0.00	0.17	0.20	0.00	0.00	0.00	0.01
Pd	30.48	27.98	31.02	26.61	25.61	26.66	26.49	22.68	23.75
Ir	0.00	0.10	0.09	0.11	0.02	0.00	0.00	0.04	0.00
Os	0.00	0.37	0.00	0.00	0.05	0.00	0.00	0.00	0.00
Rh	-	-	-	-	-	-	-	0.00	0.02
Ru	-	-	-	-	-	-	-	0.00	0.00
Fe	0.45	0.84	0.00	0.23	0.10	0.00	0.12	0.25	0.14
Ni	5.76	6.91	7.11	7.69	8.40	8.88	9.33	11.42	10.69
As	0.29	0.30	0.51	0.29	0.43	0.28	0.31	0.42	0.48
Bi	1.01	2.55	1.08	1.35	1.87	1.30	1.38	1.53	1.21
Te	31.03	31.00	31.27	32.28	31.80	31.86	32.03	32.13	32.31
Sb	30.23	30.20	29.00	30.94	30.74	30.86	31.08	31.21	30.93
S	0.00	0.06	0.01	0.02	0.02	0.00	0.01	-	-
Total	99.25	100.45	100.09	99.69	99.24	99.84	100.75	99.68	99.54
				atomic percent					
Pt	0.0	0.1	0.0	0.1	0.1	0.0	0.0	0.0	0.0
Pd	32.1	29.0	32.1	27.6	26.6	27.4	26.9	22.8	24.1
Ir	0.0	0.1	0.1	0.1	0.0	0.0	0.0	0.0	0.0
Os	0.0	0.2	0.0	0.0	0.0	0.0	0.0	0.0	0.0
Rh	-	-	-	-	-	-	-	0.0	0.0
Ru	-	-	-	-	-	-	-	0.0	0.0
Fe	0.9	1.7	0.0	0.5	0.2	0.0	0.2	0.5	0.3
Ni	11.0	13.0	13.3	14.5	15.8	16.5	17.1	20.8	19.6
As	0.4	0.4	0.8	0.4	0.6	0.4	0.5	0.6	0.7
Bi	0.5	1.3	0.6	0.7	1.0	0.7	0.7	0.8	0.6
Te	27.2	26.8	27.0	28.0	27.6	27.3	27.1	27.0	27.3
Sb	27.8	27.3	26.2	28.1	27.9	27.7	27.5	27.5	27.4
S	0.0	0.2	0.0	0.1	0.1	0.0	0.0	-	-

1. $(Pd_{0.32}Ni_{0.11}Fe_{0.01})_{0.44}(Sb_{0.28}Te_{0.27}Bi_{0.01})_{0.56}$
2. $(Pd_{0.29}Ni_{0.13}Fe_{0.02})_{0.44}(Sb_{0.27}Te_{0.27}Bi_{0.01})_{0.55}$
3. $(Pd_{0.32}Ni_{0.13})_{0.45}(Sb_{0.28}Bi_{0.01}Te_{0.27}Bi_{0.01}As_{0.01})_{0.56}$
4. $(Pd_{0.28}Ni_{0.14})_{0.42}(Sb_{0.28}Te_{0.28}Bi_{0.01})_{0.57}$
5. $(Pd_{0.27}Ni_{0.16})_{0.43}(Sb_{0.28}Te_{0.28}Bi_{0.01}As_{0.01})_{0.58}$
6. $(Pd_{0.27}Ni_{0.17})_{0.44}(Sb_{0.28}Te_{0.27}Bi_{0.01})_{0.56}$
7. $(Pd_{0.27}Ni_{0.17})_{0.44}(Sb_{0.28}Te_{0.27}Bi_{0.01})_{0.56}$
8. $(Pd_{0.23}Ni_{0.21})_{0.44}(Sb_{0.27}Te_{0.27}Bi_{0.01}As_{0.01})_{0.56}$
9. $(Pd_{0.24}Ni_{0.20})_{0.44}(Sb_{0.27}Te_{0.27}Bi_{0.01}As_{0.01})_{0.56}$

Fig. 6.3 Compositions of Thompson mine unnamed PGM in the

(Pd+Pt+Ir+Os+Rh+Ru)-(Ni+Fe)-(Te+Sb+Bi+As) system.

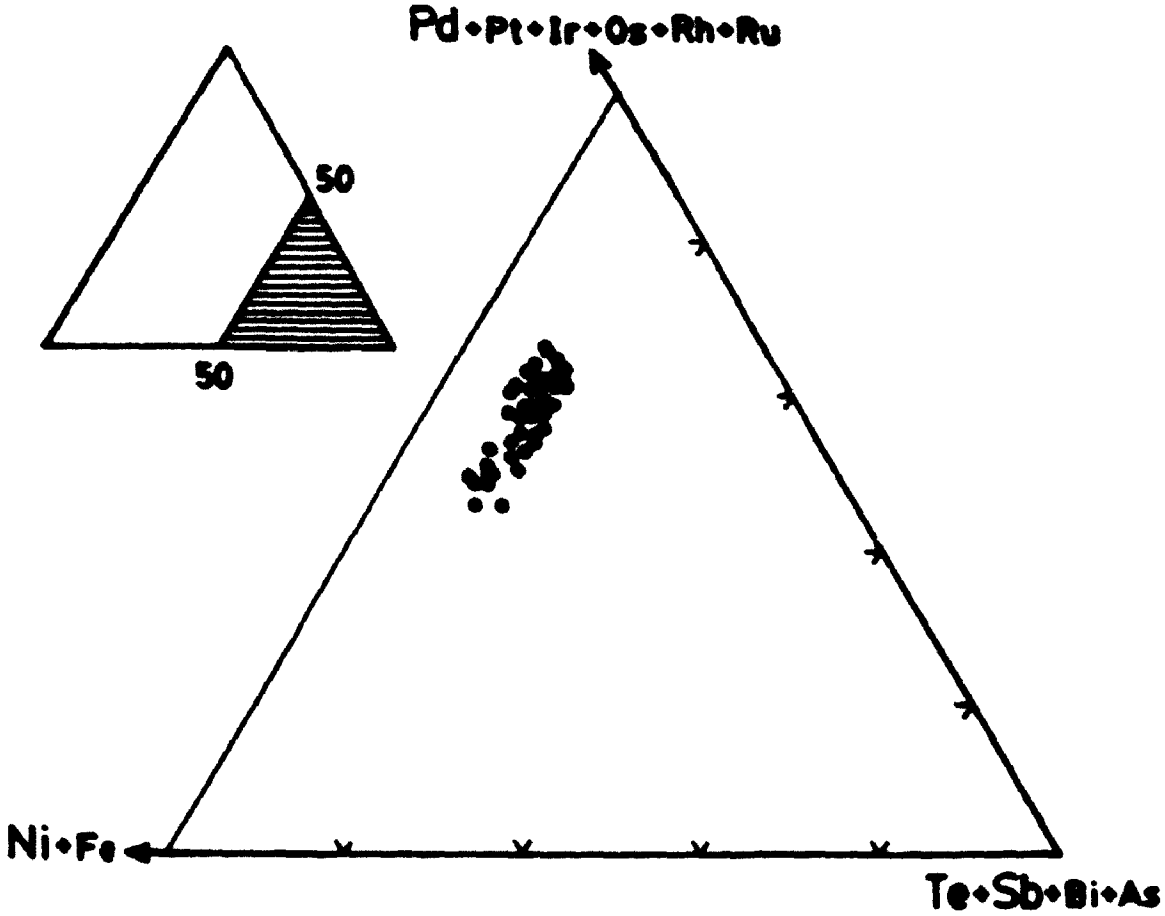
Pd•Pt•Ir•Os•Rh•Ru
50
50
Ni•Fe
Te•Sb•Bi•As

from Ni-bearing layered mafic-ultramafic massifs of the Kola region, Russia (Yakovlev et al., 1991).

In this study, majakite is observed to be the most common PGM in the Thompson mine pegmatite. The majority of majakite grains occur at the boundary between nickeline and silicate gangue minerals (Plate 4I). It also appears as elongated inclusions in nickeline. It occurs generally as subhedral to euhedral grains, 10x10 μm to 60x10 μm in size. Under reflected light, majakite appears greyish creamy with a bluish tint. Reflection pleochroism in air is weak to distinct, from greyish creamy to bluish creamy. In oil, majakite is greyish white with a distinct bluish tint with pleochroism from greyish to bluish white. Both in air and in oil, majakite is weak to moderately anisotropic, from bluish grey to brownish grey.

The compositions of majakite have been plotted on a (Pd+Pt+Os+Ir)-(Ni+Fe)-(As+Sb+Bi+Te) ternary diagram (Fig. 6.4, c.f. Appendix XVIII). Representative electron microprobe analyses of majakite are given in Table 6.5. Palladium contents range from 46.7 to 48.8 wt%, and Ni from 18.7 to 20.0 wt%. Arsenic content varies from 31.0 to 33.5 wt%, giving the formula $Pd_{1.09}Ni_{0.79}As_{1.00}$ to $Pd_{0.99}Os_{0.01}Ni_{0.74}As_{1.00}$, which shows that majakite from the Thompson mine is Ni-depleted. Maximum contents of substitutions (in wt%) are Os 0.7, Ir 0.2, Pt 0.2, Fe 0.1, Te 0.2, Bi 0.2, and Sb 0.2; Os, Ir, Pt, and Fe were detected for the first time. Osmium, Ir and Pt may substitute for Pd, and Fe for Ni, and Te, Bi, and Sb may substitute for As.

Fig. 6.4 Compositions of Thompson mine majakite (filled circles) in the (Pd+Pt+Os+Ir)-(Ni+Fe)-(As+Sb+Bi+Te) system. Triangle and open circles represent data from Kola region and Majak Mine, Russia, respectively.

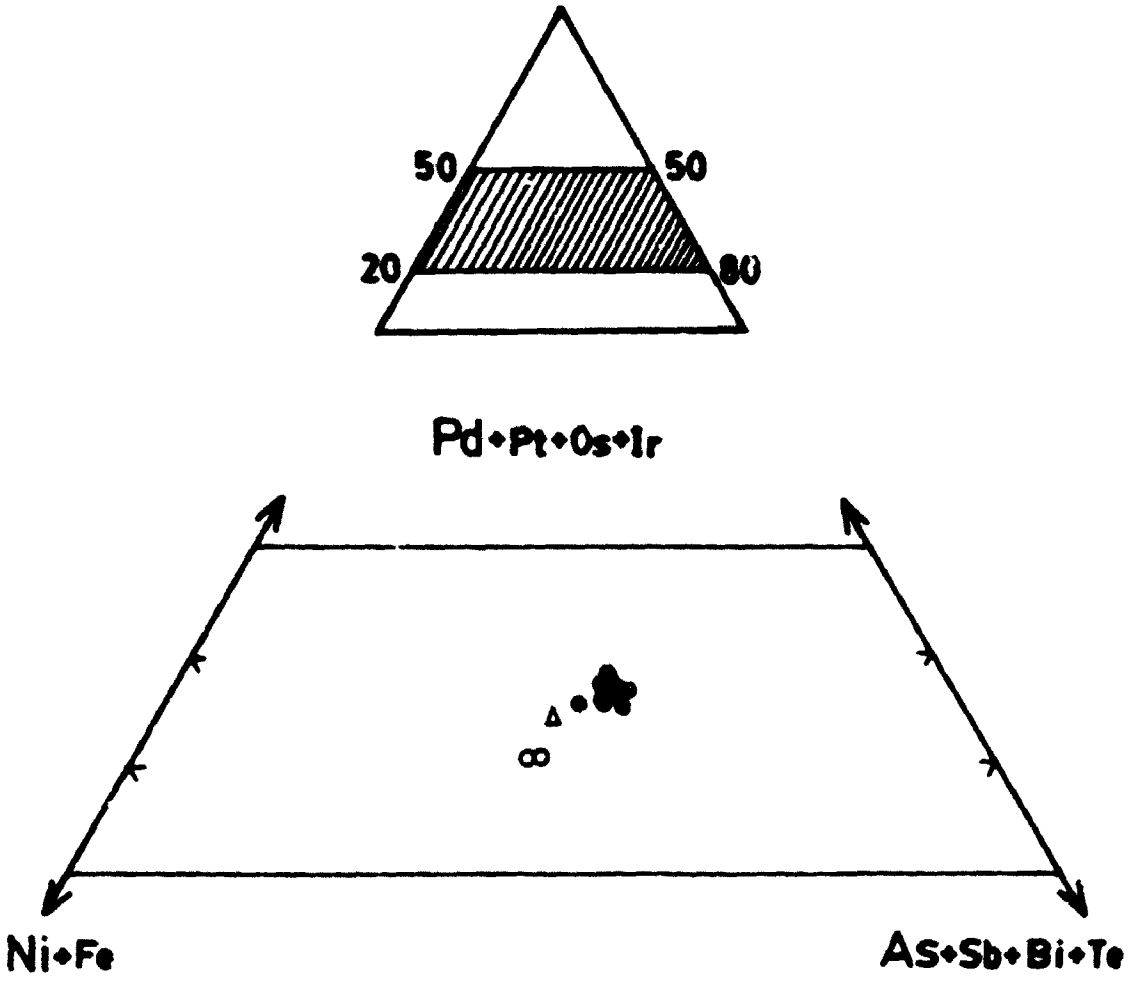
50
50
20
80
Pd+Pt+Os+Ir
Ni+Fe
As+Sb+Bi+Te

Table 6.5 Representative electron microprobe analyses of majakite from ore type IV, pegmatite host

sample	1	2	3	4	5	6	7	8
				weight percent				
Pt	0.00	0.18	0.04	0.10	0.00	0.06	0.01	0.21
Pd	46.65	46.78	47.13	48.80	48.60	47.43	47.89	48.73
Os	0.66	0.15	0.35	0.07	0.33	0.59	0.07	0.13
Ir	0.00	0.00	0.00	0.04	0.17	0.03	0.11	0.00
Au	-	-	-	-	0.09	0.00	-	-
Ag	-	-	-	-	0.00	0.01	-	-
Fe	0.03	0.02	0.08	0.04	0.06	0.02	0.06	0.08
Ni	19.98	20.04	19.45	19.58	18.75	19.34	18.68	18.85
Pb	0.00	0.10	0.00	-	-	-	-	-
As	33.21	33.32	33.49	31.58	32.32	32.70	31.01	31.56
Sb	0.20	0.20	0.20	0.00	-	-	0.00	0.00
Bi	..09	0.00	0.00	0.00	0.00	0.00	0.00	0.16
Te	0.05	0.09	0.10	0.12	0.14	0.00	0.18	0.05
S	0.01	0.00	0.04	0.00	0.01	0.05	0.00	0.01
Total	100.88	100.88	100.88	100.33	100.47	100.23	98.01	99.78
				atomic percent				
Pt	0.0	0.1	0.0	0.0	0.0	0.0	0.0	0.1
Pd	35.7	35.7	36.1	37.7	37.7	36.6	38.0	38.0
Os	0.3	0.1	0.2	0.0	0.1	0.3	0.0	0.1
Ir	0.0	0.0	0.0	0.0	0.1	0.0	0.1	0.0
Au	-	-	-	-	0.0	0.0	-	-
Ag	-	-	-	-	0.0	0.0	-	-
Fe	0.0	0.0	0.1	0.1	0.1	0.0	0.1	0.1
Ni	27.7	27.7	27.0	27.4	26.3	27.1	26.8	26.6
Pb	0.0	0.0	0.0	-	-	-	-	-
As	36.1	36.1	36.4	34.7	35.6	35.9	34.9	35.0
Sb	0.1	0.1	0.1	0.0	-	-	0.0	0.0
Bi	0.0	0.0	0.0	0.0	0.0	0.0	0.0	0.1
Te	0.0	0.1	0.1	0.1	0.1	0.0	0.1	0.0
S	0.0	0.0	0.1	0.0	0.0	0.1	0.0	0.0

1. $(Pd_{1.67}Os_{0.01})_{1.68}Ni_{0.89}As_{1.43}$
2. $Pd_{1.67}Ni_{0.87}As_{1.46}$
3. $Pd_{1.68}Ni_{0.81}As_{1.50}$
4. $Pd_{1.73}Ni_{0.82}As_{1.45}$
5. $Pd_{1.73}Ni_{0.78}As_{1.49}$
6. $(Pd_{1.77}Os_{0.01})_{1.78}Ni_{0.81}As_{1.41}$
7. $Pd_{1.74}Ni_{0.82}As_{1.44}$
8. $Pd_{1.74}Ni_{0.82}As_{1.44}$

6.5 Kotulskite

Kotulskite has been reported from Cu-Ni sulfide deposits, such as Sudbury (Cabri and Laflamme, 1976), Noril'sk, USSR (Genkin and Evstigneeva, 1986), Cu sulfide deposits, such as the New Rambler Pt-Cu-Au deposit (Nyman, 1990) and Geordie Lake intrusion, Coldwell Complex, Ontario (Mulja and Mitchell, 1990), and mafic-ultramafic layered complexes, such as Merensky Reef (Kingston and El-Dosuky, 1982; Tarkian, 1987), Kola Region, Russia (Yakovlev et al., 1991), Stillwater (Volborth et al., 1986), Penikat PGE Reef, northern Finland (Halkoaho et al., 1990a; 1990b), and Lac Des Iles Complex, Ontario (Cabri, 1981b).

In this study, kotulskite from the Thompson mine usually occurs as inclusions in nickeline. Only one grain has been recorded in gersdorffite. The inclusion size ranges from 5x10 μm to 20x5 μm. Under reflected light it is creamy, and under crossed nicols it is weakly anisotropic, grey to pale brownish grey. No reflection pleochroism is observed when the mineral is next to nickeline in air, but in oil the mineral shows weak pleochroism from creamy white to creamy. However, weak pleochroism from creamy to pale bluish creamy is observed in air when the mineral occurs next to gersdorffite, and it appears much yellower in oil. Most kotulskite grains yielded poor electron microprobe analyses due to their small size. Our best result (in wt%) was Pd 38.3, Ni 1.0, Pt 0.3, Fe 0.1, Ir 0.1, S 0.04, Bi 18.8, Te 37.0, Sb 0.2, total

95.8, corresponding to $(Pd_{0.94}Ni_{0.05}Fe_{0.01})_{1.00}(Te_{0.76}Bi_{0.24})_{1.00}$. Kotulskite from the Thompson mine appears to have a high Ni content, higher than that reported from other localities. Because no As was detected, contamination from host minerals is apparently excluded. On a (Pd+Pt+Fe+Ni+Cu)-(Bi+Te)-Te ternary diagram (Fig. 6.5), Thompson mine kotulskite plots in the same field as samples from Merensky Reef and the Penikat layered intrusion, Finland. Three of the representative analyses of kotulskite have [(Pd+Ni)/(Bi+Te)] atomic ratios greater than 1, giving formulae of $(Pd_{3.00}(Te_{1.59}Bi_{0.41})_{2.00}$, $Pd_{4.00}(Te_{2.46}Bi_{0.54})_{3.00}$, and $Pd_{6.00}(Te_{3.77}Bi_{1.23})_{5.00}$, respectively (Table 6.6). These grains contain more Pd than analyses previously reported, may represent Pd-rich kotulskite or analytical error attributable to small grain size.

6.6 Michenerite

Michenerite has been documented previously from the Pipe mine, which is located over 40 km north from the present locality along the strike of the Thompson Nickel Belt, where it occurs in sulfide veins cutting serpentinite (Cabri and Laflamme, 1981). In this study, two grains of michenerite were found coexisting with nickeline, included in gersdorffite (5x10 and 5x5 μm in size). Under reflected light, michenerite is pale blue in colour with a grey tint. In oil, it is bluish grey. The mineral is isotropic both in oil and in air. Representative compositions are given in Table 6.7 and all analyses are plotted in the ternary diagram (Pd+Pt+Fe+Ni+Cu)-(Bi+Sb)-Te (Fig. 6.5) to

Fig. 6.5 Compositions of Thompson mine kotulskite, merenskyite and michenerite (filled circles) in the (Pd+Pt+Fe+Ni+Cu)-(Bi+Sb)-Te system. Shaded areas represent data reported in the literature (Beaudoin et al., 1990; Halkaho et al., 1990; Harney and Merkle, 1990; Mulja and Mitchell, 1990; Yakovlev et al., 1991).

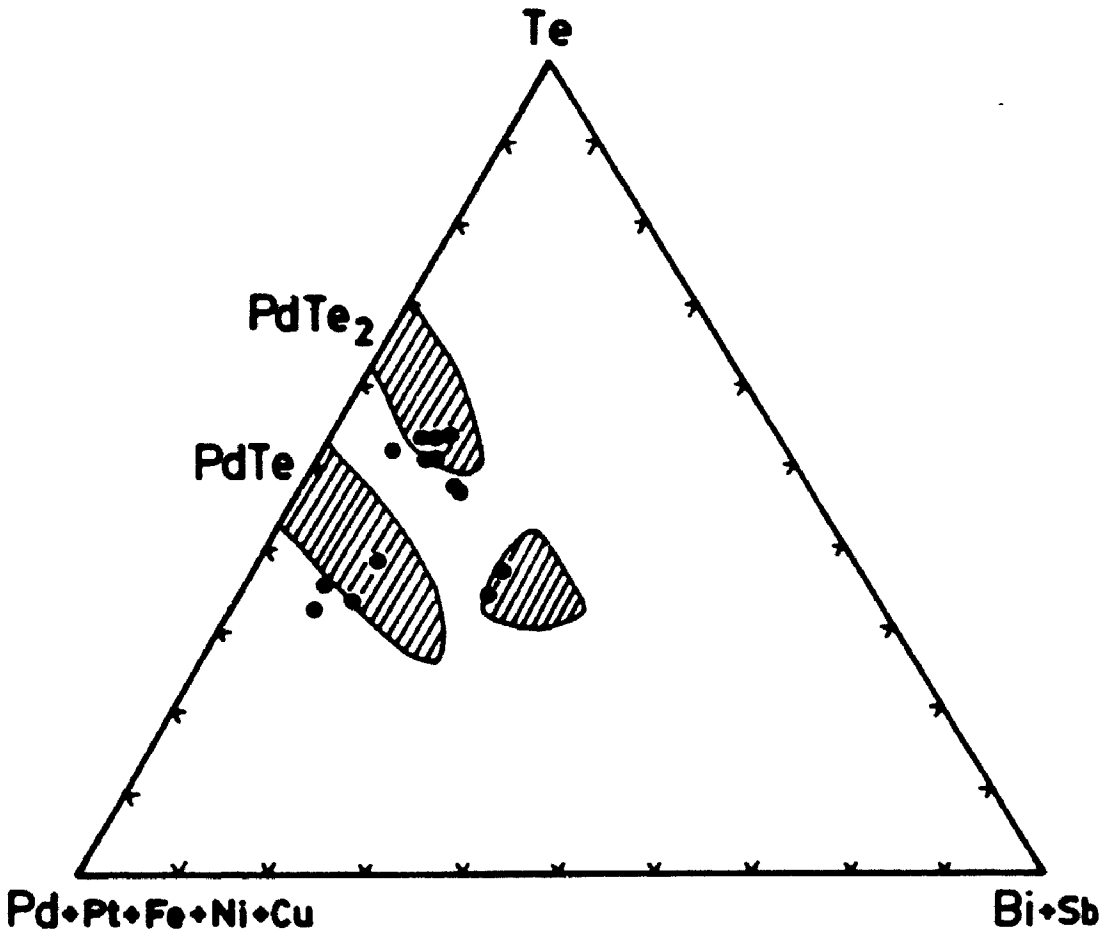
Te
PdTe2
PdTe
Pd•Pt•Fe•Ni•Cu
Bi•Sb

Table 6.6 Electron microprobe analyses of Pd-(Te,Bi) minerals from ore type IV, pegmatite host

	kotulskite	$Pd_3(Te,Bi)_2$	$Pd_4(Te,Bi)_3$	$Pd_9(Te,Bi)_5$
		weight percent		
Pd	38.31	46.04	44.73	44.52
Pt	0.31	0.00	0.00	0.00
Os	0.00	0.00	0.00	0.00
Ir	0.05	0.00	0.00	0.00
Fe	0.12	0.10	0.16	0.18
Ni	1.01	1.80	2.37	0.73
As	0.00	0.00	0.15	0.01
Sb	0.19	0.00	0.00	0.00
Bi	18.83	14.16	13.51	18.76
Te	36.97	33.28	37.43	35.21
S	0.04	0.08	0.05	0.00
Total	95.83	95.46	98.40	99.41
		atomic percent		
Pd	47.1	54.4	51.0	52.3
Pt	0.2	0.0	0.0	0.0
Os	0.0	0.0	0.0	0.0
Ir	0.0	0.0	0.0	0.0
Fe	0.3	0.2	0.4	0.4
Ni	2.3	3.8	4.9	1.6
As	0.0	0.0	0.2	0.0
Sb	0.2	0.0	0.0	0.0
Bi	11.8	8.5	7.8	11.2
Te	37.9	32.8	35.5	34.5
S	0.2	0.3	0.2	0.0

1. $(Pd_{0.94}Ni_{0.03}Fe_{0.01})_{1.00}(Te_{0.76}Bi_{0.24})_{1.00}$
2. $(Pd_{2.72}Ni_{0.19}Fe_{0.01})_{2.92}(Te_{1.04}Bi_{0.43}S_{0.01})_{2.08}$
3. $(Pd_{3.57}Ni_{0.34}Fe_{0.02})_{3.93}(Te_{2.49}Bi_{0.55}As_{0.02})_{3.06}$
4. $(Pd_{3.73}Ni_{0.17}Fe_{0.03})_{3.97}(Te_{3.79}Bi_{1.23}S_{0.01})_{5.03}$

compare with data reported from the literature. Michenerite from the Thompson mine is apparently Pd enriched. The corresponding formula is $(Pd_{1.05}Ni_{0.11}Fe_{0.01})_{1.17}(Bi_{0.78}Sb_{0.01}S_{0.01})_{0.80}Te_{1.03}$.

6.7 Merenskyite

A total of 7 grains of merenskyite were found in this study. Three grains are from metapelite-hosted ore type II. One merenskyite grain occurs in pyrrhotite, and two in gersdorffite. The other four grains of merenskyite were from ore type IV (pegmatite-hosted), in which two occur in gersdorffite, one is associated with native gold in gersdorffite, and one is in nickeline. Most of the grains are present as rounded and elongated inclusions and their sizes range from 10x10 to 10x20 μm. When next to nickeline, merenskyite is yellowish white with very weak pleochroism from white to light creamy both in air and in oil. Anisotropism is weak to distinct both in air and in oil, from bluish grey to pale yellowish grey. Merenskyite is pale greenish yellow within gersdorffite. Reflection pleochroism is nil to weak, but more distinct in oil, and is pale blue to pale yellow. The composition of merenskyite has been plotted in a (Pd+Pt+Fe+Ni+Cu)-(Bi+Sb)-Te diagram (Fig. 6.5) to compare with compositions from the literature. Merenskyite from the Thompson mine is metal enriched. Representative analyses are given in Table 6.7. Merenskyite from pegmatite contains Bi 16.8 to 19.0 wt%, with corresponding formulae of $(Pd_{0.93}Pt_{0.01}Ni_{0.10}Fe_{0.03})_{1.07}(Te_{1.62}Bi_{0.31}Sb_{0.01}S_{0.01})_{1.95}$ to

Table 6.7 Electron microprobe analyses of merenskyite and michenerite

sample	1	2	3	4	5	6	7
				weight percent			
Pt	0.42	0.29	0.59	0.38	0.30	0.65	0.00
Pd	26.44	25.69	25.87	25.06	22.75	25.41	27.12
Os	0.00	0.00	0.24	0.00	0.00	0.00	0.00
Ir	0.05	0.00	0.24	0.00	0.00	0.09	0.05
Au	-	-	-	-	-	0.00	-
Ag	-	-	-	-	-	0.13	-
Fe	0.56	0.45	0.08	0.49	2.58	0.24	0.31
Ni	1.96	1.48	1.46	2.55	2.19	2.05	1.52
Co	-	-	-	0.13	-	-	-
As	0.00	0.00	0.00	0.00	0.00	0.00	0.11
Sb	0.18	0.18	0.15	-	-	-	0.00
Bi	17.39	16.82	18.96	19.45	15.70	25.27	39.63
Te	52.77	53.82	53.05	50.37	55.11	44.43	32.02
Pb	-	-	-	-	-	-	0.03
S	0.10	0.05	0.03	0.10	0.33	0.02	0.04
Total	99.87	98.78	100.67	98.54	98.96	98.30	100.85
				atomic percent			
Pt	0.3	0.2	0.4	0.3	0.2	0.4	0.0
Pd	31.2	30.9	31.0	30.1	26.2	31.7	34.9
Os	0.0	0.0	0.2	0.0	0.0	0.0	0.0
Ir	0.0	0.0	0.2	0.0	0.0	0.1	0.0
Au	-	-	-	-	-	0.0	-
Ag	-	-	-	-	-	0.2	-
Fe	1.3	1.0	0.2	1.1	5.7	0.6	0.8
Ni	4.2	3.2	3.2	5.6	4.6	4.6	3.5
Co	-	-	-	0.3	-	-	-
As	0.0	0.0	0.0	0.0	0.0	0.0	0.2
Sb	0.2	0.2	0.2	-	-	-	0.0
Bi	10.5	10.3	11.6	11.9	9.2	16.1	26.0
Te	52.0	54.0	53.0	50.4	52.9	46.3	34.4
Pb	-	-	-	-	-	-	0.0
S	0.4	0.2	0.1	0.4	1.3	0.1	0.2

1-3. merenskyite, pegmatite host, ore type IV;
4-6. merenskyite, metapelite host, ore type II;
7. michenerite, pegmatite host, ore type IV.

1. $(Pd_{0.94}Ni_{0.13}Fe_{0.04}Pt_{0.01})_{1.12}(Te_{1.56}Bi_{0.31}Sb_{0.01}S_{0.01})_{1.89}$
2. $(Pd_{0.93}Ni_{0.10}Fe_{0.03}Pt_{0.01})_{1.07}(Te_{1.62}Bi_{0.31}Sb_{0.01}S_{0.01})_{1.95}$
3. $(Pd_{0.93}Ni_{0.10}Fe_{0.01}Pt_{0.01})_{1.05}(Te_{1.79}Bi_{0.15})_{1.94}$
4. $(Pd_{0.89}Ni_{0.17}Fe_{0.03}Co_{0.01}Pt_{0.01})_{1.12}(Te_{1.31}Bi_{0.36}S_{0.01})_{1.68}$
5. $(Pd_{0.79}Ni_{0.14}Fe_{0.17}Pt_{0.01})_{1.11}(Te_{1.79}Bi_{0.28}S_{0.04})_{1.91}$
6. $(Pd_{0.93}Ni_{0.14}Fe_{0.02}Pt_{0.01})_{1.12}(Te_{1.39}Bi_{0.48})_{1.87}$
7. $(Pd_{1.03}Ni_{0.11}Fe_{0.02})_{1.18}(Bi_{0.78}As_{0.01}S_{0.01})_{0.80}Te_{1.03}$

$Pd_{0.95}Pt_{0.01}Ni_{0.10}Fe_{0.01})_{1.05}(Te_{1.59}Bi_{0.34})_{1.93}$, respectively. Merenskyite from metapelite contains Bi 15.7 to 25.3 wt% with formulae of $(Pd_{0.79}Pt_{0.01}Ni_{0.14}Fe_{0.17})_{1.11}(Te_{1.59}Bi_{0.28}S_{0.04})_{1.91}$ to $(Pd_{0.95}Pt_{0.01}Ni_{0.14}Fe_{0.02})_{1.12}(Te_{1.59}Bi_{0.48})_{1.87}$, respectively. Maximum contents of substitutions (in wt%) are Pt 0.7, Os 0.2, Ir 0.2, Fe 0.6, Sb 0.2, Ni 2.6, Ag 0.1, and Co 0.1.

6.8 Irarsite

Irarsite has been recorded previously from Thompson Nickel Belt as inclusions in cobaltite at the Pipe mine (Cabri and Laflamme, 1981). In this study, irarsite occurs as euhedral inclusions in gersdorffite. One 20 μm grain was concentrically zoned (Table 6.8). Platinum content varies from 6.9 wt% in the core, to 8.8, and finally to 5.5 in the margin. Pt-rich areas are brighter in back-scattered electron images. The Rh content increases from core to margin (1.6 to 2.1 wt%, respectively). One location in the host gersdorffite adjacent to the irarsite inclusion contains a higher Rh content (4.1 wt%) than the irarsite itself (Plate 4J). Maximum contents of substitutions (in wt%) are Pd 0.6, Ru 0.1, Ni 2.0, Fe 0.7, and Co 0.6.

6.9 Native Gold

Native gold is a relatively common precious-metal mineral in both metapelite- and pegmatite-hosted ores (ore type II and IV). Representative

Table 6.8 Electron microprobe analyses of irarsite from ore type I, metapelite host

	margin		core
	1	2	3
	weight percent		
Fe	0.72	0.54	0.52
S	9.85	8.95	9.61
Pt	5.50	8.75	6.86
Pd	0.61	0.36	0.44
Ni	2.01	1.79	1.59
As	29.21	29.75	28.86
Co	0.62	0.37	0.46
Ru	0.06	0.06	0.06
Rh	2.14	1.37	1.55
Os	0.00	0.00	0.00
Ir	49.71	47.75	49.66
Total	100.42	99.71	99.61
	atomic percent		
Fe	1.2	0.9	0.9
S	28.7	27.0	28.8
Pt	2.6	4.3	3.4
Pd	0.5	0.3	0.4
Ni	3.2	3.0	2.6
As	36.5	38.4	37.0
Co	1.0	0.6	0.8
Ru	0.1	0.1	0.1
Rh	2.0	1.3	1.5
Os	0.0	0.0	0.0
Ir	24.2	24.0	24.8

1. $(Ir_{0.73}Pt_{0.08}Ni_{0.10}Rh_{0.04}Fe_{0.04}Pd_{0.02})_{1.01}As_{1.00}S_{0.86}$
2. $(Ir_{0.72}Pt_{0.13}Ni_{0.09}Rh_{0.04}Fe_{0.03}Pd_{0.01})_{1.02}As_{1.15}S_{0.81}$
3. $(Ir_{0.74}Pt_{0.10}Ni_{0.08}Rh_{0.04}Fe_{0.03}Pd_{0.01})_{1.00}As_{1.11}S_{0.86}$

compositions of gold from the Thompson mine are given in Table 6.9. Native gold ($Au_{68}Ag_{32}$-$Au_{69}Ag_{31}$) has been documented from three locations in thin sections of pegmatite-hosted samples. It is relatively Ag-rich. The grain size of the gold varies from a few μm in diameter to 30x10 μm. In two instances, it occurs as elongated inclusions in gersdorffite, one coexisting with merenskyite and the other with chalcopyrite. In another instance, it occurs as rounded inclusions at the boundary of gersdorffite and nickeline.

More than 32 native gold grains varying in size from a few μm in diameter to 150x90 μm were found in sample T1FP (ore type II) with compositions of $Au_{74}Ag_{26}$-$Au_{78}Ag_{22}$ (Table 6.9). A trace amount of Cu (0.2 wt%) has been detected. Most of these grains are elongated and included in gersdorffite, but others are attached to chalcopyrite, pyrrhotite, sphalerite, or chlorite. Only a few are completely included in either nickeline or pyrrhotite. Gold also coexists with PGMs, for example, testibiopalladite (2 grains, Plate 4D), unnamed PGM (2 grains, Plate 4H) and sudburyite (1 grain, Plate 4B). In ore type III (metapelite-hosted), native gold ($Au_{73}Ag_{27}$) occurs in association with bismuth telluride within chalcopyrite, and at gersdorffite/chalcopyrite grain boundaries.

Table 6.9 Representative electron microprobe analyses of native gold

sample	1	2	3	4	5
			weight percent		
Au	86.83	83.78	82.49	79.38	78.91
Ag	13.13	15.82	16.46	19.61	20.32
Pt	-	-	0.05	-	-
Hg	0.00	0.00	0.00	0.00	0.00
Cu	0.19	0.00	-	-	-
Total	100.15	99.60	99.00	98.99	99.23
			atomic percent		
Au	78.0	74.4	73.3	68.9	68.0
Ag	21.5	25.6	26.7	31.1	32.0
Pt	-	-	0.1	-	-
Cu	0.5	0.0	-	-	-

1,2. metapelite host, ore type II;
3. metapelite host, ore type III;
4,5. pegmatite host, ore type IV.

Plate 4

PGM from the Thompson mine

A: Electron back-scattered image of sudburyite (white) associated with quartz (black), gersdorffite (dark grey) and nickeline (light grey; ore type II). Sample TAB-1D.

B: Electron back-scattered image of sudburyite (grey) coexisting with gold (white) in gersdorffite matrix (black; ore type II). Sample TD-2.

C: Electron back-scattered image of sudburyite (white) coexisting with unnamed PGM in association with gersdorffite (black; ore type II). Sample TD-4.

D: Electron back-scattered image of testibiopalladite (grey) associated with gold in gersdorffite (black; ore type II). Sample TD-4.

E: Electron back-scattered image of testibiopalladite (light grey) associated with unnamed PGM (grey) in gersdorffite (black; ore type II). Sample TD 2.

F: Electron back-scattered image of testibiopalladite-Sb-michenerite grain showing compositional variation from Sb-michenerite (light grey core) to testibiopalladite (dark grey margin; ore type II). Sample TAB-1AB.

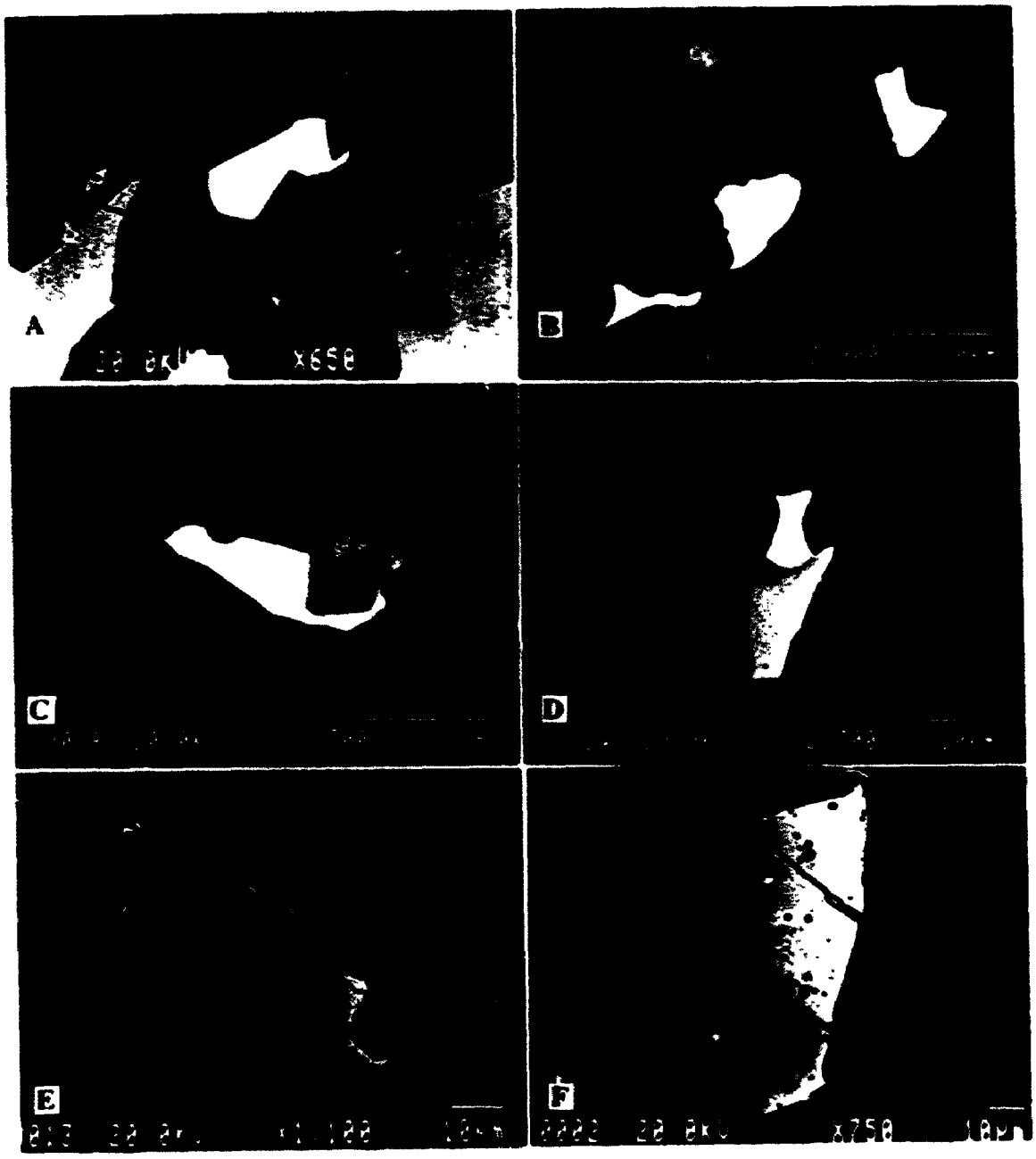
A
B
C
D
E
F

Plate 4 (continued)

G: Electron back-scattered image of unnamed PGM (white) showing cleavage, associated with gersdorffite (dark grey), nickeline (light grey) and pyrrhotite (black; ore type II). Sample TAB-1D.

H: Electron back-scattered image of unnamed PGM (light grey) and gold (white) between gersdorffite (black) and nickeline (dark grey; ore type II). Sample TD-2.

I: Electron back-scattered image of majakite (white) at the boundary between nickeline (grey) and quartz (black; ore type IV). Sample T1A4B.

J: Electron back-scattered image of irarsite (white) included in gersdorffite (grey) associated with pyrrhotite (black; ore type II). Sample TO3A.

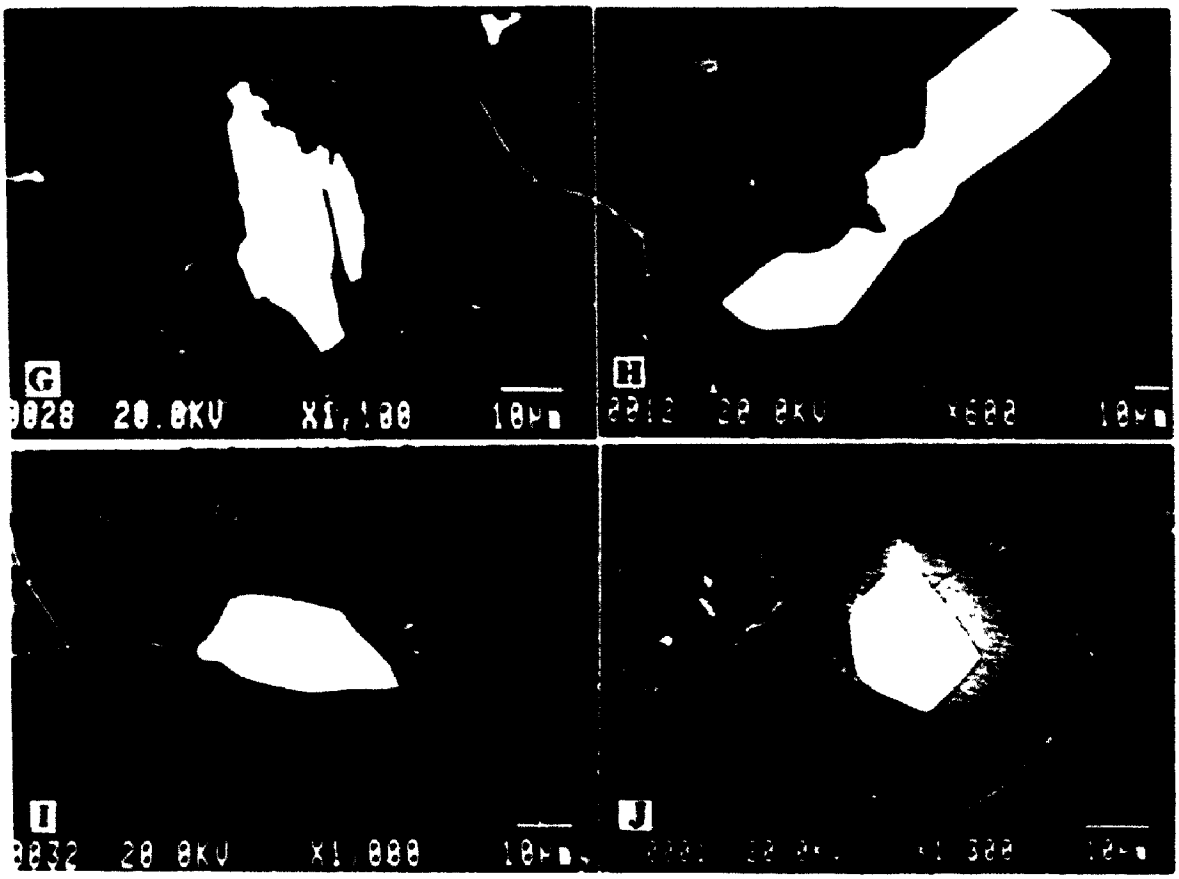
G
20.0KV
10μm
H
I
J

CHAPTER 7 GEOTHERMOMETRY AND GEOBAROMETRY

7.1 Introduction

Rocks of the Thompson Nickel Belt have a complex metamorphic history. The dominant metamorphic grade is amphibolite facies, which is generally understood to be an imprint related to the Hudsonian orogenic event (1.7 Ga, Cranstone and Turek, 1976). Island-like domains of granulite facies gneiss in the amphibolite facies terrane are interpreted as relict of an older event of Archean age, dated at 2.8 Ga (Cranstone and Turek, 1976). Bleeker (1990) proposed 700-750°C, 6-7 kbar (upper amphibolite grade) for the peak metamorphic conditions of the metapelite at the Thompson mine. In this study, in addition to confirming the peak metamorphism, a late hydrothermal event associated with the present precious-metal mineralization is also documented. This event is probably related to the late-stage retrograde alteration of the Hudsonian orogeny (Brooks and Theyer, 1981; Cumming et al., 1982). Also the metasedimentary rocks related to the sulfide mineralization have been retrograded from amphibolite facies to greenschist facies metamorphic grade, and ultramafic rocks to lower epidote-amphibolite and greenschist metamorphic grades.

The garnet-biotite geothermometer, and garnet-plagioclase-sillimanite-quartz geobarometer and geothermobarometer, using multi-equilibrium calculations, have been applied to determine the peak prograde metamorphic

conditions. The chlorite geothermometer and muscovite geobarometer are used to determine the metamorphic conditions of the late-hydrothermal alterations.

7.2 Prograde Metamorphic Conditions

7.2.1 Garnet-biotite geothermometer

The exchange of Mg and Fe between coexisting biotite and garnet is highly sensitive to temperature. With increasing temperature, biotite becomes more Fe-rich and garnet more Mg-rich, according to the following continuous exchange reaction:

$$\text{Fe-garnet} + \text{Mg-biotite} \rightleftharpoons \text{Mg-garnet} + \text{Fe-biotite}. \qquad (1)$$

Because of the common occurrence of this mineral pair in medium to high grade metamorphic rocks, the garnet-biotite Fe-Mg exchange geothermometer finds wide application. At present, various different formulations are available for calculation of temperature. Ferry and Spear (1978) experimentally calibrated the thermometer in systems where Fe/(Fe+Mg) of garnet was held within the range from 0.8 to 0.9. Perchuk (1981) also experimentally calibrated the thermometer in systems with a Fe/(Fe+Mg) value of 0.6. Thompson (1976), Goldman and Albee (1977), and Hodges and Spear (1982) empirically derived the geothermometer from natural garnet-biotite assemblages. Ideal Fe-Mg mixing in both garnet and biotite was assumed in all these formulations except

for that of Hodges and Spear (1982). Dasgupta et al. (1991) and Bhattacharya et al. (1992) proposed a refined geothermometer based on non-ideal mixing of phlogopite-annite and of Fe-Mg-Ca-Mn in garnet.

In this study an ideal mixing model is preferred because all the non-ideal mixing models require an assumed pressure, which makes the geothermometer pressure dependent. The formulation of Ferry and Spear (1978) is applied since the composition of garnet and biotite from the Thompson metasedimentary rocks is similar to those used in its calibration. Temperature is calculated using the following equation, with uncertainty of ± 50°C.

$$\ln[(Mg/Fe)_{garnet}/(Mg/Fe)_{biotite}] = -2109/T(K) + 0.782. \quad (7.1)$$

The results are given in Table 7.1. Garnet-biotite in metapelite (ore type I) from the Thompson T-3 mine gives temperature ranging from 603 to 709°C, with 649°C as the average value. The formation temperature of garnet-biotite in metapelite from the Thompson open pit is 710°C. The formation temperature of garnet-biotite from sulfide iron formation type II is lower than the other two rock types, and ranges from 546 to 618°C, with 583°C as the average value.

One of the restrictions of the Ferry and Spear (1978) geothermometer is that the ratio of $({}^{VI}Al+Ti)/({}^{VI}Al+Ti+Mg+Fe) \leq 0.15$ in biotite. The ratio of $({}^{VI}Al+Ti)/({}^{VI}Al+Ti+Mg+Fe)$ of biotite from the sulfide iron formation is 0.11, which is within the required range. The ratio in biotite from the metapelite is 0.19 which is only slightly higher than the required value. Indares and Martignole (1985) proposed a calibration of the biotite-garnet

geothermometer that includes correction for the high Ti content of biotite; but this necessitates pressure data. In general, for present assemblages, pressure data are available only after calculation of the temperature. However, in view of the low Ti concentrations in biotite, correction is not necessary.

Another restriction of Ferry and Spear's (1978) method is that the (Ca+Mn)/(Ca+Mn+Fe+Mg) ratio $\leq$ 0.2 in garnet. In this study, garnet from metapelite has a ratio $\leq$ 0.15, but garnet from the sulfide iron formation II has a ratio of 0.29. Perchuk (1981) and Perchuk and Lavrent'eva (1983) established a correction for the Mn $\leftrightarrow$ Mg substitution in garnet and proposed the following equation for temperature calculation of temperature:

$$T(K) = 3650/(\ln K_D + 2.57) + 252.25 \bullet (X_{Mn}^{Garnet} - 0.035), \quad (7.2)$$

where, $K_D = (X_{Mg}/(1 - X_{Mg})^{biotite} \bullet (1 - X_{Mg}/X_{Mg})^{Garnet}$,

$X_{Mg} = Mg/(Mg + Fe + Mn)$ and $X_{Mn} = Mn/(Mn + Fe + Mg)$.

The results calculated from this equation are also given in Table 7.1. In general, the temperatures from the two different equations are consistent with each other, probably do represent the peak temperatures during the prograde metamorphic processes. The results are also in agreement with the previous study (Bleeker, 1990).

7.2.2 Garnet-plagioclase-Al_2SiO_5-quartz geobarometer

The garnet-plagioclase-Al_2SiO_5-quartz geobarometer has become the most widely used geobarometer for medium- and high-grade metamorphic rocks due

Table 7.1 Formation temperature of garnet/biotite pairs

sample No.	garnet				biotite			T (°C)	
	Mg/Fe	X_{Mg}	X_{Mn}	Ca+Mn*	Mg/Fe	X_{Mg}	^{VI}Al+Ti*	T_1	T_2
TS171	0.209	0.160	0.071	0.103	1.061	0.513	0.177	603	589
TS172	0.218	0.166	0.070	0.102	1.041	0.510	0.192	626	600
TS173	0.188	0.146	0.079	0.112	0.909	0.476	0.150	621	599
TS341	0.127	0.109	0.036	0.067	0.497	0.331	0.182	709	646
TS342	0.130	0.111	0.038	0.067	0.536	0.348	0.179	686	634
TO5B1	0.252	0.184	0.087	0.152	0.986	0.494	0.174	710	644
TS191	0.116	0.090	0.133	0.293	0.579	0.365	0.089	609	594
TS192	0.106	0.083	0.134	0.291	0.616	0.379	0.105	557	567
TS193	0.101	0.080	0.133	0.293	0.606	0.376	0.103	546	561
TS194	0.115	0.088	0.141	0.288	0.561	0.357	0.082	618	599

Ca+Mn* = (Ca+Mn)/(Ca+Mn+Mg+Fe);

^{VI}Al+Ti* = (^{VI}Al+Ti)/(^{VI}Al+Ti+Mg+Fe);

T_1 calculated after Ferry and Spear (1978);

T_2 calculated after Perchuk (1981).

TS171-TS173, TS341 and TS342 are metapelite (ore type I) from the Thompson T-3 mine; TO5B1, metapelite (ore type III) from the Thompson open pit; TS191-TS193, sulfide iron formation type II from the Thompson T-3 mine.

to the widespread occurrence of garnet-plagioclase-Al_2SiO_5-quartz assemblages in metapelite. It was developed by Ghent (1976), and has been modified somewhat by Newton and Haselton (1981) and by Perkins et al. (1982) based on different solution models for the activity of grossular in garnet. Koziol (1988) also recalibrated the anorthite breakdown reaction.

The geobarometer is based on the reaction:

$$3CaAl_2Si_2O_8 = Ca_3Al_2Si_3O_{12} + 2Al_2SiO_5 + SiO_2. \qquad (2)$$

anorthite grossular sillimanite (kyanite) (andalusite) quartz

The quantitative application of the geobarometer stems from the thermodynamic condition for equilibrium of the above reaction. If the temperature of crystallization of the assemblage is estimated independently, the pressure is given implicitly as a function of the temperature and activities of reacting species. For any temperature, Newton and Haselton (1981) have written the equation for the geobarometer as

$$-P^\circ\Delta V^\circ + RT\ln(\alpha_{gr}/\alpha_{an})^3 + P\Delta V_m \approx 0, \qquad (7.3)$$

where P° and ΔV° are, respectively, the pressure of the end-member (pure anorthite and grossular) equilibrium at T and the volume change of the end-member. ΔV_m is the partial molal volume change at 1 bar, and the approximation sign is used because of the neglect of the effect of thermal expansion and compressibility on volumes. The partial molar volumes of $CaAl_2Si_2O_8$ in plagioclase are sensibly equal to the molar volume of anorthite

(Newton and Haselton, 1981). However, the partial molar volume of $Ca_3Al_2Si_3O_{12}$ in garnet is considerably different from the molar volume. In this study the partial molar volume of grossular was read directly from Cressey et al.'s (1978) diagram based on its mole fraction.

From experimental results, several authors have proposed an equation for the calculation of the equilibrium pressure using a known temperature. The latest one is from Koziol and Newton (1988), which is (in °C, bars)

$$P^{\circ}_{,\text{sillimanite}} = -0.0001872T^2 + 23.41T - 25. \qquad (7.4)$$

According to these authors the uncertainty of the geobarometer is ±0.6 kbar. The molar volume data for the related minerals and activity models for garnet and plagioclase solid solution are given in Table 7.3. Results are given in Table 7.4. The calculated pressure for metapelite (ore type I) from the Thompson T-5 mine ranges from 6.6 to 7.4 kbar based on temperatures obtained from the geothermometer of Ferry and Spear (1978), and 6.1 to 6.6 kbar based on temperatures from the geothermometer of Perchuk (1981).

7.2.3 Thermobarometry using multi-equilibrium calculations

Berman (1991) has presented a new method for geothermobarometry, referred to as TWEEQU (Thermobarometry with estimation of equilibration state), in which the positions of all possible equilibria implied by a given mineral assemblage are computed in P-T space by computer program TWQ. If three conditions are met: (1) the thermodynamic data are perfect, (2) the

Table 7.2 Thermodynamic data for related phases

phase	V (J/bar)
α-quartz	2.269
sillimanite	4.990
grossualr	12.530
anorthite	10.079

From Helgeson et al. (1978).

Table 7.3 Activity models for garnet and plagioclase solid solutions

activity model	source
1. Grossular:	
$\alpha_{gr} = (\gamma_{gr} \cdot X_{Ca}^{Gar})^3$	Newton and Haselton
$\gamma_{gr} = \exp[W_{CaMg}(X_{Mg}^2 + X_{Mg}X_{Fe})/RT]$	(1981), Hodges and
$W_{CaMg} = 13807 - 6.3T$ (joules)	Spear (1982)
2. Anorthite:	
$\alpha_{An} = 1/4 \cdot X_{Ca}^{M}(1 + X_{Ca}^{M})^2 \cdot$	Newton and Haselton
$\exp[(1-X_{Ca}^{M})^2 \cdot (1032 + 1726\ X_{Ca}^{M})/T]$	(1981)
$X_{Ca}^{M} = Ca/(Ca + Na + K)$	

Table 7.4 Summary of mineral compositions and estimates of temperature and pressure

sample No.	plagioclase		garnet				T (°C)		P (kbar)	
	X(An)	X(Ab)	X(Fe)	X(Mg)	X(Ca)	X(Mn)	T_1	T_2	P_1	P_2
TS171	0.271	0.720	0.742	0.155	0.035	0.068	603	589	6.6	6.4
TS172	0.278	0.713	0.738	0.161	0.035	0.067	626	600	6.9	6.6
TS173	0.299	0.687	0.747	0.141	0.036	0.076	621	599	6.6	6.3
TS341	0.241	0.754	0.828	0.105	0.033	0.034	709	646	7.4	6.6
TS342	0.252	0.734	0.826	0.107	0.030	0.037	686	634	6.8	6.1

T_1 calculated after Perry and Spear (1978); T_2 calculated after Perchuk (1981). P_1 and P_2 calculated with T_1 and T_2, respectively.

compositional data are perfect, and (3) all minerals last equilibrated at the same pressure and temperature, all equilibria will intersect at a single P-T point. On Figure 7.1 the equilibrium lines for the following two independent reactions are plotted:

grossular + quartz + 2sillimanite = 3anorthite (3)

phlogopite + almandine = annite + pyrope. (4)

The results show that the peak metamorphic conditions for the Thompson mine metapelite are at 5.5 kbar and 733°C (Fig. 7.1). These values are generally compatible with the results obtained from the geothermometry and geobarometry described above.

Overall uncertainties are difficult to assess quantitatively, because both systematic errors in thermodynamic data and random errors in analytical procedures influence the accuracy of the results. However, the application of this method repeatedly produces results that place rocks with one Al_2SiO_5 polymorph in its appropriate field of stability and rocks with two Al_2SiO_5 polymorphs thought to be at equilibrium within about 0.5 kbar of the appropriate phase-boundary (Berman, 1991). The uncertainty can also be evaluated based on geobarometer compatibility of geobarometers. Berman (1991), for example, suggested that a reasonable estimate of overall uncertainty for reaction (3) is generally around 1 kbar (2σ), except for assemblages with Ab-rich plagioclase, for which activity coefficients are poorly known. The estimate is also supported by the analysis of Kohn and Spear (1991), which

Fig. 7.1 Metamorphic P-T conditions for the Thompson mine based on multi-equilibrium calculations (Berman 1991) of independent reactions: (1) grossular + quartz + 2sillimanite = 3anorthite; (2) phlogopite + almandine = annite + pyrope. Gr=grossular, Qz=quartz, Si=sillimanite, An=anorthite, Phl=phlogopite, Alm=almandine, Ann=annite, Py=pyrope.

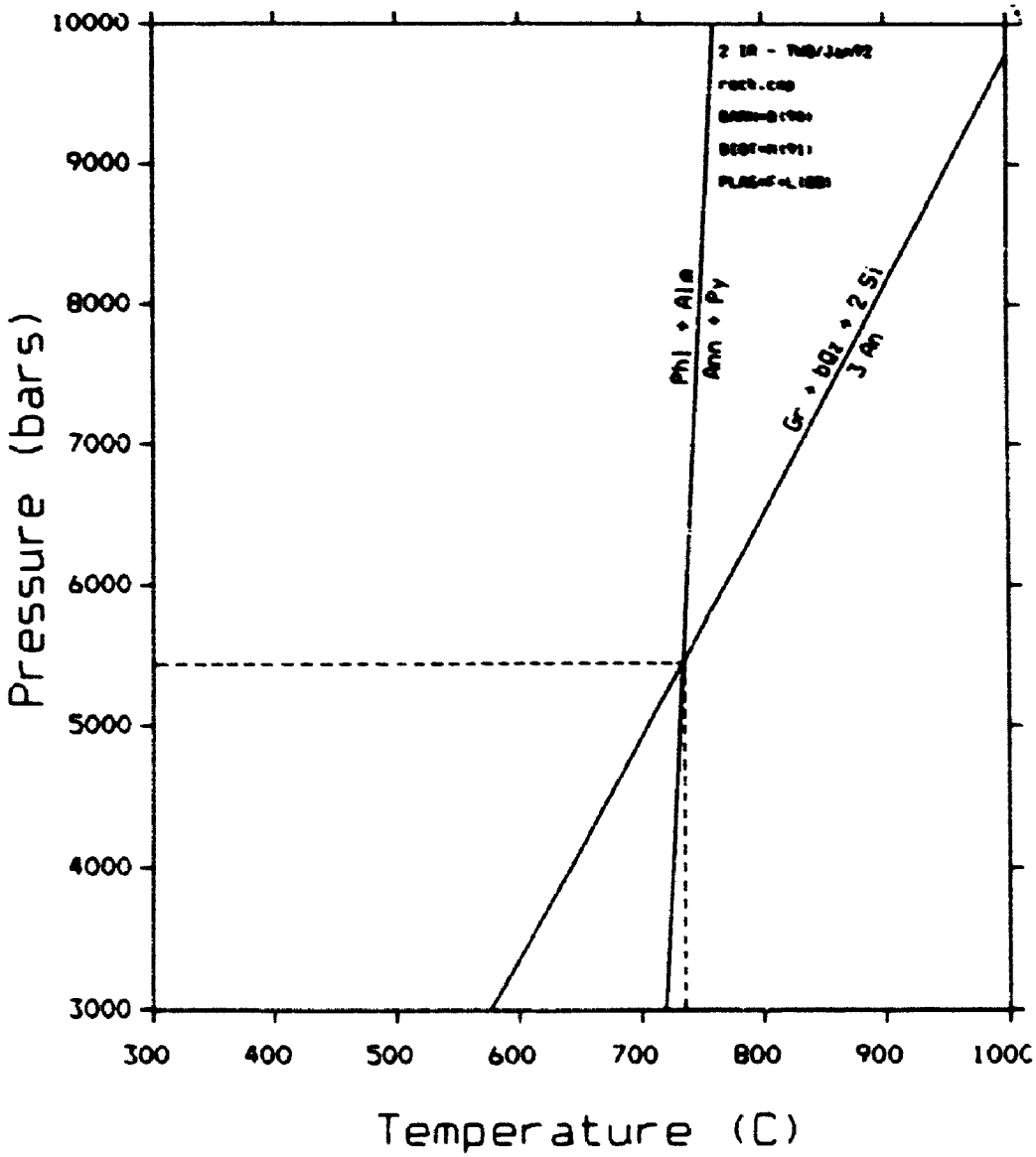
10000
9000
8000
7000
6000
5000
4000
3000
300
400
500
600
700
800
900
1000
Pressure (bars)
Temperature (C)
Phl + Ala
Ann + Py
Gr + bQz + 2 Si
3 An

suggests overall errors of 1.6-2.4 kbar.

7.3 Late hydrothermal alteration

7.3.1 Chlorite geothermometry

Cathelineau and Nieva (1985) proposed a chlorite solid solution geothermometer based on their studies on the secondary chlorite from hydrothermally altered andesites in the active geothermal system of Los Azufres (Mexico). The chlorite composition was analyzed by electron microprobe, and compared with the formation temperature of chlorite measured directly at different depths in wells, and combined with the results of microthermometric data on fluid inclusions from quartz and calcite associated with chlorite. They concluded that ^{IV}Al of chlorite is positively correlated with the formation temperature; a result which can be represented by the equation

$$^{IV}Al = 4.71 \times 10^{-3}\ T(°C) - 8.26 \times 10^{-2}.$$

Rearrangement of this equation gives

$$T(°C) = 212.3\ ^{IV}Al + 17.5.$$

In their study, the Fe/(Fe+Mg) ratio of chlorite ranged from 0.27 to 0.38, with an average value of 0.34. A correction is required for the concentration of ^{IV}Al contents with Fe/(Fe+Mg) ratio. This geothermometer also requires that the system is saturated with aluminum.

In the present study, chlorite from ultramafic rocks is formed under

aluminum-undersaturated conditions. Therefore, the geothermometer can not be used for these chlorites. However, chlorites from the metapelite and the pegmatite are crystallized under aluminum-saturated conditions.

Chlorites from the metapelite and the pegmatite have Fe/(Fe+Mg) ratios ranging from 0.57 to 0.77, which are higher than those from Los Azufres, Mexico. Correction must be made for the increase in ^{IV}Al content caused by increase in Fe content since the Fe/(Fe+Mg) ratio is positively correlated with ^{IV}Al content in the chlorites. The ^{IV}Al contents were normalized to [Fe/(Fe+Mg)]=0.34, which is the mean value for chlorite from Los Azufres (Mexico), using the regression line of ^{IV}Al vs. Fe/(Fe+Mg) obtained in this study. The correction for Fe/(Fe+Mg) ratio is then given by:

$$^{IV}Al_{corrected} = {}^{IV}Al_{measured} - 0.43\ [Fe/(Fe+Mg) - 0.34].$$

The average formation temperatures obtained for chlorite are 290±25°C for ore type I, 280±25°C for ore type II, 250±25°C for ore type III and 270±25°C for ore type IV.

7.3.2 Muscovite geobarometer

It is well known that the celadonite content of muscovite correlates with formation pressure. Velde (1967) studied the phengitic muscovite in both glaucophane schist and its enclosing pelitic greenschist facies country rocks from Ile de Groix, France. He suggested that the constancy of Si content in micas from rocks of different bulk chemical composition but closely similar

physical conditions indicated that the Si content of phengitic muscovite can be used to estimate the pressure and temperature conditions of its formation. His experimentally derived stability curves for muscovite with various amounts of celadonite solid solution under $P_{H2O} = P_{total}$ (Velde, 1965) are well known.

As described above, the average Si content of muscovite from ore types I, II and III hosted by metapelite at the Thompson mine is 3.2 cations p.f.u. Based on the alteration temperature obtained from the chlorite geothermometer, the corresponding pressure is approximately 1 kbar for ore types I, II and III, according to the stability curves of Velde (1965). The content of Si in muscovite in ore type IV hosted in pegmatite is too low to be used as an indicator of the pressure.

Powell and Evans (1983) calculated the pressure dependence of the composition of muscovite in the assemblage muscovite + biotite + chlorite + quartz on the basis of the experimental data of Velde (1965) and thermodynamic data given in Powell (1978). They suggested that the celadonite component of muscovite in the above assemblage may have the potential for a new geobarometer. Such a barometer would be helpful because the metamorphic pressures in low-grade metamorphism are often poorly constrained. Bucher-Nurminen (1987) recalculated the muscovite-biotite-chlorite geobarometer on the basis of the thermodynamic data of Massonne (1981).

In this study the geobarometer proposed by Powell and Evans (1983) has been applied rather than that of Nurminen (1987), because the recalculated

equilibrium of Nurminen shows much steeper dP/dT slopes than those calculated by the method of Powell and Evans (1983), making pressure estimation strongly dependent on the reliability of the estimated temperature of equilibrium. The geobarometer of Nurminen (1987) requires temperatures over 400°C, which are too high for the alteration assemblages in this study.

The muscovite equilibrium reaction is written using pure mineral end-members:

$$\underset{\text{celadonite}}{4KMgAlSi_4O_{10}(OH)_2} + \underset{\text{clinochlore}}{Mg_5Al_2Si_3O_{10}(OH)_8}$$

$$= \underset{\text{muscovite}}{KAl_3Si_3O_{10}(OH)_2} + \underset{\text{phlogopite}}{3KMg_3AlSi_3O_{10}(OH)_2}.$$

Activities for chlorite, celadonite and muscovite were calculated from:

$$X_{clin} = 64X^3_{Mg,M2}X^2_{Mg,M1}X_{Al,M1}X_{Al,T}X^3_{Si,T}X^8_{OH,V}$$

$$X_{cel} = 9X_{K,A}X_{Mg,M1}X_{Al,M1}X_{\square,M2}X^4_{Si,T}X^2_{OH,V}$$

$X_{mus} = 9.38X_{K,A}X^2_{Al,M1}X_{\square,M2}X_{Al,T}X^3_{Si,T}X^2_{OH,V}$ (Powell and Evans, 1983).

The activity of phlogopite component in biotite was calculated with the simple relationship proposed by Nurminen (1987):

$$X_{phl} = X_{K,A}X^3_{Mg}$$

where $X_{Mg} = N_{Mg}/(N_{Mg}+N_{Fe})$.

Since the calculation of pressure is based on electron microprobe compositions, the following assumptions were made:

(1) all iron is assumed as Fe^{2+};

(2) $[Mg/(Mg+Fe)]_{M1} = [Mg/(Mg+Fe)]_{M2} = [Mg/(Mg+Fe)]_{total}$;

(3) OH is only replaced by F and Cl;

(4) all Mg is in the M_1 site of muscovite.

The pressure calibration of the geobarometer of Powell and Evans (1983) is limited to a minimum estimated temperature of 300°C, which is slightly higher than the temperatures estimated for the alteration assemblage of Thompson mine ore. Therefore, some extrapolation was required. The results are given in Table 7.5. The pressures obtained for the same sample locations are considerably higher than those from the geobarometer of Velde (1967).

Table 7.5 Formation temperatures and pressures of ore types I, II, III and IV in the Thompson mine

sample	ore type	T (°C)	lnK	P(kbar)	n*
T3 mine	I	290±25	4.4	4.0±0.5	20
T1 mine	II	280±25	3.5	4.5±0.5	11
open pit	III	250±25	4.3	3.0±0.5	6
T1 mine	IV	270±25	7.6	1.5±0.5	3

* n is number of samples averaged.

CHAPTER 8 DISCUSSION AND CONCLUSIONS

Precious-metal minerals in the Thompson mine consist of both PGMs and argentian native gold, in approximate equal abundance, as estimated from petrographic observations (reflected light microscopy and EMP imaging) and whole-rock geochemistry. With the exception of irarsite of ore type I, the PGMs are exclusively compounds of Pd and Ni with pnictides (As, Sb, Bi) and Te. The PGMs and gold are invariably spatially associated with gersdorffite ± nickeline, which correspondingly have sporadic high contents of PGEs. Gangue minerals in all PGM-gold-bearing ore types are pervasively altered by a late hydrothermal event.

The hydrothermal alteration which post-dates the regional amphibolite-facies metamorphism is ubiquitous but variably developed and yet diverse in mineral assemblages in different rock types of the Thompson mine. Alteration assemblages in metapelites contain biotite, muscovite, chlorite, albite, calcite, siderite, allanite, quartz, and sulfides (mainly pyrite, violarite and chalcopyrite). Here, biotite, chlorite, and muscovite commonly occur as replacements after early biotite, and albite, chlorite, calcite, and muscovite after more calcic plagioclase. The primary Zn-rich spinel in ore types I and III has been modified, and some spinel grains have oscillatory zonation in chemical compositions. Ferrosilite and garnet porphyroblasts in silicate-facies banded iron formation (BIF) are extensively replaced by biotite, grunerite,

ferropyrosmalite, and pyrrhotite. Ferropyrosmalite also is present locally in cross-cutting veins. In skarn rocks, olivine is partly serpentinized and diopside is replaced by tremolite, chlorite, and phlogopite. Epidote-zoisite, titanite, and prehnite are also present. Minor chondrodite is locally present in olivine-diopside-carbonate skarn. Pegmatite has also been affected by a late hydrothermal alteration characterized by similar mineral assemblages to those in metapelites. Metapyroxenites examined in this study, both from the footwall of the Ni sulfide orebody and as inclusions in massive sulfide matrix, are strongly altered to talc, dolomite, serpentine, chlorite, actinolite, and phlogopite, with relict tremolitic hornblende, magnesio-hornblende, and spinel. Hisingerite is closely associated with late carbonate veins. Mineralized peridotite (serpentinized peridotite of Zurbrigg, 1963) collected from the T-1 mine is composed of serpentine, talc, carbonate minerals, phlogopite, and chlorite, as well as relict olivine and pyroxene. Primary spinel in the peridotite has also been modified by Cr-Zn-rich hydrothermal fluids.

Late hydrothermal alteration in the present four (PGE-Au)-mineralized ore types of the Thompson mine is similar in mineral assemblages but much more pervasive than that in the respective host rocks (metapelite and pegmatite). For example, allanite is a minor or trace constituent (< 1 vol%) in most samples of all rock types of the Thompson mine, but it is abundant (up to 5 vol%) in ore type II, in which it occurs as large isolated crystals (up to 0.2 x 0.6 mm) and aggregates associated with biotite and/or sulfides. Albite and

calcite are also most abundant in ore type II whereas in ore type III, quartz is much abundant.

One of the most interesting features of the late alteration assemblages at the Thompson mine is the high Cl concentration. Chlorine is enriched in some of the hydrothermal minerals, particularly ferropyrosmalite with up to 5 wt% Cl (Table 5.3). Pan et al. (1993) note that pyrosmalite series minerals are a local sink for Cl in metamorphosed and matasomatised massive sulfide deposits. Biotite and grunerite associated with ferropyrosmalite in BIF also contain minor amounts of Cl (both up to 0.2 wt%, Table 5.3). Although ferropyrosmalite has not been observed in the (PGE-Au)-mineralized samples, a minor amount of Cl (up to 0.2 wt%, Appendix X) has been detected in biotites from all four of the present ore types. Thus, fluids of the late hydrothermal event were undoubtedly Cl-rich. Moreover, allanite in ore types I, II, III (all hosted in metapelite) contains significant amounts of both F and Cl (up to 0.6 and 0.8 F and Cl, respectively; Table 5.4) and therefore is an unusual halogen-bearing variety (cf., Pan and Fleet, 1990). Similarly, minor contents of halogens have been detected also in allanite grains of the pegmatite-hosted ore type IV (Table 5.4). Additionally, the ubiquitous presence and local abundance of allanite in PGM-gold-bearing ore types demonstrates that rare-earth elements (REEs) were at least locally remobilized and concentrated at this time.

In this study, only one grain of titanite was observed in the As-rich nickel ore. The stability of titanite is known to be influenced by the partial

pressure of CO_2, via the reaction: titanite + CO_2 = rutile + quartz + calcite (Hunt and Kerrick, 1977; Bancroft et al., 1987). Therefore the scarcity of titanite may indicate that the hydrothermal fluids associated with PGM-Au mineralization are also CO_2 rich. In summary, the PGMs, native gold, As-rich ore minerals, and the hydrothermal mineral suite were all formed contemporaneously during a late hydrothermal event.

In addition, Bleeker (1990) observed quartz veins (up to 30 m in width) associated with brecciated Ni sulfide ore in open fractures at the Thompson open pit, and some of the highest As values occur in samples that are intimately associated with quartz veins. This is further the evidence of hydrothermal activity probably related to PGE-Au mineralization.

P-T conditions for the late hydrothermal alteration are poorly constrained due to the lack of well-calibrated geothermobarometers. Chemical compositions of chlorite yielded a temperature of 250-300°C according to the calibration of Cathelinean and Nieva (1985). A pressure of about 3-4 kbar is estimated from the geobarometer of Powell and Evans (1983) using the assemblage of muscovite + biotite + chlorite + quartz.

The Thompson Nickel Belt has experienced a complex deformation history. According to Bleeker (1990), the collision between the Proterozoic continental margin on the northwest side of the belt and Archean Superior craton on the southeast side started as early as 2.3-2.0 Ga and ended with terminal brittle faulting as late as 1.7-1.6 Ga. The collisional climax along the

Thompson Belt segment may have commenced at about 1.9 Ga, and is referred to as the Hudsonian orogeny.

It is important to note that both the As-rich ore mineral assemblage and the hydrothermal alteration assemblage transect the penetrative deformation of the host rocks, and are not themselves penetratively deformed. Although Ni sulfide deposits and individual ore minerals in the Thompson Nickel Belt apparently show evidence of deformation (Peredery et al., 1982; Cumming et al., 1982; Bleeker, 1990), the present PGM-gold-bearing ore types were clearly formed during the latest event after the peak of the Hudsonian orogeny. The peak P-T conditions for the orogeny are presently constrained around 600-700°C and 6-7 kbar.

The precious-metal mineralization at the Thompson mine is spatially related to the main Ni sulfide ores which contain trace amounts of PGEs and Au (Table 8.1), and is probably most readily ascribed to a late reworking of the ores by hydrothermal fluids during a period of dilatancy, and presumably after the peak of the Hudsonian orogeny. The ultimate origin of the Ni sulfides in the Thompson Nickel Belt is presently obscured by the complex tectonic and metamorphic history of the region. However, metasedimentary-hosted Ni sulfide ores, such as those in the Thompson mine, that are not spatially related to large volumes of mafic-ultramafic rocks, and have a very high sulfide/ultramafic ratio, are particularly troublesome for orthomagmatic models.

Eckstrand et al. (1989) and Bleeker (1990) proposed that magmatic

assimilation of sedimentary sulfide was a controlling factor. Thus, only those ultramafic sills which were intruded along sulfide iron formation generated voluminous sulfide from magmatic segregation. Both Bleeker (1990) and Cumming et al. (1982) suggested that the Thompson Belt Ni sulfides may be subdivided into "primary" and "mobilized" varieties. The primary sulfides are interstitial to silicates in the serpentinized peridotite, whereas mobilized sulfides occur in the adjacent country rocks. Typical mobilized ore is breccia Ni-ore (ore type I) which constitutes a major component of the total ore tonnage at the Thompson mine. This ore is hosted in metapelite, and the majority of the inclusions in it are metapelite and pegmatite. The very presence of "mobilized" ores (and the occurrence of the alteration assemblages) demonstrates that large volumes of Ni (and Cu-Ni) sulfides can be emplaced in the crust solely by fluid processes. To date, little consideration has been given to the conditions under which fluid transport and deposition of Ni (and Cu-Ni) sulfides occur.

The lead isotope systematics of sulfide concentrates from the Thompson Nickel Belt (Cumming et al., 1982) are interesting, if accepted uncritically, because they reveal events of four distinct ages 2.3, 2.0, 1.6, 1.1 Ga, which were interpreted to correspond to magmatic concentration and emplacement of the ore, possible early folding, a late retrograde stage of the Trans-Hudsonian orogeny, and emplacement of the MacKenzie dyke swarm. The 1.6 Ga age is similar to the 1.6 Ga date of Brooks and Thayer (1981) for the pervasive late Trans-Hudsonian retrograde alteration in the Thompson Nickel Belt. The latter

logically corresponds to the hydrothermal event associated with the present precious-metal mineralization. The 1.6 Ga age from the lead isotope systematics therefore may have significance. According to Bleeker (1990), lead isotope dating on pegmatite inclusions in breccia Ni ore (refer to as ore type I in this study) indicates that the brecciation event occurred after 1.8 Ga. Therefore, the brecciation of Ni-ore could have occurred either before or at the same time as the PGE-Au mineralization.

The enrichment of both Au and As in the Thompson mine precious-metal mineralization is most interesting and could point to contributions of these elements from the metasedimentary host rocks. Platinum, Pd, and Au are characteristically enriched together in late crystallizing (Cu-Ni) sulfides in both anhydrous (monosulfide only) and fluid systems (e.g., Fleet et al., 1992). Also, Pt, Pd, and Au are characteristically enriched together in late sulfide segregations associated with Cu-Ni sulfide deposits (e.g., Naldrett, 1989). Furthermore, Pt and Pd are equally enriched in the massive Ni sulfide ore at the Thompson mine (Table 8.1). Thus the marked fractionation of Pd from Pt in the present As-rich assemblages is surprising, and is clearly further evidence for fluid involvement in the concentration of the PGEs.

The association of pnictide and telluride PGMs with argentian gold (or electrum), other metal pnictides and tellurides, and a hydrothermal alteration suite is a common feature of most of the important PGM parageneses (perhaps only with the single exception of PGMs in ophiolite complexes). Detailed

Table 8.1 PGE, Au concentrations of Ni-sulfide ores from the Thompson mine (after Bleeker, 1990)

samples	Os	Ir	Ru	Rh	Pt	Pd	Au
			ppb				
1	216	224	498	224	1245	2738	446
2	198	165	341	198	708	1421	82

1. interstitial sulfides, ultramafic rocks;

2. ore type I.

research invariably indicates deposition from Cl-rich hydrothermal fluids (e.g., Farrow and Watkinson, 1992). The fluids in question were perhaps metamorphogenic as in the New Rambler deposit, Wyoming (McCallum et al., 1976) and at Rathbun Lake, Ontario (Rowell and Edgar, 1986) or late magmatic as in the Bushveld Igneous complex (Ballhaus and Stumpfl, 1986; Johan and Watkinson, 1987), the Duluth complex, Minnesota (Mogessie et al., 1991), and the North Range of the Sudbury Igneous Complex (Farrow and Watkinson, 1992). These researches on natural assemblages highlighted the dearth of information that existed on the physicochemical behaviour of PGEs in both magmas and natural fluids. Recent experimentation on sulfide/silicate partitioning of PGEs under magmatic conditions (e.g., Fleet et al., 1991) appears to preclude the primary concentration of PGEs in Bushveld ores by sulfide liquation. Other experiments, on the volatility of PGEs (Fleet, 1992) now demonstrate the feasibility of the quantitative transport of PGEs as (Cl, S) species under late-magmatic conditions.

PART III: PGMs FROM THE SUDBURY MINING CAMP, ONTARIO

CHAPTER 9 PGMs FROM THE LINDSLEY MINE

9.1 General Geology

The Lindsley mine of Falconbridge Limited is situated in Belzard township, 6.5 km north of the city of Sudbury. It is a polymetallic sulfide deposit, with economic values in Ni, Cu, Co, Au, Pt, and Pd, hosted in the South Range of Sudbury Igneous Complex (Fig. 9.1). The Lindsley deposit has many features typical of the South Range ore deposits, which often occur in depressions within the footwall of the Sudbury Igneous Complex and are referred to as contact or sublayer-type deposits. According to Phillips (1989), from south to north, the stratigraphic sequence is granite, basalt, sublayer and amphibole-quartz-rich norite. The granite and basalt form the footwall and the norite forms the hanging wall of the orebody above the 900 m elevation. Below this depth, the hanging wall and footwall relationships are reversed forming a nose-like structure (Fig. 9.2).

The Lindsley deposit comprises four zones of mineralization, termed zones 1 to 4. Zones 1 and 2 are on the footwall side of the sublayer 600 m and 1020 m, respectively, below surface where the basalt-sublayer contact is altered to the amphibolite facies of metamorphism. Zone 3 occurs about 1440 m below surface where the sublayer is overturned and the dip is reversed. Consequently,

Fig. 9.1 Generalized geological map of the Sudbury basin

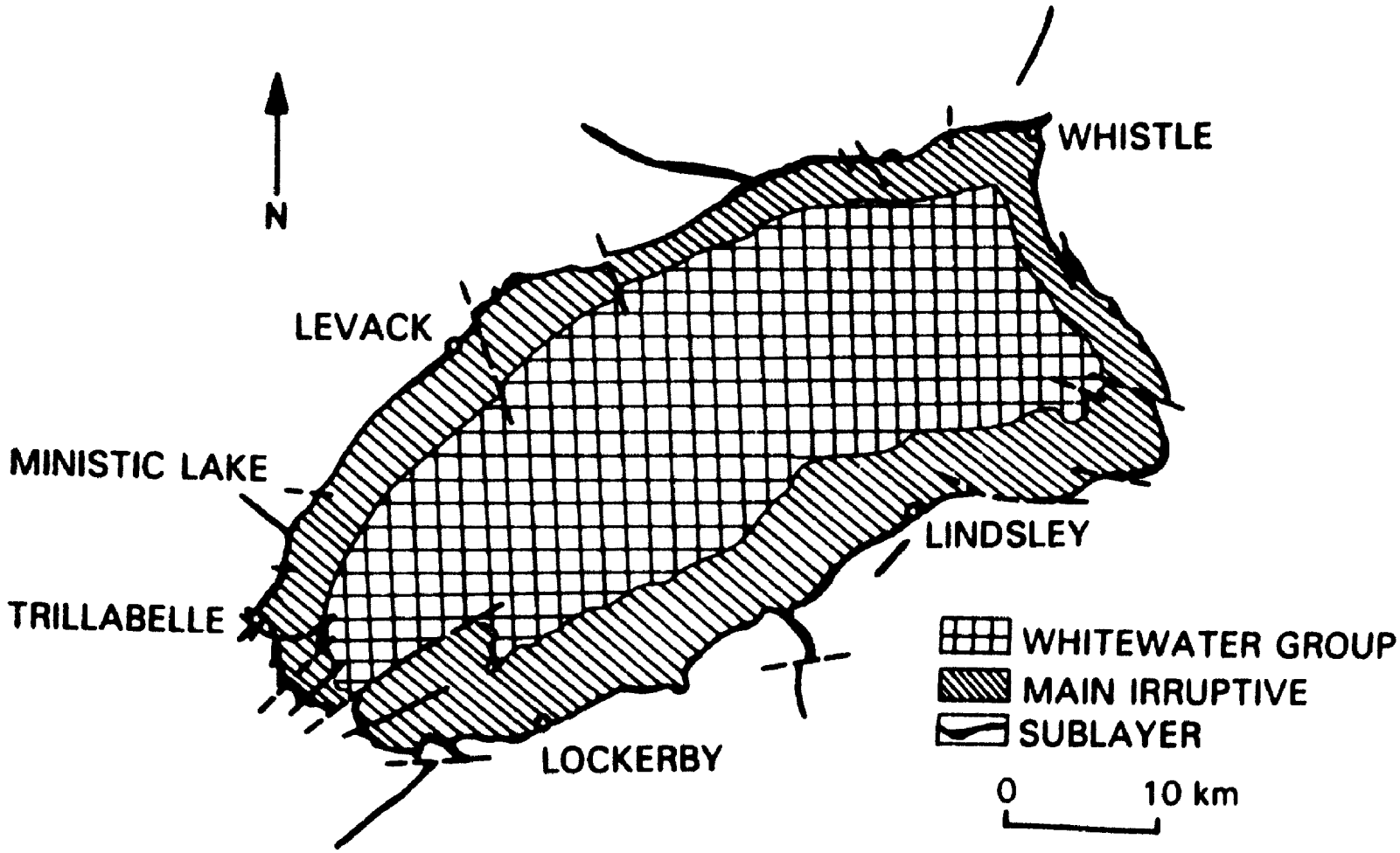
N
WHISTLE
LEVACK
MINISTIC LAKE
LINDSLEY
TRILLABELLE
LOCKERBY
WHITEWATER GROUP
MAIN IRRUPTIVE
SUBLAYER
0
10 km

Fig. 9.2 Lindsley project composite section-3600E, looking southwest

(after Phillips, 1989)

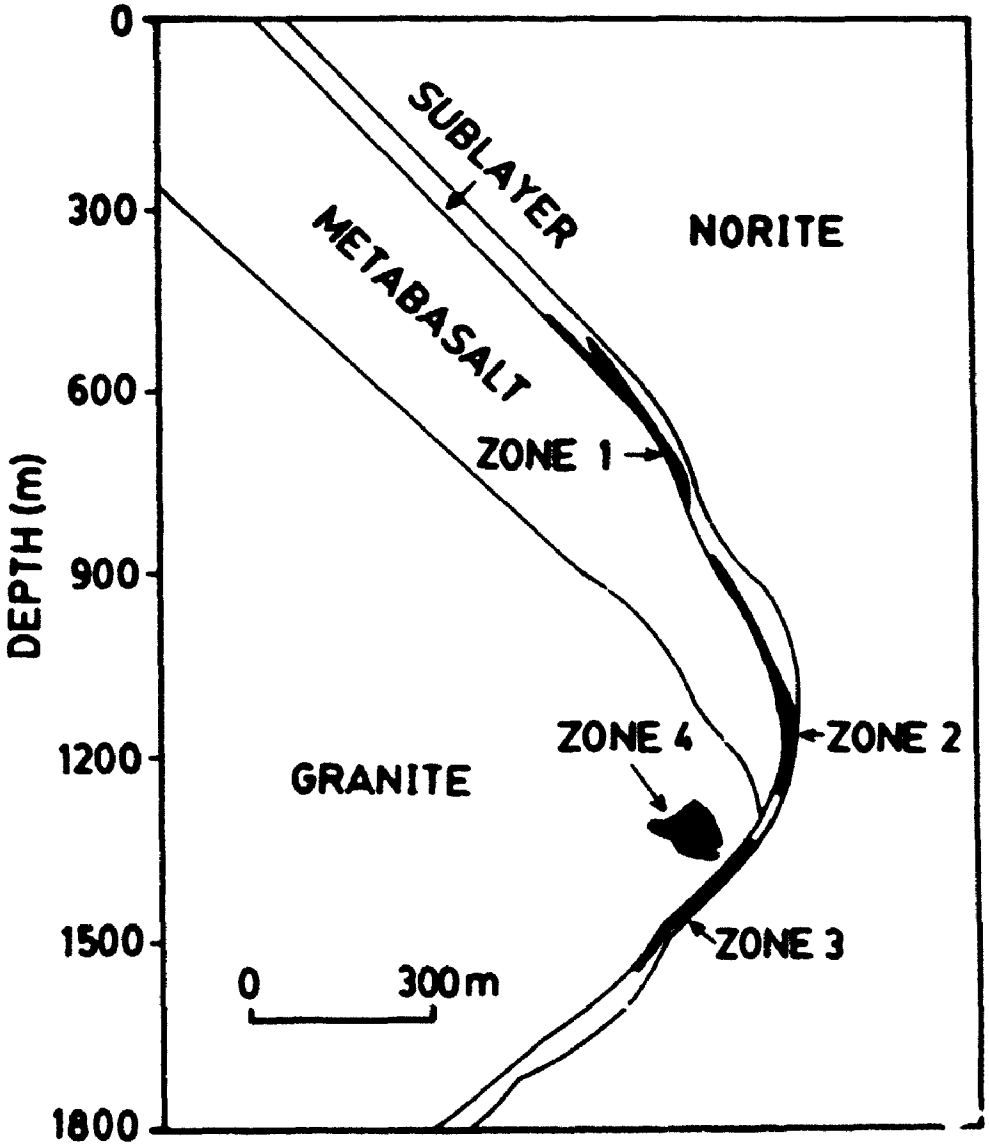
0
300
600
900
1200
1500
1800
DEPTH (m)
SUBLAYER
METABASALT
NORITE
ZONE 1
ZONE 2
ZONE 3
ZONE 4
GRANITE
0
300 m

zone 3 occurs on the hanging wall side of the sublayer. Zone 4 is centred at about 1290 m below the surface. It is similar to the massive sulfide found in the sublayer, but it is enriched in Cu, Au, Pt, and Pd and is, on average, three times the grade of all other Falconbridge mines in the Sudbury area (Phillips, 1989).

The sulfide ore sample investigated in this study was collected from a very recent underground drillhole TL-2 at 277.0 m from zone 4, and is hosted in granite. The ore contains Ni 1.27 wt%, Cu 5.11 wt%, Co 0.06 wt%, S 20.8 wt%, Pb 97 ppm, Pt 13 g/t, Pd 2.38 g/t, Au 2.27 g/t, and Ag 15.2 g/t (Severin, 1991; pers. comm.). It is a massive Cu-Ni sulfide ore, composed of pyrrhotite, pentlandite, chalcopyrite and minor magnetite, with numerous silicate inclusions, such as biotite, chlorite, plagioclase, microcline, and quartz.

9.2 Platinum-Group Minerals

Three PGM grains were observed in the present sample, one of michenerite and two of merenskyite.

9.2.1 Michenerite

The michenerite grain is about 200 x 140 μm in size and surrounded by chalcopyrite, pyrrhotite, quartz, and biotite (Plate 5A). It is isotropic, and creamy white in color with a greyish tint in air. An electron microprobe analysis is given in Table 9.1. In addition to the major components (Pd, Bi,

Table 9.1 Electron microprobe analyses of PGMs from the Lindsley mine, Sudbury

No.	1	2	3
		wt%	
Fe	0.07	0.04	0.00
S	0.04	0.03	0.03
Pt	0.59	4.99	4.77
Pd	25.19	26.00	24.38
Ni	0.00	0.05	0.03
As	0.00	0.00	0.00
Sb	0.00	0.00	0.00
Bi	40.71	20.71	20.55
Te	33.63	50.09	48.38
Pb	0.00	0.00	0.00
Os	0.17	0.00	0.00
Ir	0.09	0.00	0.00
Total	100.49	101.91	98.14
		at%	
Fe	0.18	0.09	0.00
S	0.18	0.12	0.13
Pt	0.43	3.33	3.32
Pd	34.11	32.35	31.65
Ni	0.00	0.11	0.07
As	0.00	0.00	0.00
Sb	0.00	0.00	0.00
Bi	27.59	12.90	13.35
Te	37.33	51.09	51.48
Pb	0.00	0.00	0.00
Os	0.13	0.00	0.00
Ir	0.07	0.00	0.00

1. michenerite, $(Pd_{1.02}Pt_{0.01}Fe_{0.01})_{1.04}(Bi_{0.83}Te_{1.12}S_{0.01})_{1.96}$
2. merenskyite, $(Pd_{0.97}Pt_{0.10})_{1.07}(Te_{1.34}Bi_{0.39})_{1.93}$
3. merenskyite, $(Pd_{0.95}Pt_{0.10})_{1.05}(Te_{1.33}Bi_{0.40})_{1.95}$

and Te), maximum contents of substitutions (in wt%) are Pt 0.6, Ir 0.1, Os 0.2, and Fe 0.1. The calculated structural formula is $(Pd_{1.02}Pt_{0.01}Fe_{0.01})_{1.04}(Bi_{0.83}Te_{1.12}S_{0.01})_{1.96}$.

9.2.2 Merenskyite

Merenskyite occurs in contact with quartz-biotite inclusions within pyrrhotite in grain size up to 180 x 100 μm. It is white with a pink or cream tint in air and is strongly anisotropic from bluish grey to pinkish grey. Electron microprobe analyses are given in Table 9.1. The Pt content is up to 5.0 wt%. The calculated structural formula is $(Pd_{0.97}Pt_{0.10})_{1.07}(Te_{1.54}Bi_{0.39})_{1.93}$.

CHAPTER 10 PGMs FROM THE LOCKERBY MINE

10.1 General Geology

According to an unpublished guidebook prepared by Falconbridge Limited (1990, pers. comm.), the Lockerby Cu-Ni sulfide deposit is situated in Denison township on the southwest rim of the Sudbury basin, 32 km by road west of Sudbury (Fig. 9.1). The orebody is located at the contact of norite and country rock where a nose of norite protrudes into greenstone at the west end of the Creighton granite pluton. A major fault follows the east limb of the nose. The sulfide ore occurs mainly as breccia and stringer sulfides within the fault zone, as blebs in the matrix of the breccia pipe and as disseminations in norite.

Samples examined in this study were collected from the 4000 level underground. All of the samples containing PGMs were found within greenstone in contact with the norite. They are all massive ore with greenstone inclusions. The greenstone is mainly composed of green hornblende with variable amounts of biotite, plagioclase, chlorite and quartz and minor epidote-zoisite.

The platinum-group mineralization is documented for the first time in this study, and includes michenerite (PdBiTe), Ni-rich merenskyite $(Pd,Ni)Te_2$, Pd-melonite and sperrylite ($PtAs_2$). Electron microprobe analyses of the PGMs are given in Table 10.1.

Table 10.1 Electron microprobe analyses of PGMs from the Lockerby mine, Sudbury

No.	1	2	3	4	5	6	7	8
				wt%				
Pt	1.34	1.11	1.25	1.27	0.54	0.45	0.14	54.58
Pd	24.72	25.57	24.92	24.97	15.87	18.38	10.73	0.00
Ir	0.41	0.45	0.49	0.47	0.23	0.19	0.02	0.62
Os	0.33	0.36	0.37	0.48	0.09	0.12	0.00	0.34
Fe	0.04	0.53	0.27	0.23	0.42	0.31	2.81	0.44
Ni	0.65	0.24	0.49	0.47	7.35	6.00	9.90	0.49
As	0.02	0.05	0.03	0.08	0.00	0.00	0.00	43.47
Bi	38.86	34.02	38.55	39.38	13.89	17.88	10.72	0.00
Te	32.23	32.59	31.12	30.32	60.57	55.45	63.90	0.00
Sb	1.78	4.22	1.66	1.12	0.20	0.00	0.12	0.00
S	0.04	0.04	0.03	0.03	0.03	0.03	0.21	0.26
Total	100.43	99.19	99.18	98.81	99.17	98.80	98.55	100.19
				at%				
Pt	0.97	0.80	0.91	0.94	0.33	0.29	0.08	31.46
Pd	32.74	33.44	33.38	33.75	17.97	21.45	11.45	0.00
Ir	0.30	0.32	0.36	0.35	0.14	0.13	0.01	0.36
Os	0.24	0.27	0.28	0.36	0.06	0.08	0.00	0.20
Fe	0.11	1.33	0.69	0.60	0.91	0.68	5.72	0.88
Ni	1.57	0.57	1.18	1.14	15.07	12.69	19.16	0.94
As	0.04	0.10	0.05	0.15	0.00	0.00	0.00	65.25
Bi	26.21	22.65	26.29	27.10	8.01	10.62	5.83	0.00
Te	35.59	35.54	34.76	34.17	57.19	53.96	56.89	0.00
Sb	2.06	4.82	1.95	1.32	0.19	0.00	0.11	0.00
S	0.16	0.17	0.15	0.12	0.13	0.12	0.74	0.90

1. michenerite, $(Pd_{0.99}Pt_{0.03}Ir_{0.01}Os_{0.01}Ni_{0.03})_{1.08}(Bi_{0.78}Te_{1.07}Sb_{0.06})_{1.92}$
2. michenerite, $(Pd_{1.00}Pt_{0.02}Ir_{0.01}Os_{0.01}Fe_{0.02}Ni_{0.02})_{1.10}(Bi_{0.86}Te_{1.07}Sb_{0.14})_{1.99}$
3. michenerite, $(Pd_{1.00}Pt_{0.03}Ir_{0.01}Os_{0.01}Fe_{0.02}Ni_{0.04})_{1.11}(Bi_{0.79}Te_{1.04}Sb_{0.06})_{1.89}$
4. michenerite, $(Pd_{1.01}Pt_{0.03}Ir_{0.01}Os_{0.01}Fe_{0.02}Ni_{0.03})_{1.11}(Bi_{0.81}Te_{1.04}Sb_{0.04})_{1.89}$
5. merenskyite, $(Pd_{0.64}Ni_{0.28}Pt_{0.01}Fe_{0.02})_{1.05}(Bi_{0.32}Te_{1.63})_{1.95}$
6. merenskyite, $(Pd_{0.54}Ni_{0.45}Pt_{0.01}Fe_{0.03})_{1.03}(Bi_{0.24}Te_{1.72}Sb_{0.01})_{1.97}$
7. Pd-melonite, $(Ni_{0.57}Pd_{0.34}Fe_{0.17})_{1.08}(Te_{1.72}Bi_{0.18}S_{0.02})_{1.92}$
8. sperrylite, $(Pt_{0.97}Ir_{0.01}Os_{0.01}Fe_{0.03}Ni_{0.03})_{1.01}(As_{1.98}S_{0.01})_{1.99}$

10.2 Platinum-Group Minerals

10.2.1 Michenerite

Four michenerite grains with different modes of occurrence were found. One grain coexisting with Bi-telluride occurs as an inclusion in chalcopyrite. Another grain is attached to Bi-telluride and surrounded by pyrrhotite, chalcopyrite, quartz, and plagioclase. The other two grains together with other exotic minerals occur as inclusions in pyrrhotite. One is associated with both Ag-telluride and Ni-rich merenskyite (Plate 5B) whereas the other one is in contact with cobaltite which itself has a sperrylite inclusion (Plate 5C). The size of michenerite grains ranges from 30 x 10 to 130 x 50 μm. In reflected light, michenerite is greyish white in air, and isotropic.

Calculated structural formulae vary from $(Pd_{0.98}Pt_{0.03}Ir_{0.01}Os_{0.01}Ni_{0.05})_{1.08}(Bi_{0.79}Te_{1.07}Sb_{0.06})_{1.92}$ to $(Pd_{1.01}Pt_{0.03}Ir_{0.01}Os_{0.01}Fe_{0.02}Ni_{0.03})_{1.11}(Bi_{0.81}Te_{1.04}Sb_{0.04})_{1.89}$. Maximum contents of substitutions (in wt%) in michenerite are Pt 1.3, Ir 0.5, Os 0.5, Fe 0.5, Ni 0.7, and Sb 4.2.

10.2.2 Merenskyite

Merenskyite attached to grains of Ag-telluride and michenerite forms rounded inclusions in pyrrhotite (Plate 5B). It also occurs in contact with Bi-telluride within pyrrhotite. The merenskyite is yellowish-white with a pink tint

in air, and is anisotropic, from greyish blue to brownish grey. Two merenskyite grains were analyzed by electron microprobe. In general, the merenskyite from the Lockerby mine is very Ni-rich, with Ni content ranging from 6.0 to 7.4 wt%. Maximum contents of substitutions (in wt%) in merenskyite are Pt 0.5, Ir 0.2, Os 0.1, Fe 0.4, and Sb 0.2. Structural formulae vary from $(Pd_{0.64}Ni_{0.38}Pt_{0.01}Fe_{0.02})_{1.05}(Bi_{0.32}Te_{1.63})_{1.95}$ to $(Pd_{0.54}Ni_{0.45}Pt_{0.01}Fe_{0.03})_{1.03}(Bi_{0.24}Te_{1.72}Sb_{0.01})_{1.97}$.

10.2.3 Pd-melonite

Pd-melonite occurs attached to Ag-telluride within pyrrhotite. It is white with a yellowish tint in air and is anisotropic from yellowish grey to greyish blue. Maximum contents of substitutions (in wt%) in Pd-melonite are Pt 0.1, Pd 0.7, Fe 2.8, Bi 5.8 and Sb 0.1. The structure formula is $(Ni_{0.57}Pd_{0.34}Fe_{0.17})_{1.08}(Te_{1.72}Bi_{0.18}S_{0.02})_{1.92}$.

10.3 Electrum and Ag-pentlandite

10.3.1 Electrum

Ten electrum grains in association with Ag-telluride were observed in a chalcopyrite vein cutting carbonates and silicates (chlorite, plagioclase, hornblende, biotite, quartz, and epidote). The largest electrum grain is only 15 μm in diameter. Electron microprobe analysis of this grain gave Au (76.0

wt%), and Ag (26.8 wt%). Maximum contents of substitutions (in wt%) are Pt 0.3 and Cu 0.4, giving a structure formula of $Au_{0.60}Ag_{0.39}Cu_{0.01}$.

10.3.2 Ag-pentlandite

Ag-pentlandite was observed in a Cu-rich granite-breccia Ni-sulfide ore, attached to galena, altaite (PbTe) and Bi-telluride, and included in quartz and plagioclase. Ag-pentlandite is brown in air, resembling bornite. Electron microprobe analyses gave Fe 35.9 wt%, S 31.4, Ni 18.8, Ag 13.0, and Cu 0.1, with total of 99.3. The structural formula is $[(Fe_{5.24}Ni_{2.61})Ag_{0.99}]_{8.86}S_{8.00}$.

PART IV: PGMs FROM DUNDONALD BEACH, ONTARIO

CHAPTER 11 PGMs FROM THE DUNDONALD BEACH PROPERTY

Massive Ni sulfide ore was collected by P.Davis from a new Ni sulfide showing at the Dundonald Beach exploration property of Falconbridge Limited, which is in the Archean Abitibi Belt proximal to the Dundonald Ni sulfide deposit (Muir and Comba, 1979). This komatiite-hosted deposit is described by Naldrett and Mason (1968) and Muir and Comba (1979). At the Dundonald Beach property, sulfide lenses are associated with a cumulate pyroxenite layer near the base of a peridotitic flow unit, and are up to 10 m long and 20 cm wide. The sample analyzed consists largely of massive pentlandite with minor chalcopyrite, sphalerite, and chromite. Pentlandite is extensively replaced by late violarite and minor nickeline (Plate 5D and 5F). The pyroxenite host rock and gangue have been extensively altered to talc, chlorite, and tremolite-actinolite; olivine has been completely serpentinized.

A whole-rock assay of the massive sulfide yielded: Os 455, Ir 528, Ru 2125, Rh 115, Pt 3775, Pd 7500 and Au 1250 ppb (Table 11.1). In situ analyses by microprobe SIMS revealed that Pt was about 30 times higher in the violarite than in the pentlandite it was replacing (Table 11.1). Also, Pt was slightly higher in chalcopyrite than in the pentlandite.

In the present study three varieties of PGMs and electrum were identified

Table 11.1 PGE and Au contents of the whole rock and sulfide minerals (ppb)

sample	Os	Ir	Ru	Rh	Pt	Pd	Au
whole rock*	455	528	2125	115	3775	7500	1250
violarite**	-	900	-	-	3700	-	1500
pentlandite**	-	910	-	-	110	-	700
chalcopyrite**	-	240	-	-	640	-	1000
whole rock***	-	893	-	-	1049	-	914

* INAA analysis; ** in situ microprobe SIMS; *** calculated PGE values based on mineral proportion and SIMS analyses on each mineral.

from the massive sulfide.

11.1 Froodite ($PdBi_2$)

Six grains of froodite were identified and confirmed by electron microprobe analysis (Table 11.2). Most of the grains are subhedral to anhedral with maximum size of 70 x 100 μm, and are included in both pentlandite and violarite (plate 5D). In reflected light, froodite is white with a slightly yellow tinge next to pentlandite and light brown next to parkerite. It is moderately anisotropic from brown to yellowish or light grey.

The maximum content of substitutions (in wt%) in froodite are: Os 1.2, Pt 0.9, Ir 0.6, Rh 0.1, Ru 0.2, Fe 1.2, Ni 2.0, As 0.1, Te 0.4, and Sb 0.1. Osmium, Ir, Rh, Ru, Fe, Ni and As are reported for the first time. Parkerite ($Ni_3Bi_2S_2$) coexisting with froodite also has minor contents of PGE, maximum substitutions (in wt%) being Pd 0.2, Ir 0.1 and Os 0.4.

With the exception of the occurrence at the Pipe mine, Thompson Nickel Belt, froodite is generaly associated with Cu-Ni-sulfide deposits hosted in mafic rocks, as in Sudbury, Ontario (Cabri, 1981b), Noril'sk, Siberia (Genkin and Evstigneeva, 1986), and Watefall Gorge, Pondoland (Tishler et al., 1981). This is the first occurrence of froodite from komatiite.

11.2 Unnamed Pd-Sb-Bi Phase

Six grains of an unnamed PGM phase occur as inclusions in pentlandite

Table 11.2 Compositions of froodite from the Dundonald Beach property

sample	1	2	3	4	5
			weight percent		
Pt	0.06	0.04	0.00	0.00	0.85
Pd	19.54	19.00	19.34	19.80	19.62
Ir	0.00	0.00	0.00	0.00	0.54
Os	1.11	0.95	1.08	1.18	0.90
Rh	0.05	0.03	0.02	0.00	0.00
Ru	0.00	0.00	0.00	0.00	0.15
Fe	0.05	0.04	0.20	0.28	1.16
Ni	0.08	0.08	0.38	0.48	1.95
As	0.08	0.00	0.00	0.01	0.14
Bi	79.61	78.75	77.92	79.49	75.93
Te	0.25	0.19	0.37	0.12	0.00
Sb	0.03	0.07	0.06	0.00	0.02
S	0.00	0.00	0.00	0.01	0.04
total	100.86	99.15	99.37	101.37	101.30
			atomic percent		
Pt	0.05	0.03	0.00	0.00	0.71
Pd	31.84	31.61	31.67	31.69	29.82
Ir	0.00	0.00	0.00	0.00	0.45
Os	1.01	0.88	0.99	1.06	0.77
Rh	0.08	0.05	0.03	0.00	0.00
Ru	0.00	0.00	0.00	0.00	0.24
Fe	0.16	0.13	0.62	0.85	3.36
Ni	0.24	0.24	1.13	1.39	5.37
As	0.19	0.00	0.00	0.02	0.30
Bi	66.05	66.69	64.96	64.77	58.75
Te	0.34	0.26	0.51	0.16	0.00
Sb	0.04	0.10	0.09	0.00	0.03
S	0.00	0.00	0.00	0.05	0.20

1. $(Pd_{0.95}Os_{0.03}Ni_{0.01})_{1.00}(As_{0.01}Bi_{1.98}Te_{0.01})_{2.00}$
2. $(Pd_{0.95}Os_{0.03}Ni_{0.01})_{1.00}(Bi_{1.99}Te_{0.01})_{2.00}$
3. $(Pd_{0.95}Os_{0.03}Fe_{0.02}Ni_{0.03})_{1.03}(Bi_{1.95}Te_{0.02})_{1.97}$
4. $(Pd_{0.95}Os_{0.03}Fe_{0.03}Ni_{0.04})_{1.05}Bi_{1.95}$
5. $(Pt_{0.02}Pd_{0.89}Ir_{0.01}Os_{0.02}Ru_{0.01}Fe_{0.10}Ni_{0.16})_{1.21}(As_{0.01}Bi_{1.76}S_{0.01})_{1.78}$

and violarite, with maximum size of 10 x 10 μm. The unnamed phase is white with creamy tinge, and greyish yellow next to native gold. It is strongly anistropic from light brown to light grey. The composition of the mineral is given in Table 11.3. The formula varies from $Pd(Sb_{0.66}Bi_{0.34})$ to $Pd(Sb_{0.50}Bi_{0.50})$. The electron microprobe analyses are slightly metal-rich, but this is probably attributable to the small grain size of the mineral.

11.3 Os-Ni-Fe Alloy

One grain of Os-Ni-Fe alloy was encountered. It occurs as an inclusion in late violarite with grain size of 15 x 15 μm. It is yellowish white with pink tinge in reflected light, and is anisotropic from brown to light grey. Due to its small grain size, electron microprobe analysis gave only a total of 89.25 wt%. The alloy consists of mainly Os, Ni and Fe, and small amounts of Ir and Bi (Table 11.3), and has a formula of $Os_{0.60}Ir_{0.05}Pt_{0.01}Fe_{0.19}Ni_{0.11}Bi_{0.04}$.

11.4 Electrum

Twenty-six grains of electrum were identified. Most of them occur as inclusions in violarite but some are included in pentlandite. The maximum grain size is 20 x 20 μm. Representative electron microprobe analyses are given in Table 11.4. The electrum is characterized by high Hg contents which range from 4.2 to 9.0 wt%, and increase with increasing Ag content. The formula varies from $Au_{0.53}Ag_{0.44}Hg_{0.03}$ to $Au_{0.42}Ag_{0.50}Hg_{0.07}$.

Table 11.3 Compositions of unnamed PGM phase and Os-Fe-Ni alloy from the Dundonald Beach property

sample	1	2	3	4
		weight percent		
Pt	0.15	0.13	0.37	0.80
Pd	41.54	39.72	41.83	0.00
Ir	0.15	0.17	0.00	5.41
Os	0.00	0.00	0.00	68.17
Rh	0.03	0.00	0.02	0.00
Ru	0.00	0.00	0.00	0.00
Fe	1.38	1.08	1.42	6.36
Ni	1.93	1.74	1.94	3.79
As	0.29	0.25	0.25	0.14
Bi	29.26	33.84	25.31	4.56
Te	0.41	1.84	0.19	0.00
Sb	25.17	20.76	28.40	0.00
S	0.05	0.04	0.06	0.02
Total	100.36	99.57	99.79	89.25
		atomic percent		
Pt	0.10	0.09	0.23	0.69
Pd	48.48	48.15	48.25	0.00
Ir	0.10	0.11	0.00	4.74
Os	0.00	0.00	0.00	60.40
Rh	0.04	0.00	0.02	0.00
Ru	0.00	0.00	0.00	0.00
Fe	3.07	2.49	3.12	19.19
Ni	4.08	3.82	4.06	10.88
As	0.48	0.43	0.41	0.32
Bi	17.39	20.89	14.86	3.68
Te	0.40	1.86	0.18	0.00
Sb	25.67	21.99	28.63	0.00
S	0.19	0.16	0.23	0.11

1-3. unnamed PGM phase; 4. Os-Fe-Ni alloy.

1. $Pd_{0.49}Fe_{0.03}Ni_{0.04}Bi_{0.17}Sb_{0.26}$
2. $Pd_{0.49}Fe_{0.02}Ni_{0.04}Bi_{0.21}Sb_{0.22}Te_{0.02}$
3. $Pd_{0.49}Fe_{0.03}Ni_{0.04}Bi_{0.15}Sb_{0.29}$
4. $Os_{0.63}Fe_{0.19}Ni_{0.11}Ir_{0.03}Pt_{0.01}Bi_{0.04}$

Table 11.4 Compositions of electrum from the Dundonald Beach property

sample	1	2	3	4	5	6	7	8
				weight percent				
Au	55.76	55.32	55.29	54.75	66.52	65.70	65.42	55.51
Ag	36.53	36.49	36.20	36.80	29.98	30.44	29.89	35.71
Hg	8.92	8.94	8.92	8.76	4.17	4.45	4.21	8.23
total	101.21	100.75	100.41	100.31	100.67	100.63	99.52	99.45
				atomic percent				
Au	42.49	42.32	42.48	41.94	53.06	52.27	52.70	43.10
Ag	50.83	50.97	50.79	51.48	43.67	44.22	43.97	50.63
Hg	6.68	6.72	6.73	6.59	3.26	3.52	3.33	6.28

Plate 5

PGM from Sudbury and Dundonald Beach

A: Electron back-scattered image of Lindsley mine michenerite (white) associated with magnetite (dark grey), pyrrhotite (light grey) and quartz (black). Sample B.

B: Electron back-scattered image of Lockerby mine michenerite (white), merenskyite (light grey) and Ag-telluride (dark grey) included in pyrrhotite and pentlandite (black). Sample LBT-6.

C: Electron back-scattered image of Lockerby mine michenerite (white) coexisting with cobaltite (light grey) which itself has a sperrylite inclusion (white), associated with pentlandite (dark grey) and pyrrhotite (black). Sample LBTC.

D: Electron back-scattered image of Dundonald Beach froodite (white) associated with pentlandite (light grey), violarite (dark grey) and silicate minerals (black). Sample DONS1C.

E: Electron back-scattered image of Dundonald Beach electrum (light grey) and unnamed PGM (dark grey) in association with violarite (black). Sample DONS1C.

F: Electron back-scattered image of Dundonald Beach electrum (white) associated with pentlandite (light grey), violarite (dark grey) and silicate minerals (black). Sample DONS1B.

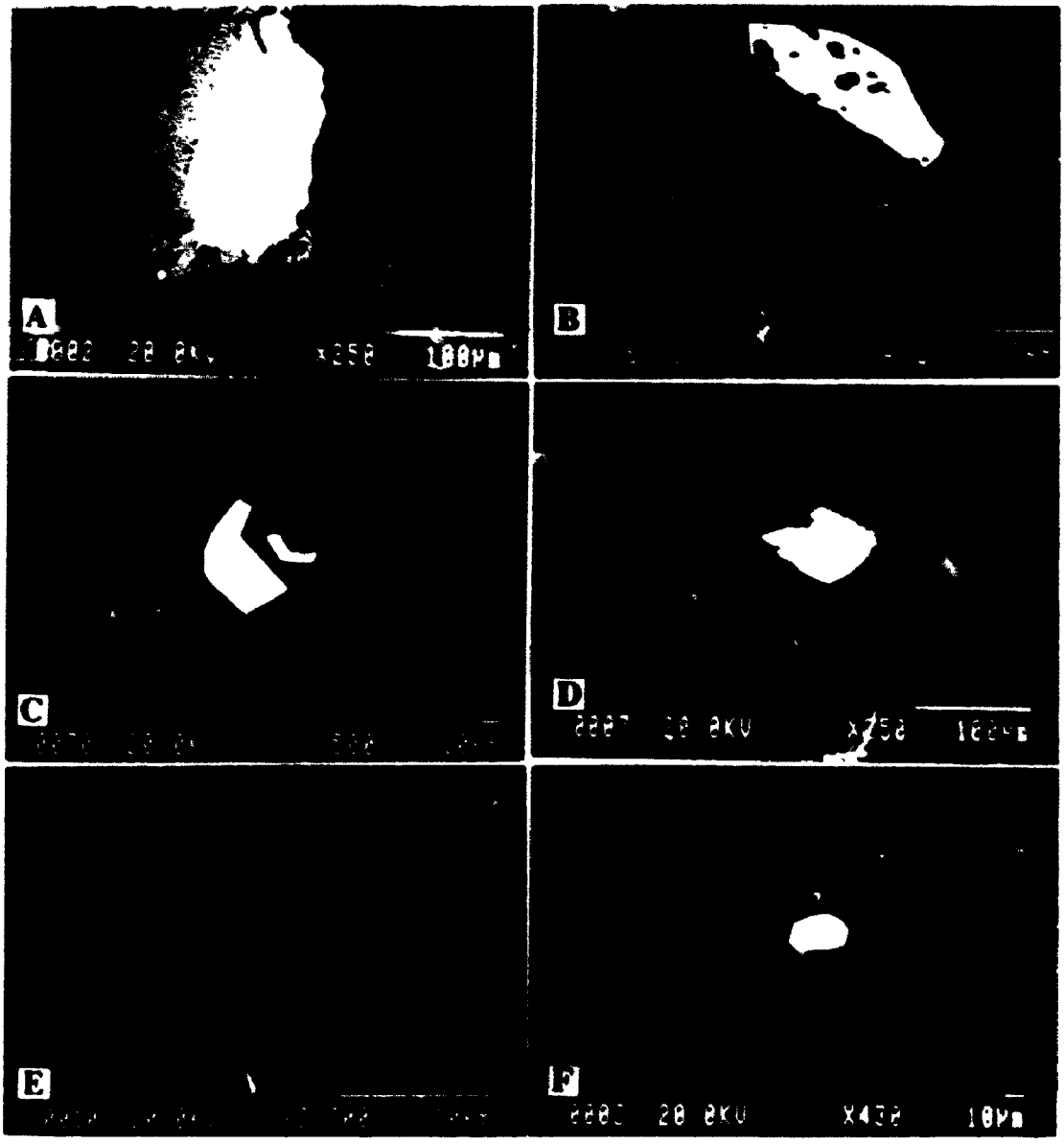
A
B
C
D
E
F

PART V: PARTITIONING OF Ni BETWEEN OLIVINE AND Fe-Ni SULFIDE

CHAPTER 12 PREVIOUS WORK

The partitioning of nickel between olivine (ol) and Fe-Ni-Cu sulfide (sulf) is most conveniently studied through the Ni/Fe exchange reaction:

$$NiSi_{1/2}O_{2,ol} + FeS_{sulf} = NiS_{sulf} + FeSi_{1/2}O_{2,ol}$$

with distribution coefficient (labelled K_{D3} by Fleet and MacRae, 1983) given by

$$K_{D3} = (X_{NiS} \bullet X_{FeSi1/2O2})/(X_{FeS} \bullet X_{NiSi1/2O2}).$$

The experimental data for this exchange reaction are now known with some confidence. Following an extensive period of laboratory experimentation (Clark and Naldrett, 1972; Fleet et al., 1977; Fleet and MacRae 1987; 1988), K_{D3} has been shown to be essentially constant at about 30 to 35 in the temperature range 900 to 1400°C for a wide range of olivine and Fe-Ni monosulfide compositions at low fO_2, and for Fe-Ni monosulfide-oxide liquids exhibits only a weak decrease from 35 to 29 over the full range of possible oxidation conditions for the upper mantle.

Boctor (1981, 1982) reported experimental K_{D3} values of 13 and 8 at 1400°C. Fleet and MacRae (1987) reinvestigated the experimental conditions of Boctor (1981, 1982), but were unable to stabilize a monosulfide liquid. Doyle

and Naldrett (1987) suggested that K_{D3} values would be reduced in nature by dilution of Fe-Ni monosulfide with oxide components, to the extent that K_{D3} for olivine and a natural sulfide-oxide liquid is expected to be less than 12. This was contradicted by Fleet (1986), who showed that, for the temperature range 900 to 1200°C, K_{D3} appears to be essentially constant within the range of fO_2 defined by the iron-silica phase-fayalite (IQF) and fayalite-magnetite-silica phase (FMQ) buffers. Fleet and MacRae (1988) also reported that ultrabasic and early-magmatic basic magmas could not support an oxygen-enriched sulfide-oxide liquid. The oxygen content of monosulfide-oxide liquid is essentially buffered by the coexisting olivine and bulk silicate melt.

In comparison with the laboratory experiments that indicate an equilibrium K_{D3} value of about 30 to 35, Cu-Ni sulfide ore deposits in host rocks that have not been metamorphosed beyond low grade conditions have K_{D3} values in the range of 2 to 5 for komatiites and 5 to 10 for layered intrusions. Fleet and MacRae (1983) suggested that the high NiO contents of olivine from these deposits appeared inconsistent with ore formation by segregation of immiscible sulfide liquid. With increasing metamorphic grade and pervasiveness of metamorphism, calculated K_{D3} values approach the experimental value, indicating that the Ni contents of sulfide and silicate phases approach equilibrium concentration (Fleet and MacRae, 1983).

CHAPTER 13 THOMPSON NICKEL BELT

A previous study (Paktunc, 1984) on an unusually fresh ultramafic body found on the 4000 level of the Thompson T-3 mine (on the east limb of the anticline) reported compositions of olivine ranging from Fo_{83} to Fo_{89}. The NiO content of olivine ranges from the limit of detection to 0.40 wt%. The MnO content ranges from 0.10 to 0.35 wt%. However, this ultramafic body does not contain Fe-Ni sulfide. The mineralized peridotite samples examined in the present study were collected from the 3-shear orebody of the Thompson T-1 mine. The peridotite body is located close to the nose of the anticline (Fig. 4.1), and contains both disseminated and brecciated veins of pentlandite and pyrrhotite. Minor amounts of chalcopyrite are also present. Ninety-nine percent of the rock is serpentinized with some relict olivine, orthopyroxene, and amphibole, and very rare relict clinopyroxene and phlogopite (Plate 6A). Massive carbonate minerals and talc are closely related to veins of Fe-Ni sulfides (Plate 6B). Zincian spinel has also been documented.

Olivine occurs as isolated islands within serpentinized matrix (Plate 6A, 6B), and its composition ranges from Fo_{88} to Fo_{90}. The NiO content of olivine is low, varying from 0.03 to 0.10 wt%, and the MnO content varies from 0.20 to 0.30 wt% (Appendix XIX). The volume proportions of the sulfides were estimated by point-counting (over 5000 points for each sample), and then calculated into weight percentage. The compositions of the sulfides and Ni/Fe

partitioning data are given in Tables 13.1 and 13.2. Most of the calculated K_{D3} values for mineralized peridotite from the Thompson T-1 mine range from 17 to 20. According to Fleet and MacRae (1983), the olivine and sulfide compositions of Ni-Cu sulfide deposits metamorphosed to or below low grade conditions yield K_{D3} values in the range 2 to 10. In contrast, K_{D3} values for Ni-Cu sulfide deposits metamorphosed to medium and high grade conditions are significantly closer to the experimental values. There is in general, a rather good correlation of increasing approach to chemical equilibration with increasing grade and pervasiveness of metamorphism. This correlation may be related to the marked temperature dependence of the mobility of Ni in olivine. The high K_{D3} value of mineralized peridotite from the Thompson T-1 mine suggests that the ultramafic rock experienced medium or high grade metamorphism after formation of the orebodies. Thus, the Ni sulfide mineralization in the Thompson Nickel Belt certainly appears to have predated the peak of the Hudsonian orogeny. This conclusion is in agreement with the radiogenic ages of Cumming et al. (1982). The depletion in the Ni content of olivine indicates that Ni was mobilized from olivine to sulfide during the medium or high grade metamorphism, enriching the Ni-content of the sulfide.

Table 13.1 Compositions of sulfide minerals from the Thompson T-1 mine

No.	Sulfides, Proportion		Composition[1] (wt%)			
		vol%[2]	wt%[3]	Fe	Ni	Cu	S
PT3	Pn	13.3	13.8	29.7	35.1		33.3
	Po	86.1	85.7	60.9	0.1		39.6
	Cp	0.6	0.6	30.4		34.6	34.9
PT7	Pn	13.3	13.8	31.2	35.9		33.6
	Po	86.1	85.7	59.1	0.1		38.3
	Cp	0.6	0.6	30.4		34.6	34.9
PT8	Pn	13.3	13.8	30.3	36.0		33.7
	Po	86.1	85.7	60.9	0.2		39.7
	Cp	0.6	0.6	30.4		34.6	34.9

Pn=pentlandite, Po=pyrrhotite, Cp=chalcopyrite.

1. Electron microprobe analyses; the ideal composition was used for chalcopyrite.
2. Estimated by point counting.
3. Calculated from volume percentage.

Table 13.2 Ni/Fe partitioning data for natural olivine/monosulfide from the Thompson T-1 mine

No.	N	Olivine (wt%)					Monosulfide (wt%)			
		SiO_2	MgO	FeO	NiO	MnO	Fe	Ni	Cu	S
PT8	33	40.66	48.70	11.34	0.07	0.25	56.2	5.1	0.2	38.6
PT7	20	40.60	49.21	10.34	0.07	0.24	56.2	5.2	0.2	38.4
PT3	30	40.09	49.47	10.19	0.05	0.24	56.3	5.0	0.2	38.6
		X_{FeSiO_2}		X_{NiSiO_2}			X_{FeS}	X_{NiS}		K_D
PT8		0.115		0.0005			0.918	0.079		20
PT7		0.105		0.0005			0.917	0.080		18
PT3		0.103		0.0005			0.920	0.077		17

N=number of microprobe spots for olivine.

CHAPTER 14 SUDBURY AREA

14.1 General geology

Since the discovery of Cu-Ni sulfide ore in 1883, the Sudbury structure has been the subject of numerous geological studies (cf., summary of Pye et al., 1984). The elliptically shaped, mid-Proterozoic basin, 60 km long by 27 km wide, consists of plutonic rocks of the Sudbury Igneous Complex overlain by and enclosing the predominantly sedimentary rocks of the Whitewater Group. Concentric outcropping rings of lower zone norite (the outermost), middle zone gabbro and upper zone granophyre (the innermost) constitute the main body of the complex. The Cu-Ni sulfide deposits are associated with a contact sublayer which is composed of fine to medium-grained noritic to gabbroic rocks, occurring around much of the outer margin of the Sudbury Nickel Irruptive as discontinuous lenses and as filling for the offset dikes. Inclusions in the sublayer are of 2 kinds, one is of adjacent country rocks and the other is of rounded mafic to ultramafic xenoliths which have no counterpart in the exposed footwall. Exotic inclusions of olivine-bearing sublayer rocks examined in this study were obtained from the field and from the research collection of INCO Limited, and included material from the Levack, Trillabelle and Whistle mines. The sample from the Ministic Lake offset dyke was provided by M.E. Fleet. No previous work on olivine from these rocks has been reported in the literature. In this study emphasis is placed on the sulfide-

silicate relationships, i.e., on the partitioning of Ni between olivine and sulfide.

14.2 Whistle Offset Mine

The Whistle deposit is located at the extreme northeast corner of the Irruptive (Fig. 9.1). Sublayer rocks overlain by basal Irruptive mafic and felsic norites to the southwest occupy a funnel-shaped depression in the footwall which merges into a poorly defined offset dyke. A well-defined zonation of sublayer rock types parallel to the contact of the Irruptive exists within the funnel; zones of orthopyroxene-rich and olivine-bearing igneous sublayer occupying the core of the funnel are succeeded by progressively more siliceous varieties of igneous sublayer as the footwall contacts are approached (Pattison, 1979). Norite samples collected from olivine-bearing igneous sublayer are mainly composed of olivine, orthopyroxene, plagioclase, and minor biotite and magnetite. Talc replaces orthopyroxene, and olivine has been strongly serpentinized (Plate 6C). The composition of olivine varies from Fo65 to Fo68, and NiO and MnO contents range from 0.09 to 0.21 wt% and 0.35 to 0.49 wt%, respectively (Appendix XX). Disseminated sulfides, composed of pyrrhotite and pentlandite with minor chalcopyrite, are quite common. Compositions of sulfides are given in Table 14.1. The calculated K_{D3} value is 14 (Table 14.2).

14.3 Levack Mine

Table 14.1 Compositions of sulfide minerals from the Sudbury area

location	No.		Sulfides, Proportion		Composition[1] (wt%)				
			vol%[2]	wt%[3]	Fe	Ni	Cu	Co	S
Whistle	WHL2A	Pn	7.8	8.2	27.0	37.2		1.5	33.3
offset		Po	87.1	87.3	59.6	0.9			39.8
		Cp	5.0	4.6	30.4		34.6		34.9
Levack	LEK1	Pn	69.5	71.2	22.7	42.3		1.0	33.3
mine		Pm	11.8	11.7	6.7	35.2		16.2	42.9
		Cp	16.9	15.2	30.4		34.6		34.9
		Py	1.8	2.0	42.6	0.5		3.3	53.8
Trillabelle	TR2	Pn	15.7	16.2	31.9	29.3		3.9	33.6
mine		Po	84.1	83.6	64.4	0.0			36.8
		Cp	0.2	0.2	30.4		34.6		34.9
	TR4	Pn	15.7	16.2	32.6	29.0		4.0	33.7
		Po	84.1	83.6	64.3	0.0			36.2
		Cp	0.2	0.2	30.4		34.6		34.9
Ministic	M1	Pn	13.5	14.0	29.5	36.0			34.5
offset		Po	86.5	86.0	60.5	0.3			39.2

Pn=pentlandite, Po=pyrrhotite, Cp=chalcopyrite, Py=pyrite, Pm=polydymite.

1. Electron microprobe analyses, the ideal composition was used for chalcopyrite;
2. Estimated by point counting;
3. Calculated from volume percentage.

Table 14.2 Ni/Fe partitioning data for natural olivine/monosulfide from the Sudbury area

No.	N	Olivine (wt%)					Monosulfide (wt%)				
		SiO_2	MgO	FeO	NiO	MnO	Fe	Ni	Cu	S	Co
WHL2A	13	36.82	33.03	29.24	0.16	0.44	55.5	3.8	1.6	39.0	0.1
LEK1	14	39.59	44.25	15.31	0.25	0.32	22.5	34.4	5.3	35.2	2.7
TR4	10	39.25	42.72	17.97	0.11	0.24	58.9	4.7	0.1	35.7	0.6
TR2	31	39.27	41.02	19.65	0.16	0.30	58.6	4.7	0.1	36.0	0.6
M1	30	37.98	38.43	23.25	0.15	0.29	56.2	5.3		38.5	
Levack West/Little Stobie mines:							58.1	3.9	5.7	32.2	0.1

	X_{FeSiO_2}	X_{NiSiO_2}	X_{FeS}	X_{NiS}	K_D	K_D*	
WHL2A	0.330	0.0015	0.915	0.060	14	14	
LEK1	0.162	0.0025	0.849	0.105	94	4	
TR4	0.190	0.0010	0.920	0.070	14	12	
TR2	0.211	0.0015	0.919	0.071	11	9	
M1	0.253	0.0015	0.918	0.082	15	11	

N=number of microprobe spots for olivine.

* K_D calculated with average compositions of sulfides from the Levack West mine and the Little Stobie mine (Hoffman et al., 1979).

The Levack deposit is located on the North Range of the basin (Fig. 9.1). Hornblende peridotite occurs as exotic xenoliths and consists of mainly olivine and hornblende with variable amounts of phlogopite and minor magnetite (Plate 6D). Olivine has been extensively serpentinized. The occurrence of sulfide is very sporadic. The sulfide assemblage is also very Ni-rich, being comprised of pentlandite, polydymite, pyrite, and chalcopyrite Polydymite (Ni_3S_4) has been reported from the Vermilion mine (Clarke and Catlett, 1889), and the Levack mine (Wandke and Hoffman, 1924). However, in view of its optical similarity to bravoite and violarite, confirmation in the absence of chemical or X-ray data is open to question (Misra and Fleet, 1973). In this study, the presence of polydymite in the Levack xenolith is confirmed by electron microprobe investigation. It is associated with pentlandite, occurring as inclusions. Polydymite is pink in reflected light and isotropic. Electron microprobe analyses show that it is a solid solution of Ni_3S_4-Co_3S_4-Fe_3S_4, containing 35.2 wt% of Ni, 16.2 wt% of Co, 6.6 wt% of Fe and 42.9 wt% of S, total 100.99. The calculated structural formula is $(Ni_{1.82}Co_{0.80}Fe_{0.38})_3S_4$.

Electron microprobe analyses of olivine are given in Appendix XXI. Olivine composition ranges from Fo81 to Fo88. The NiO and MnO contents of olivine vary from 0.18 to 0.32 wt% and 0.20 to 0.41 wt%, respectively. The Ni-rich sulfide assemblage results in an unreasonably high value of K_{D3} (94, Table 14.2). This result is not surprising, since the Ni-rich sulfide assemblage is probably not primary. According to Scott (1982), polydymite is only stable

below 356°C. Therefore, it is quite possible that polydymite was precipitated from hydrothermal fluids or is the alteration product of Fe-Ni sulfide, as suggested by Misra and Fleet (1974) for the formation of violarite.

14.4 Trillabelle Mine

The Trillabelle deposit is located on the northwest rim of the Irruptive (Fig. 9.1). Dunite inclusions collected from the sublayer contain over 90 vol% of olivine, variable amounts of amphibole, orthopyroxene and minor phlogopite (Plate 6E). Chlorite is after phlogopite, whereas talc and carbonate replace orthopyroxene. Pentlandite and pyrrhotite and minor chalcopyrite were also identified. Electron microprobe analyses of olivine are given in Appendix XXII. The composition of olivine varies from Fo 78 to Fo 81; minor MnO (0.16-0.42 wt%) and NiO (0.08-0.19 wt%) were also detected. K_{D3} values of the samples range from 11 to 14 (Table 14.2).

14.5 Ministic Lake Offset Dyke

The Ministic Lake offset is located on the northwest margin of the Irruptive (Fig. 9.1). Sublayer rocks and footwall breccia fill a small embayment structure in the proximal part of the offset dyke, but quartz diorite is the dominant facies in the distal part (Grant and Bite, 1984).

An olivine norite sample from the Ministic offset is composed mainly of hypersthene, amphibole, plagioclase and olivine with minor biotite (Plate 6F).

The sulfide assemblage includes pentlandite and pyrrhotite. Fleet et al. (1987) noted that plagioclase laths are replaced by a very fine-grained mixture of epidote and sericite. Hypersthene grains have been replaced by actinolite±cummingtonite, and occasionally by patches of talc. Green-brown and green low-Al hornblende and blue-green actinolitic hornblende formed by the replacement of primary edenite. Olivine has been replaced by serpentine. Olivine compositions are given in Appendix XXIII and the sulfide composition in Table 14.2. The calculated K_{D3} value for the Ministic offset is 15 (Table 14.2).

14.6 Discussion

The Ni-sulfide deposits from northeast and northwest of the North Range of the Sudbury basin have similar K_{D3} values, ranging from 11 to 15. These low values are consistent with Ni-C sulfide deposits that have not been metamorphosed beyond low-grade conditions.

The origin of the Cu-Ni sulfide orebodies has generally been interpreted as caused by either sulfide liquid immiscibility in silicate magma during the early magmatic stage (Naldrett, 1989; Lesher and Groves, 1986) or sulfidation of the host rocks during the late magmatic stage or high-temperature subsolidus stage (Fleet, 1979; Fleet and MacRae, 1983; Stone et al., 1989). It is generally anticipated that the geochemistry of Ni in ultramafic and mafic rocks, and particularly the partitioning of Ni between coexisting phases will provide

evidence on hypotheses of early magmatic origin of nickel sulfide deposits. Studies on unmetamorphosed to low-grade metamorphosed rocks suggested that the NiO content of olivine is commonly too high and the Ni content of the associated sulfides is too low for equilibration of sulfide liquid with magmatic olivine. This appears to be the case for the Sudbury ore as well. However, K_{D3} is significantly higher for Cu-Ni sulfide deposits metamorphosed to medium and high grade conditions (Fleet et al., 1977; Fleet, 1979; Fleet and MacRae, 1983; Fleet and Stone, 1990). Studies on Ni partitioning between olivine and monosulfide from the deposits of the North Range of the Sudbury Basin, together with the Ni partitioning data from the Thompson mine, confirm the theory described above. The K_{D3} values of olivine/monosulfide from the Thompson mine are distinctly higher than those from the Sudbury Basin. This may be attributable to their different metamorphic history.

Plate 6

Olivine-bearing rocks directly or indirectly associated with magmatic sulfide

A: Photomicrograph of strongly serpentinized Thompson mine peridotite (3-shear orebody) with relict olivine (island like) and pyroxene (high relief, with distinct cleavage). Sulfide vein (black) replacing olivine grain. Scale bar is 0.2 mm. Sample PT7.

B: Photomicrograph of altered Thompson mine peridotite with secondary talc (pseudomorphing pyroxene) and massive carbonate minerals. Scale bar is 0.2 mm. Sample PT8II.

C: Photomicrograph of olivine-bearing norite from the Whistle mine, Sudbury, illustrating olivine (small grain, high relief, no cleavage) replaced by serpentine (biac.,, orthopyroxene (larger grains, high relief) with distinct cleavage) and plagioclase (white, low relief). Scale bar is 0.2 mm. Sample WHL2A.

D: Photomicrograph of peridotite xenolith from the Levack mine, Sudbury, illustrating olivine (high relief, with irregular fractures), hornblende (dark grey), and phlogopite (light grey with (001) cleavage). Scale bar is 0.2 mm. Sample LEK-1.

E: Photomicrograph of dunite xenolith from the Trillabelle mine, Sudbury, illustrating olivine (with fractures), phlogopite (with (001) cleavage), orthopyroxene (high relief, with cleavage in one direction) and amphibole (with amphibole cleavage). Scale bar is 0.2 mm. Sample TR6.

F: Photomicrograph of olivine norite from the Ministic offset, Sudbury, illustrating olivine (small grain, high relief), orthopyroxene (high relief, clear), amphibole (with magnetite dust) and plagioclase (low relief). Scale bar is 0.2 mm. Sample BSY223A.

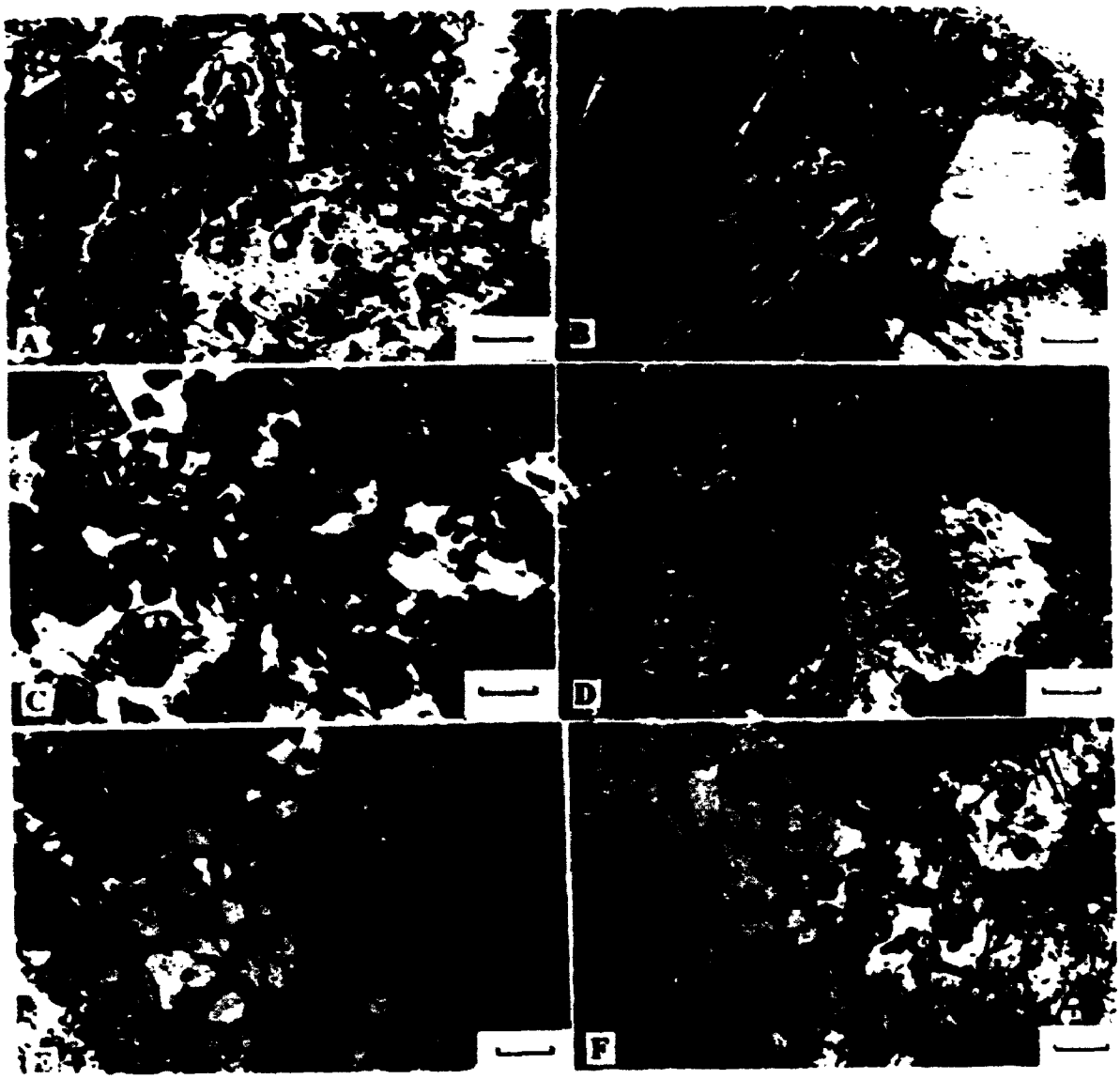
A
B
C
D
E
F

CHAPTER 15 DUNDONALD BEACH

The massive sulfide sample of Chapter 11 did not contain fresh olivine. However an olivine-bearing sample was collected by P. Davis near the base of the komatiite in the Dundonald Beach Prospect, but along strike from the massive sulfide lens. It is therefore spatially associated with the pyroxenite layer containing the PGMs and gold described in Chapter 11.

The olivine-bearing rock contains over ninety percent of olivine and has been strongly serpentinized. The composition of olivine ranges from Fo90 to Fo92. The NiO content is high, varying from 0.36 to 0.41 wt%, and average contents of MnO and Cr_2O_3 are 0.12 and 0.22 wt%, respectively (Appendix XXIV). The same method as in the previous chapters was used to estimate the proportion of sulfides (Table 15.1). The compositions of the sulfides and Ni/Fe partitioning data are given in Table 15.2. The calculated K_{D3} value is 26, which is much higher than values previously reported for low-grade metamorphosed komatiite. This high K_{D3} value could be attributed to hydrothermal alteration of Fe-Ni sulfides, giving Ni-enriched sulfides, as is commonly observed in serpentinization. Alternatively, it could also represent equilibrium between olivine and primary sulfides.

Table 15.1 Compositions of sulfide minerals from the Dundonald Beach Prospect

Sam. No.		Sulfides, Proportion		Composition[1] (wt%)				
		vol%[2]	wt%[3]	Fe	Ni	Cu	Co	S
DB	Pn	72.0	72.8	29.5	37.2		0.2	32.9
	Vl	25.8	25.3	22.5	35.3		0.3	41.7
	Cp	2.2	2.0	30.4		34.6		34.9

Pn=pentlandite, Vl=violarite, Cp=chalcopyrite.
1, 2, 3. see Table 14.1.

Table 15.2 Ni/Fe partitioning data for natural olivine/monosulfide from Dundonald Beach

Nc.	N	Olivine (wt%)					Monosulfide (wt%)				
		SiO_2	MgO	FeO	NiO	MnO	Fe	Ni	Cu	Co	S
DB	8	40.16	49.69	8.01	0.39	0.12	27.8	36.1	0.7	0.2	35.2

X_{FeSiO_2}	X_{NiSiO_2}	X_{FeS}	X_{NiS}	K_D
0.083	0.0039	0.224	0.275	26

PART VI: GENERAL CONCLUSIONS

CHAPTER 16 CONCLUSIONS

Precious-metal minerals in the Thompson Mine consist of both PGMs and argentian native gold. PGMs include irarsite, sudburyite, testibiopalladite-antimonian michenerite, unnamed PGM, merenskyite, majakite, and kotulskite. PGMs and gold occur exclusively within late gersdorffite-nickeline veins that are spatially related to the main Ni-sulfide orebody. Also, gangue minerals in all PGM-gold bearing ores are pervasively altered. All these features suggest that this local enrichment of PGEs and Au may be due to a late reworking of Ni ores by hydrothermal fluids. Mineral chemistry and P-T-X calculations indicate that the fluids were Cl-rich and probably moderately enriched in CO_2.

PGMs and gold presently reported from the Sudbury mining camp include michenerite and merenskyite at the Lindsley mine, and sperrylite, michenerite, merenskyite, Pd-melonite, and electrum at the Lockerby mine. At the Dundonald Beach exploration property, Ontario, electrum, Os-Ni-Fe alloy, froodite, and an unnamed PGM phase (Pd-Sb-Bi) occur in komatiite. The alteration assemblages in these deposits also favour the possible involvement of hydrothermal fluids in the PGE-Au mineralization.

Investigation of the partitioning of Ni between olivine and Fe-Ni monosulfide reveals that the Fe/Ni distribution coefficient (K_{D_1}) is in the range

4-15 at the Whistle, Levack, Trillabelle, and Ministic Lake mines of the Sudbury mining camp. These values are consistent with K_{D3} for Ni-Cu sulfide ores in host rocks that have not been metamorphosed beyond low grade conditions. The K_{D3} values (17-20) for the Thompson Mine peridotite on the otherhand are similar to K_{D1} for magmatic sulfide ore bodies that have experienced medium or high grade metamorphism. The komatiite from the Dundonald Beach property has a K_{D3} value of 26, which could be attributed to either hydrothermal alteration of Fe-Ni sulfide, giving Ni-enriched sulfides, or equilibrium of primary (magmatic) sulfides with olivine.

REFERENCES

ALBEE, A.L. (1962): Relationships between the mineral association, chemical composition and physical properties of the chlorite series. Am. Mineral. 47, 851-870.

AMOSSE, J. ALLIBERT, M., FISCHER, W. AND PIBOULE, M. (1990): Experimental study of the solubility of platinum and iridium in basic silicate melts——implications for the differentiation of platinum-group elements during magmatic processes. Chem. Geol. 81, 45-53.

APLONOV, V.S. AND SEREDA, E.V. (1983): Formation temperatures of quartz and hisingerite from massive copper-nickel ores of the Talnakh deposit. Geol. Geofiz. 3, 62-7 (in Russian)

AUGE, T. (1985): Platinum-group-mineral inclusions in ophiolitic chromitite from the Vourinos complex, Greece. Can. Mineral. 23, 163-171.

_____ (1986): Platinum-group-mineral inclusions in chromitites from the Oman ophiolite. Bull. Mineral. 109, 301-304.

_____ (1988): Platinum-group minerals in the Tiebaghi and Vourinos ophiolitic complexs: genetic implications. Can. Mineral. 26, 177-192.

BAILEY, S.W. (1975): Chlorites. In Soil Components, Vol. 2, Inorganic Components (Gieseking, J.E., ed.), Springer-Verlag, New York, 191-263.

_____ (1988): Chlorites: structure and crystal chemistry. In Hydrous Phyllosilicates (exclusive of micas) (Bailey, S.W., ed.), Reviews in Mineralogy 19, 347-404.

BALLHAUS, C.G. AND STUMPFL, E.F. (1986): Sulfide and platinum mineralization in the Merensky Reef: evidence from hydrous silicates and fluid inclusions. Contrib. Mineral. Petrol. 94, 193-204.

BARNES, S.J. AND NALDRETT, A.J. (1985): Geochemistry of the J-M (Howland) Reef of the Stillwater Complex, Minneapolis adit area I. Sulfide chemistry and sulfide-olivine equilibrium. Econ. Geol. 80, 627-645.

BEAUDOIN, G., LAURENT, R. AND OHNENSTETTER, D. (1990): First report of platinum-group minerals at Blue lake, Labrador Trough, Quebec. Can.

Mineral. 28, 409-418.

BEESON, M.H. AND JACKSON, E.D. (1969): Chemical composition of altered chromite from the Stillwater Complex, Montana. am. Mineral. 54, 1084-1100.

BELL, C.K. (1971): Boundary geology, Upper Nelson River area, Manitoba and Northwestern Ontario. In Geoscience Studies in Manitoba (A.C. Turnock, ed.), Geol. Assoc. Can. Spec. Pap. 9, 11-39.

BERMAN, R.G. (1991): Thermobarometry using multi-equilibrium calculations: a new technique, with petrological applications. Can. Mineral. 29, 833-855.

BHATTACHARYA, A., MOHANTY, L. MAJI, A. SEN, S.K. AND RAITH, M. (1992): Non-ideal mixing in the phlogopite-annite binary: constraints from experimental data on Mg-Fe partitioning and a reformulation of the biotite-garnet geothermometer. Contrib. Mineral. Petrol. 111, 87-93.

BLEEKER, W. (1990): Evolution of the Thompson Nickel Belt and its nickel deposits, Manitoba, Canada. unpublished Ph.D. thesis, University of New Brunswick.

BLISS, N.W. AND MACLEAN, W.H. (1975): The paragenesis of zoned chromite from central Manitoba. Geochim. Cosmochim. Acta 39, 973-990.

BOCTOR, N.Z. (1981): Partitioning of nickel between olivine and iron monosulfide melts. Carnegie. Inst. Washington Yearb. 80, 356-359.

_____ (1982): The effect of f_{O2}, f_{S2} and temperature on Ni partitioning between olivine and iron sulfide melts. Carnegie. Inst. Washington Yearb. 81, 366-369.

BOUDREAU, A.E., MATHEZ, E.A. AND MCCALLUM, I.S. (1986): Halogen geochemistry of the Stillwater and Bushveld complexes: evidence for transport of the platinum-group elements by Cl-rich fluids. J. Petrol. 27, 967-986.

BOW, C., WOLFGRAM, D., TURNER, A., BARNES, S.J., EVANS, J., ZDEPSKI, M. AND BOUDREAU. A. (1982): Investigations of the Howland Reef of the Stillwater Complex, Minneapolis adit area: Stratigraphy, structure, and mineralization. Econ. Geol. 77, 1481-1492.

BOWIE, S.H.U. (1955): Thucholite and hisingerite-pitchblende complexes from Micholson Mine Saskatchewan, Canada. Bull. Geol. Surv. Gr. Britain 10, 45-57.

BRIGATTI, M.F. (1982): Hisingerite: a review of its crystal chemistry. In Proc. Int. Caly Conf., Bologna and Pavia (H. van Olphen and F. Veniale, eds.), Elsevier, Amsterdam, 97-110.

BROOKS, C. AND THAYER, P. (1981): Rb-Sr geochronology in the Thompson Belt, Manitoba: implications for Aphebian crustal development and metallogenesis. Can. J. Earth Sci. 18, 932-943.

BUCHER-NURMINEN, K. (1987): A recalibration of the chlorite-biotite-muscovite geobarometer. Contrib. Mineral. Petrol. 96, 519-522.

CABRI, L.J., ed. (1981): Platinum-group elements: mineralogy, geology, recovery. Can. Inst. Mining Metall. Spec. Vol. 23.

_____ and LAFLAMME, J.H.G. (1974): Sudburyite, a new palladium-antimony mineral from Sudbury, Ontario. Can. Mineral. 12, 275-279.

_____ and _____ (1976): The mineralogy of the platimun-group elements from some copper-nickel deposits of the Sudbury area, Ontario. Econ. Geol. 71, 1159-1195

_____ and _____ (1981): Analyses of minerals containing platinum-group elements. In Platimum-Group Elements: Mineralogy, Geology, Recovery (L.J. Cabri, ed.), Can. Inst. Mining Met. Spec. Vol 23, 151-173.

CAMERON, E.N. (1978): The lower zone of the eastern Bushveld Complex in Olifants River trough. J. Petrology 19, 437-462.

_____ (1980): Evolution of the Lower Critical Zone, central sector, eastern Bushveld Complex and its chromite deposits. Econ. Geol. 75, 845-871.

_____ (1982): The Upper Critical Zone of the eastern Bushveld complex——precursor to the Merensky Reef. Econ. Geol. 77, 1307-1327.

CAMPBELL, I.H. AND TURNER, J.S. (1986): The role of convection in the formation of platinum and chromitite deposits in layered intrusions. Toronto, Mineralog. Assoc. Canada short course Handbook. 12. 236-

278.

_____, NALDRETT, A.J. AND BARNES, S.J. (1983): A model for the origin of the platinum-rich sulfide horizons in the Bushveld and Stillwater complexes. J. Petrology 24, 133-165.

CATHELINEAU, M. AND NIEVA, D. (1985): A chlorite solid solution geothermometer: The Los Azufres (Mexico) geothermal system. Contrib. Mineral. Petrol. 91, 235-244.

CLARK, A.M., EASTON, A.J. AND MOUNT, M. (1978): Astudy of the neotocite group. Mineral. Mag. 42, 279-280.

CLARK, T. AND NALDRETT, A.J. (1972): The distribution of Fe and Ni between synthetic olivine and sulfide at 900°C. Econ. Geol. 67, 939-952.

CLARKE, F.W. AND CATLETT, C. (1889): A platiniferous nickel ore from Canada. Am. J. Sci. 137, 372-374.

COSTA, U.R., BARNETT, R.L. AND KERRICH, R. (1983): The Mattagami Lake mine Archean Zn-Cu sulfide deposit, Quebec: hydrothermal coprecipitation of talc and sulfides in a sea-floor brine pool——evidence from geochemistry, $^{18}O/^{16}O$, and mineral chemistry. Econ. Geol. 78, 1144-1203.

COWDEN, A., DONALDSON, M.J., NALDRETT, A.J. AND CAMPBELL, I.H. (1986): Platinum-group elements and gold in the komatiite-hosted Fe-Ni-Cu sulfide deposits at Kambalda, Western Australia. Econ. Geol. 81, 1226-1235.

CRANSTONE, D.A. AND TUREK, A. (1976): Geological and geochronoiogical relationships of the Thompson Nickel Belt, Manitoba. Can. J. Earth Sci. 13, 1058-1069.

CRESSEY, G., SCHMID, R. AND WOOD, B.J. (1978): Thermodynamic properties of almandine-grossular garnet solid solutions. contrib. Mineral. Petrol. 67, 397-404.

CUMMING, G.L., ECKSTRAND, O.R. AND PEREDERY, W.V. (1982): Geochronologic interpretations of Pb isotope ratios in nickel sulfides of the Thompson Belt, Manitoba. Can. J. Earth Sci. 19, 2306-2324.

DANA, E.S. (1920): Dana's System of Mineralogy (6th. ed.). John Wiley and

Sons Inc., New York.

DASGUPTA, S., SENGUPTA, P., GUHA, D. AND FUKUOKA, M. (1991): A refined garnet-biotite Fe-Mg exchange geothermometer and its application in amphibolites and granulites. Contrib. Mineral. Petrol. 109, 130-137.

DEER, W.A., HOWIE, R.A. AND ZUSSMAN, J. (1986): Rock-Forming Minerals. 1B. Disilicates and Ring Silicates (2nd ed.). Longmans. London.

DOLLASE, W.A. (1971): Refinement of the crystal structure of epidote, allanite and hancockite. Am. Mineral. 56, 447-464.

DOYLE, C.D. AND NALDRETT, A.J. (1987): The oxygen content of "sulfide" magma and its effect on the partitionaing of nickel between coexisting olivine and molten ores. Econ. Geol. 82, 208-211.

ECKSTRAND, O.R., GRINENKO, L.N., KROUSE, H.R., PAKTUND, A.D., SCHWANN, P.L. AND SCOATES, R.F.J. (1989): Preliminary data on sulphur isotopes and Se/S ratios, and the source of sulphur in magmatic sulphides from the Fox River Sill, Molson Dykes and Thompson nickel deposits, northern Manitoba. Current Research, Part C, Geol. Surv. Can. Paper 89-1C, 235-242.

EGGLETON, R.A., PENNINGTON, T.H., FREEMAN, R.S. AND THREADGOLD, I.M. (1983): Structural aspects of the hisingerite-neotocite series. Clay Mineral. 18, 21-31.

EVANS, B.W. AND FROST, B.R. (1975): Chrome-spinel in progressive metamorphism - a preliminary analysis. Geochim. Cosmochim. Acta 39, 959-972.

_____ and GUGGENHEIN, S. (1988): Talc, pyrophyllite, and related minerals. Hydrous Phyllosilicates (exclusive of micas) (Bailey, S.W., ed.), Reviews in Mineralogy 19, 225-294.

FARROW, C.E.G. AND WATKINSON, D.H. (1992): Alteration and the role of fluids in Ni, Cu and platinum-group element deposition, Sudbury Igneous Complex contact, Onaping-Levack area, Ontario. Mineral. Petrol. 46, 67-83.

FERRARIO, A. AND GARUTI, G. (1990): Platimun-group mineral inclusions in chromitites of the Finero mafic-ultramafic complex (Ivrea-Zone, Italy).

Mineral. Petrol. 41, 125-143.

FERRY, J.M. (1979): Reaction mechanisms, physical conditions, and mass transfer during hydrothermal alteration of mica and feldspar in granitic rocks from south-central Maine, USA. Contrib. Mineral. Petrol. 68, 125-139.

_____ and SPEAR, F.S. (1978): Experimental calibration of the partitioning of Fe and Mg between biotite and garnet. Contrib. Mineral. Petrol. 66, 113-117.

FLEET, M.E. (1977): Origin of disseminated copper-nickel sulfide ore at Frood, sudbury, Ontario. Econ. Geol. 72, 1449-1456.

_____ (1979): Partitioning of Fe, Co, Ni, and Cu between sulfide liquid and basaltic melts and the composition of Ni-Cu sulfide deposits - A discussion Econ. Geol. 74, 1517-1519.

_____ (1986). Geochemistry of the J-M (Howland) Reef of the Stillwater Complex, Minneapolis adit area. I. Sulfide chemistry and sulfide-olivine equilibrium - A discussion. Econ. Geol. 81, 199-203.

_____ (1992): Experiments on the volatility of Fe, Ni, Cu, and platinum group elements (PGE) in sulfide assemblages at 1000°C. AGU, Montreal. EOS Suppl, 372.

_____ and BARNETT, R.L. (1978): Al^{IV}/Al^{VI} partitioning in calciferous amphiboles from the Frood mine, Sudbury, Ontario. Can. Mineral. 16, 527-532.

_____ and MACRAE N.D. (1983): Partition of Ni between olivine and sulfide and its application to Ni-Cu sulfide deposits. Contrib. Mineral. Petrol. 83, 75-81.

_____ and _____ (1987): Partition of Ni between olivine and sulfide: equilibrium with sulfide-oxide liquid. Contrib. Mineral. Petrol. 95, 336-342.

_____ and _____ (1988): Partition of Ni between olivine and sulfide: equilibria with sulfide-oxide liquids. Contrib. Mineral. Petrol. 100, 462-469.

_____ and STONE, W.E. (1990): Nickeliferous sulfides in xenoliths, olivine

megacrysts and basaltic glass. Contrib. Mineral. Petrol. 105, 629-636.

_____ and _____ (1991): Partition of platinum-group elements in the Fe-Ni-S system and their fractionation in nature. Geochim. Cosmochim. Acta 55, 245-253.

_____, MACRAE N.D. AND HERZBERG, C.T. (1977): Partition of nickel between olivine and sulfide: A test for immiscible sulfide liquids. Contrib. Mineral. Petrol. 65, 191-197.

_____, BARNETT, R.L. AND MORRIS, W.A. (1987): Prograde metamorphism of the Sudbury Igneous Complex. Can. Mineral. 25, 499-514.

_____, MACLEAN, P.J. AND BARBIER, J. (1989): Oscillatory-zoned As-bearing pyrite from stratabound and stratiform gold deposits: An indicator of ore fluid evolution. Econ. Geol. Monograph 6, 356-362.

_____, STONE, W.E. AND CROCKET, J.H. (1991): Partitioning of palladium, iridium, and platinum between sulfide liquid and basalt melt: Effects of melt composition, concentration, and oxygen fugacity. Geochim. Cosmochim. Acta 55, 2545-2554.

_____, CHRYSSOULIS, S.L , STONE, W.E. AND WEISENER, C.G. (1992): Laboratory partitioning of precious metals between (Fe,Ni,Cu) monosulfide liquid and solid solution by SIMS and EMP. GAC-MAC Joint Annual Meeting, Wolfville, A34.

_____, ANGELI, N. AND PAN, Y. (1992): Oriented chlorite lamellae in chromite from the Pedra Branca Mafic/Ultramafic Complex, Ceará, Brazil. Am. Mineral. (accepted).

FRISCH, T. (1971): Alteration of chrome spinel in a dunite nodule from Lanzarote, Canary Islands. Lithos 4, 83-91.

FRONDEL, C. AND BAUER, L.H. (1953): Manganpyrosmalite and its polymorphic relation to friedelite and schallerite. Am. Mineral. 38, 755-760.

FROST, B.R. (1975): Contact metamorphism of serpentinite, chloritic blackwall and rodingite at Paddy-Go-Easy Pass, Central Cascade, Washington. J. Petrol. 16, 272-313.

_____ (1991): Stability of oxide minerals in metamorphic rocks. In Oxide

Minerals: Petrologic and Magnetic Signidicance (Lindsley, D.H., ed.), Reviews in Mineralogy 25, 469-487.

FUETEN, F., ROBIN, P.Y.F. AND PICKERING, M.E. (1986): Deformation in the Thompson belt: a progress report. Geol. Surv. Can. Pap. 86-1B, 797-809.

GARUTI, G. AND RINALDI R. (1986): Mineralogy of melonite-group and other tellurides from the Ivrea-Verbano basic complex, Westerm Italian Alps. Econ. Geol. 81, 1213-1217.

_____, FIANDRI, P. AND ROSSI, A. (1986): sulfide composition and phase relations in the Fe-Ni-Cu ore deposits of the Ivrea-Verbano basic complex (western Alps, Italy). Mineral. Deposita 21, 22-34.

GENKIN, A.D., EVSTIGNEEVA, T.L. (1986): Associations of platimun-group minerals of the Noril'sk copper-nickel sulfide ores. Econ. Geol. 81, 1203-1212.

_____ and _____, TRONEVA, N.V. AND VYAL'SOV, L.N. (1978): Majakite, PdNiAs, a new mineral from copper-nickel sufide ores. Internat. Geol. Rev. 20, 96-100.

GHENT, E.D. (1976): Plagioclase-garnet-Al_2SiO_5-quartz: a potential geobarometer-geothermometer. Am. Mineral. 61, 710-714.

GUBELS, R.H., MILLARD, H.T., DESBOROUGH, G.A. AND BARTEL, A.J. (1974): Osmium, ruthenium, iridium, and uranium in silicates and chromite from the eastern Bushveld complex, South Africa. Geochim. Cosmochim. Acta 38, 319-337.

GOLDMAN, D.S. AND ALBEE, A.L. (1977): Correlation of Mg/Fe partitioning between garnet and biotite with O^{18}/O^{16} partitioning between quartz and magnetite. Am. J. Sci. 277, 750-767.

GRANT, R.W. AND BITE, A. (1984): Sudbury quartz diorite offset dikes. In The Geology and Ore Deposits of the Sudbury Structure (Pye, E.G., Naldrett, A.J. and Giblin, P.E., eds.), Ministry of Natural Resources, Ontario, 275-300.

_____ and SASSI, F.P. (1976): Muscovite as a petroganetic indicator minerla in pelitic schists. N. Jahrb. Mineral. Abh. 127, 97-142.

VON GRUENEWALDT, G. (1973): The main and upper zones of the Bushveld complex in the Roossenekal area, Eastern Transvaal. Geol. Soc. S. Afr. Trans. 76, 207-227.

_____, HULBERT, L.J. AND NALDRETT, A.J. (1989): Contrasting platinum-group element concentration patterns in cumulates of the Bushveld Complex. Mineral. Deposita 24, 219-229.

_____, DICKS, D., WET, J. D. AND HORSCH, H. (1990): PGE mineralization in the eastern Bushveld Complex. Mineral. Petrol. 42, 71-95.

GRUNER, J.W. (1934): The structures of vermiculites and their collapse by dehydration. Am. Mineral. 19, 557-585.

GUIDOTTI, C.V. (1984): Micas in metamorphic rocks. In Micas (Bailey, S.W., ed.), Reviews in Mineralogy 13, 357-455.

HAGGERTY, S.E. (1991): Oxide mineralogy of the upper mantle. In Oxide Minerals: Petrologic and Magnetic Signidicance (Lindsley, D.H., ed.), Reviews in Mineralogy 25, 355-416.

HALKOAHO, T.A.A., ALAPIETI, T.T. AND LAHTINEN, J.J. (1990a): The Sompujarvi PGM Reef in the Penikat layered intrusion, northern Finland. Mineral. Petrol. 42, 39-55.

_____, _____, _____ and LERSSI, J. M. (1990b): The Ala-Penikka PGE Reffs in the Penikat layered intrusion, Northern Finland. Mineral. Petrol. 42, 23-28.

HALL, S.T. (1975): Mineralogy, chemistry, and petrogenesis of some hypabyssal intrusions, Highland County, Virginia. M.S. Thesis, Virginia Polytechnic Institute and State University, Blacksburg, Virginia.

HARNEY, D.M.W. AND MERKLE, R.K.W. (1990): Pt-Pd minerals from the upper zone of the eastern Bushveld Complex, South Africa. Can. Mineral. 28, 619-628.

HELGESON, H.C., DELANY, J.M., NESBITT, H.W. AND BIRD, D.K. (1978): Summary and critique of the thermodynamic properties of rock-forming minerals. Am. J. Sci. 278A, 1-229.

HEY, M.H. (1954): A new review of the chlorites. Mineral. Mag. 30, 277-292.

HODGES, K.V. AND SPEAR, F.S. (1982): Geothermometry, geobarometry and the Al_2SiO_5 triple point at Mt. Moosilauke, New Hampshire. Am. Mineral. 67, 1118-1134.

HOFFMAN, E.L., NALDRETT, A.J., ALCOCK, R.A. AND HANCOCK, R.G.V. (1979): The noble-metal content of ore in the Levack West and Little Stobie mines, Ontario. Can. Mineral. 17, 437-451.

HOFFMAN, P.F. (1988): United plates of America, the birth of a craton: Early Proterozoic assembly and growth of Laurentia. Ann. Rev. Earth Planet. Sci. 16, 543-603.

HUDSON, D.R. (1986): Platinum-group minerals from the Kambalda nickel deposits, Western Australia. Econ. Geol. 81, 1218-1225.

_____ and DONALDSON, M.J. (1984): Mineralogy of platinum group elements in the Kambalda nickel deposits, Western Australia. In Sulphide Deposits in Mafic and Ultramafic Rocks (D.L. Buchanan and M.J. Jones eds.), London, Inst. Mining Metallurgy, 55-61.

_____, ROBINSON, B.W. AND VIGERS, R.B.W. (1978): Zoned michenerite-testibiopalladite from Kambalda, Western Australia. Can. Mineral. 16, 121-126.

HUHTELIN, T.A., ALAPIETI, T.T. AND LAHTINEN, J.J. (1990): The Paasivaara PGE Reef in the Pennikat layered intrusion, Northern Finland. Mineral. Petrol. 42, 57-70.

HUNT, J.A. AND KERRICK, D.M. (1977): The stability of sphene: experimental redetermination and geological implications. Geochim. Cosmochim. Acta 41, 279-288.

INDARES, A. AND MARTIGNOLE, J. (1985): Biotite-garnet geothermometry in the granulite facies: the influence of Ti and Al in biotite. Am. Mineral. 70, 272-278.

IRVINE, T.N. (1974): Petrology of the Duke Island ultramafic complex, southeastern Alaska. Geol. Sco. America Mem. 138, 240p.

_____ (1977): origin of chromite layers in the Muskox intrusion and other stratiform intrusions, a new interpretation. Geology 5, 273-277.

IVANOV, O.P., VOROB'EV, Y.K., EFREMENKO, L.Y. AND KNYAZEVA, D.N.

(1981): Acicular allanite from the Itulin deposit veins (further study of lombardite). Zap. Vses. Mineral. Obshchestva 110, 361-366 (in Russian).

JAMIESON, R.A. (1981): Metamorphism during ophiolite emplacement-the petrology of the St. Anthony complex. J. Petrol. 22, 397-449.

JOHAN, Z. AND WATKINSON, D.H. (1987): Phase fluide riche en Na-Cl-H-O-N et son rôle dans le concentration des éléments groupe de platine et de la chromite: "Upper Critical Zone", complexe de Bushveld. In: Guides de prospection pour les gisements de platinoides dans les complexes ophiolitiques et stratifiés. Rapport final: Commission des Communautés Européennes 61-85.

_____, OHNENSTETTER, M., SLANSKY, E., BAEEON, L.M. AND SUPPEL, D. (1989): Platinum mineralization in the Alaskan-type intrusive complex near Finfield, New South Wales, Australia Part 1. Platinum-group minerals in clinopyroxenites of the Kelvin Grive Prospect, Owendale intrusion. Mineral. Petrol. 40, 289-309.

JUSTER, T.C. (1987): Mineralogic domains in very low grade pelitic rocks. Geology 15, 1010-1013.

KAGER, P.C.A. AND OEN, I.S. (1983): Iron-rich talc-opal-minnesotaite spherulites and crystallochemistry relations of talc and minnesotaite. Mineral. Mag. 47, 229-231.

KINGSTON, G.A. AND EL-DOSUKY B.T. (1982): A contribution on the platinum-group mineralogy of the Merensky Reef at the Rustenburg platinum mine. Econ. Geol. 77, 1367-1384.

KINLOCH, E.D. (1982): Regional trends in the platinum-group mineralogy of the critical zone of the Bushveld complex, South Africa. Econ. Geol. 77, 1328-1347.

KLEIN, C. (1968): Coexisting amphiboles. J. Petrol. 9, 281-230.

KLEMM, D.D. (1965): Synthesen und Analysen in den Dreiecksdiagrammen FeAsS-CoAsS-NiAsS und FeS_2-CoS_2-NiS_2. N. Jb. Mineral. Abh. 103, 205-225.

KOHN, M J. AND SPEAR, F.S. (1991): Error propagation for barometers. 2. Application to natural rocks. Am. Mineral. 76, 138-147.

KOHYAMA, N. AND SUDO, T. (1975): Hisingerite occurring as a weathering product of iron-rich saponite. Clays Clay Minerals 23, 215-218.

KOSKI, R.A., LONSDALE, P.F., SHANKS, W.C., BERNDT, M.E. AND HOWE, S.S. (1985): Mineralogy and geochemistry of a sediment hosted sulfide deposit from the southern trough of Guaymas Basin, Gulf of California. J. Geophys. Res. 90(B8), 6695-6707.

KOZIOL, A.M. AND NEWTON, R.C. (1988): Redetermination of the anorthite breakdown reaction and improvement of the plagioclase-garnet-Al_2SiO_5-quartz geobarometer. Am. Mineral. 73, 216-223.

KRANIDIOTIS, P AND MACLEAN, W.H. (1987): Systematics of chlorite alteration at the Phelps Dodge massive sulfide deposit, Matagami, Quebec. Econ. Geol. 82, 1898-1911.

LAIRD, J. (1988): Chlorites: metamorphic petrology. In Hydrous Phyllosilicates (exclusive of micas) (Bailey, S.W., ed.), Reveiws in Mineralogy 19, 405-453.

LEAKE, B.E. (1965): The relationship between tetrahedral aluminium and the maximum possible octahedral aluminium in natural calciferous and subcalciferous amphiboles. Am. Mineral. 50, 843-851.

_____ (1978): Nomenclature of amphiboles. Can. Mineral. 16, 501-520.

LEBEDEV, P.I. (1936): Beitrag zur Petrographie and Mineralogie der basichen Paegmatite Volyniens. Vernadsky Jubilee volume Acad. Sci. USSR 2, 199-1012. From Miner. Abstr. 7, 199.

LEGENDRE, O. AND AUGE, T. (1986): Mineralogy of platinum-group-mineral inclusions in chromitites from different ophiolitic complexes. In Metallogeny of Basic and Ultrabasic rocks (M.J. Gallagher, R.A. Ixer, C.R. Neary and H.M. Prichard, eds.). Inst. Min. Metall., London.

LESHER, C.M. AND GROVES, D.I. (1986): Controls on formation of komatiite associated nickel-copper sulfide deposits. In Geology and metallogeny of copper deposits (G. Friedrich, A. Genkin, A.J. Naldrett, J.D. Ridge, R.H. Sillitoe and F.M. Vokes, eds.), Springer-Verlag, Heidelberg.

LEWRY, J.F., SIBBALD, T.I.I. AND SCHLEDEWITZ, D.C.P. (1985): Variation in character of Archean rocks in the western Churchill Province and its significance. In Evolution of Archean Supercrustal Sequences (L.D.

Ayres, P.C. Thurston, K.D. Card and W. Weber, eds.), Geol. Assoc. Can. Spec. Pap. 28, 239-261.

LINDQVIST, B. AND JANSSON, S. (1962): On the crystal chemistry of hisingerite. Am. Mineral. 47, 1356-1362.

LINDSLEY, D.H. (1991): Experimental studies of oxide minerals. In Oxide Minerals: Petrologic and Magnetic Signidicance (Lindsley, D.H., ed.), Reviews in Mineralogy 25, 69-106.

LONSDALE, P.F., BISCHOFF, J.L., BURNS, V.M., KASTNER, M. AND SWEENEY, R.E. (1980): A high temperature hydrothermal deposit on the seabed at a Gulf of California spreading center. Earth Planet. Sci. Letters 49, 8-20.

LUDWIG, K.R., NASH, J.T. AND NAESER, C.W. (1981): U-Pb isotope systematics and age of uranium mineralization, Midnite mine, Washington. Econ. Geol. 76, 89-110.

MARCHETTO, C.M.L. (1990): Platinum-group minerals in the O'Toole (Ni-Cu-Co) deposit, Brazil. Econ. Geol. 85, 921-927.

MARZA, I., MARZA, L. AND POSZET, T. (1974): Hisingerite from the epimetamorphosed Fagul Chetasii copper ore deposit, Bahan, Romania. Stud. Univ. Babes-bolyai, Ser. Geol.-Mineral. 19, 9-14 (in Romanian).

MASSONNE, H.J. (1981): Phengite: Eine experimentelle untersuchung ihres druck-temperatur-verhaltens im system K_2O-MgO-Al_2O_3-SiO_2-H_2O. Ph.D. thesis, University of Bochum.

MCCALLUM, M.E., LOUCKS, R.R., CARLSON, R.R., COOLEY, E.F. AND DOERGE, T.A. (1976): Platinum metals associated with hydrothermal copper ores of the New Rambler mine, Medicine Bow Mountains, Wyoming. Econ. Geol. 71, 1429-1450.

MCELDUFF, B. AND STUMFPFL, E.F. (1990): Platinum-group minerals from the Troodos ophiolite, Cyprus. Mineral. Petrol. 42, 211-232.

MICHAILIDIS, K.M. (1990): Zoned chromites with high Mn-contents in the Fe-Ni-Cr-laterite ore deposits from the Edessa area in Northern Greece. Mineralium Deposita 25, 190-197.

MIHALIK, P. JACOBSEN, J.B.E. AND HIEMSTRA, S.A. (1974): Platinum-group

minerals from a hydrothermal environment. Econ. Geol. 69, 257-262.

MISRA, K.C. AND FLEET, M.E. (1974): chemical compositions and stability of violarite. Econ. Geol. 69, 391-403.

MOGESSIE, A., STUMPFL, E.F. AND WEIBLEN, P.W. (1991): The role of fluids in the formation of platinum-group minerals, Duluth Complex, Minnesota: Mineralogic, textural and chemical evidence. Econ. Geol. 86, 1506-1518.

MOSTERT, A.B., HOFMEYR, P.K. AND POTGIETER, G.A. (1982): The platinum-group mineralogy of the Merensky Reef at the Impala platinum mines, Bophuthatswana. Econ. Geol. 77, 1385-1394.

MUIR J.E. AND COMBA, C.D.A. (1979): The Dundonald deposit: an example of volcanic-type nickel-sulfide mineralization. Can. Mineral. 17, 351-359.

MULJA, T. AND MITCHELL, R.H. (1990): Platinum-group minerals and tellurides from the Geordie Lake intrusion, Coldwell Complex, northwestern Ontario. Can. Mineral. 28, 489-501.

NALDRETT, A.J. (1981a): Platinum-group element deposits. In Platimum-Group Elements: Mineralogy, Geology, Recovery (L.J. Cabri, ed.). Can. Inst. Min. Metall., Spec. Vol. 23, 197-231.

_____ (1981b): Nickel sulfide deposits: Classification, composition, and genesis. Econ. Geol. 75th anniv. Vol., 628-685.

_____ (1989): Magmatic sulfide deposits, Oxford University Press, New York.

_____ and CABRI, L.J. (1976): Ultramafic and related mafic rocks: their classification and genesis with special reference to the concentration of nickel sulfides and platinum-group elements. Econ. Geol. 71, 1131-1158.

_____ and VON GRUENEWALDT, G. (1989): Association of platinum-group elements with chromitite in layered introsions and ophiolite complexes. Econ. Geol. 84, 180-187.

_____ and LEHMANN, J. (1988): Spinel non-stoichiometry as the explanation for Ni-, Cu-, and PGE-enriched sulphides in chromitites, In Geoplatinum '87 (H.M. Prichard, P.J. Potts, J.F.W. Bowles and S.J.

Cribb, eds.), Elsevier, London (93-110).

_____ and MASON, G.D. (1968): Contrasting Archean ultramafic igneous bodies in Dundonald and Clergue Township, Ontario. Can. J. Earth Sci. 5, 111-142.

NEWTON, R.C. AND HASELTON, H.T. (1981): Thermodynamics of the garnet-plagioclase-Al_2SiO_5-quartz geobarometer. In Thermodynamics of Minerals and Melts (R.C. Newton, A. Navrotsky and B.J. wood, eds.), Springer-Verlag, New York, 131-147.

NIL'NITSKAYA, E.F. (1967): Manganoferrous wollastonite and its alteration. Zap. Vses Min. Obshch. 96, 927-305. From Miner. Abstr. 19, 47.

NILSSON, L.P. (1990): Platinum-group mineral inclusions in chromitite from the Osthammeren ultramafic tectonite body, south central Norway. Mineral. Petrol. 42, 249-263.

_____ and HAMMACK, J.L. (1990): Mettallogeny of mafic-ultramafic rocks. In Ore Deposits, Tectonics and Mettallogeny in the Canadian cordillera. Mineral. Dep. Div. of Geol. Assoc. Can., short course Notes, Sect. 5-3.

NIXON, G.T., CABRI, L.J. AND LAFLAMME J.H.G. (1990): Platinum-group-element mineralization in lode and placer deposits associated with the Tulameen Alaskan-Type complex, British Columbia. Can. mineral. 28, 503-535.

NYMAN, M.W., SHEETS, R.W. AND BODNAR, R.J. (1990): Fluid-inclusion evidence for the physical and chemical conditions associated with intermediate-temperature PGE mineralization at the New Rembler deposit, southeastern Wyoming. Can. Mineral. 28, 629-638.

OEN, I.S., FERNANDEZ, J.C. AND MANTECA, J.I. (1975): The lead-zinc and associated ores of La Union Sierra de Cartagena, Spain. Econ. Geol. 70, 1259-1278.

OHNENSTETTER, M. (1992): Platinum group element enrichment in the upper mantle peridotite of the Monte Maggiore Ophiolitic Massif (Corsica, France): mineralogical evidence for ore-fluid metasomatism. Mineral. Petrol. 46, 85-107.

ONYEAGOCHA, A.C. (1974): Alteration of chromite from the Twin Sisters

Dunite, Washington. Am. Mineral. 59, 608-612.

OSBORNE, F.F. AND ARCHAMBAULT, M. (1950): Hisingerite from Montauban-les-Mines. Le Naturaliste Canadien, Quebec. 77, 283-290.

PAGE, N.J. AND TALKINGTON, R.W. (1984): Palladium, platinum, rhodium, ruthenium and iridium in peridotetes and chromitites from ophiolite complexes in Newfoundland. Can. Mineral. 22, 137-149.

PAKTUNC, A.D. (1984): Metamorphism of the ultramafic rocks of the Thompson Mine, Thompson Nickel Belt, northern Manitoba. Can. Mineral. 22, 77-91.

PAN, Y. AND FLEET, M.E. (1988): Metamorphic petrology of the White River Property of LAC Minerals Ltd, Hemlo, Ontario. Ont. Geol. Surv., Misc. Pap. 140, 164-176.

_____ and _____ (1990): Halogen-bearing allanite from the White River gold occurrence, Hemlo area, Ontario. Can. Mineral. 28, 67-75.

_____ and _____ (1992): Mineralogy and genesis of calc-silicates associated with Archean volcanogenic massive sulfide deposits at the Manitouwadge mining camp, Ontario. Can. J. Earth Sci. 29 (in press).

_____, _____, BARNETT, R.L. AND CHEN, Y. (1993): Pyrosmalite in Canadian Precambrian sulfide deposits: mineral chemistry, petrogenesis and significance. Can. Mineral. (in press).

PARRY, W.T. AND DOWNEY L.M. (1982): Geochemistry of hydrothermal chlorite replacing igneous biotite. Clays Clay Minerals 30, 81-90.

PATTISON, E.F. (1979): The Sudbury sublayer. Can. Mineral. 17, 257-274.

PEACH, C.L., MATHEZ, E.A. AND KEAYS, R.R. (1989): Sulfide melt-silicate melt distribution coefficients for the noble metals as deduced from MORBS. 5th Intl. Platinum Syme., Helsinki, Abstr. 58-59.

PERCHUK, L.L. (1981): Correction of the biotite-garnet thermometer in case of the Mn $\leftrightarrows$ Mg + Fe isomorphism in garnet. Dokl. USSR AS 256, 38-41.

_____ and LAVRENT'EVA, I.V. (1983): Experimental investigation of exchange equilibria in the system corcierite-garnet-biotite. In Kinetics

and Equilibrium in Mineral Reactions (S.K. Saxena, ed.). Springer-Verlag, New York.

PEREDERY, W.V. (1979): Relationship of ultramafic amphibolites to metavolcanic rocks and serpentinites in the Thompson belt, Manitoba. Can. Mineral. 17, 187-200.

_____ and GEOLOGICAL STAFF (1982): Geology and nickel sulfide deposits of the Thompson Belt, Manitoba. In Precambrian Sulfide Deposits (R.W. Hutchinson, C.D. Spence and J.M. Franklin, eds.), Geol. Assoc. Can. Spec. Pap. 25, 165-209.

PERKINS III, D., ESSENE, E.J. AND MARCOTTY, L.A. (1982): Thermometry and barometry of some amphibolite-granulite facies rocks from the Otter Lake area, southern Quebec. Can. J. Earth Sci. 19, 1759-1774.

PHILLIPS, P. (1989): A look at Lindsley. The Northern Miner Magazine, March, 11, 15.

PLATINUM METAL MINERAL RESEARCH GROUP (1974): Tellurostibnide of palladium and nickel and other new minerals and varieties of platinum metals. Geochimica 3, 169-181 (in Chinese with English abstract).

POWELL, R. (1978): Equilibrium thermodynamics in petrology, an introduction. Harper and Row, Publishers, p. 284.

_____ and EVANS J.A. (1983): A new geobarometer for the assemblage biotite-muscovite-chlorite-quartz. J. Metamorph. Geol. 1, 331-336.

PRICHARD, H.M. AND TARKIAN M. (1988): Platinum and palladium minerals from two PGE-rich localities in the Shetland ophiolite complex. Can. Mineral. 26, 979-990.

_____, NEARY, C.R. AND POTTS, P.J. (1986): Platinum-group minerals in the Shetland ophiolite. In Metallogeny of Basic and Ultrabasic rocks (M.J. Gallagher, R.A. Ixer, C.R. Neary and H.M. Prichard, eds.). Inst. Min. Metall., London.

PYE, E.G., NALDRETT, A.J. AND GIBLIN, P.E., eds. (1984): The geology and ore deposits of the Sudbury Structure. Ministry of Natural Resources, Ontario.

RAASE, P. (1974): Al and Ti contents of hornblende, indicators of pressure and

temperature of regional metamorphism. Contrib. Mineral. Petrol. 45, 231-236.

RAICEVIC, D. AND CABRI, L.J. (1976): Mineralogy and concentration of Au- and Pt-bearing placers from the Tulameen River area in British columbia. Can. Inst. Min. Metall. Bull. 69(770), 111-119.

RAO, A.T., RAO, A. AND RAO, P.P. (1979): Fluorian allanite from calc-granulite and pegmatite contacts at Garvidi, Andhra Pradesh, India. Mineral. Mag. 43, 312.

RAZIN, L.V. (1976): Geologic and genetic features of forsterite dunites and their platinum-group mineralization. Econ. Geol. 71, 1371-1376.

ROSS, J.R. AND KEAYS, R.R. (1979): Precious metals in volcanic-type nickel sulfide deposits in western Australia. Relationship with the composition of the ores and their host rocks. Can. Mineral. 17, 417-435.

ROWELL, W.F. AND EDGAR, A.D. (1986): Platinum-group element mineralization in a hydrothermal Cu-Ni sulfide occurrence, Rathbun Lake, northeastern Ontario. Econ. Geol. 81, 1272-1277.

RUSSEL, J.K. (1981): Metamorphism of the Thompson Nickel Belt gnesses. Can. J. Earth Sci. 18, 191-209.

SALES, R.H. AND MEYER, C. (1948): Wall rock alteration at Butte, Montana. Am. Inst. Min. Eng. Mining Technol. Tech. Pub. 2400, p.25.

SCOTT, S.D. (1982): The Fe-S system. In Sulfide Mineralogy (Ribbe, P.H., ed.), Reviews in Mineralogy 1, CS21-CS81.

SEITSAARI, J. (1956): Some new data on the blue-green hornblende from the Tampere Schist belt. Bull. Comm. Geol. Finland 28, 41-46.

SHEN, P., BASSETT, W.A. AND LIU, L.-G. (1983): Experimental determination of the effects of pressure and temperature on the stoichiometry and phase relations of wustite. Geochim. Coschim. Acta 47, 773-778.

_____, HWANG, S.-L., CHU, H.-T. AND JENG, R.-C. (1988): STEM study of "ferritchromite" from the Heng-Chun chromitite. Am. Mineral. 73, 383-388.

SPRY, P.G. (1982): An unusual gahnite-forming reaction, Geco base-metal

deposit, Manitouwadge, Ontario. Can. Mineral. 20, 549-553.

_____ and SCOTT, S.D. (1986): Zincian spinel and staurolite as guids to ore in the Appalachians and Scandinavian Caledonides. Can. Mineral. 24, 147-163.

ST. LOUIS, R.M.S., NESBITT, B.E. AND MORTON, R.D. (1986): Geochemistry of platimun-group elements in the Tulameen ultramafic complex, southern British Columbia. Econ. Geol. 81, 961-973.

STOCKMAN, H.W. AND HLAVA, P.F. (1984): Platinum-group minerals in alpine chromitites from southwestern Oregon. Econ. Geol. 79, 491-508.

STODDARD, E.F. (1979): Zinc-rich hercynite in high-grade metamorphic rocks: a product of the dehydration of staurolite. Am. Mineral. 64, 736-741.

STONE, W.E., FLEET, M.E. AND MACRAE, N.D. (1989): Two-phase nickeliferous monosulfide solid solution (mss) in megacrysts from Mount Shasta, California: A natural laboratory for nickel-copper sulfides. Am. Mineral. 74, 981-993.

STONE, W.E., CROCKET, J.H. AND FLEET, M.E. (1990): Partitioning of palladium, iridium, platinum, and gold between sulfide liquid and basalt melt at 1200°C. Geochim. Cosmochim. Acta 54, 2341-2344.

STUMPFL, E.F. (1986): distribution, transport and concentration of platinum group elements. In Metallogeny of Basic and Ultrabasic rocks (M.J. Gallagher, R.A. Ixer, C.R. Neary and H.M. Prichard, eds.). Inst. Min. Metall., London (379-394).

SUDO, T. AND NAKAMURA, T. (1952): Hisingerite from Japan. Am. Mineral. 37, 618-621.

SCHWARTZ, G.M. (1924): On the nature and origin of hisingerite from Parry Sound, Ontario. Am. Mineral. 9, 141-144.

TAKEUCHI, Y., KAWADA, I. IRIMAZIRI, S. AND SADANGA, R. (1969): The crytal structure and polytypism of manganpyrosmalite. Mineral. J. 5, 450-467.

TALKINGTON, R.W. AND LIPIN, B.R. (1986): Platinum-group minerals in chromite seams of the Stillwater Complex, Montana. Econ. Geol. 81, 1179-1186.

_____ and WATKINSON, D.H. (1986): Whole-rock platinum-group element in chromite-rich rocks in ophiolitic and stratiform igneous complexes. In Metallogeny of Basic and Ultrabasic Rocks (M.J. Gallagher, R.A. Ixer, C.R. Neary and H.M. Prichard, eds.). Inst. Min. Metall., London (427-440).

_____, _____, WHITTAKER, P.J. AND JONES, P.C. (1983): Platinum-group-mineral inclusions in chromite from the Bird River Sill, Manitoba. Mineralium Deposita. 246-255.

_____, _____, _____ and _____ (1984): Platinum-group minerals and other solid inclusions in chromite of ophiolitic complexes occurrences and petrological significance. Tschermaks Mineral. Petrog. Mitt. 32, 285-301.

TARKIAN, M. (1987): Compositional variations and reflectance of the common platinum-group minerals. Mineral. Petrol. 36, 169-190.

_____ and PRICHARD, H.M. (1987): Irarsite-hollongworthite solid-solution series and other associated Ru-, Os-, Ir-, and Rh-bearing PGM's from the Shetland ophiolite complex. Mineral. Deposita 22, 178-184.

THALHAMMER, O.A.R., PROCHASKA, W. AND MÜHLHANS, H.W. (1990): Solid inclusions in chrome-spinels and platinum group element concentrations from the Hochgrössen and Kraubath Ultramafic Massifs (Austria). Contrib. Mineral. Petrol. 105, 66-80.

THOMPSON, A.B. (1976): Mineral reactions in pelitic rocks: II. Calculation of some P-T-X (Fe-Mg) phase relations. Am. J. Sci. 276, 425-454.

TISCHLER, S.E., CAWTHORN, R.G., KINGSTON, G.A. AND MASKE, S. (1981): Magmatic Cu-Ni-PGE mineralization at Waterfall Gorge, Insizwa, Pondoland, Transkei. Can. Mineral. 19, 607-618.

TODD, S.G., KEITH, D.W., LE ROY, L.W., SCHISSEL, D.J., MANN, E.L. AND IRVINE, T.N. (1982): The J.M. platinum-palladium reef of the Stillwater complex, Montana. I. Stratigraphy and petrology. Econ. Geol. 77, 1454-1480.

TRELOAR, P.J. (1987): The Cr-minerals of Outokumpu - their chemistry and significance. J. Petrol. 28, 867-886.

VAL'TER, A.A., BOBONICH, F.M., POL'SHIN, E.V., KALINICHENKO, A.M.,

KHOMENKO, V.M., BURMISTROVA, V.V., GONIONDSKAYA, L.S. AND SOLOMAKHA, V.N. (1988): Nature of hisingerite from the Ternovaya astrobleme (Krivio Rog Basin). Mineral. Zh. 10, 50-63 (in Russian).

VAUGHAN, J.P. (1986): The iron end-member of the pyrosmalite series from the Pegmont zinc deposit, Queensland. Mineral. Mag. 50, 527-531.

_____(1987): Ferropysmalite and nomenclature in the pyrosmalite series. Mineral. Mag. 51, 171.

VELDE, B. (1965): Phengite micas: synthesis, stability and natural occurrence. Am. J. Sci. 263, 886-913.

_____ (1967): Si^{4+} content of natural phengites. Contrib. Mineral. Petrol. 14, 250-258.

VERMAAK, C.F. AND HENDRIKS, L.P. (1976): A review of the mineralogy of the Merensky Reef, with specific reference to new data on the precious metal mineralogy. Econ. Geol. 71, 1244-1269.

VOLBORTH, A., TARKIAN, M., STUMPFL, E.F. AND HOUSLEY, R.M. (1986): A survey of Pd-Pt mineralization along the 35-KM strike of the J-M Reef, Stillwater complex, Montana. Can. Mineral. 24, 329-346.

WANDKE, A. AND HOFFMAN, R. (1924): A study of the Sudbury ore deposits. Econ. Geol. 19, 169-204.

WEBER, W. AND SCOATES, R.F.J. (1978): Archean and Proterozoic metamorphism in the northwestern Superior Province and along the Churchill-Superoir boundary, Manitoba. In Metamorphism in the Canadian Shield (J.A. Fraser and W.W. Heywood, eds.), Geol. Surv. Can. Pap. 78-10, 5-16.

WHELAN, J.A. AND GOLDICH, S.S. (1961): New data for hisingerite and neotocite. Am. Mineral. 46, 1412-1423.

WHITTAKER, P.J. AND WATKINSON, D.H. (1984): Genesis of chromitite from the Mitchell Range, central British columbia. Can. Mineral. 22, 161-172.

WILSON, H.D.B. AND BRISBIN, W.C. (1961): Regional structure of the Thompson-Moak Lake nickel belt. Can. Inst. Mining Met. Bull. 54, 815-822.

WYLLIE, P.J. (1967): Ultramafic and related rocks. John willey and sons, New York, 464p.

WYLIE, A.G., CANDELA, P.A. AND BURKE, T.M. (1987): Compositional zoning in unusual Zn-rich chromite from the Sykesville district of Maryland and its bearing on the origin of "ferritchromite". Am. Mineral. 72, 413-422.

YAKOVLEV, Y.N., DISTLER, V.V., MITROFANOV, F.P., RAZHEV, S.A., GROKHOVSKAYA, T.L. AND VESELOVSKY, N.N. (1991): Mineralogy of PGE in the mafic-ultramafic massifs of the Kola Region. Mineral. Geol. 43, 181-192.

ZAMBONINI, F. (1901): Mineralogische Mitteilungen 12. Pyrosmalith aus der Bjulke Grube (Nordmarken). Z. Kristal. Mineral. 34, 549-561.

ZIENTEK, M.L., CZAMANSKE, G.K. AND IRVINE, T.N. (1985): Stratigraphy and nomenclature for the Stillwater Complex. In Stillwater complex (G.K. Czamanske and M.L. Zientek, eds.), Montana Bureau of Mines and Geology, Spec. Pub. No.92, 21-32.

ZURBRIGG, H.F. (1963): Thompson Mine geology. Can. Inst. Mining Met. Bull. 56, 451-460.